PARTICULATE MATTER FORMATION IN SPARK-IGNITION ENGINES

by

David Kayes

Bachelor of Science in Mechanical Engineering
University of California at Berkeley
(1994)

Master of Science in Mechanical Engineering
Massachusetts Institute of Technology
(1996)

Submitted to the Department of Mechanical Engineering
in partial fulfillment of the requirements for the degree of

DOCTOR OF PHILOSOPHY

at the

MASSACHUSETTS INSTITUTE OF TECHNOLOGY

[February 1999]
January, 1999

© 1999 Massachusetts Institute of Technology
All rights reserved

Signature of Author_____
Department of Mechanical Engineering
8 January 1999

Certified by_____
Simone Hochgreb
Associate Professor, Department of Mechanical Engineering
Thesis Supervisor

Accepted by_____
Ain A. Sonin
Chairman, Department Graduate Committee

MASSACHUSETTS INSTITUTE OF TECHNOLOGY
JUL 1 2 1999
LIBRARIES

ARCHIVES

PARTICULATE MATTER FORMATION IN SPARK-IGNITION ENGINES

by David Kayes

Submitted to the Department of Mechanical Engineering on 17 December 1998 in partial fulfillment of the requirements for the degree of Doctor of Philosophy in Mechanical Engineering

ABSTRACT

Recent health concerns over airborne particulate matter (PM) have prompted examination of the mechanisms by which PM is formed in spark ignition (SI) internal combustion engines. A study was undertaken in order to understand the effects of dilution on measured PM, to examine and model the effect of steady state engine operating conditions on engine-out PM, and to characterize the effect of transient engine conditions on particle growth and dynamics.

Particle dynamics in diluted SI and compression ignition (CI) engine exhaust are examined and discussed in the context of SI exhaust dilution. Temperature measurements in the exhaust pipe and dilution tunnel reveal the degree of mixing between exhaust and dilution air, the effect of flowrate on heat transfer from undiluted and diluted exhaust to the environment, and the minimum permissible dilution ratio for a maximum sample temperature of 52°C. Measurements of PM concentrations as a function of dilution ratio, using a Scanning Mobility Particle Sizer (SMPS), show the competing effects of temperature and particle/vapor concentrations on particle growth dynamics, which result in a range of dilution ratios — from 13 to 18 — where the effect of dilution ratio, independent of flowrate, is kept to a minimum and is therefore optimal in order to achieve repeatable PM concentration measurements. Particle dynamics in transit through the dilution tunnel are measured and compared to previous research.

PM emissions are strongly affected by steady state engine parameters that affect global and local air/fuel ratios, the concentration of liquid fuel in the cylinder, and the availability of soot precursors. PM emissions vary by up to six orders of magnitude between the fuels tested, when at the same fuel/air equivalence ratio. Minimum PM concentrations are emitted at a global fuel/air ratio within 10% of stoichiometric, with the exact value depending on the particular fuel, and concentrations can increase by more than three orders of magnitude when the fuel/air ratio is either increased or decreased 30% from stoichiometric. Burning liquid fuel is a significant source of PM, as evidenced by the fact that open valve fuel injection increases PM emissions by up to three orders of magnitude relative to closed valve injection. Coolant and oil temperatures, spark timing, and Exhaust Gas Recirculation (EGR) affect PM through their effect on intake port and cylinder temperatures, as well as through the effect on the availability of liquid fuel in the cylinder. Particles derived from oil consumption were found to be between zero and 40% of the total PM concentration for the oils used in the present experiments. Differences in PM emissions with and without the catalytic converter are not statistically significant. Particulate number and mass concentrations plus particle sizes are addressed in the present paper, as is the correlation between PM and emissions of gaseous pollutants — hydrocarbons (HCs), oxides of nitrogen (NO_x), oxides of carbon (CO and CO_2) — as well as oxygen and characteristic temperatures and pressures during the engine cycle.

A model of PM formation via homogeneous- and heterogeneous-phase reactions, growth via condensation and adsorption/absorption of vapors, and diminution via oxidation explains the observed behavior of PM emissions with respect to each of the engine, fuel, and dilution parameters above. PM emissions during transient engine operation are generally a first-order time response with characteristic times similar to those involved in the fuel evaporation process, suggesting that PM emissions respond to instantaneous engine conditions and may be modeled using a quasi-steady state application of the model.

Thesis Supervisor: Simone Hochgreb
Associate Professor of Mechanical Engineering, M.I.T.

Additional Members of Doctoral Committee:
Glen Cass, Professor of Environmental Engineering Science, Caltech
John Heywood, Professor of Mechanical Engineering, M.I.T.
Jack Howard, Professor of Chemical Engineering, M.I.T.

ACKNOWLEDGMENTS

I imagine that the acknowledgments are the most read part of any thesis: the rest is stuffy technical writing that, if it is of real value, will be published in a reputable journal. (I've got my fingers crossed regarding acceptance of the papers I've sent out!) But the acknowledgments are the only place where the author can display a shred of warmth and humor. If you, the reader, glance at no other page than this one, I hope you will realize just how large a debt of gratitude I owe to the people acknowledged here; without their guidance and interaction, I might well have become that humorless, stuffy person in whose voice the remainder of this thesis is written, while thanks to them, I am...um...ahem.... In any case, they tried their best!

Several professors deserve my gratitude: Professor Simone Hochgreb for accepting the gamble inherent in a project as new to our as lab as my proposed particulate project was, and for guiding me during the frequent occasions when my modeling attempts went awry; Professors Glen Cass, John Heywood, and Jack Howard for the exceptional expertise they demonstrated both during and outside of our committee meetings; and Professor James Keck for his questions and insights, which always send me in new directions and introduce me to a variety of ways in which I might think about a given phenomenon.

I would like to further thank Professor Glen Cass as well as James Schauer of Caltech for their assistance with the design of the dilution tunnel and their expertise on particle measurement. Invaluable assistance was lent by undergraduate assistant Scott Whitehead, who collected filter samples, and post-masters assistant Helen Liu, who performed several of the transient engine experiments; but even more importantly, both supplied a fresh perspective and new insight regarding the project. Behind every great research project is an even greater technical support staff who, more often than not, do not get their just recognition; so — no matter what your opinion of my work — you must applaud the immeasurable support given to me by Brian Corkum, Pete Menard, and Nancy Cook.

In the acknowledgments of my master's thesis, I suggested that while a successful professor is one who is cited in the references of numerous papers, a successful student is one who is cited in the acknowledgments of numerous theses. Many of the following students are cited for the second time in this, the second of my theses, but all are experts in the extracurricular arts: Doug Whittington, Bob Murry, Bob Kennedy, Greg Dudley, and the rest of the chemists, Brad VanDerWege, Mark Dawson, Mike Shelby, Robert Meyer, Chris O'Brien, Helen Liu, Micha Weigel, and the rest of the Sloan Lab, as well as friends from undergrad — John and Rachel Horsch, Beahrs!, Greg Artiles, Jerris Mungai, Jay Ashford, Henrik Gullman — whom I wish I could see more often.

I would like to thank the following for sponsoring this project: EPA Center On Airborne Organics at MIT, the MIT Engine-Fuels Interaction Consortium (DaimlerChrysler, Ford, General Motors, Mobil, Peugeot, Renault, Shell, and Volvo), and the National Science Foundation. The researchers in the interaction consortium deserve special thanks for the insight they supplied during our frequent meetings. In addition, I would like to thank Matti Maricq, Diane Podsiadlik, and Dick Chase of Ford for welcoming me to their lab and giving me free rein to run experiments (or, at least, so it seemed); I think ours is a healthy research collaboration, and I hope it will continue in the future. I would also like to thank Scott Carpenter and the rest of the engineers at GM Saturn who helped build the engine controller. Lastly, I would like to thank the anonymous people who reviewed my journal submissions: the harsher the reviews, the more I learned, and fortunately you helped me learn a lot!

Dave Kayes
5 January 1999

TABLE OF CONTENTS

ABSTRACT 3

ACKNOWLEDGMENTS 5

TABLE OF CONTENTS 7

LIST OF TABLES 9

LIST OF FIGURES 10

NOMENCLATURE 17

CHAPTER 1. INTRODUCTION 20
- 1.1 Background 20
- 1.2 Dilution Issues 21
- 1.3 Effect of Steady State Engine Parameters 23
- 1.4 Effect of Transient Engine Operation 27
- 1.5 Objectives 29

CHAPTER 2. EXPERIMENTAL APPARATUS AND PROCEDURE 31
- 2.1 Apparatus and Procedure for Dilution and Steady State Engine Experiments 31
- 2.2 Apparatus and Procedure for Transient Experiments 35
- 2.3 Verification of Dilution Tunnel Design 37
- 2.4 Apparatus Conditioning 40

CHAPTER 3. DATA ANALYSIS 44
- 3.1 Analysis of Steady State Data 44
- 3.2 Analysis of Transient Data 45
- 3.3 Uncertainty Analysis 48

CHAPTER 4. RESULTS OF DILUTION EXPERIMENTS 60
- 4.1 Experimental Methodology and Conditions 60
- 4.2 Temperature Along the Tunnel 60
- 4.3 Effect of Dilution Ratio on PM 62
- 4.4 Particle Number Losses and Volume Gain at Fixed Dilution Ratio 65
- 4.5 Comparison Between Filter Analyses and SMPS 69

CHAPTER 5. RESULTS OF STEADY STATE ENGINE EXPERIMENTS 74
- 5.1 Experimental Methodology and Conditions 74
- 5.2 Effect of Engine Parameters on PM Emissions 76
- 5.3 Effect of Fuel Parameters on PM Emissions 89
- 5.4 Effect of Oil Parameters on PM Emissions 97
- 5.5 Effect of Catalytic Converter on PM Emissions 99

CHAPTER 6. CORRELATIONS BETWEEN PM AND ENGINE/EXHAUST PARAMETERS 109
- 6.1 Methodology 109
- 6.2 Correlations Between PM And HC Emissions 109
- 6.3 Correlations Between PM And NO_x Emissions 111
- 6.4 Correlations Between PM And CO, CO_2, And O_2 Emissions 111
- 6.5 Correlations Between PM Emissions And Characteristic Temperatures and Pressures 112

CHAPTER 7. MODEL OF PM EMISSIONS 117
- 7.1 Background 117

7.2 Model 120
7.3 Dilution Issues 137
7.4 Calculation Of Model Coefficients 138

CHAPTER 8. MODEL RESULTS AND DISCUSSION 142
8.1 Matrix of Operating Conditions 142
8.2 Experimental Comparison 143
8.3 Discussion 149

CHAPTER 9. TRANSIENT PM EMISSIONS 153
9.1 Experimental Methodology and Conditions 153
9.2 Time Response of Individual Components 154
9.3 Results 157
9.4 Discussion 165

CHAPTER 10. CONCLUSIONS 174
10.1 Dilution Experiments 174
10.2 Steady State Experiments 176
10.3 Model of PM Formation During Steady State Operation 177
10.4 PM Formation During Transient Operation 178

REFERENCES 180

APPENDICES 185
APPENDIX 1. Model Prediction Of PM Versus Fuel Control Strategy 185
APPENDIX 2. Chemical Analyses of PM 186
APPENDIX 3. PM Emissions During FTP Test 189
APPENDIX 4. Data Used In Chapter 6 191

LIST OF TABLES

Table 1.1 Estimates of total particulate emissions by vehicle class and driving location (estimates of 1993 vehicle fleet) 21

Table 2.1 Engine specifications 32

Table 2.2 Baseline engine operating conditions 35

Table 5.1 Parameters varied about the baseline conditions 74

Table 7.1 Unitless scaling factor A_{sp} for each fuel used 122

Table 7.2 Coefficients for model of PM emission and the equations in which they are used 139

Table 9.1 Time constants measured for rising and falling edges of particulate response for experiments with varying intake manifold pressure 158

Table 9.2 Time constants measured for rising and falling edges of particulate response for experiments with varying fuel/air equivalence ratio 160

LIST OF FIGURES

Figure 2.1 Schematic of engine, dilution tunnel, and SMPS. Units: cm..... 42

Figure 2.2 Tracer (propane) concentration across the radius of the dilution tunnel. Traverses A..... 43
and B are along lines perpendicular to each other, at the monitoring port of the dilution tunnel. Error bars represent 4% measurement imprecision. All concentrations are normalized to the mean as described in the text.

Figure 3.1 Schematic of procedure for analyzing data..... 57

Figure 3.2 Size distributions of particles drawn from undiluted diesel exhaust in fourteen..... 58
consecutive tests, taken over a period of one hour.

Figure 3.3 Size distributions from seven consecutive tests on the SI engine, using the dilution..... 58
tunnel. Corrected for dilution ratios of 13:1 to 15:1, as discussed in Data Analysis section. Baseline engine operating conditions specified in text. Samples were taken over the course of one hour.

Figure 3.4 Post-dilution number and volume size distribution characteristics for seven..... 58
consecutive tests within one hour, using SI engine. Engine operating conditions same as in previous figure. Error bars represent standard deviations.

Figure 3.5 Size distributions from seven consecutive tests on the SI engine, weighted on a..... 58
volume (or mass) basis. Engine operating conditions same as in previous figure.

Figure 3.6 Response of PM emissions to transient intake pressure for two different lengths..... 59
of time steps. Particle size: 25nm. Baseline conditions at the 40 kPa IMAP case; baseline conditions at the 70 kPa IMAP case except for intake pressure. Duration of time steps: (a) 30 seconds, (b) 120 seconds.

Figure 4.1 Calculated diluted exhaust temperature as a function of dilution ratio for four..... 71
exhaust gas temperatures, assuming constant specific heat and adiabatic mixing.

Figure 4.2 Measured temperatures at various points in the experimental setup: exhaust port,..... 71
end of exhaust pipe, and four locations in the dilution tunnel, plus blow-up of temperatures in the dilution tunnel. Calculated temperatures of diluted exhaust (presented in the blow-up) are taken from Figure 4.1 for the corresponding exhaust temperatures.

Figure 4.3 Measured diluted exhaust temperatures at the monitoring port location (2.8 meters..... 72
downstream of the mixing location) as a function of dilution ratio for diluted exhaust flowrates of 950 and 6400 lpm. Curves represent approximate fits to data.

Figure 4.4 PM concentration versus dilution ratio for SI engine, Re ≈ 57000. Open symbols..... 72
and dashes show data from experiment 1: 2000 rpm, 0.4 bar IMAP, standard engine fuel injection controller. Filled symbols and solid lines show data from experiment 2: 2000 rpm, 0.3 bar IMAP, computerized proportional/integral (PI) fuel injection controller. Concentrations are corrected for dilution ratio, and therefore reflect only the effect of particle dynamics on the engine-out concentrations. Units of number concentration are particles/cm^3, volume concentration nm^3/cm^3. Bracketed data are outliers.

Figure 4.5 PM concentrations versus dilution ratio for SI engine, Re ≈ 9000. Engine operating.....73
conditions: 2000 rpm, 0.4 bar IMAP, standard engine fuel injection controller. Concentrations are corrected for dilution ratio, and therefore only reflect effect of particle dynamics on the measured engine-out concentrations. Units of number concentration are particles/cm^3, volume concentration nm^3/cm^3.

Figure 4.6 Particle concentrations (number- and volume-weighted) as a function of location within....73
the dilution tunnel. Curves represent average of data at each location. Dilution tunnel flowrate = 950 lpm, Re = 9000. Dilution tunnel temperatures held fixed. PM generated by diesel engine. Uncertainty in measurements of number concentration is 20%, in volume concentration is 25%.

Figure 4.7 Particle sizes as a function of location within the dilution tunnel (same conditions.....73
as in previous figure). Uncertainties in measurements of mode sizes are 10%, those in mean sizes are 3%.

Figure 4.8 Comparison of concurrent SMPS and filter measurements. Several engine operating.....73
conditions: equivalence ratios from 0.7 to 1.3, spark timings from 5 to 55°CA BTC, EGR from 0% to 100% of amount needed to stall engine. Dilution ratio: 15 ± 2. Filter collection time: 50 minutes. Only glass-fiber filter measurements presented. Threshold (dotted line) corresponds to approximately 3% of HCs being adsorbed on filters, as discussed in the text.

Figure 5.1 PM as a function of fuel/air equivalence ratio. Baseline engine operating conditions..... 102
except equivalence ratio and dilution ratio, as explained in text. Data taken on both Ford and Saturn engines. Data corrected for dilution ratio, in order to represent PM concentration in the cooled engine exhaust.

Figure 5.2 HC and oxygen emissions as a function of fuel/air equivalence ratio. Baseline engine..... 102
operating conditions except equivalence ratio. Emissions were measured on Ford engine and corrected in order to represent mole fraction in the "wet" exhaust gas.

Figure 5.3 Flame temperature as a function of fuel/air equivalence ratio, calculated using GM..... 102
Engine-Simulation Program [51]. Baseline engine operating conditions except equivalence ratio, isooctane fuel.

Figure 5.4 Number-weighted mean and mode particle sizes as a function of equivalence ratio,..... 102
measured on both Ford and Saturn engines. Baseline conditions except equivalence ratio and dilution ratio, as explained in text.

Figure 5.5 HC and PM emissions as a function of the time in Crank Angle Degrees (CAD)..... 103
after intake top-dead center (AITDC) at which injected fuel hits the intake valves. Baseline engine operating conditions except fuel injection timing.

Figure 5.6 HC, NO_x, and mass-weighted PM emissions as a function of coolant and oil..... 103
temperature. Baseline operating conditions except for coolant and oil temperatures.

Figure 5.7 PM emissions as a function of spark timing. Baseline operating conditions except..... 103
spark timing. Tests repeated on two days: data shown as filled and open symbols. Outlier shown in parentheses.

Figure 5.8 HC emissions, peak flame temperature, and exhaust port temperature as a function..... 103
of spark timing. Baseline operating conditions except spark timing. Symbols represent data; curves accompanying HC mole fractions and exhaust temperatures represent fit to data. Peak flame temperature calculated using GM Engine-Simulation Program [51].

Figure 5.9 Number- and mass-weighted mean and mode particle sizes as a function of spark..... 104
timing. Baseline engine operating conditions except spark timing.

Figure 5.10 Number- and mass-weighted PM emissions as a function of EGR rate. Baseline..... 104
conditions except EGR rate. Lines represent fits to data, described in text.

Figure 5.11 Intake manifold temperature, exhaust HC concentration, and exhaust NO_x..... 104
concentration as a function of EGR rate. Baseline engine operating conditions except EGR rate.

Figure 5.12 Particle sizes as a function of EGR rate: mean sizes on both number- and mass-..... 104
weighted bases, plus mode sizes on number-weighted basis. Baseline engine operating conditions except EGR rate. Mode sizes on mass-weighted basis are too scattered and thus are not plotted.

Figure 5.13 Number-weighted PM concentrations as a function of intake pressure (engine..... 105
load). Three engine speeds, all other conditions same as baseline.

Figure 5.14 Mass-weighted PM concentrations as a function of intake pressure (engine load)..... 105
Three engine speeds, all other conditions same as baseline.

Figure 5.15 Number-weighted PM concentrations as a function of engine speed. Three intake..... 105
pressures, all other conditions same as baseline.

Figure 5.16 Mass-weighted PM concentrations as a function of engine speed. Three intake..... 105
pressures, all other conditions same as baseline.

Figure 5.17 Number-weighted PM concentrations as a function of fuel/air equivalence ratio..... 106
using five fuels (both Ford and Saturn engines used). Baseline conditions except for fuel type and equivalence ratio. Dilution ratio in indolene test on Ford engine is between 8 and 9 as discussed in text.

Figure 5.18 Mass-weighted PM concentrations as a function of fuel/air equivalence ratio using..... 106
five fuels (both Ford and Saturn engines used). Baseline conditions except for fuel type and equivalence ratio. Dilution ratio in indolene test on Ford engine is between 8 and 9 as discussed in text.

Figure 5.19 Number-weighted mean and mode particle sizes as a function of fuel/air equivalence..... 106
ratio for indolene/MTBE mixture, toluene, and isooctane. Baseline conditions except for fuel type and equivalence ratio. All data taken on Saturn engine.

Figure 5.20 HC emissions as a function of fuel/air equivalence ratio using five fuels (both Ford..... 106
and Saturn engines used). Baseline conditions except for fuel type and equivalence ratio.

Figure 5.21 Number- and mass-weighted PM concentration as a function of oil viscosity and..... 107
composition. Baseline conditions except for oil type.

Figure 5.22 Catalyst efficiency at eliminating PM as a function of measured catalyst temperature,..... 107
plus blow-up of data taken at catalyst temperature above 400°C. Three speed and load conditions, all other conditions same as baseline.

Figure 5.23 Change in particle sizes — expressed as engine-out particle size minus catalyst-out..... 108
particle size divided by engine-out particle size — at the various engine operating conditions as a function of the measured catalyst temperature, plus blow-up of data above -40% on ordinate axis. Three speed and load conditions, all other conditions same as baseline.

Figure 6.1 Comparison between PM and HC concentrations in various experiments..... 114

Figure 6.2 Comparison between PM and HC concentrations in experiments with rich air/fuel..... 114
ratios. Symbols represent same things as in previous figure. Exponential curve fit to data and corresponding R^2 correlation coefficient shown.

Figure 6.3 Comparison between mean PM size and HC concentrations in various experiments:..... 114
(a) number-weighted, (b) mass-weighted. Symbols represent same things as in previous figures.

Figure 6.4 Comparison between PM and NO_x concentrations in various experiments. Symbols..... 115
represent same things as in previous figures.

Figure 6.5 Comparison between PM and CO concentrations in various experiments. Symbols..... 115
represent same things as in previous figures.

Figure 6.6 Comparison between PM and CO_2 concentrations in various experiments. Symbols..... 115
represent same things as in previous figures.

Figure 6.7 Comparison between PM and O_2 concentrations in various experiments. Symbols..... 115
represent same things as in previous figures.

Figure 6.8 Comparison between PM concentration and peak temperature. Peak temperature..... 116
calculated by GM Engine-Simulation Program [51]. Symbols represent same things as in previous figures.

Figure 6.9 Comparison between PM concentration and exhaust temperature for tests in which..... 116
exhaust temperature data is available. Exhaust temperature measured by thermocouples in exhaust ports. Symbols represent same things as in previous figures.

Figure 6.10 Comparison between PM concentration and peak cylinder pressure. Peak cylinder..... 116
pressure calculated by GM Engine-Simulation Program [51]. Symbols represent same things as in previous figures.

Figure 7.1 Comparison between modeled and experimentally measured PM concentrations..... 141
All data scaled relative to PM concentration at baseline conditions.

Figure 8.1 Modeled and experimentally measured PM concentrations as a function of fuel/air..... 150
equivalence ratio. All data scaled relative to PM concentration at baseline conditions.

Figure 8.2 Fractional contributions of each mechanism to the total PM mass as a function of..... 150
fuel/air equivalence ratio, and fractional change in mass due to oxidation. Note that the left hand scale is logarithmic. "Ad/ab" is mass from the adsorption/absorption mechanism; "GP" is from gas phase nucleation mechanism; "LP" is from liquid phase nucleation mechanism; "Ox" is fractional change in mass due to oxidation.

Figure 8.3 Modeled and experimentally measured PM concentrations as a function of fuel..... 150
injection timing. All data scaled relative to PM concentration at baseline conditions.

Figure 8.4 Modeled and experimentally measured PM concentrations as a function of EGR..... 150
rate (measured as the fraction of the amount necessary to stall the engine). All data scaled relative to PM concentration at baseline conditions. Curve labeled "fit to experiment" is an exponential fit to the experimental data.

Figure 8.5 Fractional contributions of each mechanism to the total PM mass as a function of..... 151
EGR rate, and fractional change in mass due to oxidation. Note that the left hand scale is logarithmic. Definitions of symbols same as in Figure 8.2.

Figure 8.6 Modeled and experimentally measured PM concentrations as a function of spark..... 151
timing. All data scaled relative to PM concentration at baseline conditions. Curve labeled "fit to experiment" is a fourth order polynomial fit to the experimental data.

Figure 8.7 Modeled and experimentally measured PM concentrations as a function of load (intake..... 151
manifold absolute pressure). All data scaled relative to PM concentration at baseline conditions.

Figure 8.8 Modeled and experimentally measured PM concentrations as a function of engine..... 151
speed. All data scaled relative to PM concentration at baseline conditions.

Figure 8.9 Modeled and experimentally measured PM concentrations as a function of dilution..... 152
ratio in the high flowrate case (Re = 57,000). All data scaled relative to PM concentration at baseline conditions. PM concentration at dilution ratio of unity could not be measured accurately: subsequent measurements will be progressively lower; therefore the datum presented in this figure is the maximum measured concentration at $\Lambda = 1$.

Figure 8.10 Modeled and experimentally measured PM concentrations as a function of dilution..... 152
ratio in the low flowrate case (Re = 9,000). All data scaled relative to PM concentration at baseline conditions. PM concentration at dilution ratio of unity could not be measured at all, so datum in figure is the extrapolation of the curve through the other data, as explained in the text.

Figure 8.11 Modeled and experimentally measured PM concentrations using the different fuels..... 152
at the baseline operating conditions. All data scaled relative to PM concentration using indolene fuel.

Figure 9.1 Time response of SMPS to step changes in PM concentration. Particle size measured:..... 170
(a) 50 nm, (b) 75 nm. The 50 nm PM emissions have a non-differentiability in the time response, while at 75 nm, if such a non-differentiability exists, it is indistinguishable from measurement noise.

Figure 9.2 Time response of exhaust piping, dilution tunnel, and SMPS to step changes in PM..... 171
concentration. Particle size measured: 25 nm. Time between step changes: several minutes (in order for conditions to reach steady state before any step change in input conditions). Vertical dashed line at time = 0 denotes beginning of transient response after the steady state period during time < 0.

Figure 9.3 Response of PM emissions to transient intake pressure. Particle size: (a) 50 nm, (b)..... 171
12.5 nm. Baseline conditions at the 40 kPa IMAP case, with a dilution ratio of 7:1. Baseline conditions except for intake pressure at the 70 kPa IMAP case, with a dilution ratio of 5:1. Air/fuel ratio remains within same bounds about stoichiometric as in Figure 3.1b, and thus is not plotted. Although the durations of the time steps differ between figures a and b (1 and 2 minutes, respectively), Chapter 3 has shown that the duration does not affect the particulate time response.

Figure 9.4 Response of PM emissions to transient equivalence ratio. Particle size: (a) 25 nm, (b)..... 172
50 nm. Baseline conditions except equivalence ratio. Dilution ratio = 7:1. Time between step changes: 2 minutes. Figure 9.4a shows no drift, and Figure 9.4b shows unrepeatable drift following first order response. Drift is within the 30% uncertainty bounds for all but the two second period circled in Figure 9.4b.

Figure 9.5 PM emissions during repeated start-up and shut-down experiments and schematic..... 172
representation of fuel/air equivalence ratio. Conditions: baseline engine operating conditions when the engine is firing; when it is being motored, speed and throttle position remain same as in firing conditions, but no fuel is injected and the spark is not ignited. Dilution ratio = 7:1. Time between ignition on and ignition off events: 2 minutes.

Figure 9.6 Schematics of (a) PM emissions as might be measured in the exhaust during start-up..... 173
and shut-down experiments (bursts of particles and baseline level shown as solid lines) and the measured PM emissions that result from the first-order time lag between exhaust and SMPS (dotted lines); (b) PM size distribution — plotted versus the log of particle size, D_p — shifting upward and to larger particle sizes: dotted curve is original size distribution, longer dashes is that size distribution scaled up in particle concentration, solid curve is the scaled size distribution moving along the size axis toward larger particles.

Figure 9.7 Response of PM emissions to transient intake manifold pressure. Particle size: (a)..... 173
12.5 nm, (b) 50 nm. Baseline conditions at the 40 kPa IMAP case, with a dilution ratio of 22:1. Baseline conditions except for intake pressure at the 70 kPa IMAP case, with a dilution ratio of 11:1. IMAP and equivalence ratio (ϕ) plotted. Time between step changes: 10 minutes.

Figure A2.1 (a) Chromatogram (page 1) of diluted exhaust PM. Dilution ratio = 15:1..... 187
Conditions: fully warmed operation, 2000 rpm, ½ throttle.

Figure A2.1 (b) Chromatogram (page 2) of diluted exhaust PM. Dilution ratio = 15:1..... 188
Conditions: fully warmed operation, 2000 rpm, ½ throttle.

Figure A3.1 Modeled PM emissions during Bag 1 of the FTP and experimental data for a..... 190
V8 blank-brick catalyst vehicle. PM emissions are plotted relative to the peak PM concentration. Plotted on the second ordinate axis is the trace of speed versus time for Bag 1 of the FTP, in order to show that peaks of PM emissions occur during acceleration periods.

Figure A4.1 Peak flame temperature as a function of fuel/air equivalence ratio as calculated for..... 192
Otto Cycle and for real cycle, the latter using the GM Engine-Simulation Program [51]. Inputs: baseline engine operating conditions except equivalence ratio, with engine geometry equal to that for Ford Zetec.

Figure A4.2 Peak cylinder pressure as a function of fuel/air equivalence ratio as calculated using..... 192
the GM Engine-Simulation Program [51]. Inputs: baseline engine operating conditions except equivalence ratio, with engine geometry equal to that for Ford Zetec. Isooctane fuel.

Figure A4.3 Measured exhaust temperature as a function of fuel/air equivalence ratio. Baseline..... 192
engine operating conditions except equivalence ratio, using Saturn engine. Data for propane (using Ford Zetec engine) not available.

Figure A4.4 Measured exhaust concentrations of CO, CO_2, and O_2 as a function of fuel/air..... 193
equivalence ratio. Baseline engine operating conditions except equivalence ratio. Symbols represent same things as in previous figure.

Figure A4.5 Measured exhaust concentrations of NO_x as a function of fuel/air equivalence ratio..... 193
Baseline engine operating conditions except equivalence ratio. Symbols represent same things as in previous figures.

Figure A4.6 Peak cylinder temperature and pressure as a function of IMAP as calculated using..... 193
the GM Engine-Simulation Program [51]. Inputs: baseline engine operating conditions except IMAP, with engine geometry equal to that for Ford Zetec. Isooctane fuel.

Figure A4.7 Peak cylinder temperature as a function of engine speed as calculated using the GM..... 193
Engine-Simulation Program [51]. Inputs: baseline engine operating conditions except speed, with engine geometry equal to that for Ford Zetec. Isooctane fuel.

Figure A4.8 Peak cylinder temperature and pressure, as well as Brake Mean Effective Pressure..... 194
Pressure (BMEP), as a function of engine spark timing as calculated using the GM Engine-Simulation Program [51]. Inputs: baseline engine operating conditions except speed, with engine geometry equal to that for Ford Zetec. Isooctane fuel.

Figure A4.9 Peak cylinder temperature, NO_x emissions, and Brake Mean Effective Pressure..... 194
(BMEP) as a function of EGR mass fraction as calculated using the GM Engine-Simulation Program [51]. Calculated EGR mass fraction corresponding to 100% of that needed to stall the engine (the metric used in the text) is 64%. Inputs to engine-simulation program: baseline engine operating conditions except residual gas fraction, with engine geometry equal to that for Ford Zetec. Isooctane fuel.

NOMENCLATURE

ACRONYMS —

ATC	After Top Center
BMEP	Brake Mean Effective Pressure
BTC	Before Top Center
CA	Crank Angle
CI	Compression Ignition
CNG	Compressed Natural Gas
CPC	Condensation Particle Counter
CVI	Closed Valve Injection
DOHC	Dual Overhead Cam
EEC IV	Stock controller for Ford Zetec engine
EGR	Exhaust Gas Recirculation
EVC	Exhaust Valve Closes
EVO	Exhaust Valve Opens
FID	Flame Ionization Detector
FFID	Fast-response Flame Ionization Detector
FTP	Federal Test Procedure
HC	Hydrocarbon
HEPA	High Efficiency Particulate Air (Filter)
HO2S	Heated O_2 Sensor
IMAP	Intake Manifold Absolute Pressure
IVC	Intake Valve Closes
IVO	Intake Valve Opens
lpm	Liters Per Minute
MBT	Maximum Brake Torque
MTBE	Methyl Tert-Butyl Ether
NDIR	Non-Dispersive Infrared
nm	Nanometer
OVI	Open Valve Injection
PAH	Polycyclic Aromatic Hydrocarbon
PFI	Port Fuel Injection
PI	Proportional/Integral (controller)
PM	Particulate Matter
rpm	Revolutions per minute
RVP	Reid Vapor Pressure
SI	Spark Ignition
SMPS	Scanning Mobility Particle Sizer
STP	Standard Temperature and Pressure
UEGO	Universal Exhaust Gas O_2 (Sensor)
USEPA	United States Environmental Protection Agency
VMT	Vehicle Miles Traveled

SYMBOLS —

A	Rate coefficient
B	Pre-exponential factor for the Damköhler Number
CO	Carbon Monoxide
CO_2	Carbon Dioxide
c_p	Specific heat of the gas
D	Diameter (either particle diameter, D_p, or droplet diameter, D_{dr})
Da	Damköhler number
d_∞	Diffusivity of fuel in the bulk gas
f	Fraction, as in fraction of HC emissions derived from liquid fuel droplets
F	Fuel

HC	Hydrocarbon
h_{fg}	Heat of vaporization
k	Arrhenius rate
m_f	Mass of fuel
M	Molecular weight
NO_x	Oxides of nitrogen
O_2	Oxygen
OVI	Open Valve Injection
p	pressure
P_i	Probability of ignition
ppmC1	Parts of carbon per million
PM	Particulate Matter
Q	Lower heating value of the fuel (heat release per unit mass of fuel consumed)
r	Rate of absorption or desorption
R^2	Correlation coefficient
Re	Reynolds' number
R_g	Universal gas constant
S_{ee}	Soot formed (modeled by the Edelman expression)
t	Time
T	Temperature
T_a	Activation temperature
x	Intensive property
X	Mole fraction
Y	Mass fraction
β	Constant of proportionality in adsorption or absorption mechanism
Θ	Fraction of sites occupied by adsorbed molecules for adsorption model, or equivalently the fraction of $[PM]_{sa}$ that is absorbed or adsorbed material for combined adsorption/absorption model, or equivalently fraction of adsorption/absorption "sites" occupied by adsorbed/absorbed molecules for combined adsorption/absorption model
Λ	Dilution ratio
Π	Final PM mass per unit original PM mass for growth and oxidation mechanisms
ρ	Density
τ	Time available for the occurrence of a mechanism or time constant
ϕ	Fuel/air equivalence ratio
Ψ_{dr}	Nondimensional droplet vaporization rate
ψ	Mass of adsorbate or absorbate per unit area
ω	Surface mass recession rate due to oxidation

SUBSCRIPTS —

a	activation
ab	combined absorption/adsorption mechanism
ad	adsorption mechanism
bc	baseline conditions
c	carbon dioxide
cd	combustion duration
con	condensation mechanism
d	diluted exhaust
da	diluent air
de	desorption
dr	droplet: either a characteristic of droplets or droplet nucleation mechanism
e	exhaust (undiluted)
ee	Edelman expression
ev	evaporation
ex	experiment

f	fuel
fe	falling edge (referring to time constant)
fg	fluid to gas (subscript used in heat of vaporization)
fin	final
g	gas constant
gp	gas phase nucleation mechanism
HC	hydrocarbon
i	ignition
in	intake
l	liquid
lf	liquid fuel
m	mass-weighted
mo	model
n	nucleation mechanisms
o	original
OVI	Open Valve Injection
ox	oxidation mechanism or oxidizer
p	particle
pf	peak flame
re	rising edge (referring to time constant)
rel	relative or normalized (referring to PM concentrations)
sa	surface area-weighted
sp	soot precursors
sr	surface recession
v	volume-weighted
w	water
∞	surroundings or bulk gas

SUPERSCRIPTS —

a, b, c	Exponents used in Edelman expression
d, e	Exponents used in liquid fuel nucleation mechanism
f, g	Exponents used in oxidation mechanism

CHAPTER 1

INTRODUCTION

1.1 Background

Recent studies suggest that atmospheric particulate matter (PM) is an important factor associated with mortality and morbidity in urban areas, contributing to the order of 10,000 deaths per year in the United States alone [1, 2]. The health problems associated with inhaled PM are cancer, mutations, cardiopulmonary ailments, lung damage, and exacerbation of pre-existing health problems especially among children and the elderly [2, 3]. In addition, due to the fact that airborne particles are approximately the same size as the wavelengths of sunlight, these particles have been found to obstruct visibility by up to 70% relative to natural levels [3]. Furthermore, particle deposition causes soiling and damage to clothing and structures [4]. Due mainly to adverse health effects from atmospheric PM, the United States Environmental Protection Agency (USEPA) recently enacted stricter National Ambient Air Quality Standards limiting permissible concentrations of fine particles (meaning PM less than 2.5 microns in diameter) in the atmosphere [5].

A substantial fraction of the total PM is contributed by internal combustion engines; in particular, they contribute more than 21% of the fine particulate organic carbon emitted to the Los Angeles basin [6]. Although diesels emit significantly higher concentrations of PM than Spark-Ignition (SI) engines, the number of total vehicle-miles traveled (VMT) by gasoline-powered vehicles greatly exceeds that of diesels. Hence, the estimated contribution of gasoline engines to the integrated urban vehicle-related PM can be from 0.4% to 68% of the total, as detailed in Table 1.1. This table covers all particles emitted by gasoline and diesel engines, which are predominantly between 10 and 500 nm [7, 8, 9]; however, during their residence time in the atmosphere, the particles may undergo significant growth and chemical reaction such that inhaled particles may vary significantly from emitted ones. Because many cities are in the process of switching their fleets to natural gas or electric powered buses, PM emission from buses — whose mileage constitutes from 0.7 to 3.8% of total urban diesel-vehicle miles traveled [10] — will further decline in significance, hence buses are omitted from Table 1.1. Moreover, since the mean size of diesel particles is

larger than SI particles (80 nm versus 50 nm), gasoline engines may contribute from 1.6% to 90% of the total urban PM on a number-weighted basis [11].

Since engines emit primarily fine particles (below 2.5 microns, as opposed to the coarse ones previously regulated), the USEPA's new air quality standards restricting fine PM will likely result in stricter limits on the levels of PM emissions permissible to automobiles in the near future. Therefore, it has become increasingly important to understand how PM is formed in SI engines, and how it might be mitigated. Moreover, it is important to understand not only the number- or mass-weighted emissions, but also the size distribution characteristics insofar as they influence respirability.

Table 1.1 Estimates of total particulate emissions by vehicle class and driving location (estimates of 1993 vehicle fleet)[a]

	Gasoline powered vehicles (cars, motorcycles, and light-duty gasoline powered trucks)	Diesel powered vehicles (light-duty and heavy-duty diesel powered vehicles)[b]
PM emissions (mg/mile)	5 to 40	400 to 3500
Total annual urban vehicle travel within the U.S. (10^9 miles)	960 to 1200[c]	60 to 320[c]
Total annual urban PM emissions (10^6 kg)	4.8 to 49	23 to 1100
Total annual rural vehicle travel within the U.S. (10^9 miles)	580 to 790[c]	90 to 300[c]
Total annual rural PM emissions (10^6 kg)	2.9 to 32	37 to 1100
Total annual PM emissions, both urban and rural (10^6 kg)	7.7 to 81	60 to 2200

[a] Sources: [10, 12, 13, 14]

[b] Since many cities are switching to electric or natural gas powered buses, mileage for buses is omitted from this category. Vehicle miles traveled by buses constitute from 0.7 to 3.8% of total urban diesel-vehicle miles traveled [10].

[c] Broad range of estimates reflects variety of engine types classified jointly as "light-duty trucks" by Motor Vehicle Manufacturers Association [10].

1.2 Dilution Issues

While the effects of the dilution process and related particle dynamics have been analyzed in detail for diesel exhaust (e.g.: [15, 16, 17, 18]), they have not been studied as thoroughly in the context of gasoline engine exhaust. The fact that particle and vapor characteristics may differ between the two engine types warrants study of particle dynamics during dilution in the context of SI engines.

Particles emitted by engines undergo a number of processes — such as coagulation, deposition, and growth via condensation, adsorption, or absorption of vapors — when they are diluted by the atmosphere [15]. Coagulation is the process in which two particles collide and stick together, forming one

larger particle. Deposition or loss is when particles are removed from the air, for example when sticking to available surface area. Condensation occurs when temperatures decrease such that the saturation vapor pressure is reached, causing vapors to condense on available surfaces such as particles. Adsorption involves the adherence of vapors on surfaces due to chemical or physical forces. Absorption is the process in which adsorbate on particles traps vapor [16]. The combined particle dynamics — coagulation and losses of particles, plus condensation, adsorption, and absorption of vapors — depend upon prevailing exhaust and dilution conditions such as particle concentration, vapor concentration, and temperature. For example, condensation, adsorption, and absorption of vapors on PM are strongly affected by the temperature of the diluted exhaust and by the particle and vapor concentrations, all of which decrease dramatically as the exhaust becomes more dilute [15]. Insofar as the objective of research into PM emissions is to examine the effect of those emissions on the atmosphere, it is important to understand and whenever possible duplicate the atmospheric dilution process that so strongly affects atmospheric particulate concentrations.

Since the dilution process strongly affects particle concentrations and size distributions, discrepancies between dilution processes used in different experiments could result in significantly different measurements of particle concentrations and size distributions. Consequently, in order to allow for comparisons between PM measurements made using different techniques, the USEPA mandates a maximum post-dilution temperature of 52°C (125°F) in all such PM measurements. This constrains the minimum dilution ratio that can be used when measuring the particle concentrations within engine exhaust, for a given exhaust gas temperature. However, other dilution parameters — such as the flowrates of exhaust and diluent through the dilution tunnel, tunnel diameter, and the residence time within the tunnel — are not constrained by regulations. In order to expedite the design and optimization of dilution systems for automotive PM collection, a systematic study was undertaken to determine how dilution parameters affect the measured particulate emissions. The results discussed in this thesis serve as a guide to selecting dilution tunnel parameters such as dilution ratio and flowrates, in order to be within the permissible temperature range, minimize losses, and optimize repeatability. A further objective of the present work is to discuss the effects of different dilution parameters on measured particle characteristics in order to facilitate comparison between data collected with dissimilar dilution systems.

1.3 Effect of Steady State Engine Parameters

The results of previous investigations of PM formation will be examined in order to elucidate some of the possible mechanisms by which SI engines form PM. Correlations between HC and PM emissions observed in previous research [12, 19, 20] as well as the necessity of HC for PM formation suggest that the mechanisms of HC and PM emission may be similar. Just as rich and extremely lean air/fuel ratios have been observed to cause high HC emissions [21, 22, 23], so have they been found to cause high PM emissions [20, 24, 25, 26]. Moreover, cold engines temperatures and cold intake air have been found to produce more PM than warm ones during transient driving schedules [12, 20, 27], presumably because of the same reason that they emit more HCs [28]: they inhibit liquid fuel vaporization, thus increasing the amount of liquid fuel in the combustion chamber, which cannot burn completely before being emitted to the exhaust [29, 30]. However, the correlation between HC and PM emissions is not perfect; for example, Quader (using a Bosch Smoke Meter) found that increased engine load increases smoke emissions but decreases HC emissions [20].

Even if there were a correlation between HC and PM emissions, it would not necessarily imply similarity of causation. For instance, HC emissions arise from such sources as leaky exhaust valves and crevices inside of which HCs escape the chemical oxidation reaction. However, PM is formed by chemical reaction; therefore, these mechanisms may not contribute directly to PM formation. Rather, HC and PM emissions need to be examined over a broad range of engine and fuel conditions in order to establish under whether they are correlated and, if so, why: specifically, what are the origins of PM in SI engines?

By contrast to HC emissions, no work has been done to investigate whether there exists a correlation between PM and NO_x emissions as engine operating parameters are varied. Williams *et al.* performed tests on a fleet of vehicles operating specified driving schedules, and found no correlation between PM and NO_x emissions [12]. Because all of Williams' *et al.* vehicles were operated over a similar if not identical series of engine operating conditions (specifically, the vehicles were operated over identical driving cycles), rather than varying engine operating conditions for a fixed vehicle, these data do not rule out the existence of a relationship between the two emission rates as engine operating conditions are varied, as exists in diesels. Since Williams' *et al.* data does not conclusive rule out a relation between PM and NO_x emissions, effort must be directed toward understanding how PM and NO_x emission rates vary as a function

of single engine parameters or control strategies in order to learn how they might be simultaneously mitigated.

Previous researchers have found fuel structure to profoundly impact PM emissions, much like it does HC emissions. The present paper addresses this research and extends the measurements. Quader, for example, used a Bosch Smoke Meter to analyze smoke emissions from a test engine operated at steady state on toluene, indolene, and isopentane, and found that toluene led to the highest smoke and HC emissions, indolene lower smoke and HC emissions, and isopentane still lower HC emissions but dramatically lower smoke emissions [20]. Since toluene has the highest aromatic content but also the lowest Reid Vapor Pressure (RVP, or equivalent measure of volatility), both of which can cause high HC emissions [31] and may (depending if the mechanisms of HC and PM emissions are similar) cause high PM emissions, Quader's data do not isolate the mechanism for increased PM emissions [20]. Pedersen *et al.* used an isokinetic sampler, cyclone batteries, and filter collection for particles plus filtered freeze traps for Polycyclic Aromatic Hydrocarbons (PAHs, a source of PM) during steady state engine tests; they found that PAH emissions increase and that particle-bound PAHs increase almost linearly with fuel aromatic content [24]. Nonetheless, they found that PM emissions on the whole do not vary significantly with aromaticity [24]. (Although Pedersen *et al.* held the octane number fixed between different fuels, it is not clear whether the RVP remained fixed as well.) Conversely, when operating an engine on the Federal Test Procedure (FTP) and using filter analysis according to the technique specified in the Federal Register, Westerholm *et al.* did not measure a linear or even a monotonic increase in either PM or particle-bound PAHs with increased fuel aromatic content [32]. But they did measure a monotonic increase in PM with increased fuel PAH content; plus, their data shows that that increasing particulate emissions correlates with increasing PAH emission in both gas and particle-bound phases [32]. Fanick *et al.*, using a cascade impactor for engine tests during an FTP cycle, found that gaseous fuels such as liquefied petroleum gas and compressed natural gas (CNG) have lower PM emissions than does gasoline [25]. However, when using a mobility analyzer, Greenwood *et al.* found that CNG vehicles may emit more PM than gasoline vehicles at certain steady state engine operating conditions, but less at other conditions [8].

In order to understand how fuel chemistry, volatility, and air/fuel ratio individually affect PM formation, the present experiments investigate PM emissions using a variety of fuel types — indolene,

isooctane, propane, toluene, and indolene doped with Methyl Tert-Butyl Ether (MTBE) — and air/fuel ratios. The present paper examines the effect of vaporization by comparison of PM emissions using warm and cold intake ports, and it examines the effect of boiling point or molecular weight among chemical classes by comparison between emissions of isooctane and propane. It also examines the effect of chemical composition with only minor effect from boiling point by comparison between emissions of toluene and isooctane (which have boiling points of 111 and 99°C, respectively) [33]. Furthermore, the present paper examines not only number- or mass-weighted emissions (as did many of the investigations reviewed above), but both measures as well as particle size distribution characteristics, and uses a model of PM formation to show how fuel vaporization parameters (such as heat of vaporization and intake port temperature) and chemical composition affect PM formation.

Although a significant fraction of the PM generated in SI engine combustion comes from the fuel itself, oil generated particles have been found to contribute as much as 15% by mass of the total PM emitted during an FTP cycle, when using leaded fuel [12]. Considering that current unleaded fuels generate significantly less PM than do leaded fuels, the fractional contribution of oil consumption to the PM emission may be significantly higher than 15%. Hildemann *et al.* analyzed the chemical composition of PM generated by both catalyst-equipped and non-catalyst-equipped automobiles operating on the FTP cycle (trapping particles on filters via cyclone separators) and found that organic carbon comprised 38 to 75% of the particulate mass [34]; this shows that either atomized/evaporated oil or unburned fuel adheres to PM nucleated in the combustion process, though it does not prove whether oil or fuel is the more significant source of PM mass. Pedersen *et al.* varied lubricant temperature — thus varying parameters involved in oil consumption such as volatility and viscosity — in tests at steady state engine operating condition and found that the oil temperature did not significantly affect PAH emissions [24]. And since organic carbon, such as that in PAHs, is a significant source of PM, Pedersen *et al.*'s results suggest that oil consumption may have a small effect on PM emissions. However, Pedersen *et al.* found that oil composition can affect PM emission rate during steady state engine operation; specifically, synthetic lubricant increased the oil consumption rate relative to their conventional commercial SAE 15w-50 oil by a factor of ten, which caused the particle mass emission rate to increase by a factor of 2.5 to 3 [24]. Plus, when the oil was doped with a PAH, they found that exhaust PAH emissions increased [24], which gives further evidence for a possible

link between oil breakdown and PM formation. In the present work, the contribution of oil to exhaust PM is isolated and evaluated. Additional measurements are made of exhaust PM using both synthetic and conventional mineral oils. Since tests on a diesel engine at steady conditions showed a inverse correlation between oil viscosity and PM emissions [35], the effect of viscosity on PM emissions is also explored in the present work.

Given the efficiency of the catalyst at oxidizing HCs, and given that HC vapors condense and adsorb on particles to form a significant fraction of the total post-dilution PM mass [34], it may be suspected that the catalyst would reduce the post-dilution PM mass. To date, only limited tests have been performed to find the effect of the catalytic converter on particulate matter, and most of those tests involve a comparison of different vehicles — catalyst equipped versus non-catalyst equipped — convoluting the effect of a catalyst on PM with the effects of different engines and control technologies. For instance, Rickeard *et al.* and Hildemann *et al.* performed tests to compare the emissions from catalyst-equipped and non-catalyst-equipped vehicles, either during steady state operating conditions using a Scanning Mobility Particle Sizer (SMPS) and cascade impaction or during a FTP using cyclone separators and filter collection, respectively [7, 34]. Although the non-catalyst cars generally have higher PM emission rates (a malfunctioning catalyst-equipped vehicle being the largest exception), difficulties arise in comparing the data between the two classes of automobiles because the non-catalyst cars are either older or have different fuel metering technologies than the catalyst-equipped cars. However, Rickeard *et al.* found that when they operated at a steady, high road-load power — equivalent to 120 km/h — the catalyst-equipped car had approximately the same number-weighted PM emission rate as did the non-catalyst car, and that the particles had roughly the same mean size [7]. Consequently, the particulate mass emission rate from the two vehicles at this operating condition is roughly the same. The fact that the emission rates from the two cars can, in certain cases, be approximately equal indicates that the efficiency of the catalyst at removing particulate matter may depend on engine operating conditions and *may* drop to zero at some conditions. Conversely, this evidence may indicate nothing more than the overwhelming effect of fuel metering and control strategies on PM emissions. The present work examines the effect of the catalyst on PM number and mass emissions as well as PM size from one fixed engine with fixed fuel/engine controls, in order to evaluate whether and how the catalyst effects PM emission rates.

Researchers have used mobility analyzers such as the SMPS (defined above) to measure the size distributions and size characteristics of exhaust particles. For example, Greenwood *et al.* measured the number density of particles emitted by SI engines under a variety of steady state road-load powers and found that for all three vehicles tested at all load conditions, the mean and mode particle sizes are on the order of 50 nm [8]. Further, they found that only one of the vehicles emitted what they call a "significant particulate density" above 300 nm. Rickeard *et al.*, operating catalyst-equipped and non-catalyst-equipped gasoline vehicles at three steady state road-load powers, confirmed that mean particle sizes are from 50 to 100 nm, and that the largest number of particles have an electrical mobility diameter between 50 and 200 nm [7]. Since mass is proportional to the third power of diameter, mass-weighted percentage is more biased toward large particles than is number-weighted percentage, the result being that supermicron sized particles may comprise as much as 10 to 30% of the total particulate mass though much less than 1% of the particulate number [7, 12]. The present work investigates the size distribution of particles in order to understand whether engine operating parameters affect particle sizes; in particular, the contribution of HCs to PM growth mechanisms, as evidenced by particle size characteristics, is evaluated.

1.4 Effect of Transient Engine Operation

PM emissions during transient operation may greatly exceed that during steady state. For instance, SI automobiles operating the FTP (defined above) have the highest rates of PM emissions during acceleration transients — particularly during the rapid acceleration during the cold phase of the test (Bag 1), and to a lesser extent during the warm phase (Bag 3) — as measured in [36] and as inferred in [12]. Nonetheless, the measurements of time-resolved transient PM emissions cited above do not isolate the mechanism by which the particles are formed: the tests involve simultaneous variations in engine temperatures, air/fuel ratios, dilution ratios, engine speeds, and loads, thus convoluting the individual effects of each parameter. In addition, complexities of the engine control systems in the vehicles tested may contribute to or reduce the PM emissions in a non-trivial fashion; for example, open loop engine control (before the oxygen sensor is warm enough to operate properly) could cause overshoots or undershoots in the air/fuel ratio with respect to stoichiometric, which would then lead to high PM emissions, as will be discussed in an upcoming chapter. Moreover, some closed loop engine control strategies involve

enrichment at high load conditions, which would also lead to high PM emissions, particularly during periods of vehicle acceleration.

Consequently, several questions are left unanswered by prior studies of transient PM emissions. Specifically, why are PM emissions high during transients: because of high load, or deviations in air/fuel ratio from stoichiometric, or fuel injection timing that does not allow sufficient fuel evaporation in the intake port? Or are PM emissions high because of a combination of these PM sources? In order to answer these questions without confounding the study of transient engine operation by allowing multiple parameters to vary at any one time, a series of tests were performed, each of which isolated the effects of individual transient parameters on PM emissions.

The objective of these tests is to measure PM emissions during repeated changes of each operating parameter that can vary during a transient driving schedule such as the FTP. The engine operating conditions that vary during the FTP are engine load and speed; as a result of these conditions, the temperature of the engine warms up from its initial cooled state, spark timing varies (in response to load and speed demands, as well as temperature conditions, i.e., becoming retarded for faster warm-up), and the air/fuel ratio may vary (particularly, during throttle transients and/or before the oxygen sensor is significantly warm). Consequently, the present tests examine controlled transients in engine load and air/fuel ratio; repeatable tests of transient engine speed were not possible with the present dynamometer setup. Experiments were not performed in which engine temperature was the controlled variable for two reasons. Firstly, to achieve a repeated engine temperature transient, the engine must be allowed to cool overnight, which would result in uncertainty due to day-to-day variations in PM emissions; as will be discussed in an upcoming section, these day-to-day variations may be as large or larger than the deviations in PM emissions that result from temperature variations. Secondly, the time scale over which it is possible to achieve repeatable engine temperature transients is approximately the same as that over which measurement drift can occur. Therefore, transient temperature effects cannot be reasonably separated from day-to-day variations and/or gradual drifts in PM emissions. Moreover, experiments were not performed in which spark timing was the controlled variable because spark timing during warmed-up operation is a function of load and speed, rather than an independently specified variable. For the present experiments,

spark timing is held fixed with respect to maximum brake torque timing, as is the case for real-world, warmed-up engine operation.

Along another line, the first two minutes of the 41 minute-long FTP contribute as much as 60 to 80% of the total HC emissions, due in particular to cold engine and catalyst operation as well as fuel rich conditions [37, 38]. Insofar as these same conditions lead to high PM emissions in steady state operation (as will be discussed in an upcoming section), the present project investigates how the PM emission rate responds to start-up conditions, in particular, looking at the first two minutes after a repeated start-up. The start-up tests are performed at fully warmed-up conditions in order to be sufficiently repeatable and to isolate the effect of transient ignition and fuel injection conditions on PM emissions, rather than convoluting the effect of those conditions with that of varying engine temperatures. The effect of engine temperature on engine-out PM emissions during transients is inferred from the present experiments and the model of PM formation (Chapter 7), as is discussed in an upcoming section.

1.5 Objectives

The present project is divided into four parts: examination of the dilution process, experimental examination of the effect of steady state engine/fuel/oil/catalyst parameters on PM emissions, modeling of PM emissions, and examination of transient engine operation on PM emissions.

Specific objectives of the dilution examination are as follows: to quantify uncertainties in measured particle concentrations and sizes, to verify the repeatability of measurements made via a dilution tunnel system such as the one described in the present work, to discuss the optimal choices for the variety of parameters in dilution tunnel design, and to examine the effect of dilution ratio and individual flowrates on the measured particle concentrations and sizes. Of particular interest is finding an 'optimal' dilution ratio, defined as a dilution ratio that satisfies the USEPA temperature mandate and at which PM number and volume concentrations are the most repeatable, i.e., the least sensitive to slight deviations in dilution ratio.

The objectives of the examination into the effect of steady state engine/fuel/oil/catalyst conditions on PM emissions are to expand previous research, which has focused largely on single characteristics of particles — either number emissions, mass emissions, or size distribution characteristics — in a limited set of steady state operating conditions, or has examined the integrated result of some of these characteristics

over a transient driving schedule, but has not systematically investigated the effect of a variety of steady state conditions on all three characteristics. Specifically, objectives of the second phase of the present work are to examine the effect of engine operating parameters (air/fuel ratio, speed, load, spark timing, Exhaust Gas Recirculation or EGR, and operating temperature), fuel parameters (fuel chemistry, injection timing, and control strategy), lubricating oil parameters (composition and viscosity), and catalytic converter parameters on PM number and mass emissions, as well as characteristic particle sizes. Further objectives are to compare characteristics of PM emissions — concentrations and particle sizes — with concentrations of gaseous chemical species and a variety of engine parameters in order to establish whether PM emissions correlate with any parameter and if so, why. Objectives of the third phase of the project are to formulate a model of PM emissions and to compare it to experimentally measured PM concentrations in order to understand which are the important mechanisms in the PM emission process.

Objectives of the final phase of the study — the examination of PM emissions during transient engine operation — after evaluating the time-response capability of the various components of the experimental apparatus, are to examine how engine-out PM emissions respond to transient engine conditions. In particular, objectives are to find the time-scale over which the response occurs and the analytical form to which the response might be fit, and then to explain why. A further objective, with implications on the modeling of PM emissions, is to determine whether (a) transient PM emission rates can be described as a quasi-steady variation between initial and final emission rates, for which the instantaneous rate at any given time is merely a function of the instantaneous engine conditions, or whether (b) a more complicated response occurs due to transient effects in the engine, for which the history of engine operating conditions affects PM emissions. Moreover, the objectives are to examine the PM emissions during repeatable engine start-up and shut-down events, in order to determine if PM emissions are high during these events, and if possible, determine why.

CHAPTER 2

EXPERIMENTAL APPARATUS AND PROCEDURE

2.1 Apparatus and Procedure for Dilution and Steady State Engine Experiments

The experimental setup is shown in Figure 2.1. Engine exhaust flows through a muffler and is introduced into the centerline of the dilution tunnel, where it is mixed with filtered air. Diluent air for the dilution tunnel is drawn through a carbon filter to remove organics and a High Efficiency Particulate Air (HEPA) filter, with a measured particle trapping efficiency of 99.8% by mass. The dilution tunnel has an inner diameter of 15 cm, and consists entirely of stainless steel and Teflon, since other materials may retain and release organic vapors [39].

A constriction in the dilution tunnel, approximately 0.1 meters downstream from the location where the exhaust is introduced, enhances turbulence and therefore increases the extent of mixing between dilution air and exhaust. At the monitoring port, 2.8 meters downstream from exhaust inlet, samples are drawn from the diluted exhaust for particle measurement via a Scanning Mobility Particle Sizer (SMPS), the operation of which will be discussed shortly. Relative humidity is monitored at this location, in order to insure that water does not condense on the particles or on the walls of the tunnel. However, no condensation has been found to occur at the monitoring port, since the relative humidity of the diluted exhaust is quite low (about 40%, as measured by a Cole Parmer Model 37950-00 Thermohygrometer). At various locations along the flow path, thermocouples are used to measure the gas temperature. Eight by ten inch (20 cm by 25 cm) preconditioned glass-fiber or Teflon filters were collected at a temperature of 30°C ± 5°C, in two locations, each 0.8 meters downstream of the SMPS sampling location, and weighed on an Ohaus Explorer scale accurate to 10^{-4}g. Pressure measurements across both filters were used to calculate the relative flowrate through each, although the flowrates never differed by more than 2%. Filter analysis of PM concentrations proved inaccurate (as will be discussed), so only SMPS data is presented in this work.

Engine-out exhaust (no catalytic converter) is supplied by either a Ford Zetec or a Saturn DOHC four-cylinder spark-ignition engine, the specifications of which are listed in Table 2.1. Both engines drive

dynamometers and operate on Port Fuel Injected (PFI) indolene unless specified. Unless specified, exhaust is taken directly from the engines (no catalytic converter), in order to isolate PM formation processes in the engine, rather than in the combined engine/after-treatment system. The fuel injection of the Ford Zetec engine can be controlled by either the stock engine controller or by a manual computerized Proportional/Integral (PI) controller, the latter of which proved to maintain the air/fuel ratio within a more narrow range than the former. Spark timing for the Ford engine can be controlled by a manual controller and is MBT unless specified. A manufacturer-supplied computer that overrides the set points in the stock engine controller controls the fuel injection and spark timing for the Saturn engine. Again, spark timing is MBT unless specified. In a limited set of experiments regarding the effect of dilution on PM, exhaust is supplied by a Kubota EA300 single-cylinder, 309-cc, 2-valve diesel engine operated at idle using a low sulfur fuel.

Table 2.1 Engine specifications [a]

Engine	Ford Zetec	Saturn DOHC
Number of cylinders	4	4
Number of valves per cylinder	4	4
Bore x stroke (mm)	85 x 88	82 x 90
Displacement (liters)	2.0	1.9
Compression ratio	9.6	9.5
Combustion chamber design	Pent roof	Pent roof
Fuel system	PFI	PFI
Intake valve opens (IVO)	10°CA BTC	16°CA BTC
Intake valve closes (IVC)	230°CA ATC	232°CA ATC
Exhaust valve opens (EVO)	488°CA ATC	494°CA ATC
Exhaust valve closes (EVC)	8°CA ATC	14°CA ATC

[a] crank angles (CA) are referenced to intake top center: before (BTC) or after (ATC).

The SMPS, which is a differential mobility analyzer produced by TSI Incorporated, operates as follows. A vacuum pump draws a particle-laden stream from the monitoring port of the dilution tunnel through an impactor, which separates large particles (in the configuration used here, particles bigger than 418 nm), and into an Electrostatic Classifier. In the classifier, the particles pass through a Kr-85 Bipolar Charger where they are given an electrostatic charge. The flow is then sent through an annulus, in the center of which sits an electrostatically charged tube with a small slit at the end. Particles with a positive charge are drawn toward this tube through a concentric flow of highly filtered air, called the sheath air. Particles with too little aerodynamic drag (too small a diameter) are drawn toward the charged tube so

quickly that they impact the walls before reaching the hole, and are held fixed by electrostatic attraction. Particles with too high a drag (large diameter) are not drawn in sufficiently far toward the tube to enter the slit. Hence, only a certain size range of particles passes through the slit and into the Condensation Particle Counter (CPC), which condenses an alcohol vapor on the particles, thereby increasing their size so they are large enough to be counted optically [40]. The SMPS is capable of measuring concentrations from 1 to 10^7 particles per cubic centimeter within a given size range [40]. The flowrates used — in this work, 0.7 liters per minute (lpm) of particle-laden gas and 7 lpm of sheath air — determine the measurable size range; in this case, the flows were chosen to cover the range 9 to 378 nm. Measurements of the smallest particles (electrical mobility diameter ≈ 10 to 20 nm) are subject to the largest uncertainties because (a) potential losses in the SMPS transfer tubes increase as particle size decreases and (b) deviations in the charge on the electrostatically charged tube correspond to a larger fraction of the total charge when small particles are being measured. The SMPS measurement range (9 to 378 nm) was optimized for diluted engine exhaust number-weighted particle concentrations; according to measurements Rickeard *et al.* made of particle concentrations using two types of particle analyzers, less than 1% of the particles on a number-weighted basis should fall above the SMPS measurement range [7]. Because mass-weighted particle concentrations are biased toward large particles, the finite SMPS measurement range may impose an uncertainty in the measurement of mass concentrations insofar as a portion of the tail of the mass-weighted size distribution may be cut off. Uncertainties in the SMPS measurements will be quantified in the Uncertainty Analysis section of this paper.

The SMPS software corrects for the flowrate, multiply charged particles, and negatively charged particles (which are propelled away from the tube and thus never measured). The final outputs are the particle size distribution, as well as integrated results: concentrations, mean particle sizes, and mode particle sizes, all of which are given on number, surface area, and volume-weighted bases [40]. The volume-weighted concentration (or volume fraction) is directly related to the mass concentration by the particulate density. Most researchers assume a density of 1,000 kg/m^3 [9, 41, 42] to 2,000 kg/m^3 [43, 44, 45, 46] to the 2,260 kg/m^3 density of solid carbon [47]; an assumed density of 2,000 kg/m^3 — the median and the average of the above values (using the available 1 digit accuracy) — is used in the calculation of all

mass concentrations in the present work. A density of 1,000 kg/m^3, which is closer to the density of the organic carbon vapor that may make up 38 to 75% of the particle mass [34], could just as well have been assumed, in which case all PM mass concentrations would be one-half the presently quoted values. Volume-weighted sizes are equivalent to mass-weighted sizes for uniform density particles. Quoted particles sizes are the electrical mobility diameter, which is the size of a sphere that would have the same amount of drag as the particle when being drawn through air by an electric charge.

The baseline engine operating conditions used in the present experiments are listed in Table 2.2. These conditions represent a mid-speed, mid-load condition typical of on-road driving. In these conditions, exhaust flowrate is approximately 600 lpm. Several flowrates of diluted exhaust were used; this paper will present results using the flowrate of 950 lpm (Re = 9000), a higher one of 6400 lpm (Re = 57000), and a medium one — the average of those two. The diluted exhaust flowrate can be adjusted by changing the diameter of the critical orifice; since flow through the orifice is choked, the flowrate is proportional to the cross-sectional area of the orifice. For the rate of exhaust flow in the baseline operating conditions, the minimum achievable dilution ratio is approximately 10:1 in the high flowrate case and 1.5:1 in the low flowrate case. Motivation for the choice of dilution tunnel flowrates is a compromise between allowing dilution ratios comparable to those researchers have used in the past while achieving acceptable signal to noise ratios. The upper limit on dilution tunnel flowrate is that which would allow dilution ratios as low as those used in the past: between 10 and 20:1 [8, 24, 32]. On the other hand, the lower bound on flowrate is determined by particle deposition in the pipes/valves between the exhaust and the dilution tunnel. As flowrate decreases while dilution ratio remains fixed, exhaust flow must be throttled using small piping and/or small openings in valves between the exhaust pipes and the dilution tunnel: 950 lpm allows acceptable measurement signal to noise ratios at the dilution ratios used in the present experiments.

Samples are drawn isokinetically from the monitoring region of the dilution tunnel, in cases where the flowrate of diluted exhaust was 950 lpm (Re=9000). In all other cases, sampling is nonisokinetic. However, since the particles within the diluted exhaust have electrical mobility diameters on the order of 100 nm, they are expected to follow the gas flowstreams quite well [48]; hence, isokinetic sampling is not thought to be necessary.

Table 2.2 Baseline engine operating conditions

Parameter	Value
Engine speed	2000 (± 10) rpm
IMAP [a]	0.4 (± 0.04) bar, absolute
ϕ [b]	1.00 (± 0.02)
Fuel injection timing	CVI [c]
Fuel injection control strategy	PI control using UEGO sensor for Ford engine; manual override of setpoints for stock controller for Saturn engine, monitored by heated oxygen sensor [d]
Spark timing	MBT (± 3°CA) [e]
Coolant and oil temperatures	87 (± 2) °C
EGR [f]	None
Fuel type	Indolene [g]
Lubricating oil type	Conventional 30 weight mineral oil
Catalyst	None (measurements are engine-out emissions)
Exhaust dilution ratio	15 (± 2) : 1

[a] IMAP = Intake manifold air pressure, [b] ϕ = fuel-to-air equivalence ratio, [c] CVI = Closed Valve Injection, as opposed to Open Valve Injection (OVI), [d] PI = Proportional/Integral control, UEGO sensor = Universal Exhaust Gas O_2 Sensor, [e] MBT = spark timing for Maximum Brake Torque, °CA = crank angle degrees, [f] EGR = Exhaust Gas Recirculation, [g] indolene = a research gasoline with low sulfur content.

Concentrations of gas phase HCs, NO_x, CO, CO_2, and O_2 in the exhaust are measured in order to investigate correlations between the various emission rates. HCs are measured with a Rosemount Analytical Model 402 Hydrocarbon Analyzer, which is a Flame Ionization Detector (FID) with a heated inlet line. Water is not purged from exhaust before entering the FID, so the measurements represent "wet" HC concentrations. CO_2 concentrations are measured with a Rosemount Analytical Model 880A NDIR Analyzer. CO concentrations are measured with a Beckman Model 864 Infrared (NDIR) Analyzer. NO_x concentrations are measured with a Thermo Environmental Instruments Model 10 Chemiluminescence Analyzer. O_2 concentrations are measured with a Beckman Model OM-11 EA Meter. Prior to measurement of CO, CO_2, NO_x, and O_2, the exhaust is desiccated, so the measurements represent "dry" concentrations.

2.2 Apparatus and Procedure for Transient Experiments

The experimental setup used in the analysis of transient PM emissions is the same as shown in Figure 2.1; however, the engine and diagnostics are operated in a different manner, as will be discussed presently. For the transient experiments, only the Saturn engine is used, and rather than maintaining one steady state operating condition, the engine is cycled repeatedly between two operating conditions, for example, cycling between 0.4 bar IMAP and 0.7 bar IMAP at one minute intervals. (Operating procedure

will be described shortly.) Only one engine operating condition is varied from the baseline conditions at a time, so if IMAP is being varied, all other engine operating conditions are maintained at the values specified in Table 2.2.

Repeated tests of transient operating conditions are performed by supplying a "square wave" input to the engine controller, be it a square wave in IMAP, ϕ, or fuel/ignition supply. Simultaneous to a change in IMAP, the engine controller changes the spark timing to maintain MBT timing to within $\pm$ 3° crank angle. Engine data is monitored throughout transient operation, simultaneously to measurement of particulate concentrations (transient SMPS particle measurements will be described shortly). Engine speed and brake torque are measured by the dynamometer although the engine speed is fixed at 2000 $\pm$ 60 rpm for all experiments. Air/fuel ratio is measured using a NTK Air/Fuel Ratio Meter, which is a heated universal exhaust gas oxygen sensor. Intake manifold pressure is measured with a pressure transducer mounted in the intake plenum. All signals, as well as SMPS output, are recorded at one second intervals by a dedicated data acquisition computer. An attempt was made to incorporate Fast-response Flame Ionization Detector (FFID) measurements of exhaust HC concentrations into the experiments insofar as PM and HC emissions are related in certain cases (as will be discussed in Chapter 6). However, the FFID had a poor signal to noise ratio, so simultaneous FFID measurements are not addressed in the present work.

A second computer controls intake pressure, and a third controls all other engine parameters. The computers are used to produce step inputs in individual operating parameters at repeated time intervals; time intervals are on the order of one minute, chosen separately for each test in order to minimize the amount of data storage while not cutting off a transient response in progress. The choice of time intervals was found to have no statistically significant effect on measured data, as will be discussed in the Uncertainty Analysis; durations of time steps are designated in the following figures. The time scale over which input step changes occur is on the order of 1 second; the time scale over which measured PM emission rates change in response to those transient input conditions is on the order of tens of seconds, as will be shown in upcoming sections.

Although the steady state operation of the SMPS has been described above, its operation in transient mode is slightly different, as follows. In steady state experiments, the voltage on the tube in the

Electrostatic Classifier is adjusted every second during the scanning procedure, in order to measure a range of particle sizes. In the transient experiments, measurement of a range of sizes must be forgone in favor of time resolution at one particular size. The flowrates — in this work, 0.7 liters per minute of particle-laden gas and 7 liters per minute of sheath air — and the voltage on the charged tube determine the measurable size range; in this case, the voltages are chosen to examine particles of nominal size 12.5, 25, 50, 100, and 200 nm. In certain cases, an additional voltage is used in order to examine the nominal particle size of 75 nm, insofar as the peak particle concentration generally occurs at this size. The data output from the SMPS is the number of particles per cubic centimeter of diluted exhaust on a second-by-second basis; data analysis is described in an upcoming section.

The dilution tunnel is a constant volume sampler, but in tests of variable intake manifold pressure, the flowrate of exhaust varies; consequently, the dilution ratio varies. While research regarding steady state experiments (to be presented in this paper) shows that dilution ratio can have a significant impact on post-dilution particulate concentrations, the effect of dilution ratio was not deemed relevant to the transient experiments. Rather, the steady state experiments isolate the effect of steady state operation parameters (including dilution ratio) on the *steady state* PM emissions, while the transient experiments isolate PM emissions during *transition between* steady state levels, as opposed to focusing on the starting and ending points of those transitions. Dilution ratios are generally chosen to be around 15:1, which is the ratio at which PM concentrations have the least sensitivity to dilution ratio; however, in any specific experiment, the dilution ratio is chosen to give optimal sensitivity to PM concentrations at the two conditions used. Dilution ratios are specified in the figures that follow.

2.3 Verification of Dilution Tunnel Design

RADIAL MIXING IN THE DILUTION TUNNEL

In order to ensure that all of the particulates undergo the same extent of condensation, adsorption, absorption, and coagulation, mixing across the radius of the dilution tunnel must be thorough. Otherwise these processes may occur at different rates in local pockets with discrepant particle and vapor concentrations, leading to differences in the particle concentration across a plug of gas, which would

complicate interpretation of the measured particle concentrations. (As a precaution to enhance turbulence and mixing, an orifice was built inside the tunnel approximately a tenth of a meter downstream of the initial exhaust/air mixing location.) To verify the extent of mixing, the following test was performed: With the dilution tunnel drawing either 950 or 6400 lpm and with the engine off, propane was injected into the dilution tunnel through the exhaust pipe. Propane concentrations were measured at various locations along the diameter of the tunnel at the monitoring location, and plotted relative to the mean measured concentration for the five radial locations in each traverse. The results (Figure 2.2) show that the propane tracer does indeed become well mixed (to within the ± 4% uncertainty) by the time the flow reaches the monitoring location. Since particles as small as those emitted by engines (around 0.1 microns) follow a flowstream essentially like a gas [48], it can reasonably be assumed that the particles are also well mixed. One datum, circled in Figure 2.2, was 6% below the mean; however, the difference is not statistically significant. Different mean concentrations were used in the various traverses in case degree of mixing was somehow related to absolute concentration: traverse A at 950 lpm was 3650 ppmC1; traverse B at 950 lpm, 4700 ppmC1; traverses A and B at 6400 lpm, 2400 ppmC1.

CONDENSATION PROPERTIES

Condensation of water in the small passageways within the SMPS proved to be an important but avoidable problem. Specifically, in tests where the relative humidity at the SMPS was 100% — when the dilution ratio was sufficiently small, as for example when undiluted SI engine exhaust was sampled — water condensed within the small diameter transfer tubes of the SMPS. The condensed water causes a source of uncertainty as well as repeatability problems because it may form a site where PM can be absorbed, stored, and released. In addition, these droplets can restrict the flowrate through the tubes, a condition which worsens as the droplets grow. Because the flowrate through the SMPS impactor and through the CPC are measured via the pressure drop across them, an increased flow restriction (as caused by a water droplet constricting the cross-sectional area of flow) causes the actual flowrate to decrease even though the pressure drop along the tube (hence the measured flowrate) remains fixed. Moreover, since the SMPS software

calculates particle mobility (hence particle size) and concentration using this measured flowrate, the error in measuring flowrate propagates to an error in calculated sizes and concentrations [40].

In one of the experiments regarding the effect of dilution on PM to be discussed in the present paper, in which samples of diluted SI engine exhaust were drawn from various locations in the dilution tunnel, water was found to condense in the SMPS when sampling from a location 0.3 meters downstream of the initial mixing location. Samples were drawn from the tunnel centerline, the location where the exhaust is injected, so it was presumed that the exhaust and diluent air had not been given significant time to mix and equilibrate before samples were drawn (only 1/3 of a second transit time). Samples drawn one meter downstream from this location (1.3 meters from the initial mixing location) were not plagued by a supersaturation of water, so it is believed that this distance — equivalent to a transit time of 1.5 seconds given the flowrate of 950 lpm — is sufficient to avoid the condensation problem. (An experiment, which will be described in the Dilution Experiments section, required sampling prior to the 1.5 second equilibration, and therefore required an alternative to SI engine exhaust. The alternative and the qualitative comparison to SI engine exhaust will be discussed.)

Condensation of water, oil, or unburned HCs can also take place in the dilution tunnel, providing a potential source of storage and release of PM. During normal operation, the vapor pressures in the tunnel are not sufficient to cause condensation: condensation of indolene in the tunnel would require an exhaust emission mole fraction on the order of 5×10^4 ppmC1, while the maximum observed value was approximately 1.3×10^4 ppmC1 in a case where extreme exhaust gas recirculation caused frequent misfires. However, condensation may occur during erratic or transient operation. On one occasion, a pool of condensed matter formed just below the outlet of the tube through which exhaust is injected into the dilution tunnel. The problem was circumvented by installing a liquid trap in the muffler before the inlet to the dilution tunnel, consisting of a small drain at the lowest point of the muffler to drain any condensed liquid. Because PM concentrations and parameters needed to calculate dilution ratio are measured downstream of the liquid trap, exhaust flowing through the trap has no more effect on measured particle concentrations or dilution ratios than does exhaust diverted from the dilution tunnel to the lab exhaust system at the exhaust tee (Figure 2.1). Thus, the presence of the trap should not lead to a source of measurement uncertainty.

DISCUSSION OF TUNNEL DESIGN

The best design of a dilution tunnel is one that minimizes vapor and particle losses. Since particle losses from a gas to the pipe walls increase with the contact surface area per unit volume, the losses are minimized by using a large diameter pipe [39]. However, thorough mixing between the exhaust and dilution air requires highly turbulent flow, which either requires a small diameter pipe or high mass flow rates, which in turn requires a more powerful, costly air pump or vacuum source. Hence, a compromise must be made between diameter and flowrate. While only one dilution tunnel diameter was used in the present experiments, this work does evaluate the effect of flowrates on measured particle concentrations.

An additional factor of concern is that the diluted exhaust must reside in the dilution tunnel long enough that particle dynamics have adequate time to occur, so that particle concentrations and sizes can equilibrate to a steady state level. Moreover, the exhaust and diluent air must have time to mix enough that relative humidity levels do not present condensation problems, as discussed above. The question of what is an adequate time based on these constraints will be experimentally evaluated in the present work.

Another factor of concern is the cleanliness of the inside of the tunnel. It is useful to allow optical access to the dilution tunnel at its lowest point with which to check for condensation, which may lead to problems as discussed above. Optical access may be gained, for example, by removing a thermocouple and inserting a boroscope. Samples of diluent air without engine exhaust should be analyzed before every day of experiments to verify that the filtered dilution air has a significantly lower particle concentration than the atmosphere; if it does not, there may either be a problem with the HEPA filter or there may be a source of particles within the tunnel, such as a pool of liquid, which can confound measured data.

2.4 Apparatus Conditioning

The following is a description of testing procedures. Unless specified, each test, in which one parameter was swept about the baseline value, is performed on a single day in order to insure that day-to-day engine variations will not be an issue and that diluent air characteristics remained consistent. Conditioning of the dilution tunnel is performed as follows. At the beginning of a test day, the SMPS is warmed up and used to measure the atmospheric particulate concentration. Then the SMPS is used to measure the particle concentration in the diluent air, i.e., the air (without any engine exhaust) drawn into the

dilution tunnel through the HEPA and charcoal filters. Experiments begin only after the particulate mass concentration in the diluent air drops below 0.4% of the atmospheric concentration, which corresponds to less 0.1% of the measured particle concentration at the baseline engine operating conditions and approximately 0.4% of the minimum measured PM concentration (corrected for dilution ratio) using indolene fuel.

Engine conditioning is handled as follows: before any day of experiments, the engine is warmed up at the baseline engine speed and load until the temperatures of the coolant and oil are within 2° of the 87°C set point. Once the engine is fully warmed, the dilution ratio is adjusted until it is within 10% of 15:1, except in the case of transient experiments, when dilution ratio is chosen for optimal sensitivity at the variety of engine conditions used. Between any two engine operating conditions in a steady state experiment, the engine is conditioned for a minimum of ten minutes at the new operating condition. The ten minute conditioning period was deemed more than sufficient based upon measurements that five minutes after a step change in the operating conditions, the PM concentration are within 1% of the steady state value. By comparison, Graskow *et al.*, who used a similar SMPS apparatus on a SI engine connected to a dilution tunnel, found that conditioning takes only five to six minutes [49]. During the conditioning period at the beginning of any day of testing, the SMPS records size distribution measurements; however, they are not repeatable and are not analyzed in the current work. Analysis of the start-up process on individual particle sizes is present in an upcoming section.

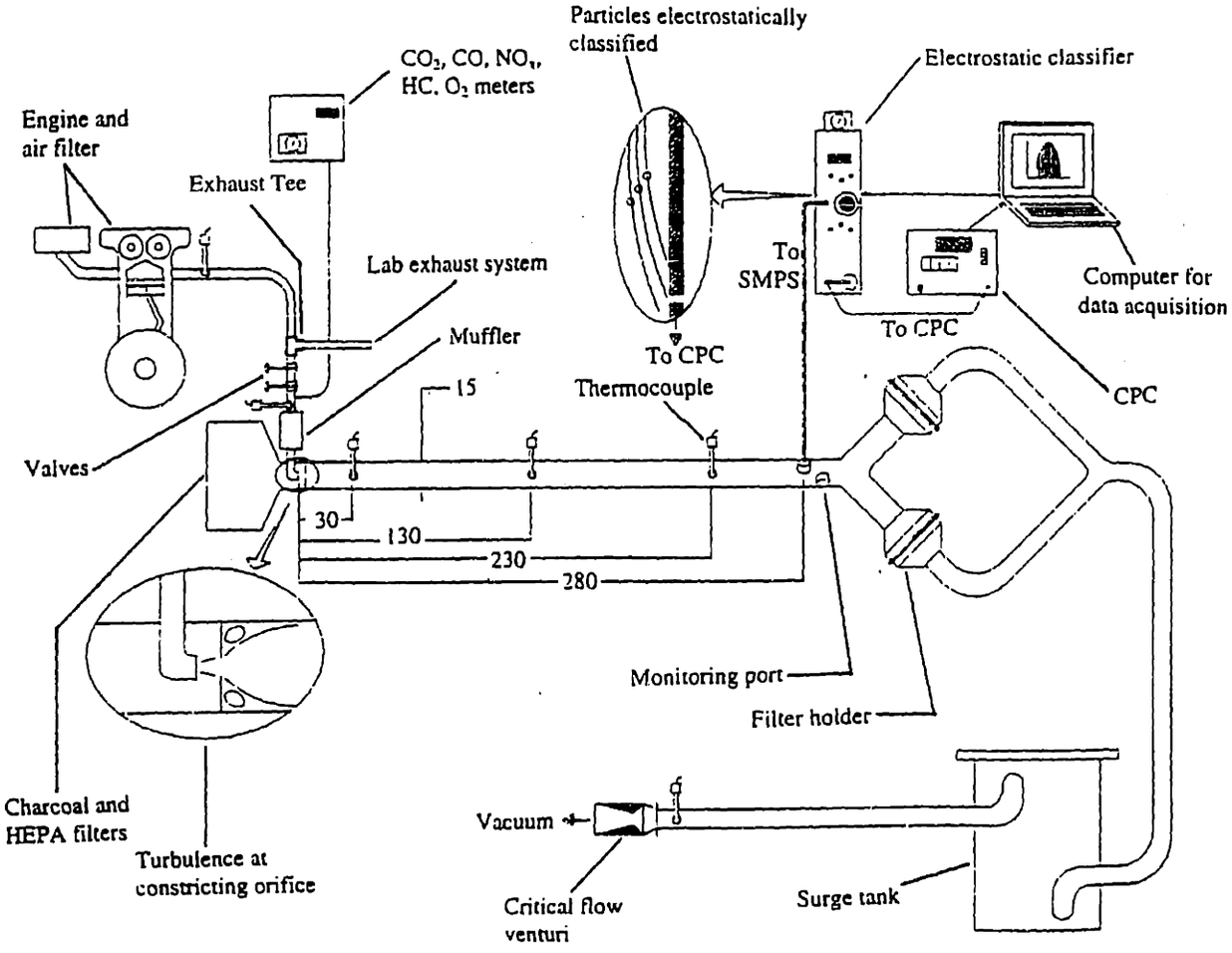

Figure 2.1 Schematic of engine, dilution tunnel, and SMPS. Units: cm.

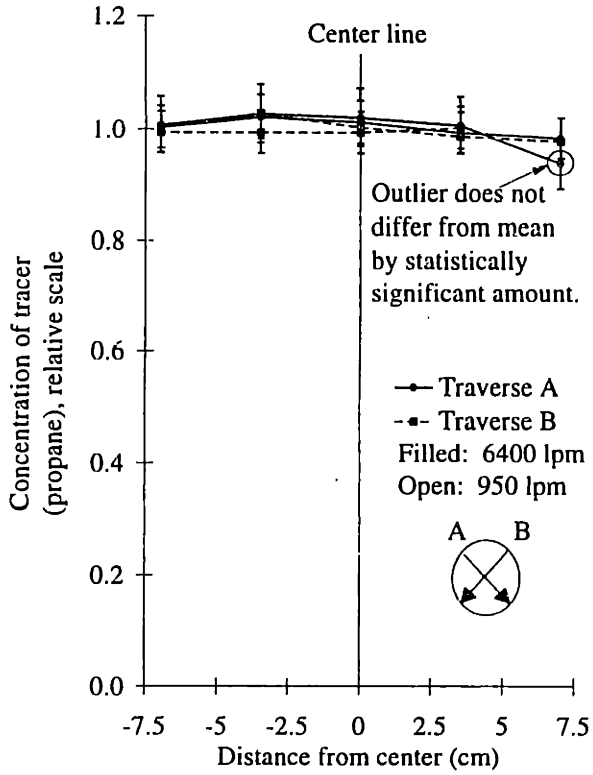

Figure 2.2 Tracer (propane) concentration across the radius of the dilution tunnel. Traverses A and B are along lines perpendicular to each other, at the monitoring port of the dilution tunnel. Error bars represent 4% measurement imprecision. All concentrations are normalized to the mean as described in the text.

CHAPTER 3

DATA ANALYSIS

3.1 Analysis of Steady State Data

Equilibrium values of intensive properties at the dilution tunnel exit are related to those properties in the exhaust and diluent through:

$$x_d = \frac{x_e + (\Lambda - 1)x_{da}}{\Lambda} \tag{3.1}$$

where x is the intensive property and Λ is the dilution ratio, defined as the ratio of mass flowrates of diluted exhaust to undiluted exhaust, with Λ = 1 corresponding to undiluted exhaust. Subscripts *d*, *e*, and *da* are diluted exhaust, undiluted exhaust, and diluent air respectively. Equation (3.1) is used to calculate the temperature of the diluted exhaust and to correct the measured PM concentrations for the dilution process (i.e., to calculate the PM emissions per unit volume of exhaust gas).

The dilution ratio is measured by comparing the mass fractions of carbon dioxide in the diluted exhaust, undiluted exhaust, and diluent air according to equation (3.1). Carbon dioxide is chosen because of its high concentration in the exhaust and low reactivity in the dilution tunnel, and is measured using a Nondispersive Infrared (NDIR) CO_2 meter. Since the NDIR requires removal of water vapor from the gas stream, the mass concentrations determined in the dry measurements must be corrected by the concentration of water vapor in the original gas. For both the dilution air and the diluted exhaust, the concentration of water vapor is sufficiently low that the correction factor is nearly unity. Because the measured concentrations from the NDIR are on a molar basis of the dry mixture, the dilution ratio can be expressed as:

$$\Lambda = \frac{X_{c,e}(1 - X_{w,e}) - X_{c,da} M_{da}/M_e}{X_{c,d} - X_{c,da} M_{da}/M_d} \cdot \frac{M_e}{M_d} \tag{3.2}$$

where X_c represents the dry molar concentrations of carbon dioxide measured by the NDIR, $X_{w,e}$ is the mole fraction of water in the exhaust (calculated based on the hydrogen/carbon ratio of the fuel and the air/fuel ratio), and M is the molecular weight of each stream. Since the concentration of carbon dioxide in ambient

air is small, the approximation that the molecular weight ratios associated with the air stream are unity leads to less than 1% error. Conservative estimates of one to eight percent uncertainty in the measurements of the three CO_2 mole fractions lead to a total uncertainty of approximately 10% in the calculation of Λ.

SMPS particulate measurements, taken in the dilution tunnel and shown in figures that follow, are corrected for dilution ratio the following equation so that they reflect the particle number or mass per unit volume of exhaust, $[PM]_e$, cooled to standard temperature and pressure:

$$[PM]_e = \Lambda \cdot [PM]_d - (\Lambda - 1) \cdot [PM]_{da} \qquad (3.3)$$

where $[PM]_d$ is the particulate number or mass concentration measured in the diluted exhaust, Λ is the dilution ratio, and $[PM]_{da}$ is the particulate concentration measured in the diluent air.

3.2 Analysis of Transient Data

The procedure for analyzing data is illustrated in Figure 3.1. The square wave input to the computer controller (Figure 3.1a) designates the desired intake manifold pressure; an analogous procedure is used when a condition other than intake manifold pressure is varied. The measured data (Figure 3.1b) shows the resulting intake manifold pressure, which differs from that desired only by virtue of the added noise. The data in Figure 3.1b also shows the measured brake engine torque, which approximately scales with the desired intake manifold pressure, but is subject to more noise due to cycle-to-cycle variability. In addition, the data in Figure 3.1b shows the equivalence ratio, which the engine controller maintains nominally at stoichiometric even during throttle transients. The top section of the data in Figure 3.1b shows the measured particulate concentrations during the transients; Figure 3.1c shows a blow-up of the particulate data so that the details can be better examined in the upcoming discussion. In particular, the form of the particulate response function will be discussed in more detail shortly. The particulate data are offset in time from the intake manifold data because of the transit time from the engine, through exhaust pipes, through the dilution tunnel, and into the SMPS. Calculation of the transit time is trivial, and hence is not discussed.

The behavior of PM concentrations — shown in Figure 3.1b and blown-up in Figure 3.1c — is illustrative of the phenomena taking place during transient engine operation. Firstly, PM concentrations vary according to changes in load, with a time scale for response on the order of ten seconds. And

secondly, a gradual decay in peak PM concentrations occurs over a time scale on the order of minutes (shown as dashed lines along the envelope of peak particle concentrations in Figure 3.1c). The short time-scale response function is of fundamental interest here, the objectives being to examine what the analytic form of the time response is and what the underlying reasons are for this response. The long time-scale response function reflects the strong dependence of PM emissions on engine/dilution system temperatures, which undergo a thermal equilibration from conditions before experiments (when the engine is operating only at the baseline conditions) to the transient experimental conditions (when operating alternately at the baseline conditions and generally hotter high-load conditions). Since the drift in steady state PM emission levels is difficult to investigate — i.e., it is difficult to repeatedly investigate the response of PM emissions to long scale temperature changes, as discussed in Chapter 1 — but is easily explained in terms of the gradual engine warm-up, the research of transient PM emissions concentrates on understanding the PM behavior occurring on the shorter time-scales. That is, the time response of interest is that occurring *between* steady state or peak emissions levels, rather than the decay in peak PM concentrations.

The objective behind the data analysis procedure is to (a) filter out the long time-scale drift in the PM signal and (b) overlay corresponding parts of the particulate responses so that the aspects of a single, repeated response function can be analyzed. The manner in which long time-scale drift is filtered out of the data is by normalizing each individual PM response such that it starts at a level of approximately zero and peaks at approximately unity. While it would be ideally preferable to analyze each individual response on its own, fit each to an analytical function, and then compare the series of analytical functions, it is not possible to distinguish unrepeatable noise from the underlying response function of any single response curve. Rather, a number of individual responses must be compared to each other in order to find the underlying response function. Accordingly, the manner in which unrepeatable noise is separated from the repeated transient response function is by overlaying the normalized response functions: the PM emission curve in response to each individual transient is plotted on a graph of relative PM concentration versus the time since the PM response began.

Although the normalization procedure eliminates any information about the absolute concentration of PM at each of the particle diameters, that information can be found in Chapter 5, which details the effect

of engine operating conditions on particle concentrations and sizes. As can be seen in figures that follow (e.g., Figure 3.3), particles in the 200 nm size range are sparsely concentrated, the result of which is poor signal to noise in transient engine experiments. Consequently, results in Chapter 9 do not include information about the time constant for 200 nm particles' response to transient engine conditions.

With only one exception (which will be discussed in Chapter 9), the overlaid, normalized PM emission curves can be best fit to a first order response[1], which is the response of a simple filling/emptying system when subject to a step change in input conditions. (An example of analyzed data is presented in Figure 3.1d. The note in Figure 3.1d about the imprecision of time steps will be explained in the Uncertainty Analysis section.) The first order response for the rising edge of the particulate response can be expressed as:

$$[PM]_{rel} = 1 - \exp(-t/\tau_{re}) \tag{3.4}$$

where $[PM]_{rel}$ is the relative or normalized PM concentration measured in the diluted exhaust gas, t is the time from the start of PM response (equal to the difference between the time from the start of the IMAP response and the transit time through the exhaust, dilution tunnel, and SMPS), and τ_{re} is the time constant for the rising edge of the first order fit. The first order response for the falling edge of the particulate response is one minus the right hand side of equation (3.4), the time constant for which will be labeled τ_{fe} in subsequent figures.

The first order response curve of the form in equation (3.4) that best fits the data is the one that represents an average or median value of the measured data. Similarly, the time constant (τ_{re} or τ_{fe}) in this best fit response curve represents a median time constant. The most conservative estimate for the upper and lower bounds on the first order fitting functions are those that encompass the entirety of the data, with the exception of noise (the distinction between noise and signal will be discussed in the Uncertainty Analysis to follow). The time constants in these upper and lower bounding functions are taken as the most conservative estimate of the upper and lower bounds on time constants for the particulate response function. Figure 3.1d

[1] The presence of noise in the PM data and the finite resolution of measurement diagnostics make it impossible to distinguish between true first order responses and either (a) responses which are a series of first order terms where one dominates, or (b) second order overdamped responses, both of which may look very similar to the simple first order response described by equation (3.4).

shows an example of the final result of the data analysis procedure: the normalized, overlaid particulate data representing a repeated response to the short time-scale engine transients; the median time response function; the upper and lower bounds on the time response functions; and the time constants for each of those three first order functions (listed as the median value plus and minus an uncertainty range). When the magnitude of two time constants are compared in the present paper, they will be said to differ by a statistically significant amount if the lower bound of one (calculated in the above manner) exceeds the upper bound of the other.

Before transient PM emissions can be presented and analyzed via the above technique, the time response of individual diagnostics and apparatus components must be quantified and an uncertainty analysis must be performed. Section 3.3 discusses the uncertainty analysis. Analysis of the time response for individual diagnostic and apparatus components is left to Chapter 9, as is analysis of the engine's time response.

3.3 Uncertainty Analysis

UNCERTAINTY IN STEADY STATE TESTS

Quantification Of Repeatability — In order to quantify the sources of measurement uncertainty in the various subsystems of the dilution tunnel and SMPS setup, tests for repeatability of PM size and concentration measurements were performed. In the course of these experiments, the individual components of the SI-engine/tunnel/SMPS system were isolated and tested for individual uncertainties. First, the SMPS sampled particles emitted by a steady particle generator, as described below. Second, the generator was connected to the dilution tunnel, with the SMPS measuring diluted particles in order to measure the uncertainty of the tunnel/SMPS combined. Finally, the SI engine, operating at steady state conditions, was used to generate exhaust particles, and the diluted exhaust particles were sampled from the monitoring port in the dilution tunnel and measured by the SMPS. Comparison between variabilities associated with the different sub-systems of the engine/tunnel/SMPS system indicates the uncertainty associated with each individual component. These tests show that the increase in variability due to the dilution process was negligible compared to the combined scatter produced of the SI engine and SMPS. Therefore, only the tests isolating the SMPS and SI engine will be described.

The repeatability of the SMPS alone (i.e., without the dilution tunnel) was tested by taking samples from the undiluted exhaust of the Compression-Ignition (CI) engine rather than a SI engine, for two reasons. First, Graskow *et al.* suggest diesel engines have steady, consistent emissions [49], thus allowing a steady stream of particles with which to isolate variability in SMPS measurements. Second, isolation of the SMPS (i.e., sampling undiluted engine exhaust) requires use of exhaust with less humidity than is present in SI exhaust, for reasons discussed in the previous chapter; thus only a CI engine could be used. Figure 3.2 shows the results of fourteen consecutive sets of size distribution measurements. All samples were drawn from the undiluted diesel engine exhaust during the course of one hour while the engine was operating at essentially steady state conditions. (In fact, the coolant and oil temperatures may have drifted upwards during testing.) Maximum and minimum concentrations in individual channels differ from the mean by approximately 20%, and much of this difference may be attributable to the warm-up, which has been found to reduce PM emissions [12, 13]. Therefore, the estimated 20% uncertainty may be the upper bound on the true uncertainty of the SMPS.

The total number and volume concentrations (the integral of the size distributions weighted by number and volume, respectively) deviate from the mean no more than 16%, and 12%, respectively. The standard deviations are 10% and 7% of the mean measured concentrations on a number and volume basis, respectively. Again, the gradual warming and the related decrease in PM emissions may make these overestimates of the true uncertainty of the SMPS itself.

Standard deviations of the mean number- and volume-weighted particle sizes are 2% of the average measured values; for mode number- and volume-weighted particle sizes, 3 and 4% of the average measured values, respectively. Maximum deviations of the mean number- and volume-weighted particle sizes from the average measured values are 3% of the average measured values; for mode number- and volume-weighted particle sizes, 6 and 7% of the average measured values, respectively.

Having estimated the measurement uncertainty due to the SMPS alone, the next step was to estimate that due to the dilution tunnel and SMPS in combination. Again, the particle source was the diesel engine for the sake of verified consistency [49]. The repeatability of the measurements was similar to the variation found without dilution described above, so that the uncertainty added by virtue of the dilution process was found to be negligible.

Finally, an experiment was performed in which the dilution tunnel and SMPS system was connected to the SI engine, and concentrations were measured repeatedly, thereby giving a measure of the repeatability of the entire system, particularly the SI engine, which Graskow *et al.* have reported to be prone to severely unstable PM emission rates [49]. Seven samples were taken in the course of one hour while all engine and dilution parameters were held fixed. The size distributions obtained (Figure 3.3) show a maximum deviation from the mean of about 20%, except at the very smallest particle sizes around 10 to 20 nm. Deviations of 20% are equal to those found in the test where the SMPS was isolated using the diesel engine as a source. The reasons for the relatively large variability at the smallest particles sizes, as discussed in the previous chapter, are that (a) particle losses in the SMPS transfer tubes increase as particle size decreases below about 20 nm, and (b) when the SMPS measures small particles, the charge on the electrostatically charged tube is small, so deviations are a relatively large fraction of the total charge, which leads to a relatively large deviation in measured PM mobilities and concentrations. Although measurements of particle concentrations below 10 nm have as much as a 50% uncertainty and those below 20 nm may have as much as a 30% uncertainty (Figure 3.3), the small size range over which this uncertainty is significant leads to a small contribution to the total or integrated number and volume concentrations.

The integrated concentrations deviate from the measured mean by no more than $\pm$ 15% on a number-weighted basis, and 18% on a volume-weighted basis. The standard deviations are 11% of the mean measured concentrations, on both number- and volume-weighted bases. Then the 95% confidence band is approximately $\pm$ 20% on both number- and volume-weighted bases (using only one digit accuracy).

The data taken using diluted diesel exhaust and presented in Figure 4.6 of the upcoming Results section has as much as a 19% scatter in number-weighted concentration and 31% scatter in volume concentration. Although this larger variability — which is statistically significant in the case of volume concentration, but not in the case of number concentration — may suggest that the data of Figure 4.6 more fully captures the true data scatter than does the 15 and 18% measured in the present test, the added variability in Figure 4.6 may on the other hand simply be a result of the sampling locations being further upstream. That is, the present test involved sampling from only the monitoring port 2.8 meters downstream of the exhaust/air mixing location, where mixing has been verified to be thorough — as was described in section 2.3: Radial Mixing In The Dilution Tunnel. Conversely, the data in Figure 4.6 were sampled at

locations prior to the monitoring port where mixing may not be complete, and thus may account for the added variability. In any case, the uncertainty band assigned to number and volume concentration data from the SI engine, diluted in the tunnel, sampled from the monitoring port, and measured with the SMPS is 20%.

While the above experiments suggest that, in a given experiment, variability is on the order of 20% of average concentrations, other researchers have suggested that variability may be significantly higher. For example, Graskow *et al.*, measuring PM emissions via a similar SMPS setup, find PM emissions from their General Motors Quad-4 SI engine to be significantly more unstable — occasionally jumping two orders of magnitude from the base emission level — than found in present experiments [49]. The difference may be due to engine-to-engine discrepancies, particularly differences in the engine controllers and control strategies, such as the fuel injection strategies to which PM emissions are extremely sensitive.

Measurements were made to quantify day-to-day variability of the engine/tunnel/SMPS system. PM number and volume concentration were measured at the baseline engine operating conditions during each day of testing. While the measured concentrations were generally within 50% of each other, on a few days the concentration was approximately an order of magnitude higher or lower than the average. Nevertheless, concentrations measured during repeated experiments on any one day (including these very high or low concentration days) did not vary by significantly more than the 20% uncertainty band discussed above. Because the source of this day-to-day variability has not yet been explained, the present paper makes comparisons only between data sets collected on the same day of experimentation where possible, in order not to be susceptible to errors derived from day-to-day variability. The only experiments that could not be performed entirely on one day were those in which particle concentrations were measured when operating on fuels other than indolene and in which catalyst efficiencies were measured.

The explanation for the large day-to-day variability is unknown, but its existence means that differences between PM concentrations measured using the different fuels are not necessarily statistically significant, nor are differences in engine-out and catalyst-out PM concentrations. Rather, differences in PM emissions from the different fuels can only be assumed statistically significant if the measured emissions vary by at least two orders of magnitude. For example, when emissions using propane and indolene at the baseline conditions are compared, the indolene is found to emit 160 to 1300 times as much PM on a

number-weighted basis and 450 to 700 times on a mass-weighted basis. Thus, these two fuels have a statistically significant difference in PM emissions. On the other hand, PM emissions measured in tests using indolene fuel and the indolene/MTBE fuel blend vary by no more than 60% of the value measured with indolene/MTBE blend, which is so small a difference as to be indistinguishable from day-to-day variability. Similarly, differences in PM emissions with and without the catalyst can only be assumed statistically significant if the measured emissions vary by at least two orders of magnitude; statistically significant differences were never observed, and the implications of the lack of difference will be discussed in an upcoming section.

Characteristic post-dilution sizes of particles emitted from the SI engine are quite consistent from test to test (Figure 3.4), indicating that not only are the measured particle concentrations approximately constant, but so are the particles size distribution characteristics. Note that the mode is expected to vary from test to test more than the mean because the mean is an averaged value, while the mode is simply the size at which the maximum occurs, irrespective of the mean. The standard deviation in number-weighted mean size is 1% of the average measurement, 10% for number-weighted mode, 0.5% for volume-weighted mean, and 6% for volume-weighted mode. These uncertainties are represented as error bars in Figure 3.4, but are so small as to be imperceptible for the number- and volume-weighted mean sizes.

Quantification Of Bias Error — Experiments were performed in order to measure the zero-offset error — the measurement made when a zero input is supplied — for the various components of the experimental setup. The zero-offset error of the SMPS was measured by drawing gases through a HEPA filter and into the SMPS for particle measurement. The steady state SMPS reading was zero particles per cubic centimeter, suggesting that the SMPS internal circuit has no zero-offset error. The zero-offset error of the tunnel/SMPS system was measured as follows. When the engine was not running but air was being drawn through the dilution tunnel, that air had a measured particle concentration of 0.1 to 0.2% of the ambient PM concentration, or approximately 20 particles/cm^3 and 2 x 10^7 nm^3/cm^3. Because 20 particles/cm^3 and 2 x 10^7 nm^3/cm^3 are negligible compared to diluted engine-out emission concentrations, of the order of 6 x 10^4 particles/cm^3 and 4 x 10^{10} nm^3/cm^3, the zero-offset error for the tunnel/SMPS system is negligible. A zero-offset error for the engine/tunnel/SMPS system was also approximated. Although the

engine/tunnel system does not necessarily have a "zero" particle emission level (i.e., the engine may emit particles under all operating conditions), the SMPS did measure a particle concentration of 130 particles/cm^3 and 3 x 10^7 nm^3/cm^3 (0.06 μg/m^3) when the engine was operated on propane fuel. Insofar as low molecular weight gaseous fuels are expected to produce very low PM concentrations, it seems sufficient to estimate the "zero" particle emission level for the engine/tunnel/SMPS system as 130 particles/cm^3 and 3 x 10^7 nm^3/cm^3. However, this offset is also negligible compared to typical measured concentration levels for diluted SI engine exhaust. Concern has been raised whether the standard engine air-filter sufficiently filters particles out of the intake air, so that intake particles do not confound measurements. Given that the results of the experiment using propane fuel show a negligibly low baseline engine-out particle concentration, one can conclude that the standard air-filter is sufficient.

Scale error — the complement to zero-offset error, in which measurements err by a certain percentage — can occur in the SMPS diagnostics as a result of either particles obtaining multiple charges in the Kr-85 Bipolar Charger or optical interference between multiple particles in the CPC. However, the SMPS software can predict and correct for both of these sources of error [40].

A systematic error may occur in the measurement of PM volume (or mass) concentration because of the finite size range over which the SMPS can measure particles. The SMPS measurement range was optimized so that it cuts off less than 1% of the particles on a number-weighted basis, but an estimate of the volume- (or mass-) weighted fraction of particles cut off is approximately 15%. The manner in which this estimate is made is that the PM volume distribution (Figure 3.5) is assumed either symmetric about its peak or log-normal in shape (the two assumptions are equivalent, for the purposes of the present calculation), and the integrated volume under the mirror image portion of the curve (which is not cut off by the SMPS) is calculated. The 15% uncertainty is on the order of the other uncertainties, discussed above.

A bias error may occur in the measurement of particle sizes. If flowrates of the SMPS sheath air and aerosol-laden flows drift from the values input to the software, then the software will erroneously calculate the particle mobility for particles in each channel of SMPS measurement, causing a bias in the measured particle sizes. However, the flowrates are all specified, set, and frequently verified to be within 0.5% of their nominal values, which translates to a bias of ± 0.1 nm at 9 nm and ± 0.6 nm at 378 nm.

The total uncertainty is approximated here as the square-root of the sum of each error squared. For number concentration measurements made using the total engine/tunnel/SMPS system, variability is 20% and bias errors are less than 1%, so the total uncertainty is approximately 20%. For volume (or mass) concentration measurements made using the total system, variability is 20% and bias errors are approximately 15%, so the total uncertainty is approximately 25%. For measurements of the mean diameter, variability is 3% (as measured in the test isolating the SMPS) and bias errors are 0.5%, so the total uncertainty is 3%. And for measurements of the mode diameters, variability is 10% and bias errors are 0.5%, so the total uncertainty is 10%.

UNCERTAINTY IN TRANSIENT TESTS

Emissions of particles of a single size during steady state operation (as opposed to the scanning SMPS operation used for tests of PM emissions steady state engine operation) were examined in order to find the magnitude of the steady state PM fluctuations, insofar as differentiating between transient and steady state emissions requires a knowledge of when a steady state condition is reached. The engine and dilution system were operated at steady state at the baseline engine operating conditions and at 70 kPa IMAP (all other conditions equal to the baseline conditions) with the SMPS constantly measuring the concentration of particles at one of several fixed nominal sizes within the range of 12.5 to 200 nm used in the transient experiments. On only one occasion did the measured PM concentration vary by more than 20%, which is the uncertainty ascribed above to the measurement of integrated PM concentrations (i.e., the concentration of particles across all size ranges) for the present experimental system in steady state. On that one occasion, steady state PM emissions at one particle size varied by nearly 30% from the mean value; consequently, 30% is designated as the uncertainty in particulate concentrations in any one size range during steady state conditions. (Note that this 30% fluctuation equals that measured at a single particle size using the SMPS in scanning mode, discussed in the steady state part of the current section.) In order to account for this uncertainty, when measured transient PM emissions are fit with a first order response varying between zero and unity as in equation (3.4), the period of interest lies between a $[PM]_{rel}$ of 0.3 and 0.7. In other words, the period during which first order response functions are compared and fit to PM data is the period between 30% and 70% of the complete response. (As can be seen from the figures that follow,

though, fluctuations are rarely as large as 30%, so the range over which $[PM]_{rel}$ can be fit often exceeds the limited 0.3 to 0.7 range, and extends closer to the bounds of zero and unity.)

The data normalization procedure described in section 3.2 eliminates any uncertainty arising from drift in engine conditions such as gradual temperature changes, day-to-day drift or variability, and drift in the precision to which repeated transients can be performed. That is, even though the computerized engine controller has a slight inaccuracy when producing step changes in operating conditions, and even though particulate emissions are strongly sensitive to operating conditions (as will be discussed in Chapter 5), the normalization procedure removes these inaccuracies as sources of measurement uncertainty.

The method of finding the range of values for $\tau_{r,}$ and $\tau_{f,}$ (described above) gives the most conservative estimate of the uncertainty in the time constant, insofar as the bounds on the time constants are those that bound all of the data, as opposed to a statistical technique, which may bound only 95 or 99% of the data, depending upon the chosen confidence interval. However, uncertainty in finding the time constants does arise from slight imprecisions in the length of time steps (noted in Figure 3.1d). Specifically, when signals are plotted such that the beginning of each rising edge response occurs at time zero along the abscissa, a slight imprecision in the length of time steps between operating condition changes will result in imprecise alignment of the falling edge data along the abscissa. Further, the imprecision with which successive time steps can be aligned along the abscissa axis limits the precision with which a time constant can be fit. Therefore, imprecise alignment of the data may appear to be drift or noise in the data, which then translates to wider bounds on the time response functions than if no such imprecision exists. This imprecision is small but unavoidable, and the uncertainty that arises is inherently incorporated into the bounding values of the time constants by virtue of the data analysis procedure.

On the other hand, uncertainty does not arise from the chosen length of time steps. Specifically, tests were performed to find whether the time duration between step changes of the input wave in Figure 3.1a (or, in other words, the wavelength) affects the time responses measured for PM emissions. But time constants for the PM response functions measured using different durations of time steps did not differ by a statistically significant amount. Figure 3.6, for example, shows the time response of particle emissions to identical transients in intake manifold pressure, the only difference being the length of the time steps. Figure 3.6 also shows time constants measured for the different step lengths, which do not differ by a

statistically significant margin. The result of the insensitivity of particulate response functions to the duration between changes in engine operating conditions is that these changes can be chosen arbitrarily, without impacting results such as the measured time constants; a variety of time steps are used in experiments presented in upcoming sections.

Repeatability was found to be a problem on only two occasions. Firstly, while time responses to transient operating conditions were generally found to be first order, a non-first order response to transient emissions was observed on one occasion; this will be discussed in Chapter 9. Secondly, while time constants measured in repeated experiments (whether on the same day or on different days) were generally equal or differed by less than a statistically significant margin (as defined in section 3.2), on one occasion, the time constants in a repeated experiment were found to differ significantly. Specifically, in the case where 100 nm particles were measured during transients in intake pressure, the time constant for the transition from 40 to 70 kPa IMAP was found to be 4 ± 1 seconds on one day and 21 ± 9 seconds on another. (In contrast, the time constant for the transition from 70 to 40 kPa IMAP was not found to differ by a significant amount: 4 ± 1 second on the first day and 7 ± 3 seconds on the second.)

Figure 3.1 Schematic of procedure for analyzing data

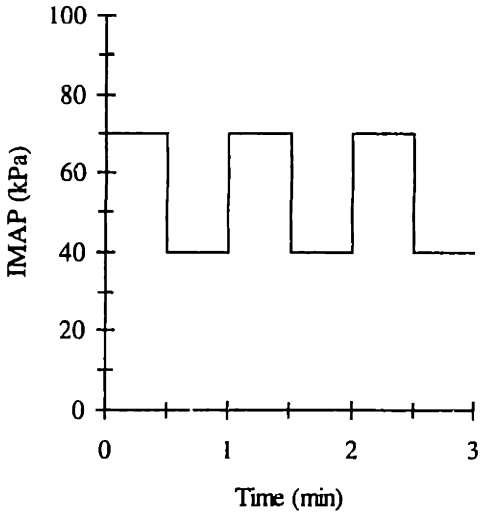

(a) Input signal. Time steps: 30 seconds.

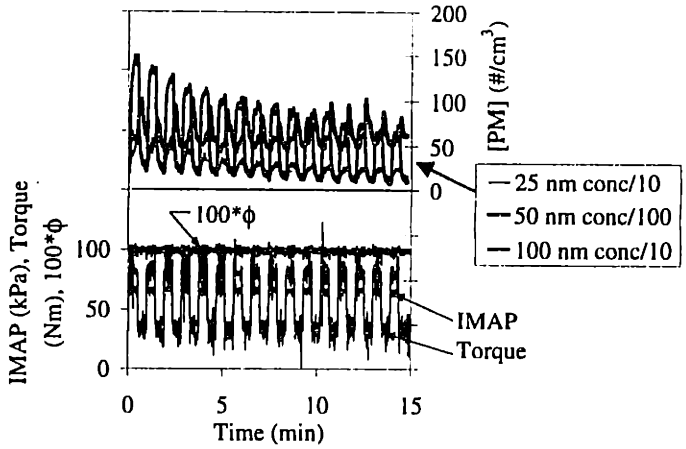

(b) Example of raw data: IMAP, torque, and equivalence ratio (ϕ) in lower portion of figure; particle concentrations at 25, 50, and 100 nm in upper portion of figure. Time steps: 30 seconds.

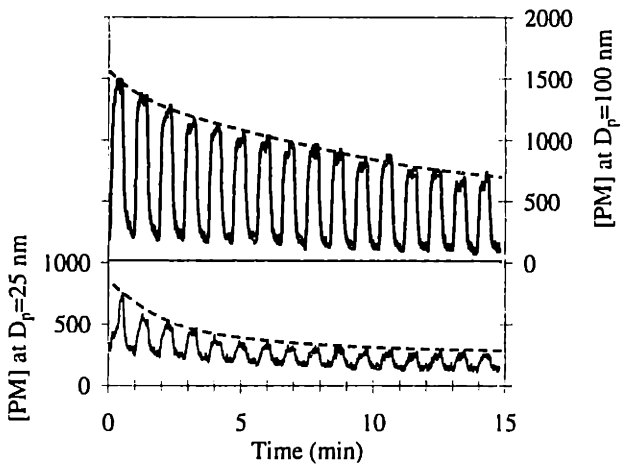

(c) Enlargement of raw data from part (b) of present figure: particulate concentrations at the 25 and 100 nm particle sizes. Dashed lines represent envelope of decay in peak particulate emissions, due to long time-scale engine processes.

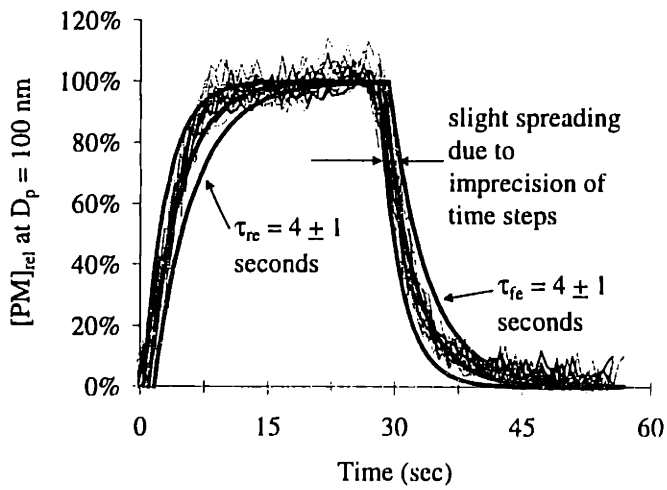

(d) Example of analyzed data: normalized, overlaid particle concentrations at one particle size (100 nm) with first order time responses superimposed: time constant for response is 4 ± 1 seconds for both the rising edge (τ_{re}) and falling edge (τ_{fe}). Conditions: intake pressure varying between 40 and 70 kPa as illustrated in Figure 2b. Time steps: 30 seconds. Data denoted as thin lines, first order time responses as thick lines.

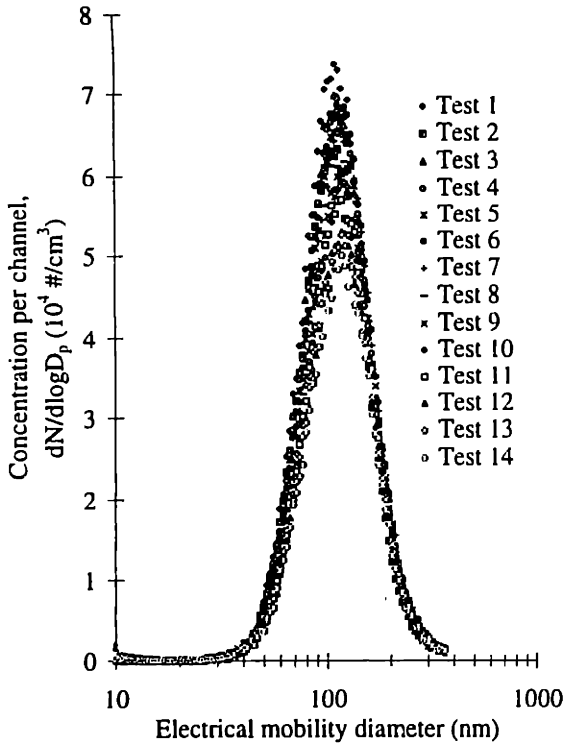

Figure 3.2 Size distributions of particles drawn from undiluted diesel exhaust in fourteen consecutive tests, taken over a period of one hour.

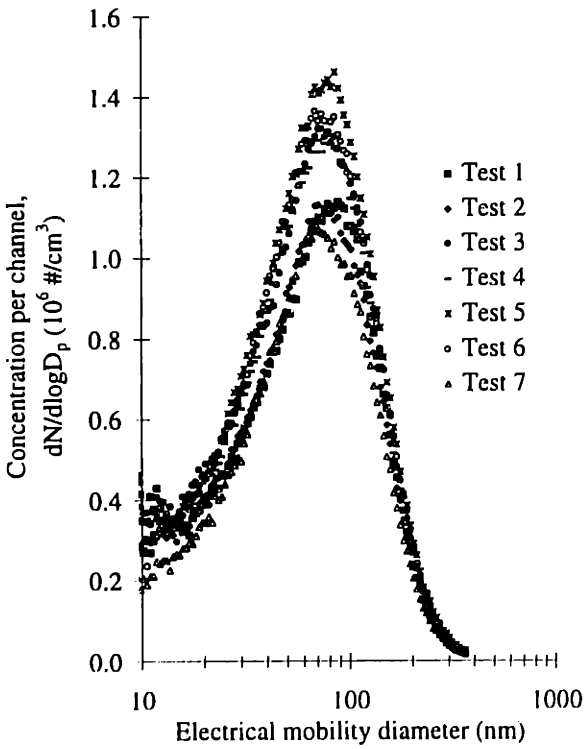

Figure 3.3 Size distributions from seven consecutive tests on the SI engine, using the dilution tunnel. Corrected for dilution ratios of 13:1 to 15:1, as discussed in Data Analysis section. Baseline engine operating conditions specified in text. Samples were taken over the course of one hour.

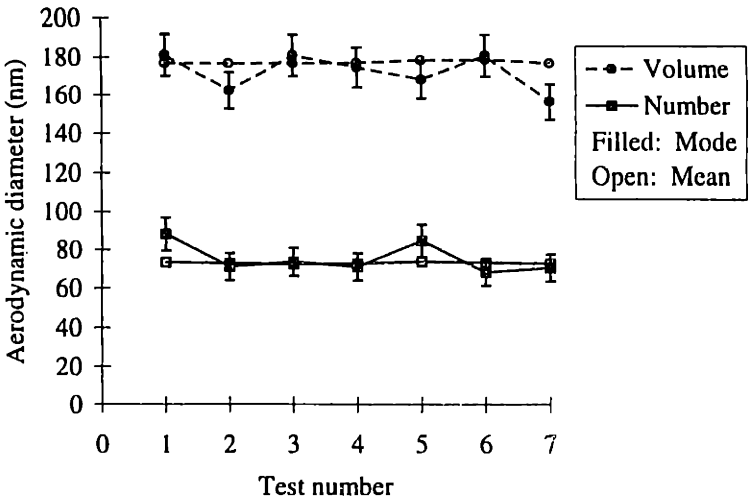

Figure 3.4 Post-dilution number and volume size distribution characteristics for seven consecutive tests within one hour, using SI engine. Engine operating conditions same as in previous figure. Error bars represent standard deviations.

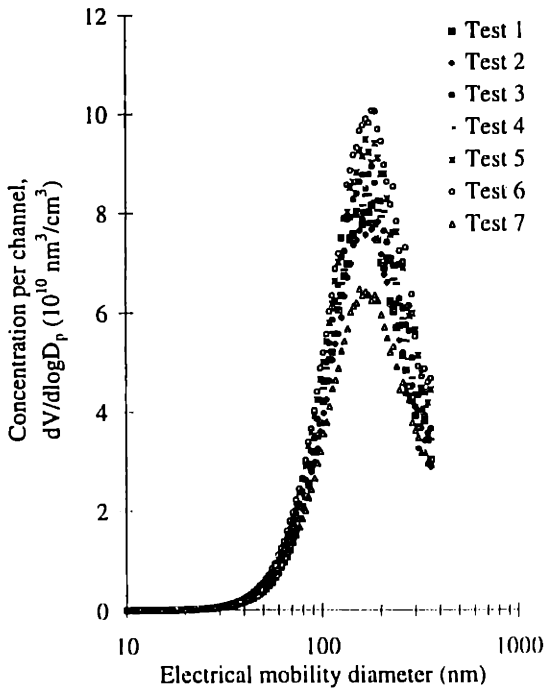

Figure 3.5 Size distributions from seven consecutive tests on the SI engine, weighted on a volume (or mass) basis. Engine operating conditions same as in previous figure.

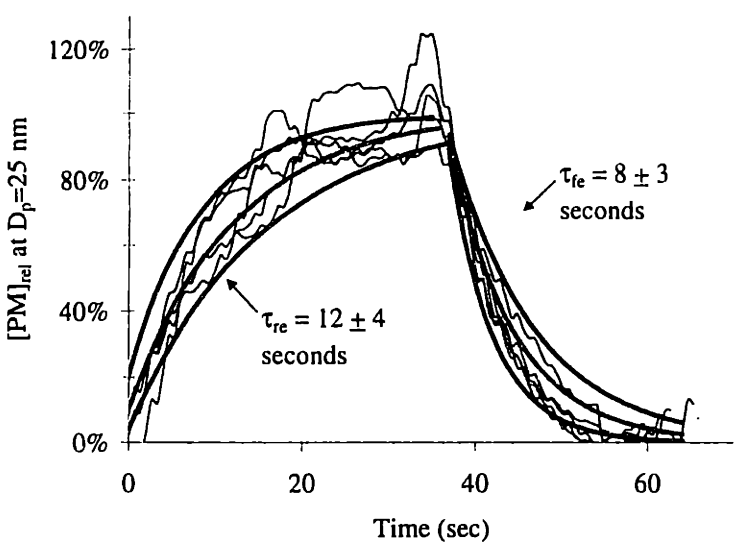

(a) Time steps: 30 seconds

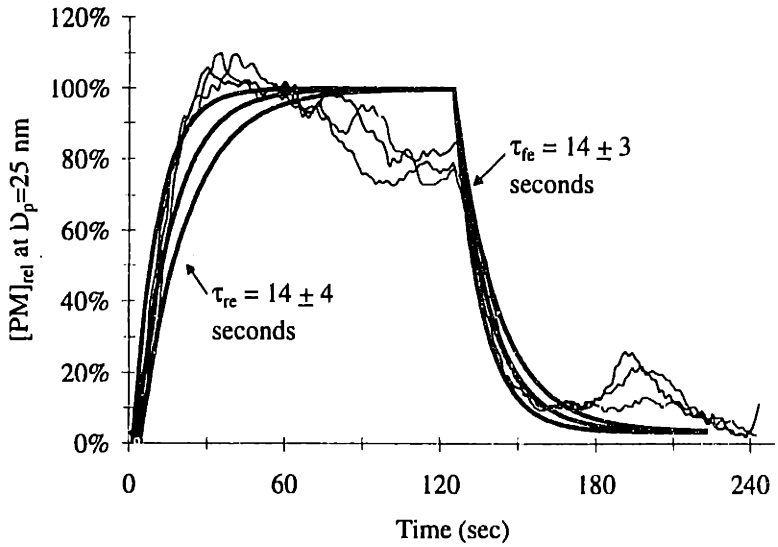

(b) Time steps: 120 seconds

Figure 3.6 Response of PM emissions to transient intake pressure for two different lengths of time steps. Particle size: 25nm. Baseline conditions at the 40 kPa IMAP case; baseline conditions at the 70 kPa IMAP case except for intake pressure. Duration of time steps: (a) 30 seconds, (b) 120 seconds.

CHAPTER 4

RESULTS OF DILUTION EXPERIMENTS

4.1 Experimental Methodology and Conditions

A series of experiments were performed to characterize relevant parameters of the dilution system and their impact on dilution related particle dynamics as measured with the SMPS — temperatures, flowrates, dilution ratio, and residence time. The engine used for these experiments was the Ford Zetec operated at the baseline conditions, except in the case where the effect of residence time was measured, when the Kubota diesel engine was required as will be discussed in section 4.4; results from this experiment will be generalized in order to draw implications on the dilution process for gasoline-derived particulate.

Additional experiments were performed to compare the particle concentrations measured via the SMPS with those measured via traditional gravimetric analyses. These experiments were performed on the Saturn engine using a matrix of engine operating conditions that centers about the baseline conditions summarized in Chapter 2.

4.2 Temperature Along the Tunnel

Knowledge of the temperature profile within the dilution tunnel is important because the temperature of the diluted exhaust strongly affects the condensation and adsorption/absorption processes [13], as recognized by USEPA regulations in requiring a maximum post-dilution temperature of 52°C. Figure 4.1 shows the final temperature of the diluted exhaust gas as a function of dilution ratio calculated from equation (3.1), assuming constant specific heats and adiabatic mixing, and using four temperatures representative of the exhaust gas at the outlet of the muffler (i.e., the inlet to the dilution tunnel). The dilution ratio required to satisfy the 52°C requirement depends on the exhaust temperature at the inlet of the dilution tunnel; the result of calculations shown in Figure 4.1 is that, for the temperatures prior to mixing shown in the figure, the required dilution ratio is on the order of 3 to 12.

The calculations in Figure 4.1 neglect heat loss from the diluted exhaust through the dilution tunnel to the environment; however, this heat loss can significantly affect the final diluted exhaust temperature if

either the temperature gradient between the exhaust and environment is large or the residence time in the dilution tunnel is long. For example, in an experiment with a diluted exhaust flowrate of 6400 lpm and a dilution ratio of 8:1 (higher exhaust flowrate than in baseline engine operating conditions), the diluted exhaust temperature was high enough relative to the atmosphere that heat loss through the stainless steel dilution tunnel resulted in a 5°C temperature decrease along the length of the tunnel (Figure 4.2). Nevertheless, the diluted exhaust temperature did not drop to 52°C, indicating that in this case the dilution ratio was not high enough. On the other hand, in the case where the 950 lpm flowrate was used, the time for heat transfer was long enough to allow the exhaust (at a temperature of approximately 100°C prior to entering the dilution tunnel) to reach 30 ± 2°C once diluted to dilution ratios between 6 and 30 (Figure 4.3).

Another significant source of heat loss in the dilution sampler is the exhaust pipe leading up to and through the muffler and then to the dilution tunnel. Heat loss in the exhaust pipe depends on the flowrate and residence time in the pipe (for fixed initial exhaust temperature). If the dilution ratio increases at fixed diluted exhaust flowrate, the flowrate of undiluted exhaust decreases, and although the rate of heat transfer decreases, the time for heat transfer increases by a larger portion. The result is that the temperature of the exhaust immediately prior to dilution is lower for higher dilution ratios. Similarly, if the diluted exhaust flowrate decreases at fixed dilution ratio, then the undiluted exhaust flowrate decreases, resulting in decreased temperature prior to dilution.

Measured temperature profiles in the exhaust runner and dilution tunnel are shown in Figure 4.2. These data were measured using a diluted exhaust flowrate of 6400 lpm on a summer day when the dilution air temperature was 33°C. As can be seen, higher dilution ratio results in more heat transfer within the exhaust pipe and thus lower temperatures immediately prior to dilution. Further, the most significant temperature decrease in the dilution tunnel is that due to mixing; by the point it has traveled even two tunnel diameters (the first sampling location in the dilution tunnel on Figure 4.2) the temperature has essentially equilibrated. For data presented in Figure 4.2, the residence time in the dilution tunnel is less than 0.5 seconds, so there is relatively little chance for heat transfer to the surroundings; it is only in the case with dilution ratio 8:1 — in which the diluted exhaust temperature is sufficiently high to allow heat transfer to

the environment (as discussed above) — where the temperature is observed to decrease after the initial mixing.

Figure 4.3 shows experimentally measured diluted exhaust temperatures as a function of dilution ratio for diluted exhaust flowrates of 950 and 6400 lpm. At 6400 lpm, the time for heat transfer to the environment is short enough that the mixing-induced temperature drop controls the final temperature, as per calculations shown in Figure 4.1. Conversely, at 950 lpm, heat transfer dominates such that final diluted exhaust temperatures are 30 ± 2°C for all dilution ratios, which ranged from 6 to 30. Moreover, Figure 4.3 shows that the reduction in flowrate from 6400 to 950 lpm at fixed dilution ratio results in decreased final diluted exhaust temperature, for reasons analogous to those stated above in the context of undiluted exhaust. The implication of the fact that both flowrate and dilution ratio affect temperature is that they both affect particle dynamics, as will be discussed in the next section.

4.3 Effect of Dilution Ratio on PM

Because the dilution process can have a profound effect on the particulate emissions — on number and volume concentrations as well as particle sizes — experiments were performed in order to determine the 'optimum' dilution characteristics. The 'optimum' dilution ratio is defined in the present work as a dilution ratio that satisfies the USEPA maximum temperature requirement and, more importantly, at which PM number and volume concentrations are the least sensitive to slight deviations in dilution ratio, hence the most repeatable. Primary concerns are the selection of dilution ratio and the flowrates of both exhaust and dilution air (although only two of these parameters are independent). The tests were run in two regimes: a high flowrate case (dilution tunnel flowrate of 6400 lpm, Re ≈ 57000), characterized by a short time for heat transfer from the diluted exhaust to the environment (residence time ≈ 0.5 seconds); and a low flowrate case (950 lpm, Re ≈ 9000), with a large residence time (3.4 seconds). If the time for heat loss to the environment is short, then the mixture of dilution air and exhaust is essentially adiabatic, so the mixture's final temperature depends primarily on the initial gas temperatures and the dilution ratio, as discussed in the previous section. If however the time for heat loss is long, then the mixture temperature may approach the ambient temperature regardless of the dilution ratio, also as discussed in that section.

The following discussion separates the effects of flowrate and dilution ratio on heat loss in order to provide insight into the effect of each on particle dynamics. (In the discussion and figures that follow, measured concentrations are corrected by multiplying them by the dilution ratio and subtracting the diluent particle concentration following equation (3.1) in order to reflect the number or volume of PM per unit volume of exhaust cooled to standard temperature and pressure, thus separating the two factors: dilution ratio and post-dilution PM concentration per unit volume of exhaust gas.)

In the high flowrate case, variations in the dilution ratio affect two parameters: the concentration of PM and the diluted exhaust temperature, both of which affect PM growth rates. The concentrations of both vapor and particles decrease with increasing dilution ratio, hence decreasing the propensity of condensation, adsorption/absorption, and coagulation, as collisions between particles and either vapor molecules or other particles become less frequent. On the other hand, as the dilution ratio increases, the final temperature decreases, thus increasing the propensity for condensation and adsorption/absorption, thereby increasing the size, volume fraction, and mass of the particles. The effect is more pronounced at low dilution ratios, where the mixture temperature is very sensitive to dilution, while at high dilution ratios, large increases in dilution ratio barely affect the mixture temperature (Figure 4.1).

The net result of the competing dilution and cooling effects is that, as the dilution ratio is increased from unity, PM number and volume (or mass) concentrations initially increase, but as the dilution ratio is increased still further, concentrations reach a maximum and then decrease and eventually level off. In other words, as the dilution ratio is increased from unity, the temperature drops so sharply that the increased propensity for condensation, adsorption, and absorption due to decreased temperature overwhelms the decreased propensity for condensation, adsorption, absorption, and coagulation due to dilution. But when the dilution ratio is increased still further, the temperature effect is overwhelmed by the dilution effect.

The explanation above is consistent with the measured concentration as a function of dilution ratio, shown in Figure 4.4. This experiment was performed at two different engine operating conditions (with correspondingly different particle emission rates) as described in the figure. Measured concentrations increase as dilution ratio is increased from the minimum attainable value (around 10:1) until approximately 13 to 18:1, while at higher dilution ratios, the concentration decreases. The dilution ratio at which concentrations are maximized and sensitivity to dilution ratio is minimized occurs in the range of 13 to 18.

This behavior, where concentration peaks at a dilution ratio of 13 to 18, is similar to that for diesel exhaust concentrations, as modeled by Amann *et al.*, MacDonald *et al.*, and Plee and MacDonald [15, 16, 17].

Beyond a dilution ratio of 23 or 25, concentrations of particles in the diluted exhaust become so small that measurement uncertainty begins to overwhelm and mask true variations in PM concentrations. At some dilution ratio, the particles and vapor become so dilute that particle dynamics are effectively halted, so further increases in dilution ratio do not affect measured particle concentrations. Amann *et al.*, MacDonald *et al.*, and Plee and MacDonald find that this occurs at dilution ratios as low as 30 and as high as 1000, but remark that the specific dilution ratio depends upon exhaust conditions such as particle and vapor concentrations and temperature [15, 16, 17].

In the low flowrate regime at Re ≈ 9000 (Figure 4.5), the final temperature becomes decoupled from the degree of dilution because the time for heat transfer to the surroundings is large. In this case, the temperature of the diluted exhaust as a function of dilution ratio differs from that plotted in Figure 4.1, in that the temperature remains constant (Figure 4.3). Hence the only effect of increased dilution is the decrease in concentration of vapors and particles, and thus the increase in resistance to condensation, adsorption/absorption, and coagulation. Therefore, the increased dilution ratio gradually inhibits the tendency for particles to grow and for particulate concentrations to increase beyond the levels reached in the exhaust. Sufficiently high dilution ratio effectively stops particle interaction and dynamics in the dilution tunnel: above this dilution ratio further increases in dilution do not affect measured particle concentrations. Experimental verification of the above phenomena is shown in Figure 4.5. The threshold dilution ratio above which particle interaction and dynamics in the dilution tunnel are halted was found to be between approximately 13 and 15:1.

The above experiments elucidate the choice of the 'optimal' dilution ratio. The optimal dilution ratio is one at which PM concentrations have the least sensitivity to dilution so that unavoidable imprecision in setting dilution ratio will not render different data sets incomparable. That is, optimal dilution ratio is that at which the curve of PM concentration (corrected for dilution ratio) versus dilution ratio is flat, corresponding to a point where the balance between the condensation, adsorption/absorption, and coagulation processes are not affected by slight changes in dilution ratio. At other dilution ratios, variations in the dilution ratio will change the PM concentration in a complicated fashion, thereby complicating the

comparison between data taken under different conditions. With both flowrates shown here (Figures 4.4 and 4.5), the minimum sensitivity to dilution ratio occurs from dilution ratios of 13:1 to 18:1.

4.4 Particle Number Losses and Volume Gain at Fixed Dilution Ratio

As discussed above, particles undergo the dynamic processes of condensation, adsorption, absorption, and coagulation during the dilution process. In addition, as they move through a dilution tunnel, they may be lost via collision with walls. Insofar as these particle dynamic processes affect measured particle concentrations, it is important to quantify their effects. In order to study these processes, an experiment was performed to quantify (a) particle number losses as a result of coagulation and particles sticking to the dilution tunnel walls and (b) particle volume or mass gain as a result of condensation, adsorption, and absorption of HC vapors. A steady stream of engine exhaust and PM was injected into the dilution tunnel, and the SMPS was used to measure the PM concentrations along the tunnel centerline at 0.3, 1.3, and 2.3 meters from the location where exhaust and dilution air are initially mixed. The conditions of the test were: total flowrate of 950 lpm (Re ≈ 9000) and a dilution ratio of 15:1. (The choice of this dilution ratio was based on the reasoning given above.) A single set of sampling tubes was used for all three locations, in order to assure that losses within the sampler did not create measurement artifacts.

Insofar as the purpose of the present work is to examine the effects of dilution on SI engine exhaust, it would have been preferable to use SI engine-generated exhaust and particles for the present experiment. However, when the SI engine was used, it was discovered that samples taken from the point 0.3 meters downstream of the mixing location contained enough water vapor that water was condensing in the SMPS tubing. This accumulation of water in the SMPS suggests that there may not be enough time during the 0.3 meters traveled from the mixing location to the probe (corresponding to 1/3 of a second) for the exhaust and diluent air to fully equilibrate, so that the suddenly cooled moisture condenses in the sampling tubes leading to the SMPS. Because the engine exhaust cannot be desiccated without drastically altering the PM characteristics, the use of the SI engine was virtually prohibited for this experiment. Measurements of PM concentrations at the 1.3 and 2.3 meter locations do not differ by a statistically significant amount, suggesting that particle dynamics may occur to a measurable extent only in the first 1.3

meters of dilution flow, after which the diluted exhaust has equilibrated. Hence, examination of the first 1.3 meters of flow is crucial to the understanding of tunnel particle dynamics.

In order to resolve the aforementioned water accumulation problem while still allowing sampling throughout the length of the dilution tunnel, exhaust and particles are drawn from the closest possible substitute with sufficiently low water vapor concentration: a diesel engine (here, a Kubota diesel engine operated at idle with an extremely lean air/fuel ratio of 90). Admittedly, (a) diesel particulate emissions and dilution have been studied extensively and (b) the particle/exhaust characteristics of diesel and gasoline engines are not identical. The justification for performing this experiment using a CI engine despite these two limitations is the following. First, the objective of this experiment is to gain knowledge of the behavior of SI exhaust particles, even if by only qualitatively comparing CI engine processes with those in SI engines. Although similar research has been done on diesels, the comparison with SI engines has not. Second, CI engines emit particles of similar size (around 80 nm number-weighted mean diameter versus 50 nm for SI engines [11]) and similar chemical composition (both contain approximately 70% elemental and organic carbon with only trace amounts, i.e. less than 4%, of any other single chemical compound [34]). Moreover, the number concentration of particles from a CI engine operated at low load such as that used in the present experiment falls within the range of PM emissions obtained using a SI engine in experiments to be discussed in Chapter 5: 70 particles/cm^3 in the diluted exhaust operating the SI engine on propane fuel at the baseline operating conditions, to 7 x 10^4 using indolene, to 1 x 10^7 using toluene at the same conditions, compared with 7 x 10^4 using the CI engine. So while the size, composition, and concentration of the CI and SI particles are not identical, they may be similar enough that the diesel exhaust should be an adequate substitute for the purpose of quantifying particle losses and coagulation. However, because the concentration of HC vapors emitted from a diesel engine at low load is lower than that from a SI engine, use of the diesel will result in an underestimation of the magnitude of condensation, adsorption, and absorption taking place in diluted SI engine exhaust; the qualitative implications of this difference will be discussed.

The theoretical expectation is the following. When the particles travel downstream from the initial mixing location, some should coagulate to form larger particles. Thus the inherent growth trend of coagulation should tend to increase the particle mean and mode sizes, but decrease the particle number concentration. In addition, particle losses to the tunnel walls should decrease the number and volume

concentration. But at the same time, condensation and adsorption/absorption of vapors should increase the particle volume concentration. Moreover, a significant number of particles that were originally too small to be measured by the SMPS may undergo condensation, adsorption/absorption, and coagulation to such an extent that they grow into the SMPS measurement range, thereby increasing the measured number concentration at the same time as they increase the volume concentration. (Although it may also happen that large particles grow out of the SMPS measurement range, the condensation and adsorption/absorption rates scale with available surface area and thus favor the greatly more populous ultrafine particles, as opposed to the scarce large particles. Similarly, the coagulation rate scales with number density squared and thus favors the ultrafine particles.) The net result is that, even though particles may be lost to tunnel walls, the volume (or mass) concentration should increase due to the other mechanisms of particle dynamics.

Experimentally measured PM concentrations are plotted in Figure 4.6, as are curves representing the average concentrations measured at each location. Number-weighted particle concentration decreases by 3% during the 2 meters of travel, as calculated from the slope of the best-fit line through data from ten tests. Volume concentration increases by 12%, calculated in the same manner. Clearly, the magnitude of changes in particle concentrations due to particle dynamics is small compared to the scatter. Thus, the data cannot corroborate whether PM number concentration truly decreases because of losses and coagulation and whether volume concentration increases because of the combination of particle dynamic mechanisms. Nor does the data suggest whether there is a minimum time required for particulate-laden exhaust and diluent air to mix; rather, the time it takes for particle dynamics in the recently-diluted exhaust to equilibrate may be less than or approximately equal to the time required to travel from the initial mixing location to the first sampling location (about 1/3 of a second).

Experimentally measured characteristic PM sizes are plotted in Figure 4.7. Again no statistically significant trend can be observed. Standard deviations of mean particle sizes (number- or volume-weighted) range from 3 to 6% of the average measured value. Standard deviations of mode particle sizes (number- or volume-weighted) range from 2 to 8% of the average measured value. Hence, mean particle sizes do not have statistically significant variation (with 95% confidence) compared to the 3% uncertainty, nor do mode sizes compared to the 10% uncertainty.

Hildemann *et al.* used a similar dilution tunnel with diameter 15 cm and Re = 10000 to isolate and measure particle losses. Particles of known sizes (1.3 to 6.2 microns diameter) were injected into the dilution tunnel with air lacking condensable material [39]. The measured loss rate was 0.6 to 1.1% per meter of flow. The loss rate for 0.1 micron diameter particles in the present case may be smaller than that for 1.3 to 6.2 micron particles. However, *if* the decrease in number concentration calculated by a best-fit line through the in Figure 4.6 represents a decrease in concentration due to number losses and not mere scatter in the data, then those losses amount to a similar value of 1.5% per meter. These conclusions are specific to the diameter of tunnel used, as discussed above in the Discussion Of Tunnel Design (section 2.3); a smaller tunnel may have more significant losses.

Abbass *et al.* used filter samples in a dilution tunnel operating at 30:1 dilution ratio to measure the increase in mass of PM generated by a diesel engine during transit through the tunnel [18]. Based on their data, approximately 10% PM mass increase occurred within the first approximately 2.3 meters of transit, and 20% by the end of the 3.5 meter long tunnel, which translates to 4 to 6% increase per meter of flow. *If* the increase in volume (or mass) concentration calculated by a best-fit line through the data in Figure 4.6 represents a increase in concentration due to adsorption/absorption and not mere scatter in the data, then that increase amounts to a similar value of 5% per meter.

Qualitative implications on SI engine exhaust that can be ascertained from the insignificant decrease in number concentration of CI-generated PM along the tunnel are the following. The degree of particle loss and coagulation should constitute a similar fraction of the total particulate number for SI engines as for the present CI engine, since losses and coagulation depend only on flow conditions and the number concentration of particles. Engine/tunnel flowrates are held fixed, regardless which engine is used, and diluted exhaust temperatures are between 300 and 325 K for all conditions encountered using both engine types; thus, differences in flow conditions are not significant. And, as discussed above, the number concentration of particles using the CI engine is within the range of those encountered for a SI engine. Therefore, losses and coagulation for SI engine exhaust diluted in a similar fashion should be indistinguishable from noise.

On the other hand, volume (or mass) accretion by condensation, adsorption, and absorption should be more significant for SI "engine-out" exhaust (i.e., non-catalyzed exhaust) than for CI exhaust because the

HC vapor concentration is on the order of five times higher [50], and therefore the adsorption/absorption rate should be five times higher, following the work of [16]. Hildemann *et al.* chemically analyzed post-dilution PM generated by SI engines during the Federal Test Procedure and found that 38 to 75% of the total mass comes from organic carbon (much of which attaches to particle nuclei as a result of adsorption/absorption) [34]. If 12% of the CI particle volume (or mass) is accreted during the dilution process (i.e., *if* the 12% fractional accretion measured in the present experiment can truly be attributed to growth and not uncertainty), and if the adsorption/absorption rate is five times higher for SI engines [50], then approximately 40% (60% divided by unity plus 60%) of the PM mass for SI engines should be due to adsorption/absorption of vapors in the dilution tunnel. Forty percent accretion is approximately consistent with the 38 to 75% measured by Hildemann *et al.* [34].

4.5 Comparison Between Filter Analyses and SMPS

In an attempt to confirm SMPS measurements, PM volume concentrations measured with the SMPS are compared to PM mass concentrations measured via gravimetric filter analysis. (The scaling factor between the two measurements is particle density, taken to be approximately 2,000 kg/m^3 as discussed previously.) Although filters are collected concurrently with SMPS measurements, the concurrence introduces no error to the SMPS measurement and no more than a 2% error in filter measurements (2% being the fraction of flow diverted out of the dilution tunnel to the SMPS before reaching the filters).

In experiments where the SMPS measures orders of magnitude variation in PM volume concentration with respect to variations of an engine operating condition (example, PM as a function of equivalence ratio or spark timing), filter analyses measure data scattered by ±20 to 30% about a single PM mass concentration. Figure 4.8 shows a comparison of concurrent SMPS and filter measurements, with SMPS measurements scaled by 2,000 kg/m^3. Unless the actual PM density changes in such a way to offset changes in PM volume concentration (and there is no reason to believe that PM density changes by orders of magnitude when engine parameters such as equivalence ratio or spark timing change), the error must lie in one or the other measurement technique.

Filter analyses are deemed faulty because of HC adsorption on the filters. Measurement of HC concentrations upstream and downstream of filters show as much as a 20% decrease in the case of glass-fiber filters and 2% decrease in the case of Teflon filters. A deposition rate of 20% of HCs is approximately 3000 times the expected mass deposition rate of PM (given the PM concentrations measured by the SMPS and the assumed density), such that the HC mass trapped on the filters overwhelms the PM mass. Consequently, gravimetric filter measurement of PM mass is impossible in the HC-rich exhaust streams of uncatalyzed gasoline engine exhaust. As a result of the inaccuracy of gravimetric filter measurement, filter results are deemed non-quantitative, so only SMPS data are presented in the results sections of the present paper.

Also plotted on Figure 4.8 is a threshold value corresponding to the amount of HC mass per unit volume of diluted exhaust flow generally trapped on the glass-fiber filters. If the full 20% of the HCs were trapped on the filters, then the filters observed concentration of HCs plus PM would be approximately 80,000 $\mu g/m^3$. The fact that the observed concentration is significantly less — closer to 12,000 $\mu g/m^3$ or about 15% of the value of the full 20% of HCs were adsorbed on the filters — indicates that the rate of HC adsorption starts out as high as 20% when the filter has little HCs, but drops as adsorption sites get filled. As a result, the final mass of HCs and PM trapped on the filters is about 3% of the HC mass passing through them.

Additional evidence that HCs adsorbed to the filters is the fact that matter trapped on the filters is volatile like gasoline, and often has the same yellowish color as gasoline. Although opacity measurements (like the Bosch Smoke Test) are not used in this research, they may prove more effective than gravimetric filter tests. Specifically, when the SMPS registers high PM volume concentrations, filters often obtain a greyish or blackish hue. Conversely, when the SMPS registers low PM concentrations, filters remain white or turned the yellowish color of the fuel. Quantitative measurement of PM via opacity techniques is beyond the scope of the present research.

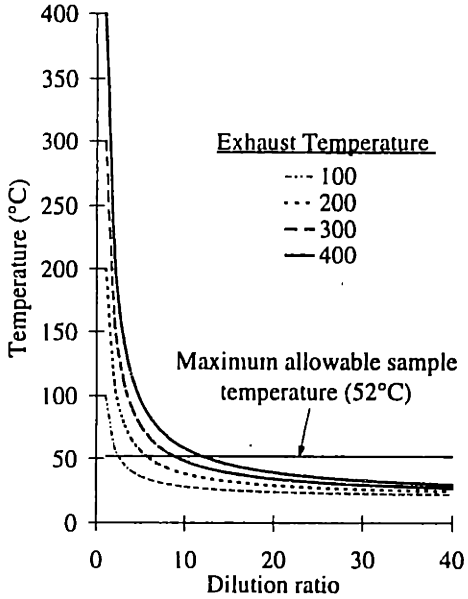

Figure 4.1 Calculated diluted exhaust temperature as a function of dilution ratio for four exhaust gas temperatures, assuming constant specific heat and adiabatic mixing.

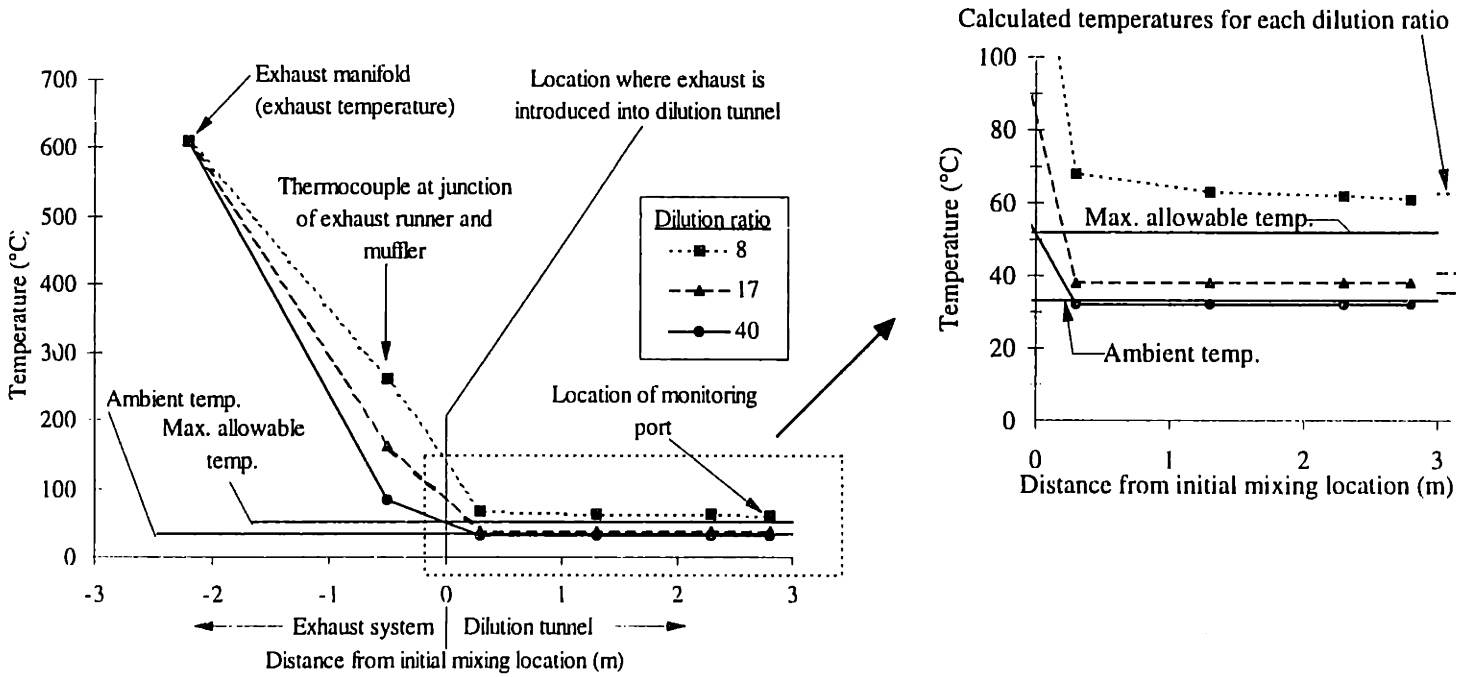

Figure 4.2 Measured temperatures at various points in the experimental setup: exhaust port, end of exhaust pipe, and four locations in the dilution tunnel, plus blow-up of temperatures in the dilution tunnel. Calculated temperatures of diluted exhaust (presented in the blow-up) are taken from Figure 4.1 for the corresponding exhaust temperatures.

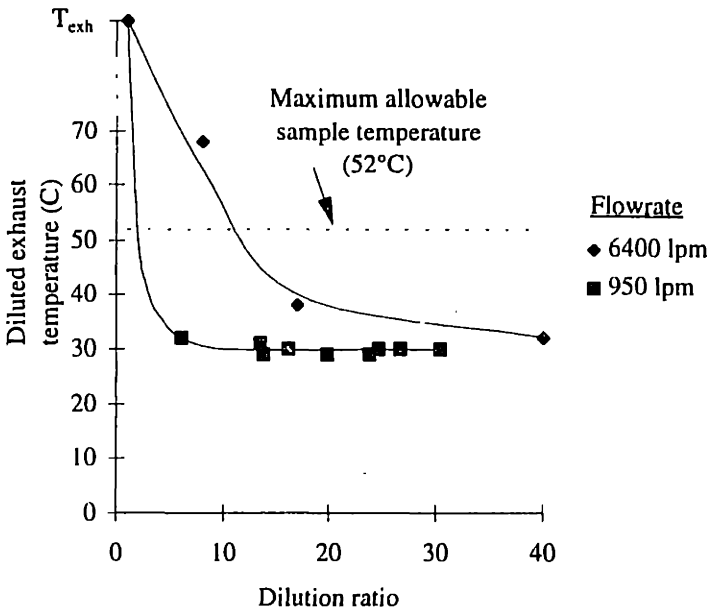

Figure 4.3 Measured diluted exhaust temperatures at the monitoring port location (2.8 meters downstream of the mixing location) as a function of dilution ratio for diluted exhaust flowrates of 950 and 6400 lpm. Curves represent approximate fits to data.

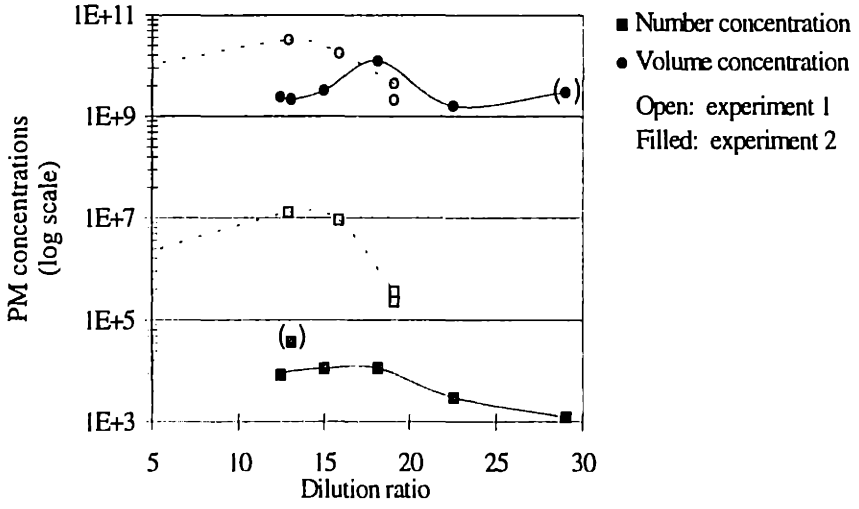

Figure 4.4 PM concentration versus dilution ratio for SI engine, Re ≈ 57000. Open symbols and dashes show data from experiment 1: 2000 rpm, 0.4 bar IMAP, standard engine fuel injection controller. Filled symbols and solid lines show data from experiment 2: 2000 rpm, 0.3 bar IMAP, computerized proportional/integral (PI) fuel injection controller. Concentrations are corrected for dilution ratio, and therefore reflect only the effect of particle dynamics on the engine-out concentrations. Units of number concentration are particles/cm^3, volume concentration nm^3/cm^3. Bracketed data are outliers.

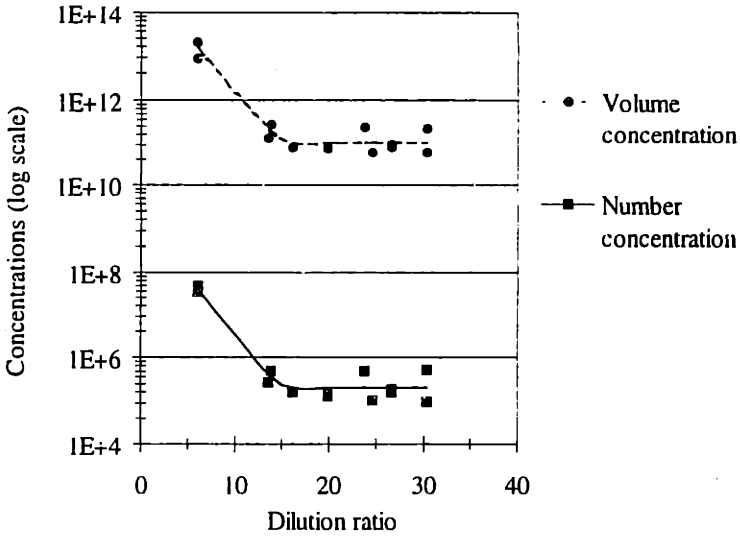

Figure 4.5 PM concentrations versus dilution ratio for SI engine, Re ≈ 9000. Engine operating conditions: 2000 rpm, 0.4 bar IMAP, standard engine fuel injection controller. Concentrations are corrected for dilution ratio, and therefore only reflect effect of particle dynamics on the measured engine-out concentrations. Units of number concentration are particles/cm^3, volume concentration nm^3/cm^3.

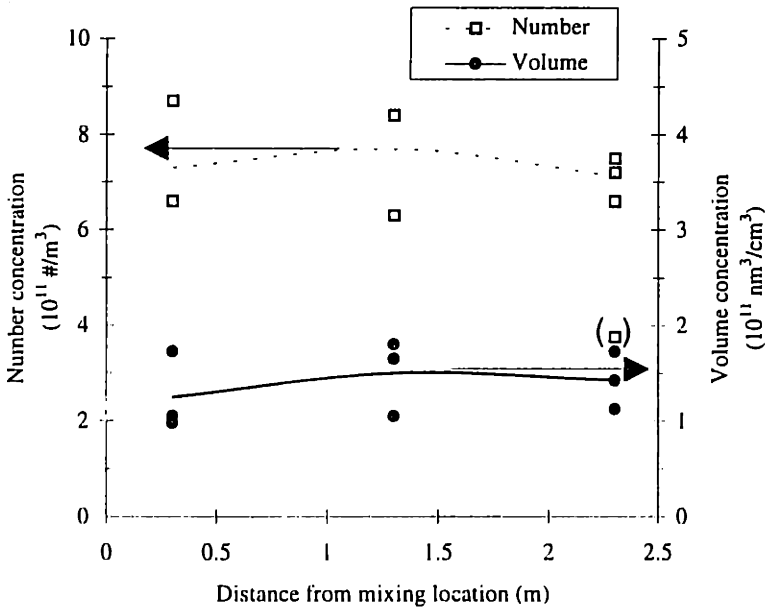

Figure 4.6 Particle concentrations (number- and volume-weighted) as a function of location within the dilution tunnel. Curves represent average of data at each location. Dilution tunnel flowrate = 950 lpm, Re = 9000. Dilution tunnel temperatures held fixed. PM generated by diesel engine. Uncertainty in measurements of number concentration is 20%, in volume concentration is 25%.

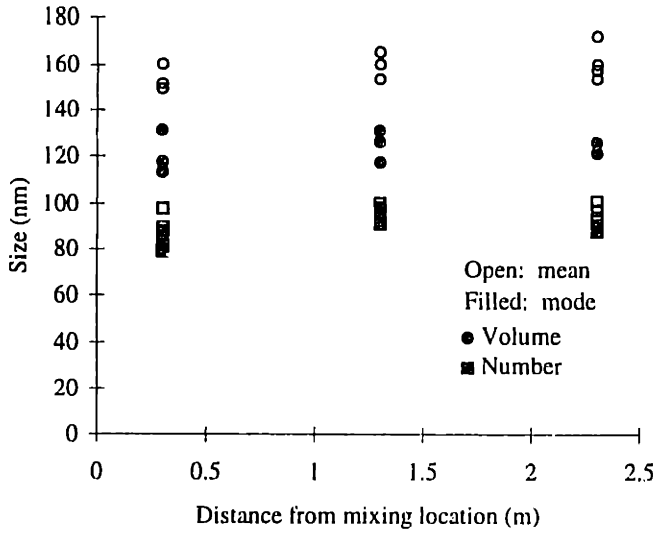

Figure 4.7 Particle sizes as a function of location within the dilution tunnel (same conditions as in previous figure). Uncertainties in measurements of mode sizes are 10%, those in mean sizes are 3%.

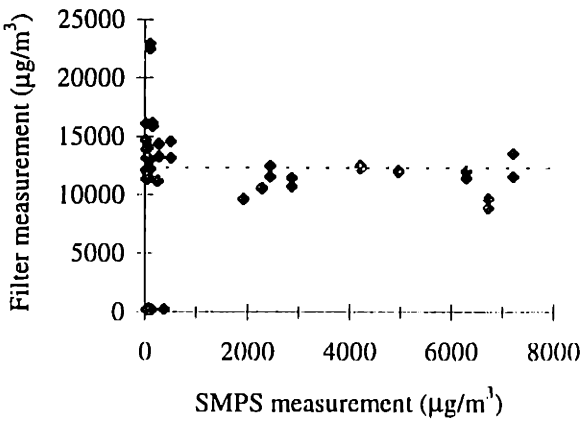

Figure 4.8 Comparison of concurrent SMPS and filter measurements. Several engine operating conditions: equivalence ratios from 0.7 to 1.3, spark timings from 5 to 55°CA BTC, EGR from 0% to 100% of amount needed to stall engine. Dilution ratio: 15 ± 2. Filter collection time: 50 minutes. Only glass-fiber filter measurements presented. Threshold (dotted line) corresponds to approximately 3% of HCs being adsorbed on filters, as discussed in the text.

CHAPTER 5

RESULTS OF STEADY STATE ENGINE EXPERIMENTS

5.1 Experimental Methodology and Conditions

A series of experiments were performed to characterize the effect of engine, fuel, oil, and catalyst parameters on number- and mass-weighted PM emissions as well as particle sizes. The experimental matrix of operating conditions centers about the "baseline operating conditions" listed in Table 2.2. Table 5.1 lists the parameters varied in the test matrix and the values assigned. Some tests in the matrix were performed on the Ford Zetec engine and some on the Saturn engine, with two sets of tests performed on both engines in order to compare their respective emissions; the comparison will be discussed in section 5.2. The lubricants used in both engines were *SAE* 30 weight oils, although the Ford engine used a 5w-30 supplied by the manufacturer and the Saturn a 10w-30. Because emissions from the two engines are compared only for warmed-up operation (oil temperature = 87°C), the difference between winter weight specifications is not deemed relevant.

Table 5.1 Parameters varied about the baseline conditions (symbols defined previously)

Parameter	**Value**
Engine speed	1500, 2000, 2500 (± 10) rpm
IMAP	0.4, 0.7, 1.0 (± 0.04) bar, absolute
ϕ	0.7 to 1.3 in 0.1 increments
Fuel injection timing	100°CA increments during CVI and 25°CA increments during open valve injection (OVI)
Fuel injection control strategy	Standard Ford engine control strategy (EEC IV) using Heated O_2 Sensor (HO2S) and PI control using UEGO
Spark timing	20°CA before MBT timing to 25°CA after MBT timing in 5°CA increments (from 5 to 55°CA BTC)
Steady state coolant and oil temperatures	34 (± 6) °C or 87 (± 2) °C
EGR rate	0, 25%, 50%, 75%, 100% of that needed to "stall" (i.e., produce no brake torque while dynamometer maintains engine speed at 2000 rpm)
Fuel type	Indolene, propane, isooctane, toluene, and indolene doped with MTBE at 10:1 on a volume basis (all fuels used over range of equivalence ratios specified above)
Lubricating oil composition and viscosity	30 weight mineral oil (10w-30), 40 weight mineral oil (15w-40), and 30 weight synthetic oil (10w-30)
Catalyst	With and without Platinum-Iridium catalyst

Apparatus conditioning was described in Chapter 2; the following is a description of the methodology specific to experiments described in the present chapter. For experiments in which a liquid fuel other than the base fuel (indolene) was used, the fuel system was purged of indolene prior to experiments using a flush-fill-flush technique. The old fuel was drained from the gas tank and from purge valves upstream of the fuel pump and filter. Next the engine was operated on what little fuel remained in the fuel system until it stalled. Then the gas tank was filled with the new fuel, and the fuel return line from the engine was connected to a waste fuel container. The engine was operated on the new fuel for several minutes, while the fuel returning to the waste fuel container was visually examined. Since indolene is yellow, while toluene and isooctane are clear, the visual examination was deemed sufficient to determine whether the toluene or isooctane successfully purged the isooctane. However, in the case where the fuel system was purged of indolene and replaced by indolene doped with MTBE the visual examination could not be used to discern whether the new fuel had completely purged the old. Consequently, the engine was motored by the dynamometer with the fuel pump and injectors operating for approximately five minutes beyond when it stalled, in order to insure that all fuel had been drained; then gas tank and fuel lines were filled with indolene doped with MTBE and the procedure was repeated. After experiments with the non-baseline fuels were completed, the fuel system was drained in a similar manner and flushed with indolene. For experiments using propane fuel, propane was metered into the intake manifold with the fuel injectors disconnected.

For experiments in which an oil other than the base oil (conventional 30 weight mineral oil) was used, the oil was purged using the flush-fill-motor-flush-fill technique. The engine was drained of oil by opening the sump and manually operating the oil pump. Then the old oil filter was replaced with a new one, and the oil system was filled with the new oil. Next the dynamometer motored the engine at 2000 rpm for fifteen minutes, with the oil pump and oil heater operating. At the end of fifteen minutes, the procedure was repeated, using a fresh supply of oil and a new oil filter. Finally, the engine was fired at the baseline engine operating conditions with the oil heater operating until the oil temperature reached 87° ± 2° C, at which point testing began. Prior to experiments, the used conventional 10w-30 mineral oil that had previously been in the engine was drained following the above procedure, and the oil system was refilled with a fresh

supply of the same oil. Tests were performed in the following order: conventional 10w-30 mineral oil, then conventional 15w-40 mineral oil, then synthetic 10w-30 oil.

In order to test the efficiency of the catalytic converter at eliminating PM, the Ford Zetec engine was operated at three speeds and three loads (for a total of nine points) with either a Platinum-Iridium catalytic converter between the exhaust manifold and the muffler or with a section of stainless steel tubing of equal length in its place. When the catalytic converter was used, it was wrapped in heater tape and electrically heated, although the exhaust temperature and flowrate were the main factors determining the catalyst temperature. Catalyst temperature was measured with a thermocouple mounted between the two catalyst blocks, halfway between the entrance and exit of the catalytic converter. Emissions were measured only once the thermocouple registered a steady state temperature. Tests with and without the catalyst were performed on different days because pipes in the exhaust system could not be disassembled when hot. Comparison between PM emissions on the two days (with and without the catalyst) are present with the caveat that the effect of the catalyst on PM may be masked by day-to-day variability. As discussed previously, PM concentrations measured with and without the catalytic converter are considered to differ by a statistically significant amount relative to the large day-to-day variability only if measurements differ by two orders of magnitude.

5.2 Effect of Engine Parameters on PM Emissions

PM AS A FUNCTION OF EQUIVALENCE RATIO

In experiments where the fuel/air equivalence ratio (ϕ) is varied while MBT spark timing is maintained, PM number and mass concentrations are a minimum at approximately stoichiometric ($\phi = 1.0$) and increase as ϕ is made either lean or rich (Figure 5.1). As opposed to HC emissions (Figure 5.2), which vary by less than an order of magnitude over the range $\phi = 0.7$ to 1.3, PM number and mass concentrations vary by one and two orders of magnitude, respectively. (The difference between the increases in number and mass concentrations is due to the change in particle sizes with respect to ϕ, as will be discussed.) Experiments by other researchers have shown that PM emissions from SI engines reach a minimum at

approximately 10 to 20% lean of the stoichiometric air/fuel ratio, and increase at rich or extremely lean ϕ [24, 26].

Experimental measurement of the variation in PM emission with respect to ϕ was performed on both the Ford and the Saturn engines. In the experiment on the Ford engine, the dilution ratio of 15 was originally thought to be so high that it would result in a low signal to noise ratio at the ϕ with the minimum PM concentration; consequently, for this experiment a dilution ratio between 8 and 9 was used. Data are corrected for dilution ratio in order to represent PM concentration per unit of exhaust gas cooled to STP, according to equation (3.3). In order to verify (a) that the choice of dilution ratio does not significantly affect PM concentrations and (b) that the trend in PM as a function of ϕ measured on the Ford engine is consistent with that measured on other engines, the experiment was repeated on the Saturn engine, this time with a dilution ratio of 15. Figure 5.1 shows both sets of data, corrected for dilution ratio. The behavior — minimum measured emissions at (or within 10% of) stoichiometric and increased emissions at lean or rich ϕ — are consistent, as are the magnitudes of the corrected PM concentration.

A combination of mechanisms contribute to the behavior of PM with respect to equivalence ratio: nucleation, oxidation, and growth. Particle nucleation is affected by temperature and the availability of particle precursors, such as liquid fuel droplets or pools, fuel-rich regions, and products of incomplete fuel oxidation. Similarly, oxidation is affected by temperature and oxygen availability. Growth is affected by the amount of HCs available for adsorption/absorption, the amount of surface area available on which HCs can adhere, and the number of particles with which any one particle can coagulate. The following discussion details the effects of air/fuel ratio on these various mechanisms and the factors controlling them.

Formation of particles in gas phase reactions depends on soot precursor availability and temperature. As the fuel/air ratio is increased, greater HC concentrations in the flame lead to greater concentrations of soot precursors. Moreover, as the fuel/air ratio is increased from $\phi = 0.7$ to 1.1, cylinder temperatures increase: for example, peak flame temperature (estimated using the GM Engine-Simulation Program [51][2]) increases from about 2350 K to 2600 K (Figure 5.3). But as ϕ is increased from 1.1 to 1.3,

[2] Although the GM Engine-Simulation Program simulations were performed based on isooctane fuel, peak flame temperature varies by no more than 3% or 100 K at any given ϕ between indolene and isooctane [52].

peak cylinder temperatures decrease by 70 K (Figure 5.3). The combined result of the soot precursor availability and temperature (as discussed in the modeling section of the present paper) is that peak particle formation via gas phase reactions occurs at ϕ = 1.2, and monotonically decreases on either side of that value. While these gas phase reactions explain the general increase in PM as ϕ increases up to 1.2, the model (presented in an upcoming section) suggests that liquid fuel combustion is the cause of increasing PM as ϕ is decreased below 1.0.

Formation of particles in heterogeneous phase reactions — i.e., generation of particles from burning droplets or pools of liquid fuel — depends on the availability of the liquid fuel and oxygen necessary for combustion, as well as on the temperature necessary to ignite the mixture. Witze and Green have used optical techniques to show that pool fires can occur after flame passage when temperatures are high but oxygen concentrations are significantly lower than in the unburned charge [28]. According to the model, the probability that a liquid fuel droplet or pool will ignite in the post-flame environment is so strongly dependent upon post-flame oxygen concentration that ignition is several orders of magnitude more likely at ϕ = 0.7 where post-flame oxygen mole-fraction is approximately 7% than at 1.0 where oxygen mole-fraction is 0.7%, despite approximately 30% less liquid fuel and the 230 K lower flame temperature (Figure 5.3) [51]. Since formation of PM from a liquid fuel requires that the liquid ignite (rather than escape the combustion chamber completely unburned), and the concentration of post-flame oxygen required for ignition decreases monotonically with increased ϕ, PM concentrations formed by heterogeneous phase reactions decrease monotonically with increased ϕ.

Particle oxidation follows an Arrhenius dependence on oxygen concentration and temperature. Although in-cylinder temperatures reach a maximum at ϕ = 1.1, oxygen availability is a maximum at the minimum ϕ and decreases monotonically with increased ϕ (Figure 5.2). The result of this competition between temperature and oxygen availability, based on calculations following the model presented in Chapter 7, is that the fraction of PM oxidized is a maximum at the leanest ϕ and decreases monotonically as ϕ is increased.

Thus engine-simulation results using isooctane fuel should be generalizable to indolene. The same applies to the other fuels used in the present project, as well.

Growth of particles via adsorption/absorption depends primarily on the availability of HCs and PM surface area. Adsorption/absorption, as modeled by for vapors on plane surfaces by Langmuir and adapted for HCs on diesel particles by Plee and MacDonald [16, 53], is enhanced by low temperatures and high concentrations of both unburned HCs and particle surface area. While adsorption/absorption begins as soon as particles and vapors are brought in contact inside the combustion chamber, it contributes most substantially to PM mass when the exhaust is cooled and diluted. But regardless of ϕ, the exhaust is diluted to approximately 30°C in the dilution tunnel, so temperature should not affect the relative amount of adsorption/absorption as a function of ϕ. Rather, HC availability in the dilution tunnel (which, at fixed dilution ratio, is a minimum at $\phi = 0.8$ and is proportional to mole fractions shown in Figure 5.2) and the amount of surface area on which adsorption/absorption can occur (which is proportional to the amount of particles nucleated minus the amount oxidized) govern the amount of mass accreted. Growth via coagulation of particles scales with the number of particles squared: thus like mass accretion via adsorption/absorption, coagulation depends strongly on the number of particles nucleated and results in ever increasing sizes of aggregate particles. Therefore, coagulation should cause the most growth at the leanest and richest air/fuel ratios. In summary, cases with the highest concentrations of particles and HC before the growth processes should yield the highest PM mass concentrations after the growth processes; the end product from the formation, adsorption, absorption, and coagulation processes is the final PM concentration shown in Figure 5.1.

Comparison of mean and mode particle sizes at the various air/fuel ratios corroborates the above explanation of PM emissions (Figure 5.4). On a number-weighted basis, the minimum particle sizes occur at $\phi = 1.0$ to 1.1, while particle size increases by as much as a factor of three at both rich and lean equivalence ratios, presumably because of coagulation and adsorption/absorption, as discussed above. By contrast, measured mass-weighted mean and mode sizes are scattered enough that that no trends are apparent, possibly because of the limited SMPS measurement range: it cannot measure the few massive particles that may dominate volume (or mass) measurements.

The occurrence of minimum PM emissions stoichiometric air/fuel ratio suggests that PM emissions can be minimized by tightening the control of air/fuel ratio around $\phi = 1$. A test was performed in order to

confirm this: two engine control strategies were employed, one allowing larger ϕ fluctuations than the other, but with all other conditions (including spark timing) fixed. In one case, the standard Ford engine controller (the EEC IV) was used with the standard heated oxygen sensor (HO2S), and in the other, a computerized proportional/integral (PI) controller with a universal exhaust gas oxygen (UEGO) sensor. The PI controller with the UEGO sensor allowed ϕ to fluctuate within about $\pm 1\%$ of stoichiometric, while the EEC IV with the HO2S allowed ± 2-3% fluctuation. PM number concentration is a factor of 7 lower (as measured in repeated tests) with the PI controller than with the EEC IV controller; mass concentration is a factor 10 lower; HC mole fraction is 250 ppmC1 (about 10% of the total HC mole fraction) lower. Number-weighted mean particle sizes are 15% smaller for PI control, presumably due to less HC adsorption, absorption, and coagulation. However, number-weighted mode and mass-weighted mean and mode for the different control strategies are all within 10% of each other, which is within measurement uncertainty. Hence, finer control of ϕ results in smaller, less concentrated particles, as well as less HCs.

PM AS A FUNCTION OF FUEL INJECTION TIMING

The effect of fuel injection timing (particularly, closed versus open valve injection) was investigated by varying the start of fuel injection at 25°CA intervals throughout the OVI period and 100°CA intervals throughout the CVI period. The experiments were performed on the Ford engine which has IVO at 10°CA BTC and IVC at 230°CA ATC, as listed in Table 2.1. Fuel injection timings were corrected by an estimate of the average time necessary for fuel droplets to travel from the injector to the intake valve, assumed approximately equal to the average transit time from intake air from the injectors to the intake valves, based upon an a force balance analysis following Ladommatos and Rose [54], so that injection timings in Figure 5.5 represent the time at which injected fuel hits the intake valves. The air and/or fuel transit time is essentially the distance of travel divided by the average air speed during the intake process, which was calculated using the GM Engine-Simulation Program [51].

HC and PM emissions (Figure 5.5) are insensitive to fuel injection timing during most of the CVI period. However, the injection timing immediately before IVO — shown as 23°CA before IVO on Figure 5.5 — results in 10% higher HC emissions that than the CVI average, while PM number- and mass-

weighted concentrations for this injection timing are both five times the CVI level. During the OVI period, HC concentrations increase by as much as 67% over the CVI level, while PM concentrations on either number- or mass-weighted bases increase by nearly three orders of magnitude. Both HC and PM concentrations have a trough at injection timings about the middle of the intake stroke.

The following is a plausible explanation for the measured trends above. Fuel injected onto the closed valves sufficiently advanced of IVO resides in the intake port long enough to allow vaporization. Thus, for these injection timings, a relatively small amount of liquid fuel enters the combustion chamber, which in turn results in low HC emissions. The fact that HC emissions are insensitive to fuel injection timing during the CVI period at steady state operation has been observed by Arcoumanis *et al.*, Alkidas, and Quader [20, 55, 56]. Analogously, fuel injection timings that allow significant evaporation time likely results in low PM emissions, presumably because of the absence of liquid fuel needed for sooty droplet or pool fires.

By contrast, fuel injected through the open valves has a short-circuit by which it can arrive in the combustion chamber without undergoing vaporization. Meyer and Heywood estimate that as much as seven times more fuel survives in liquid phase until spark ignition if it entered the cylinder via OVI as compared with CVI [57]. A number of studies have shown that OVI leads to higher steady state HC emissions than CVI precisely because of the added liquid fuel present [20, 55, 56, 58]. While OVI leads to high HC emissions by allowing some of the fuel to escape full oxidation in the flame, it generates PM in two ways. Primarily, burning droplets or pools of liquid fuel nucleate particles, as observed qualitatively by Witze and Green [28], and as discussed above in reference to the fuel-lean PM production. Of lesser importance is the fact that liquid fuel does not burn fully and thus leads to HC emissions, which may then adsorb/absorb onto existing particles, thereby increasing their mass. The reason that this mechanism is believed to be of lesser importance is that HC concentration increases by only 67%, while PM concentrations increase by orders of magnitude; if such a small change in HC concentration could create such a large change in PM concentration, then the correlation between the PM and HC emission rates would be stronger than that observed both in past work [12, 19, 20], as well as in the present work (R^2 correlation coefficient between PM and HC concentrations for the experiments described in the present paper is approximately 0.2, as will be discussed in Chapter 6). As for other PM formation mechanisms, fuel injection timing has a negligible

effect on cylinder temperatures (as demonstrated by the NO_x emissions, which varied by no more than the measurement uncertainty) and thus should not affect the amount of particulate generated through gas phase nucleation reactions, which are Arrhenius in nature [59]. Moreover, the small effect of injection timing on in-cylinder temperature and the lack of significant effect on in-cylinder oxygen concentration should lead to negligible variation in the PM oxidation rate with injection timing.

The trough in HC and PM emissions at 50 to 70°CA appears to be the result of injecting fuel into the fast-moving intake air-stream. High relative velocities result in a high heat transfer rate from intake air to the droplets and hence a relatively high evaporation rate. Moreover, injection into fast moving air streams may facilitate droplet break-up [54, 60], which increases the surface to volume ratio, and thus further enhances the evaporation rate.

Particle sizes vary by no more than the measurement uncertainty when fuel injection timing changes. The lack of variation in particle sizes corroborates the assertion that the difference between emission rates at the different injection timings is primarily due to the number of particles nucleated by burning liquid fuel. That is, if a combination of nucleation and growth mechanisms led to the measured particles, then the particles generated with OVI and thus having the most HC available for growth would be the largest. But the observed insensitivity of PM size to injection timing suggests that no one injection timing leads to more growth than another. Consequently, the amount of nucleation must dominate the observed differences in particle concentrations.

The implications of this test are that direct injection spark-ignition engines — for which the number of liquid fuel droplets inside the cylinder greatly exceeds that in standard PFI engines — should have much higher PM emissions than PFI engines at similar conditions.

PM AS A FUNCTION OF ENGINE OIL/COOLANT TEMPERATURE

In light of research by Williams *et al.* and Maricq *et al.* showing that PM emissions during Bag 1 of the Federal Test Procedure (cold test phase) are higher than those during Bag 3 (warmed test phase) [12, 36], a test was performed in order to measure the effect of steady state coolant and oil temperature on steady state PM emissions. An additional heat exchanger was added to the cooling circuits for the coolant and lubricating oil, allowing the coolant and oil to be maintained at either the baseline conditions or at a

temperature of 34 ± 6°C during steady state operation. The heat exchanger circuits consisted of copper pipes submerged (a) in ice baths in order to maintain the temperature of 34°C or (b) in ambient air in order to maintain the baseline temperature of 87°C. Besides the temperature reservoir in which the heat exchanger circuits were positioned, no changes were made to the engine between tests at the two temperatures, in order to minimize measurement artifacts.

Decreased coolant and oil temperature leads to decreased intake port and manifold temperature by virtue of the added heat transfer to the coolant and oil. However, there is not a one-to-one correlation between decreased coolant/oil temperature and decreased port/manifold temperature, in part because of compression and combustion heating of the intake valves. Nevertheless, decreased coolant and oil temperatures result in lower rates of fuel evaporation in the intake port, thus higher concentrations of in-cylinder liquid fuel; and greater concentrations of in-cylinder liquid fuel have, in the past, been observed to lead to higher HC emissions [29, 61]. Similarly, the added presence of liquid fuel in the cylinder due to cooler component temperatures should produce higher PM emissions, not only because the liquid fuel in the cylinder can burn and produce soot, but also because the increased HC emissions can adsorb/absorb on the particles.

Experimental measurements show that the 53°C decrease in coolant and oil temperature leads to a 20°C decrease in intake port and manifold temperature (as measured with a thermocouple inserted in the intake manifold approximately 11 cm upstream of the port). Figure 5.6 shows that a 53°C decrease in coolant and oil temperature results in a measured 19% increase in HCs, presumably due to the added liquid fuel presence. NO_x emission levels — a surrogate for in-cylinder temperatures — decrease by only 2% from the warm condition to the cold, which is a statistically insignificant decrease compared to the approximate 10% uncertainty. The decreased coolant and oil temperatures result in a 60% increase in mass-weighted PM emissions. (However, number-weighted PM emissions differ by less than the measured scatter.) Mass-weighted particle sizes vary by no more than 14% from the cold conditions to the warm ones, suggesting the difference in mass emission rates is primarily due to a difference in nucleation rates and only secondarily due to a difference in PM surface growth, much like the case where fuel injection timing was varied.

PM AS A FUNCTION OF SPARK TIMING

A test was performed where the spark timing was varied from 5 to 55°CA BTC, with all other conditions held fixed. (The test was performed on both the Ford and Saturn engines; however, the Ford spark timing controller was not found robust enough to vary spark timings beyond 5°CA from MBT. Hence, only results on the Saturn engine, for which the controller is sufficiently robust, are discussed in the present paper.) The effect of advanced spark timing is an increase in number- and mass-weighted PM emissions from spark timings of 5 to 40°CA BTC (the latter of which is about 5°CA advanced of MBT timing), after which further advance results in decreased emissions (Figure 5.7). Similarly, advancing spark timing up to 40°CA BTC results in increased HC emissions; but as spark timing is advanced beyond 40°CA BTC, HC emissions remain constant to within the measurement uncertainty (Figure 5.8).

The effect of spark timing on PM is not as simple as that on HCs: the behavior of HCs with respect to spark timing is consistent with an increased rate of oxidation at the higher post-flame temperatures associated with more retarded spark timings (for example, exhaust temperatures shown in Figure 5.8). On the other hand, the variation in PM concentrations with respect to spark timing reflects the competing effects of both flame and post-flame temperatures on nucleation and oxidation, as well as the effect of HC concentrations on adsorption/absorption. Advancing spark timing results in increased in peak temperature (Figure 5.8) and thus raises the rate of Arrhenius-dependent PM nucleation rates [51]. However, post-flame oxidation in the cylinder can significantly reduce PM concentrations because it too is Arrhenius-dependent [62, 63]. As spark timing is advanced, exhaust temperatures decrease (Figure 5.8), thus slowing post-flame HC oxidation and leaving more HCs available for adsorption/absorption. However, as spark timing is advanced beyond 40°CA BTC, exhaust temperatures decrease no more than the 1-2% measurement uncertainty; consequently, the Arrhenius-dependent rate of HC oxidation does not decrease significantly, resulting in the plateau in HC emissions. So, as spark timing is advanced beyond 40°CA BTC, nucleation rates increase, in-cylinder oxidation rates increase, exhaust oxidation rates remain approximately fixed, and the amount of HCs available for surface growth remains fixed; thus, the fact that PM concentrations decrease suggests that the increase in the particle oxidation rate is greater than that for nucleation. Mean and mode particle sizes vary by no more than 10% and 15% respectively (both on

number- and mass-weighted bases) as spark timing is changed, and no monotonic trend in sizes is observed (Figure 5.9).

PM AS A FUNCTION OF EGR

Experiments were performed in which the level of exhaust gas recirculated to the intake was varied with all other conditions (including IMAP and engine speed) fixed. EGR was varied from the baseline level (no EGR) to the level such that the brake torque produced by the engine was approximately zero. (Even when the engine produces no brake torque, the dynamometer maintains the engine speed at 2000 rpm.) EGR levels are referenced as the percentage of the EGR rate necessary to stall the engine, i.e., produce zero brake torque.

Experimental results show that, as the level of EGR increases, the PM number and mass emissions decrease exponentially (Figure 5.10); number- and mass-weighted PM emissions are two orders of magnitude lower at the maximum EGR case than at the baseline conditions. The number- and mass-weighted emissions have R^2 correlation coefficients of 0.78 and 0.71 for their respective exponential fits, showing that the data has a fair amount of scatter, despite the fact that as many as five measurements were made at each EGR level. The scatter in the data may not be an artifact of the PM measurement process, but may reflect real variability in PM emissions; this conclusion is consistent with the fact that at the high EGR levels used in this experiment, misfires and partial burn cycles are frequent though not necessarily periodic.

The decrease in PM emissions with increased EGR is consistent with the effect of EGR on characteristic temperatures and species concentrations in the engine. Increased EGR results in increased intake port/manifold temperature but decreased flame and post-flame temperatures, as indicated by both direct and indirect measurements. In particular, measured temperatures in the intake manifold increase monotonically from 50°C to 88°C when EGR is increased from 0 to 100% of that needed to stall (Figure 5.11) since the hot exhaust gas is recirculated directly into the intake manifold; thus, increased EGR enhances liquid fuel vaporization rates. On the other hand, peak temperatures decrease, as evidenced by NO_x emissions, which decrease from 2,400 ppm to 25 ppm as EGR is increased (Figure 5.11). While EGR does displace nitrogen and oxygen, the main reason for the decreased NO_x formation is that EGR acts as a diluent and therefore holds the peak cylinder temperatures down [64]. Similarly, as EGR increases, post-

flame temperatures decrease. For example, as EGR is increased from 0 to 100% of the level to stall, measured exhaust port temperature decreases from approximately 560°C to approximately 490°C. Moreover, HC emissions increase from 2,400 ppmC1 to 13,200 ppmC1 (Figure 5.11); the reason for this is two-fold: increased frequency of misfires and partial burn cycles wherein HCs escape oxidation in the flame, plus decreased post-flame and exhaust temperatures during non-misfire cycles, thus leading to decreased post-flame oxidation.

Given these measurements, the theoretical expectation why increased EGR results in an exponential decrease in PM is the following. As more hot exhaust gas is introduced into the intake manifold, the intake temperature rises and results in more rapid evaporation of liquid fuel. Plus, the recirculated exhaust gas displaces fresh charge in order to maintain fixed intake manifold pressure. (Estimates of the burned gas fraction in the cylinder prior to combustion made using the GM Engine-Simulation Code — varying burned gas fraction until spark timing and brake torque matched measured values — are that burned gas fraction increases from approximately 10% in the zero EGR case to approximately 70% in the maximum EGR case [51].) The combination of increased vaporization rate and decreased amount of charge supplied to the engine is that the in-cylinder gas phase fuel concentration decreases by an estimated 2/3, while the in-cylinder liquid fuel concentration decreases by an estimated 80 to 90% (as will be discussed in the model results chapter of the present paper). PM nucleation mechanisms depend strongly on the gas and liquid phase fuel concentrations, as well as temperature according to [59] and the model of PM formation (to be presented in an upcoming section), so that the decreases in concentration of both fuel phases, combined with the decrease in in-cylinder temperatures (discussed above) results in a sharp decrease in PM nucleation with increased EGR.

However, as EGR increases, oxidation rates should decrease and growth rates should increase — effects that compete with the decreased PM nucleation. Specifically, the decreased peak/exhaust temperatures and oxygen concentration result in decreased PM oxidation, since the oxidation rate depends on oxygen and exponentially on temperature, as suggested by [62, 63] and the model to be presented. Further, as EGR increases, exhaust HC concentration increases, so the amount of vapor available for adsorption/absorption increases. However, as EGR increases the increase in vapor available for growth is potentially offset by the decrease in available surface area on particle nuclei. The combined result, as

demonstrated by experimental results (Figure 5.10), is that the decreased nucleation overwhelms the decreased oxidation and potentially increased growth.

While number-weighted mean particle sizes generally decrease with increased EGR, mass-weighted mean particle sizes increase (Figure 5.12). However, neither the number- nor mass-weighted size has a monotonic trend with respect to EGR. Number-weighted mean particle sizes are approximately 40 nm at the zero EGR case and decrease to 20 nm at 75% EGR, but increase to 25 nm at 100% EGR. Mass-weighted mean particle sizes are approximately 100 nm with zero EGR, but increase from 83 nm to 170 nm as EGR is increased from 25% to 100%. The simultaneous decrease in number-weighted sizes and increase in mass-weighted sizes is due to a general though non-monotonic spreading of the size distribution as EGR is increased: the standard deviation of the size distribution is a minimum between 25% and 50% EGR, and increases as EGR is either increased or decreased from those levels.

The spreading of the size distribution is consistent with the following physical phenomena. As EGR is increased, the average size of particle nuclei decreases, presumably for the same reasons that the concentration of nuclei decreases, as discussed above. However, as EGR is increased, the increased HC concentration encourages growth. The particles that are most likely to grow are those with the most surface area: thus the largest particles grow faster than the smaller particles. The combined result of the competing nucleation and growth effects is that nucleation-mode particles are smaller at high levels of EGR than at low level of EGR, while the agglomeration-mode particles are larger at high levels of EGR than at the low levels. The reason why both number and mass-weighted mean particle sizes are smaller at 25% EGR than at zero EGR may be that the decreased size of nuclei (due to decreased liquid and gas phase fuel concentrations as well as decreased temperatures) overwhelms the slight increase in HCs available for growth (2,400 ppmC1 at zero EGR versus 2,550 ppmC1 at 25% EGR).

PM AS A FUNCTION OF ENGINE LOAD

The effect of engine load on PM number (Figure 5.13) and mass (Figure 5.14) emissions was measured at three engine speeds. All conditions besides speed and load were the baseline conditions. (Even though the torque-meter measured MBT spark timing at 7 to 10°CA BTC for the three wide open throttle conditions, light and erratic knock occurred at those conditions.)

As load is increased, PM concentrations increase monotonically. Number concentrations increase relative to concentrations at the baseline engine load by a factor of 7 at 2500 rpm, a factor of 90 at 2000 rpm, and a factor of 430 at 1500 rpm. Mass concentrations increase by 30% at 2500 rpm, by a factor of 80 at 2000 rpm, and by a factor of 370 at 1500 rpm. Measured intake manifold temperature decreases by 4°C as IMAP is increased from 0.4 to 1.0 bar at 2000 rpm. Measured exhaust temperatures increase monotonically by 80 to 120°C as load is increased at all three speeds, and (perhaps as a result of increasing oxidation) exhaust HC emissions decrease monotonically by 390 to 450 ppmC1 (a decrease of 21 to 27% of the average HC mole fractions) at the three speeds.

Increased load may cause increased PM for the following reasons. As load is increased, the mass of fresh charge drawn into the cylinder increases, because intake air and fuel flowrates increase and because the residual gas fraction in the cylinder decreases [65]. But increased intake flowrates result in decreased intake temperatures. The result is that, not only does the concentration of gas phase fuel increase, but so does the amount of liquid fuel, since the liquid fuel is less likely to evaporate due to lower port/manifold temperatures [66]. Moreover, as load increases, peak cylinder temperatures and pressures increase, as calculated using the GM Engine-Simulation Code [51]. Consequently, the amount of particulate nucleated — which depends strongly on gas and liquid phase fuel availability as well as temperature — should increase as load increases. Further, the decreased residual gas fraction and increased cylinder pressure result in higher oxygen concentrations at higher loads; since the probability of liquid fuel ignition and subsequent soot production is strongly dependent on oxygen concentration (as discussed above), the increased oxygen concentration with increased load should further increase the amount of PM nucleated through liquid fuel burning.

Conversely, as load increases, in-cylinder and exhaust temperatures increase as does the partial pressure of oxygen, thus facilitating PM oxidation. Increased load also results in decreased mole fractions of exhaust HCs, thus resulting in a decreased concentration of HC vapor available for adsorption/absorption. Nevertheless, as demonstrated by the general increase in PM with increased load (Figures 5.13 and 5.14), the increased nucleation rate overwhelms the increased oxidation and decreased growth.

Characteristic PM sizes show no universal trends as a function of engine load. Mass-weighted sizes decrease monotonically as IMAP is increased from 0.4 to 1.0 bar, although by different amounts depending on engine speed: by as little as 4%, which is statistically insignificant, to as much as 47%, which is statistically significant. Number-weighted sizes show non-monotonic behavior: increasing with IMAP at some speeds and loads, decreasing at others.

PM AS A FUNCTION OF ENGINE SPEED

In conjunction with measurements of PM at different load conditions, number- and mass-weighted PM concentrations were measured as a function of engine speed at three load conditions (Figures 5.15 and 5.16). Neither the number nor the mass concentration showed a universal, monotonic trend with respect to engine speed.

Increased engine speed results in higher gas temperatures (both in-cylinder and exhaust) [22, 51] and in lower residence times. Higher peak temperatures increase both PM formation and oxidation rates, whereas the reduced residence time limits the duration over which the rates extend. The competing factors are reflected in the rise and fall of PM number concentrations with speed, and in the load-dependent behavior of mass-weighted PM concentrations as a function of speed. HC mole fractions vary by no more than 14% as a function of engine speed, and do not vary monotonically with speed. Therefore, HCs should not contribute to a significant, monotonic trend in growth via adsorption/absorption as a function of speed.

Characteristic PM sizes show no universal trends as a function of engine speed. Number- and mass-weighted sizes increase with speed at some speeds and loads, but decrease at others. As with particle concentrations, the lack of monotonic trends may reflect competing formation, growth, and oxidation mechanisms.

5.3 Effect of Fuel Parameters on PM Emissions

PM number and mass concentrations were measured as a function of fuel/air equivalence ratio for a variety of fuel types. Toluene, isooctane (2,2,4 trimethyl-pentane), and propane were the single component fuels used. In addition to indolene, a multicomponent fuel combining indolene and MTBE at a

10:1 volume ratio was used. (The 10:1 volume ratio is approximately that used in California Phase 2 Reformulated Gasoline to achieve the 1.8%-mass oxygen mandate [67].)

Note that PM concentration using each different fuel except propane was measured on a different day (due to experimental constraints), and that unlike other experiments in the present paper, which were performed entirely during one day, comparison of PM emissions from the different fuels is subject to uncertainty arising from day-to-day variability. (Measurement of PM concentrations using propane fuel did not necessitate flushing the engine fuel system, consequently it could be performed on the same day as measurement using indolene.) The magnitude of day-to-day variability was discussed in the Uncertainty Analysis above, but to reiterate: differences in PM emissions from the different fuels can only be assumed statistically significant if the measured emissions vary by at least two orders of magnitude.

The number- and mass-weighted concentrations (Figures 5.17 and 5.18) using the various fuels have the same general trend as did indolene (shown in Figure 5.1 and discussed above): minimum emissions within 10% of stoichiometric with emissions increasing by as much as three orders of magnitude at rich or lean ϕ. (Data taken with indolene on both the Ford Zetec and Saturn DOHC engines are shown here for comparison.) In general, mass emissions are more sensitive to ϕ than are number emissions, owing to the dependence of PM size on ϕ, which increases away from stoichiometric (Figure 5.19).

The behavior of particle sizes generated by each of the fuels as a function of equivalence ratio (Figure 5.19) is ostensibly like that for indolene. On a number-weighted basis, the minimum particle sizes occur between $\phi = 0.9$ and 1.1, with increases at both rich and lean equivalence ratios. Propane number-weighted mean particle sizes are between 30 and 46 nm, but show more scatter than trend; mode sizes are between 10 and 36, and also show no trend. At all ϕ except 0.7, toluene number-weighted mean particle diameters are larger than those of indolene and the indolene/MTBE blend by a statistically significant margin. Neither propane- nor isooctane-derived particles show a statistically significant difference in mean particle size from indolene or indolene/MTBE particles. On a mass-weighted basis, scatter is large enough that no trends are apparent for the sizes of particles generated by most of the fuels.

CO_2, CO, O_2, and NO_x emissions, measured as a function of ϕ for the different fuels, are similar for all fuels with minor but predictable differences due to the different hydrogen to carbon ratios of each fuel.

HC concentrations were also measured (Figure 5.20); for all fuels, minimum emissions occur at ϕ = 0.8 to 0.9 and increase on either side. Propane has the lowest HC emissions at all ϕ, isooctane the highest at ϕ from 0.7 to 1.0, and toluene the highest at ϕ from 1.1 to 1.3.

The fact that particle concentrations and sizes as a function of fuel/air equivalence ratio for the different fuels generally follow the same trends suggests a general similarity in the PM formation, oxidation, and growth mechanisms for each fuel; the following is a general discussion of the mechanisms and their effects on PM concentrations and sizes, and afterward is a discussion of the implications of the differences between emissions using the different fuels. These discussions extend the information about PM concentrations and sizes using indolene (presented above) based upon conclusions drawn with the help of the PM emission model (to be presented in an upcoming chapter).

Particle nucleation in the gas phase has an Arrhenius rate proportional to the presence of soot precursors and exponentially dependent upon temperature (as suggested by an extension of the model in [59], which will be discussed in Chapter 7). Therefore, gas phase nucleation is enhanced by increased equivalence ratios up to ϕ = 1.2, above which the declining temperatures overwhelm the increasing HC availability, hence causing the formation rate to decrease. Formation of particles in heterogeneous-phase reactions (i.e., when droplets or pools of liquid fuel burn) is enhanced by the presence of liquid fuel plus the oxygen and high temperature needed to ignite the liquid fuel; the PM emission model suggests that the dependence on oxygen concentration is so strong that it overwhelms the dependence upon liquid fuel availability (which varies by no more than 86% across the range of ϕ) and flame temperatures (which vary by 250 K), the net result being that as equivalence ratio increases, the amount of PM nucleated by heterogeneous phase reactions decreases monotonically. According to the model, heterogeneous phase PM nucleation is more significant than homogeneous; however, post-nucleation growth and oxidation result in the fact that experimentally observed PM emissions are a minimum near ϕ = 1.0 and increase at both rich and lean ϕ.

Post-nucleation particulate oxidation depends strongly on oxygen availability, the result (according to the oxidation model to be presented in Chapter 7) being that the fraction of PM oxidized decreases monotonically with increased ϕ. Particulate growth via adsorption/absorption is enhanced by availability of

HC vapors and PM surface area [16]; therefore, maximum growth occurs at the leanest and rich air/fuel ratios used, where both vapor and PM surface area concentrations are high. The combined effects of the nucleation, oxidation, and growth mechanisms account for the behavior of PM concentrations as a function of ϕ for each fuel (Figures 5.17 and 5.18).

As discussed in the case of indolene fuel, particle sizes are largest at the richest and leanest ϕ (for fixed fuel type) presumably because at those ϕ: (a) high HC emissions facilitate growth via HC adsorption/absorption and (b) high concentrations of particles facilitate coagulation. Differences in fuel type at any fixed ϕ generally lead to small and often statistically insignificant differences in particle sizes presumably because fuel type affects the propensity for particles to nucleate via a given mechanism (e.g., the propensity for gas phase soot precursor formation) more than it affects the size of the nuclei generated by the given mechanism. Furthermore, while the extreme rich and lean conditions lead to large amounts of HC adsorption/absorption for all fuels, the amount of HCs available at fixed ϕ does not vary by orders of magnitude between fuels (Figure 5.20); consequently, the mass adsorbed/absorbed on a per-particle basis should not vary significantly between the different liquid phase fuels.

Having discussed the PM formation, oxidation, and growth mechanisms insofar as they generally affect PM emissions for all the fuels, the discussion will differentiate between the particulate emissions for the different fuels, followed by a discussion elucidating further implications toward the processes involved in PM emissions.

Propane emissions — Propane has the lowest PM emissions of all of the fuels tested: from 2 x 10^{-5} times that of toluene to 4 x 10^{-2} times that of isooctane on a number-weighted basis, and 2 x 10^{-6} times that of toluene to 1 x 10^{-3} times that of indolene on a mass-weighted basis at the baseline operating conditions. (Isooctane is the only fuel for which number-weighted PM emissions do not differ from those of propane by a statistically significant margin. On a mass-weighted basis, PM emissions from all fuels differ from those of propane by a statistically significant margin.) Mass-weighted PM emissions from propane at stoichiometric equivalence ratio are so close to the background PM concentrations in the dilution tunnel (themselves orders of magnitude lower than atmospheric particulate concentrations) that when the particle concentration per unit of exhaust gas volume is calculated, which requires subtracting the diluent air

particle concentration from the diluted exhaust particle concentration as per equation (3.3), the calculated concentration is barely discernible from noise. Rather, mass-weighted PM emissions from propane at stoichiometric equivalence ratio are so low that it cannot be conclusively stated that propane forms any particles at this ϕ. The virtual lack of exhaust particles implies two things. Firstly, either the stock intake air filter sufficiently filters ambient-air particles or those particles are sufficiently burned in the cylinder, such that intake air is a negligible source of particles compared to the amount of nuclei generated by any of the liquid fuels. Secondly, PM emissions derived by oil consumption — i.e., emissions of partially burned oil droplets — are negligible in comparison in comparison to those derived by fuel consumption. The second conclusion is valid only for the conventional lubricating oil used in this experiment; the effect of oil type and viscosity will be discussed in an upcoming section. However, this conclusion can be extended to all fuel types: oil consumption is independent of fuel type, so if it is negligible with one fuel type, it is negligible with all.

Toluene emissions — Toluene results in the highest PM emissions of all of the fuels tested: from 15 times that of indolene to 4×10^4 times that of propane on a number-weighted basis, and 90 times that of indolene to 5×10^5 times that of propane on a mass-weighted basis at the baseline operating conditions. (Number-weighted PM emissions from toluene differ from those of isooctane and propane by a statistically significant margin, while mass-weighted PM emissions from toluene differ from those of all but indolene by a statistically significant margin.) Toluene emits high PM concentrations because of two factors: (a) gas-phase particulate formation, in which partial oxidation of toluene forms benzene followed by growth into PAHs, which facilitate PM nucleation, and (b) toluene is less volatile than indolene (heat of vaporization is 410 J/kg for toluene, compared to 350 for indolene [50]), leading to more liquid fuel droplets/pools in the cylinder, the combustion of which is locally fuel-rich and has been observed to form soot [28]. At the ϕ = 0.7, 1.1, and 1.3 conditions, the SMPS measured particle number concentrations from toluene are 10 to 90% above the SMPS's stated maximum measurable concentration of 10^7 particles/cm^3; although the SMPS software does correct for high concentrations, its accuracy above 10^7 particles/cm^3 is unknown [40]. Increasing the dilution ratio would have remedied the possible instrument saturation problem; however, changing dilution ratio by the required 90% can alter dilution characteristics (diluted exhaust temperature,

as well as particle and HC concentrations), which in turn alters concentrations by as much as an order of magnitude or more (Chapter 4), such that the data may not be comparable to data at the 15:1 dilution ratio. Consequently, measured PM emissions using toluene at ϕ = 0.7, 1.1, and 1.3 must be accepted with the caveat that the measured concentrations may underestimate the actual ones.

Isooctane emissions — Using isooctane, number-weighted PM emissions are a minimum at stoichiometric, but mass-weighted PM emissions are a minimum at ϕ 10% lean of stoichiometric. Moreover, isooctane displays the largest change in PM concentration from minimum to maximum concentration of any fuel tested: more than three orders of magnitude. This may indicate that particle formation from isooctane fuel is significantly more sensitive to oxygen concentrations and liquid fuel availability than in the case of the other fuels. Again, for ϕ = 1.3, the SMPS measured a particle number concentration above its stated maximum measurable concentration so this datum is accepted with the caveat that the measured concentration may be lower than the actual one. The data at this ϕ = 1.3 condition were measured seven times and displayed significantly larger scatter than the typical measurement uncertainty (Chapter 3); the explanation may be the inaccuracy of the SMPS at this condition.

Indolene/MTBE blend emissions — Emissions using the indolene/MTBE blend on the Saturn engine are approximately equal to the concentrations measured using pure indolene on the same engine. (Given the magnitude of day-to-day variations, the observed differences are well within the bounds of uncertainty.) The fact that 9%-volume MTBE dopant does not change the PM emissions either suggests that the dopant does not significantly change either chemical properties (such as the propensity of the fuel to partially oxidize into the acetylene, benzene, or PAHs that nucleate PM) or physical properties (such as fuel volatility), or that the effects of the dopant on chemical and physical properties offset each other.

Comparison between emissions with different fuels — Insofar as is possible, the present discussion attempts to separate the different effects of fuel volatility and chemical composition on PM emissions. Results in section 5.2 showed the strong effect of in-cylinder liquid fuel on PM emissions by virtue of experiments where fuel injection timing was varied (thus varying the time available for fuel evaporation) and where intake temperatures were varied (thus varying the rate of fuel evaporation). In much the same way, the present experiments show the strong effect that molecular weight or boiling point has on PM

formation: since day-to-day variations in PM emissions are much smaller than the difference between PM emissions with propane and isooctane fuels, the orders of magnitude difference in their respective emissions implies a strong effect of volatility and/or molecular weight on PM formation.

One major source of PM — burning liquid fuel — is eliminated by use of propane, by virtue of its gaseous phase. But another major source of PM — gas phase partial oxidation products that combine to form soot — should not be so markedly different for propane and isooctane, given that the structure and concentrations of soot precursors produced by each fuel are comparable, unless because of the fact that the molecular weights of the soot precursors may differ. Specifically, both fuels break down into methane and olefins such as ethylene and propylene, while isooctane also breaks down into heavier paraffins and olefins such as isobutene, plus relatively small amounts of acetylene [21]. Furthermore, the fraction of fuel oxidation products that are soot precursors is similar. In particular, acetylene, an important building block of soot, comprises 2-9% by mass of exhaust HCs for isooctane, compared to 2-11% for propane (as measured by Kaiser *et al.* in the exhaust of a spark-ignition engine at conditions both above and below stoichiometric) [68]. Propane does not produce measurable amounts of aromatics, while less than 1% by mass of the HCs emitted using isooctane are aromatics at the same operating conditions [21, 68]. Although this similarity in fractional concentration of soot precursors in the exhaust does not necessarily indicate a similar disparity in the cylinder or flame, no information suggests that a disparity exists within the flame. Thus isooctane and propane are approximately equally likely to produce a given mass of soot precursors per unit mass of HC produced by partial fuel oxidation; the only difference being that partial oxidation products of isooctane can have higher molecular weights than those of propane [21, 68]. Isooctane does generate higher HC emissions than propane (Figure 5.20); however, differences in total HCs are not found to correlate with PM emissions as strongly as do differences in factors that influence liquid fuel burn-up and gas-phase soot production (correlations between PM and HC emissions are discussed in Chapter 6).

Hence, the virtual absence of PM emissions using propane relative to those using isooctane suggests that either the PM nucleation at sites of burning liquid fuel or PM nucleation from high molecular weight partial oxidation products is what facilitates greater rates of PM nucleation for isooctane than for propane. By contrast, differences in the chemical structure or abundance of HCs cannot account for the vast

disparity in PM concentrations. These implications apply to both number- and mass-weighted PM emissions.

Number-weighted mean particle sizes are between 30 and 46 nm with propane fuel, but may be as high as 80 nm with isooctane fuel, which is a statistically significant difference. The difference in particle sizes is likely the combined result of coagulation and adsorption/absorption: since isooctane-derived particles are more concentrated, they are more likely to coagulate into larger particles. Moreover, since isooctane fuel results in higher HC emissions, isooctane-derived particles are more likely to grow in size via adsorption/absorption of HCs. In summary, molecular weight and boiling point of a fuel can indirectly affect particle sizes, by virtue of the effects on particle and vapor concentrations.

The effect of chemical composition on PM formation may be just as significant as that of boiling point. Although the measured number-weighted PM emissions using toluene and isooctane fuel (which have similar boiling points, as discussed above) are of the same order of magnitude at $\phi = 0.7$ and $\phi = 1.3$, emissions of toluene at all other ϕ are orders of magnitude higher than those of isooctane (a statistically significant difference). Moreover, the mass-weighted PM emissions are more than an order of magnitude higher than those of isooctane at all ϕ (a statistically significant difference from $\phi = 0.8$ to 1.1). Previous research, speciating the emissions when using the two fuels, has shown that the partial oxidation products of toluene are considerably more likely to be soot precursors (acetylene or aromatic compounds) than those of isooctane [21, 68]. Specifically, Kaiser *et al.* speciated the exhaust HCs of a test engine operated on isooctane at both lean and rich operating conditions, and found that only 2-9% by mass of the HCs were acetylene or benzene, while no measurable concentration of other aromatics was formed [68]. On the other hand, in the case of toluene fuel, 96-98% was acetylene or aromatic. Again, although this disparity in fractional concentration of soot precursors in the exhaust does not necessarily indicate a similar disparity in the cylinder or flame, it can be inferred that a similar (if not exactly proportional) disparity exists: toluene is more likely than the paraffin fuels to generate the soot precursors that nucleate PAHs which in turn grow into the particles observed in the dilution tunnel.

By contrast, the similarity between the boiling points of toluene and isooctane (differing by only 12°C [33]) and heats of vaporization (differing by only 25% [50]) indicates that, at identical engine

operating conditions, a similar amount of each fuel should be in liquid phase inside the combustion chamber; hence the likelihood of burning liquid fuel droplets or pools should be the same for each fuel. If, however, the amount of particulate nucleated from a burning liquid fuel droplet or pool depends on the amount of soot precursor produced during the oxidation of that fuel, then the toluene would again be expected to produce more PM. A model for growth via adsorption/absorption presented in Chapter 7, based on the work of Langmuir [53], has been fit with experimental data from the various fuels in the present experiments; the parameters of the model — found via comparison to the experimental data presented here — are identical for the various fuels, which suggests that growth is more strongly dependent upon temperature and vapor concentration than fuel type.

Number-weighted mean particle sizes (Figure 5.19) for toluene are larger than those of isooctane by a statistically significant margin at all ϕ except 1.0, which seems to be an outlying isooctane point. Number-weighted mode particle sizes for toluene are also larger than those of isooctane, but because of the larger uncertainty with mode size measurements, the difference is statistically significant only at ϕ = 0.8, 0.9, and 1.2. Since toluene does not have higher HC emissions at all ϕ (Figure 5.20), the difference in sizes could not be due to a higher growth rate (via adsorption/absorption) per particle; rather, toluene must nucleate larger particles or their sizes must increase due to increased rates of coagulation.

5.4 Effect of Oil Parameters on PM Emissions

Although experiments using propane fuel and the base oil (30 weight conventional mineral oil) show that emissions of oil-derived particles are negligible in comparison to those derived by liquid fuel combustion, an experiment was performed in order to determine whether oil composition or viscosity could measurably affect PM emissions. The experimental procedure was described above. The synthetic 30 weight oil was Pennzoil Performax 100. The conventional (or mineral) 30 and 40 weight oils were generic SAE-certified oils supplied by the author's laboratory supplier, Fleetline of Chelsea, Massachusetts. All experiments were performed on the same day to eliminate artifacts due to day-to-day variability.

Measured PM number- and mass-weighted emissions are equal for both the 30 weight and the 40 weight conventional oils, suggesting that if the inverse relation between exhaust particulate and oil viscosity

observed for diesel engines (as discussed in the Introduction) does hold for SI engines, then the magnitude of its effect is negligible compared to the concentration of fuel-derived particles. Experiments using propane fuel imply that the contribution of oil consumption to PM emissions is negligible for the baseline lubricating oil (the 30 weight mineral oil); given that combustion conditions are identical in the case of the two oils (so fuel-derived particles should be equally concentrated), comparison between the 30 and 40 weight oils suggests that that contribution is also negligible for the 40 weight oil. However, the contribution from oil consumption is not negligible when a synthetic oil is used (Figure 5.21). Specifically, PM number- and mass-weighted concentrations using the 30 weight synthetic oil (same viscosity as the base oil) are 70% higher than those for the mineral oils. HC emissions using the three fuels vary by no more than 3%, which is a statistically insignificant difference.

The trend measured in the present experiments is qualitatively the same as that measured in the past (see Chapter 1). Specifically, the present measurements show a factor of 1.7 increase when switching from conventional to synthetic oil, while Pedersen *et al.* measured a factor of 2.5 to 3 increase [24]. Moreover, the present experiments show a small effect of viscosity on PM emission rates, compared to Pedersen *et al.*'s experiments showing that oil temperature — which affects parameters involved in oil consumption such as volatility and viscosity — does not significantly affect PAH emissions and further suggests that these parameters do not affect PM emissions [24].

While the data in Figure 5.21 suggests that synthetic oil is more readily atomized and burned into a sooty particle, it does not yield information about the chemical mechanism of the atomization/burning process or the difference between that mechanism with the different oil types.

Particle sizes show no distinct trends as a function of oil type. Number-weighted mean sizes are within 8% of each other, while number-weighted mode sizes are within 11%. The number-weighted mean for the synthetic oil is between that of the two conventional oils and does not vary from either by a statistically significant amount. Number-weighted mode is equal to that for the conventional 40 weight and 11% more than that for the conventional 30 weight, which is not a statistically significant difference. Mass-weighted mean sizes using the three oils are within 31% of each other, while mass-weighted modes are within 7%. The mass-weighted mean for the synthetic oil is between that of the two conventional oils: it is 21% larger than that of the conventional 40 weight and 11% smaller than that of the conventional 30 weight

(compared to the 3% measurement uncertainty). Mass-weighted mode for the synthetic oil is equal to that for the conventional 40 weight oil and 7% more than that for the conventional 30 weight, which is not a statistically significant difference. The lack of universal trends in number- and mass-weighted particle sizes for the different oils hinders speculation about differences in particle nucleation, growth, and oxidation mechanisms.

5.5 Effect of Catalytic Converter on PM Emissions

Catalyst efficiency was measured by comparing gaseous and PM emissions at nine speed and load points both with and without a Platinum-Iridium catalyst, as discussed in section 5.1. The flow pattern is different between the straight pipe and the catalytic converter, which may convolute the separate effects of flow pattern and catalysis on particle dynamics. Tests with and without the catalyst had to be taken on different days, so day-to-day engine variability in PM emissions may be a source of error in the estimates of catalyst efficiency. Consequently, the following discussion compares emissions with and without the catalyst, in order to ascertain whether statistically significant differences are observed, with differences between the two cases being listed as a measured "catalytic efficiency" of particulate and gaseous pollutant reduction — the difference between emissions measured with and without the catalyst, divided by the value measured without the catalyst. Because of the limitations of the author's experimental apparatus, the present experiments are described with the recommendation that these experiments be repeated using a blank catalyst rather than a straight pipe (in order to match the exhaust flow patterns in the various conditions) and with all measurements taken on one day (in order to eliminate possible error from day-to-day variability).

While the measured catalyst efficiency is 78 to 99% for oxidizing HCs, 86 to 95% for oxidizing CO, and 98.8 to 99.7% for reducing NO_x (all statistically significant), its measured efficiency at eliminating PM is considerably lower (Figure 5.22). (The fact that the NO_x-reduction efficiency is higher than either oxidation efficiency suggests that, although the oxygen sensors were calibrated, their outputs may have a bias toward lean air/fuel ratios, which is estimated at 0.8% of an equivalence ratio unit based on the work of Kummer [69].) Two separate tests — the results of which are shown in Figure 5.22 and the subsequent figure — have coincident temperatures of 470°C: 1500 rpm, 0.7 bar IMAP; and 2500 rpm, 0.4 bar IMAP.

Particulate data shown at any temperature are the average of all repeated tests at any condition, with any one test being the average of four SMPS size distribution measurements.

The maximum measured efficiency for eliminating PM is 92% on a number-weighted basis and 85% on a mass-weighted basis, although neither value reaches the level of statistical significance (two orders of magnitude difference between measurements). In two cases, the measured number and/or mass concentration is higher *with* the catalyst than without, although the difference is not statistically significant given the magnitude of day-to-day variability. (Catalyst-out emissions at these operating conditions were repeated on the same day of testing, in order to verify the results.)

If the cases where higher emissions were observed with the catalyst than without were not due to day-to-day variability, then they *might* be attributable to particle storage within the exhaust pipes and catalyst. That is, particles might be stored on the walls of flow passages during a period of high PM formation in the engine only to be released at a subsequent operating condition. However, the sequence of engine operating conditions was held fixed for the two tests so that storage and release would be the same with and without the catalyst, albeit with the possible exception of that occurring in the catalyst itself. And since ample time was allowed for conditioning before taking PM measurements (in the case of these experiments, sufficiently more than ten minutes, as compared to the five to six minutes deemed sufficient, as discussed in section 2.4), possible storage/release effects should be minimal. Hence, storage effects are eliminated as the explanation of higher post-catalyst emissions: the remaining explanations being day-to-day variability and possible catalytic enhancement of PM formation and/or growth.

Figure 5.23 shows the change in particle sizes at the various engine operating conditions as a function of the measured catalyst temperature. Changes in particle sizes are displayed as the size of the engine-out (non-catalyst) particles minus that of the catalyst particles, divided by the size of the non-catalyst particles, thereby representing fractional reductions in particle sizes resulting from catalysis (labeled shrinkage on Figure 5.23). Measured fractional changes in the particle sizes — whether statistically significant or not — show more scatter than trend, and show neither consistent shrinkage nor consistent growth.

The theoretical expectation was that catalyst would reduce PM emissions on a mass basis and result in smaller particle sizes, since it oxidizes the HCs that contribute to growth via adsorption/absorption.

Even if the few negative catalyst efficiencies in Figure 5.22 could be attributed to measurement error/variability or outlying data, the results in Figure 5.23 do not support the above conjecture. Rather, other processes — such as coagulation or surface reactions — might be intensified by the flow and temperature conditions in the catalyst to such an extent that they mask the effects of HC oxidation on particle sizes.

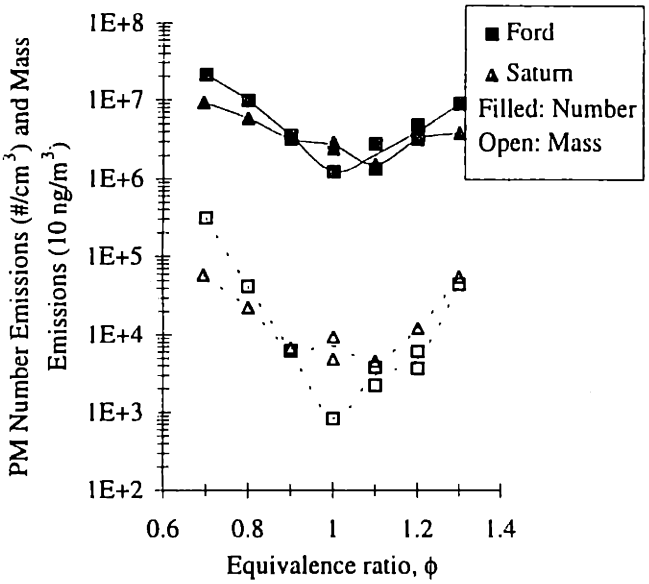

Figure 5.1 PM as a function of fuel/air equivalence ratio. Baseline engine operating conditions except equivalence ratio and dilution ratio, as explained in text. Data taken on both Ford and Saturn engines. Data corrected for dilution ratio, in order to represent PM concentration in the cooled engine exhaust.

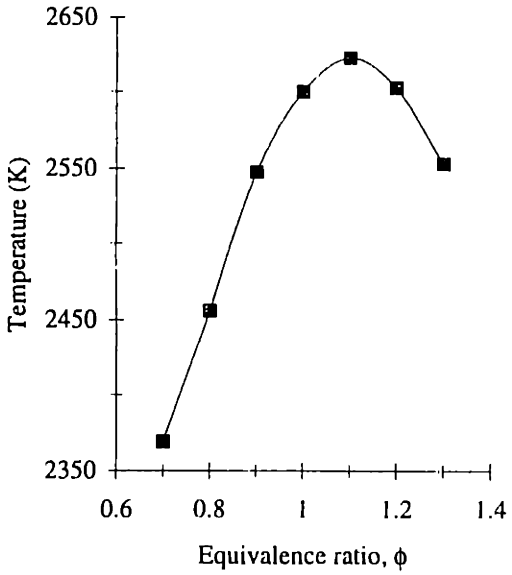

Figure 5.3 Flame temperature as a function of fuel/air equivalence ratio, calculated using GM Engine-Simulation Program [51]. Baseline engine operating conditions except equivalence ratio, iso-octane fuel.

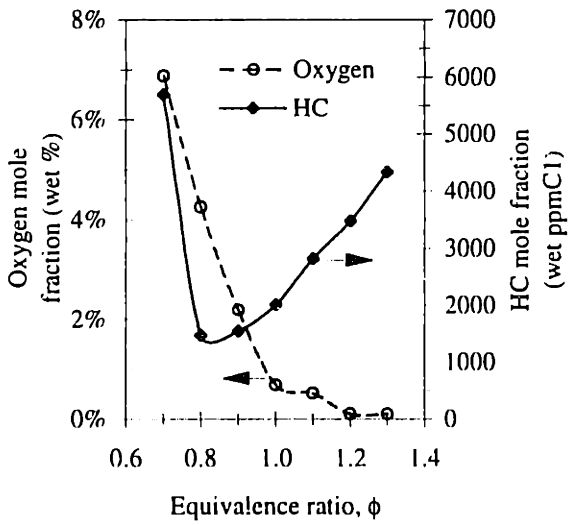

Figure 5.2 HC and oxygen emissions as a function of fuel/air equivalence ratio. Baseline engine operating conditions except equivalence ratio. Emissions were measured on Ford engine and corrected in order to represent mole fraction in the "wet" exhaust gas.

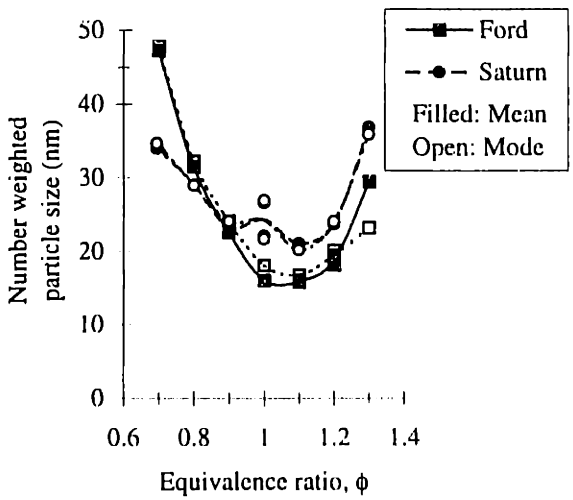

Figure 5.4 Number-weighted mean and mode particle sizes as a function of equivalence ratio, measured on both Ford and Saturn engines. Baseline conditions except equivalence ratio and dilution ratio, as explained in text.

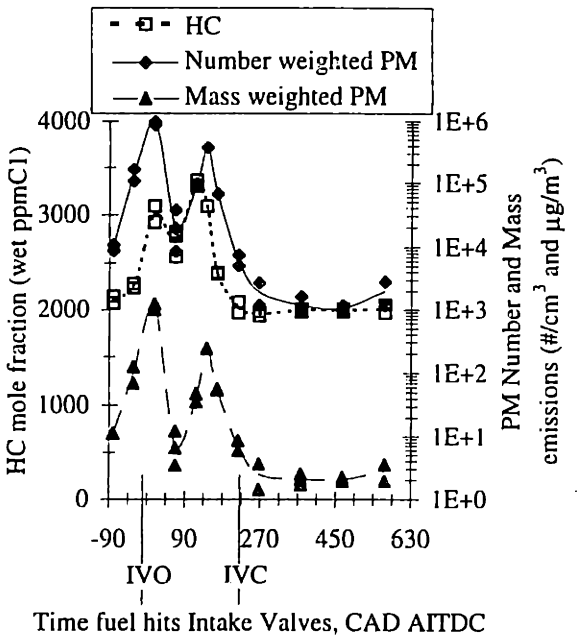

Figure 5.5 HC and PM emissions as a function of the time in Crank Angle Degrees (CAD) after intake top-dead center (AITDC) at which injected fuel hits the intake valves. Baseline engine operating conditions except fuel injection timing.

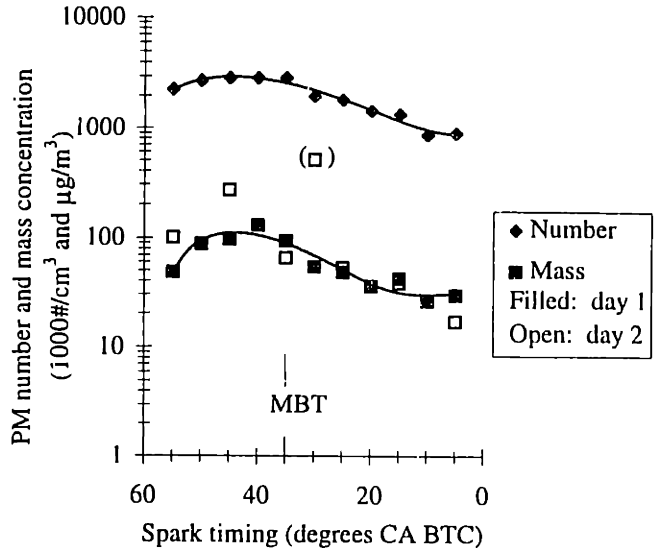

Figure 5.7 PM emissions as a function of spark timing. Baseline operating conditions except spark timing. Tests repeated on two days: data shown as filled and open symbols. Outlier shown in parentheses.

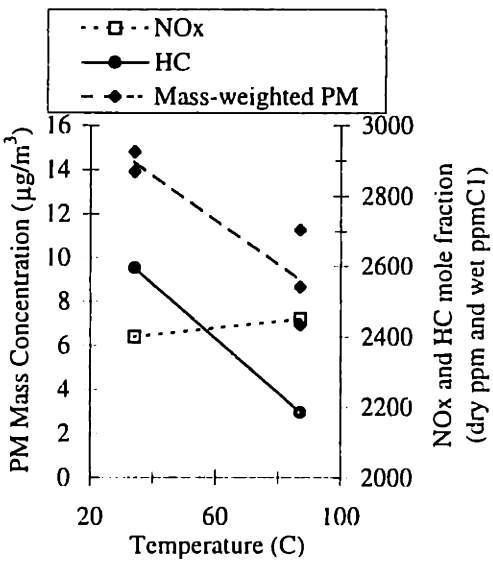

Figure 5.6 HC, NO_x, and mass-weighted PM emissions as a function of coolant and oil temperature. Baseline operating conditions except for coolant and oil temperatures.

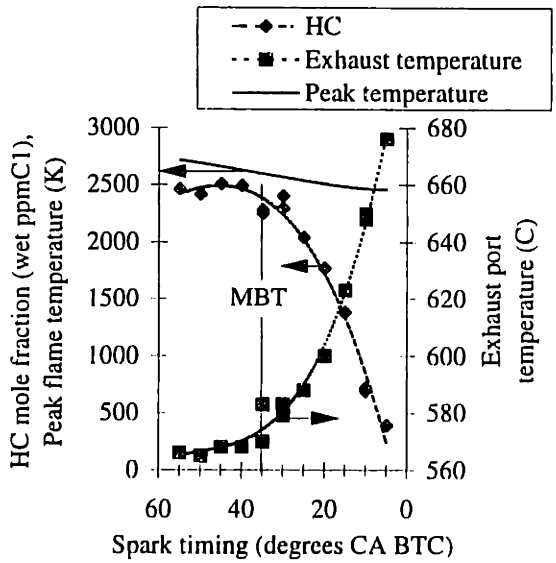

Figure 5.8 HC emissions, peak flame temperature, and exhaust port temperature as a function of spark timing. Baseline operating conditions except spark timing. Symbols represent data; curves accompanying HC mole fractions and exhaust temperatures represent fit to data. Peak flame temperature calculated using GM Engine-Simulation Program [51].

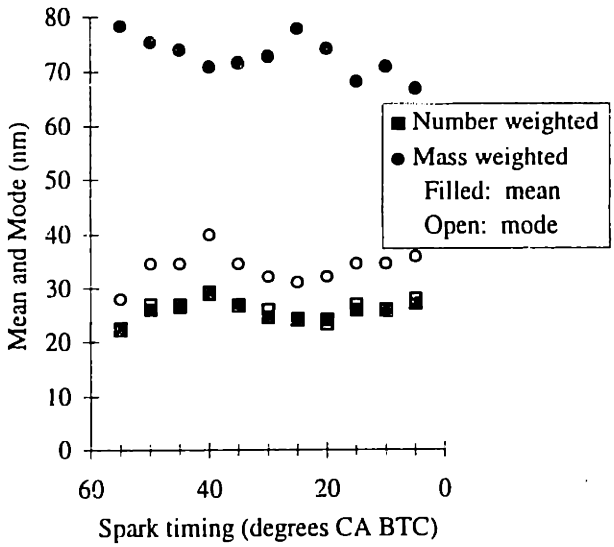

Figure 5.9 Number- and mass-weighted mean and mode particle sizes as a function of spark timing. Baseline engine operating conditions except spark timing.

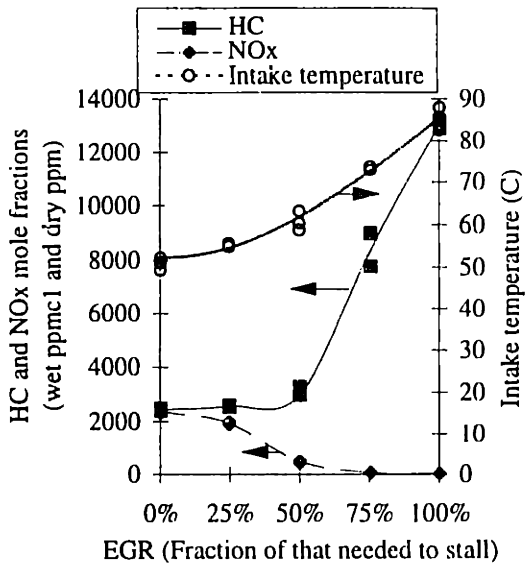

Figure 5.11 Intake manifold temperature, exhaust HC concentration, and exhaust NO_x concentration as a function of EGR rate. Baseline engine operating conditions except EGR rate.

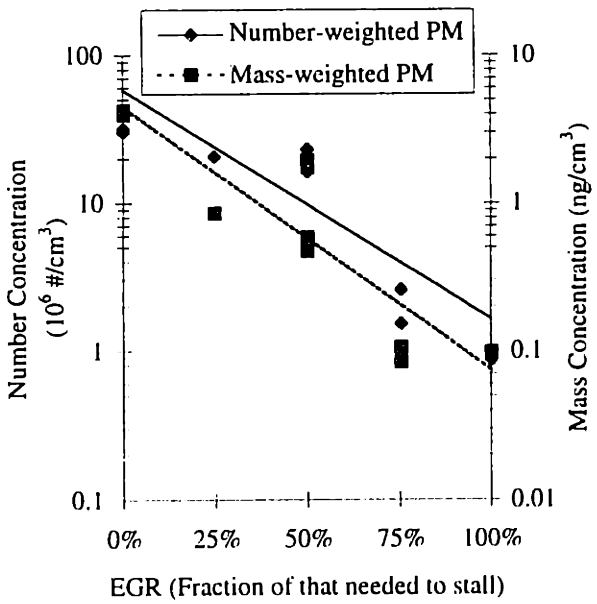

Figure 5.10 Number- and mass-weighted PM emissions as a function of EGR rate. Baseline conditions except EGR rate. Lines represent fits to data, described in text.

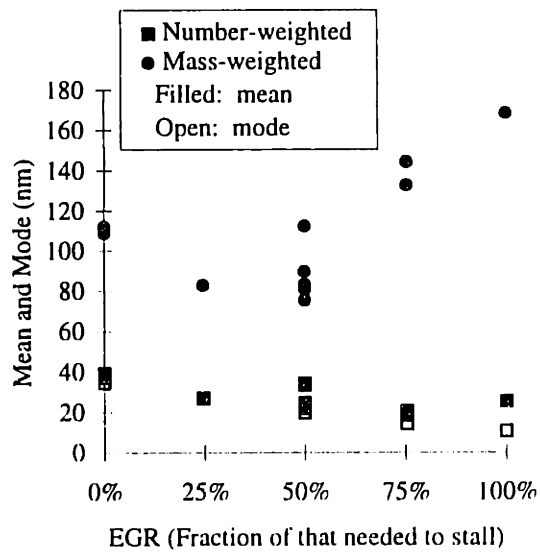

Figure 5.12 Particle sizes as a function of EGR rate: mean sizes on both number- and mass-weighted bases, plus mode sizes on number-weighted basis. Baseline engine operating conditions except EGR rate. Mode sizes on mass-weighted basis are too scattered and thus are not plotted.

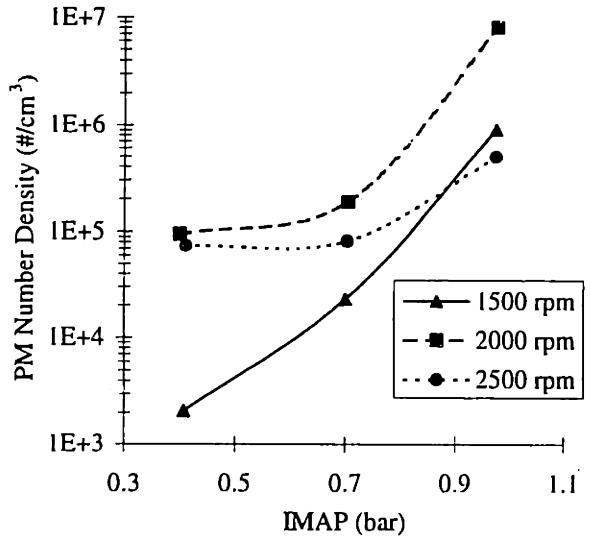

Figure 5.13 Number-weighted PM concentrations as a function of intake pressure (engine load). Three engine speeds, all other conditions same as baseline.

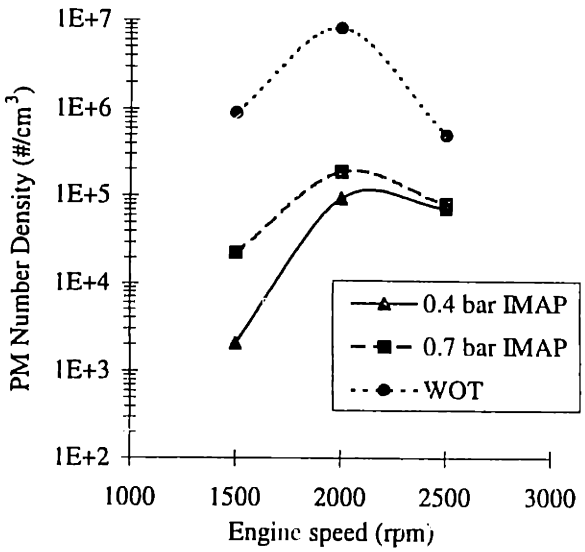

Figure 5.15 Number-weighted PM concentrations as a function of engine speed. Three intake pressures, all other conditions same as baseline.

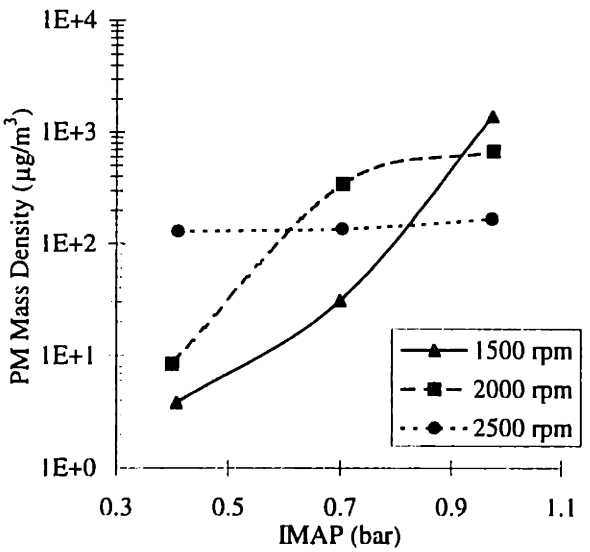

Figure 5.14 Mass-weighted PM concentrations as a function of intake pressure (engine load). Three engine speeds, all other conditions same as baseline.

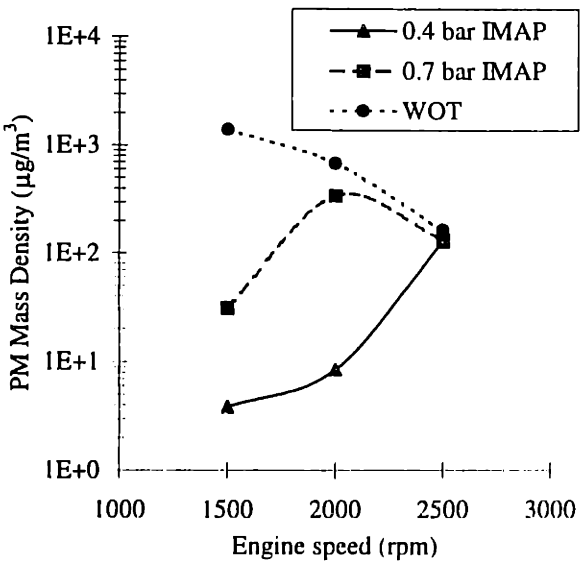

Figure 5.16 Mass-weighted PM concentrations as a function of engine speed. Three intake pressures, all other conditions same as baseline.

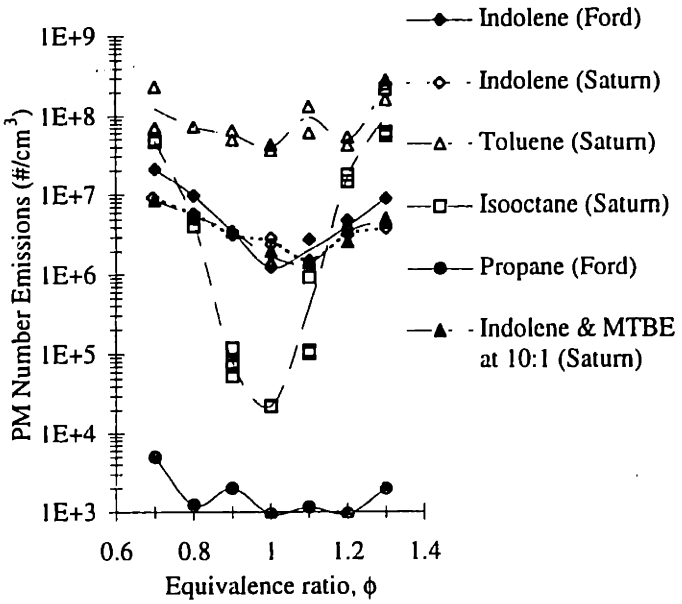

Figure 5.17 Number-weighted PM concentrations as a function of fuel/air equivalence ratio using five fuels (both Ford and Saturn engines used). Baseline conditions except for fuel type and equivalence ratio. Dilution ratio in indolene test on Ford engine is between 8 and 9 as discussed in text.

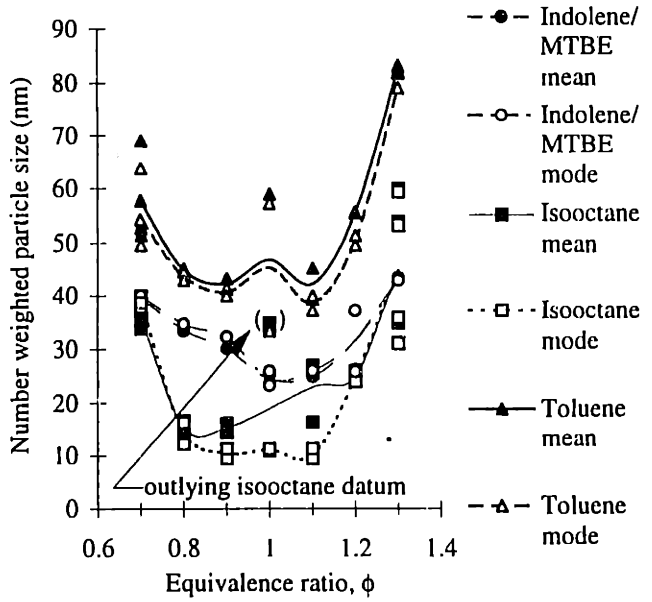

Figure 5.19 Number-weighted mean and mode particle sizes as a function of fuel/air equivalence ratio for indolene/MTBE mixture, toluene, and isooctane. Baseline conditions except for fuel type and equivalence ratio. All data taken on Saturn engine.

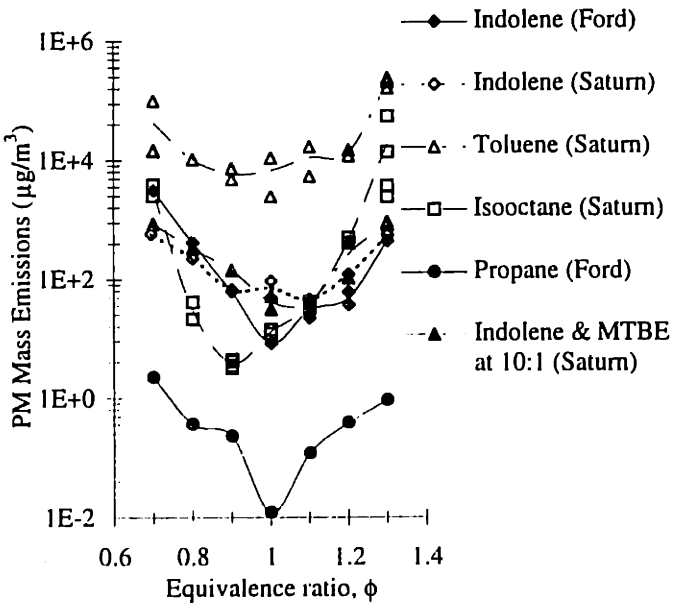

Figure 5.18 Mass-weighted PM concentrations as a function of fuel/air equivalence ratio using five fuels (both Ford and Saturn engines used). Baseline conditions except for fuel type and equivalence ratio. Dilution ratio in indolene test on Ford engine is between 8 and 9 as discussed in text.

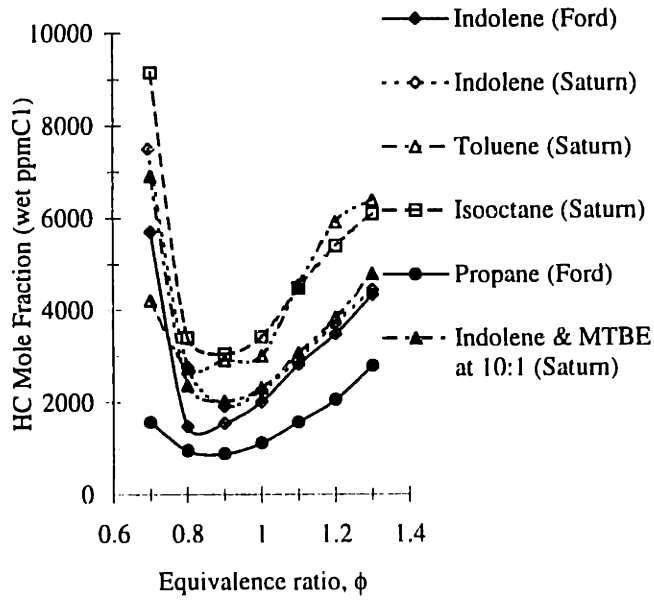

Figure 5.20 HC emissions as a function of fuel/air equivalence ratio using five fuels (both Ford and Saturn engines used). Baseline conditions except for fuel type and equivalence ratio.

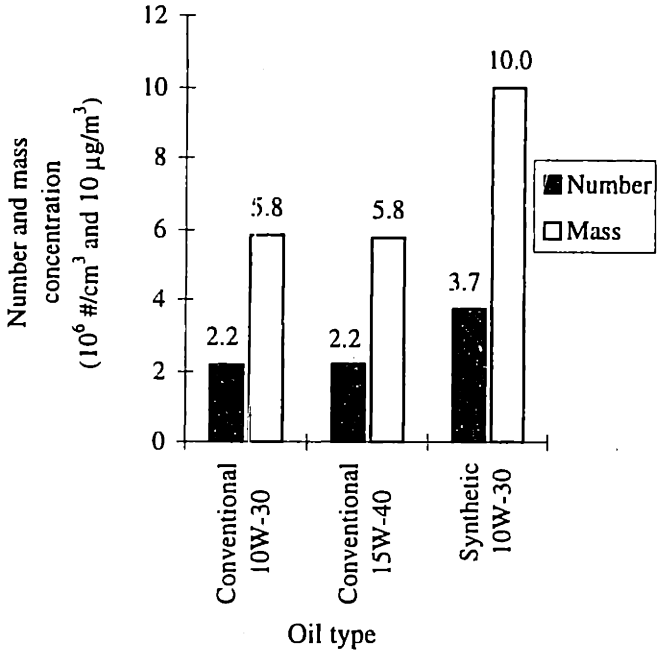

Figure 5.21 Number- and mass-weighted PM concentration as a function of oil viscosity and composition. Baseline conditions except for oil type.

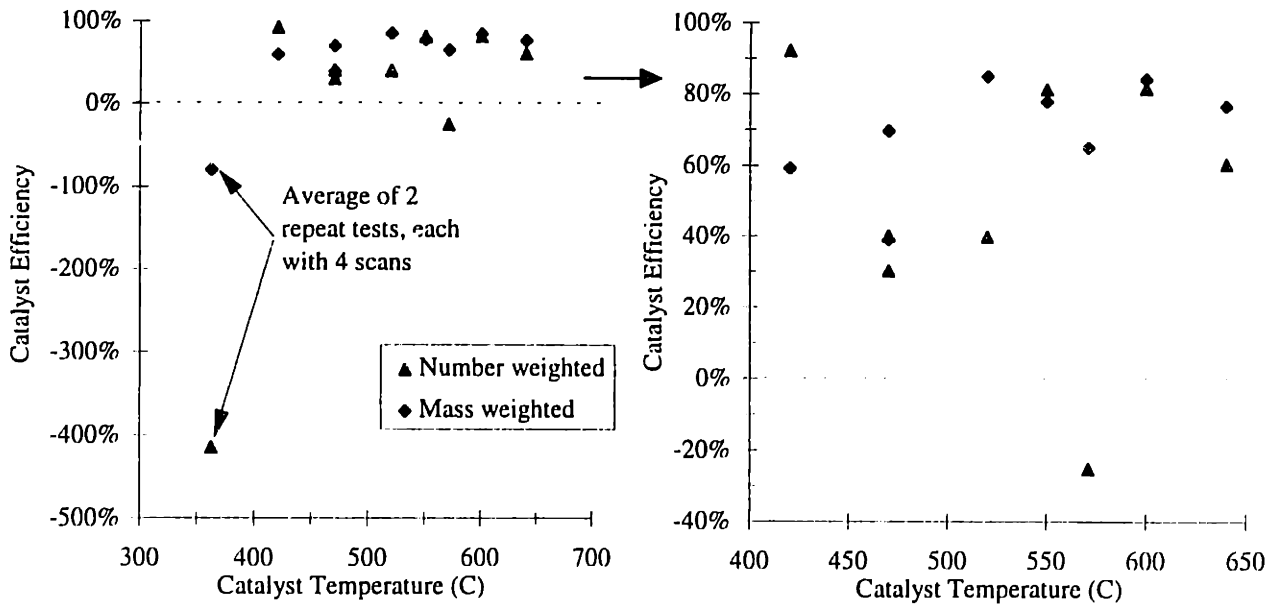

Figure 5.22 Catalyst efficiency at eliminating PM as a function of measured catalyst temperature, plus blow-up of data taken at catalyst temperature above 400°C. Three speed and load conditions, all other conditions same as baseline.

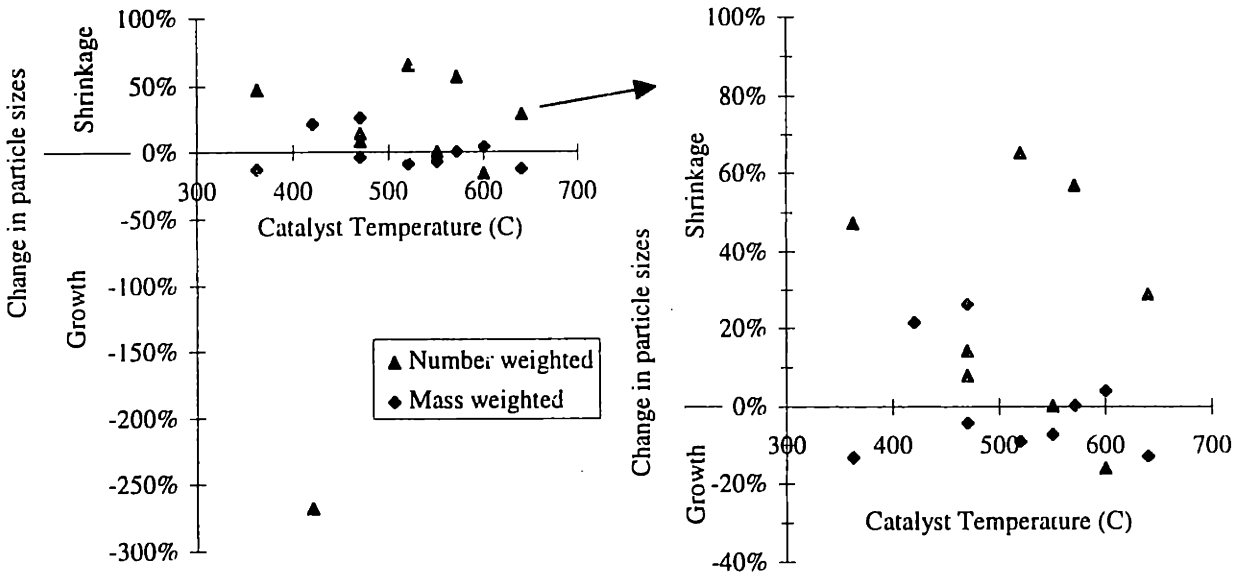

Figure 5.23 Change in particle sizes — expressed as engine-out particle size minus catalyst-out particle size divided by engine-out particle size —- at the various engine operating conditions as a function of the measured catalyst temperature, plus blow-up of data above -40% on ordinate axis. Three speed and load conditions, all other conditions same as baseline.

CHAPTER 6

CORRELATIONS BETWEEN PM AND ENGINE/EXHAUST PARAMETERS

6.1 Methodology

In the present chapter, PM emissions are compared to various gas phase species emissions, characteristic engine temperatures, and characteristic engine pressures at the same engine conditions in order to investigate whether existing correlations could shed light on the possible mechanisms of PM formation. For example, if PM emissions were correlated directly to HC emissions, then the respective emissions mechanisms might be similar or identical. Relations examined in this chapter serve as an introduction to the next chapter, which deals with the model of PM formation and emissions.

PM emissions were measured via the SMPS, in the context of experiments presented in the previous chapter. Species emissions were measured concurrently to PM measurements, as were temperatures in the exhaust port. In-cylinder temperatures and pressures were calculated using the GM Engine-Simulation Program [51] (refer to footnote 2 in Chapter 5). Units of PM emissions are those of mass concentration, while those of gas phase exhaust emissions are mole fractions, which are directly proportional to mass concentration.

6.2 Correlations Between PM And HC Emissions

Although the sources of exhaust HCs and PM are similar — liquid fuel in the combustion chamber, incomplete combustion, partial post-flame oxidation (refer to previous chapter and [61]) — the sources are not so similar that high HC emissions necessarily equates to high PM emissions (Figure 6.1). This plot of PM mass concentration in any given experiment versus the HC concentration in the same test shows that, while the lowest PM emissions do correspond to the lowest HC emissions and vice versa, the correlation between the two emission rates is poor (R^2 correlation coefficient is approximately 0.2). In particular, the conditions with the highest HC emissions, generally do not have high PM emissions. In specific experiments, HC and PM are anticorrelated: for example, when EGR is increased, HC emissions increase while PM emissions decrease (section 5.2). Even though PM emissions (plotted on a log scale) vary by

nearly seven orders of magnitude from one engine condition to another, HC emissions (plotted on a linear scale) vary by no more than a factor of six from the baseline conditions.

Poor correlation between HCs and PM reflects the fundamental difference between their respective formation and emission mechanisms: while HCs can be emitted simply by escaping oxidation, particles must be generated in some sort of partial oxidation reaction, such as gas phase nucleation or liquid fuel combustion. A major mechanism by which HCs escape combustion in steady state operation is storage in crevices [61], but this mechanism does little more for PM formation than supply a source of HCs for adsorption/absorption, while not necessarily supplying nuclei on which HCs can adsorb/absorb.

By contrast, Williams *et al.* did measure a correlation between HC and PM emissions in FTP tests on a fleet of vehicles [12]. The reason for this correlation may be the range of emissions control technology available on vehicles: older cars with poor HC control technology generally have poor PM control as well, and vice versa. So even though the specific engine conditions that lead to high HC and high PM differ, the fleet tests show a correlation. Quader compared smoke and HC emissions at a variety of engine operating conditions on one engine and found a general increase in smoke as HC increased, but that certain conditions led to high HC but low smoke [20].

Subsets of the experimental data exist in which PM and HC emissions are correlated. For instance, if PM and HC are plotted for only the cases with rich equivalence ratios, the correlation is exponential with R^2 correlation coefficient of 0.72 (Figure 6.2). The correlation between HC and PM emissions in this subset of experiments reflects the fact that, in the fuel-rich regime, the mechanisms causing emissions of the two pollutants are similar. In particular, increasing ϕ above unity results in an excess of HCs relative to the amount of oxygen available and thus increases HC emissions; similarly, increasing ϕ above unity enhances particulate formation by increasing the availability of the soot precursors and incompletely oxidized HCs that nucleate particles and/or adhere to particulate surfaces.

PM size characteristics (for example, mean particle sizes) do not correlate with HC emissions (Figures 6.3a and b). Rather, mean particle sizes are almost independent of engine operating conditions. Mean sizes are from 20 to 80 nm on a number-weighted basis (Figure 6.3a). Mean sizes on a mass-

weighted basis fall either between 50 and 100 nm for the Saturn engine and 150 to 250 nm for the Ford engine (Figure 6.3b).

The theoretical expectation was that increased presence of HC vapors would lead to increased adsorption/absorption growth and thus larger particle sizes. In the exclusive case of rich air/fuel ratios, number-weighted particle sizes and HC concentrations are correlated; however, the correlation does not extend to all of the data (i.e., stoichiometric and lean cases as well). Rather, the experimental evidence cannot confirm a general increase in particle sizes due to HC adsorption/absorption because of confounding factors such as cylinder temperatures, which may simultaneously affect both particle nucleation and oxidation, as well as growth via HC adsorption/absorption. Chapter 7 presents a model of the particle formation, oxidation, and growth processes and separates the effect of HC concentrations on particulate formation, growth, and emissions.

6.3 Correlations Between PM And NO_x Emissions

While operating conditions of a diesel engine affect nitrogen oxide (NO_x) and PM emissions in inverse fashion (lower emissions of one coming at the expense of higher emissions of the other) [70], no such anti-correlation exists between PM and NO_x in SI engines (Figure 6.4). In diesel engines, rich regions in the fuel spray facilitate soot formation, while the high temperature, oxygen-rich regions that produce NO_x also oxidize soot, thus leading to the anti-correlation. By contrast, in SI engines, the PM formation mechanisms depends upon a greater variety of factors including the amount of liquid-phase fuel, the maximum temperature, and soot precursor availability, while NO_x formation depends primarily upon maximum temperature. High temperatures stimulate PM formation via gas phase reactions as well as PM oxidation, but hamper nucleation via liquid fuel combustion by increasing the vaporization rate. The fortunate consequence is that, for SI engines, engine control strategies can be chosen in order to simultaneously mitigate PM and NO_x.

6.4 Correlations Between PM And CO, CO_2, And O_2 Emissions

The concentrations of the other measured gas phase species (CO, CO_2, O_2) were compared to the PM emissions, but none showed a strong correlation (Figures 6.5, 6.6, and 6.7 respectively). For example,

CO mole fraction is sensitive to rich air/fuel ratios, but not to lean ones, while the opposite is the case for O_2; conversely, PM is sensitive for both. Similarly, CO_2 mole fraction is largely insensitive to anything but air/fuel ratio, while PM can be quite sensitive. (The reason why most CO_2 data fall on one vertical line is that the greatest fraction of the experiments were performed at stoichiometric air/fuel ratio, the CO_2 mole fraction for which is 14.2%, but the PM emissions for which vary significantly.) The result is that O_2, CO, and CO_2 are correlated or anticorrelated to PM concentrations only in specific cases; the relationships between the emission rates do not suggest similar emission mechanisms.

6.5 Correlations Between PM Emissions And Characteristic Temperatures and Pressures

Comparison between PM emissions and peak cylinder temperature under the corresponding conditions show weak correlation (Figure 6.8). Peak cylinder temperatures were calculated using the GM Engine-Simulation Program [51]. As discussed in Footnote 2 above in the context of indolene fuel, the program does not take into account the different properties of each fuel such as the heating value; however, no more than 3% error (or 100 K) is incurred as a result of using the program to calculate peak temperature for all of the fuels used in the present experiments.

The R^2 correlation coefficient between PM and peak cylinder temperature is 0.05, demonstrating poor correlation. As discussed in section 6.3, while high in-cylinder temperatures facilitate the Arrhenius dependent gas-phase PM formation mechanism, they enhance fuel evaporation, thus limiting PM nucleation from liquid fuel. The combined effect is that PM and peak temperatures are not strongly correlated.

Similarly, comparison between PM emissions and exhaust temperature under the corresponding conditions show weak correlation (Figure 6.9). Exhaust temperatures were measured with thermocouples placed in the exhaust ports. The R^2 correlation coefficient is 0.11, demonstrating poor correlation. While an anticorrelation might be expected insofar as high exhaust temperatures should facilitate oxidation of both PM and the HC vapors that adsorb to PM, the low correlation coefficient reflects either the existence of confounding factors or a small influence of exhaust oxidation on post-dilution PM emissions. (As will be discussed in Chapter 7, the model of PM emissions predicts a negligibly small rate of PM oxidation in the exhaust, contrary to that of HC oxidation [21].)

Furthermore, PM emissions correlate poorly with peak cylinder pressures, which were calculated using the GM Engine-Simulation Program; the R^2 correlation coefficient is 0.03 (Figure 6.10) [51]. However, in certain subsets, PM concentration and peak pressure displayed strong correlation. For example, in experiments when load is varied with all other conditions fixed, PM concentration can be fit via a logarithmic expression to peak pressure with an R^2 correlation coefficient of 0.98. Nonetheless, the correlation in this particular subset of the data does not necessarily suggest that high peak pressure causes high PM emissions. Rather, the reason why increased peak pressure, for example at high load, results in high exhaust PM concentration with all other conditions equal may be the relationship between the amount of liquid fuel in the cylinder and the load, as explained in Chapter 5. However, factors like equivalence ratio and fuel injection timing affect PM very strongly, but do not affect peak pressure, resulting in poor correlation when all data (as opposed merely to subsets thereof) are compared. In conclusion, PM concentrations may be more strongly associated with measures like the amount of liquid fuel in the cylinder than with characteristic temperatures and/or pressures. The next chapter incorporates measures like the amount of liquid fuel in the cylinder into a model of PM formation; while engine temperatures and pressures are parameters in the model, they show up in a variety of mechanisms — nucleation and growth as well as oxidation — so that (for example) high temperature is predicted to stimulate both PM mass increase via some mechanisms and mass decrease via another, the net result being a poor correlation between temperature and PM emissions.

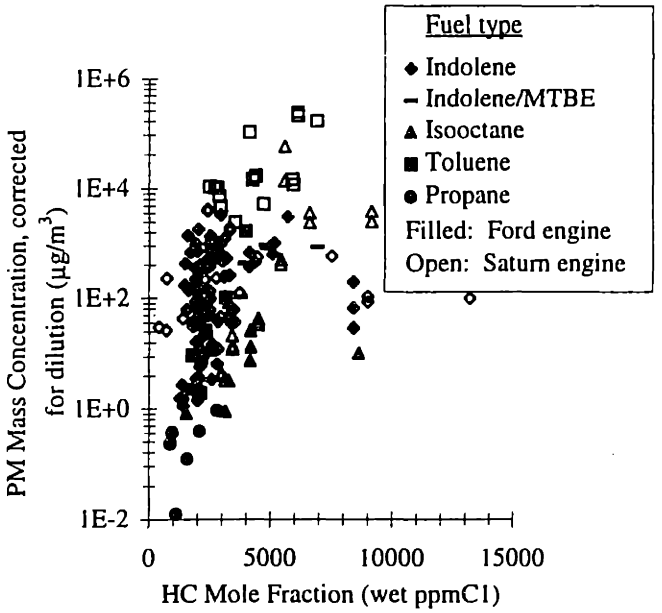

Figure 6.1 Comparison between PM and HC concentrations in various experiments.

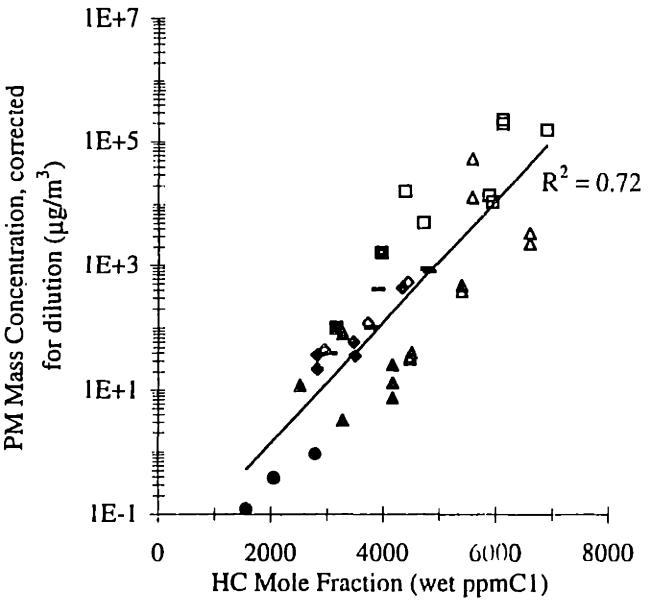

Figure 6.2 Comparison between PM and HC concentrations in experiments with rich air/fuel ratios. Symbols represent same things as in previous figure. Exponential curve fit to data and corresponding R^2 correlation coefficient shown.

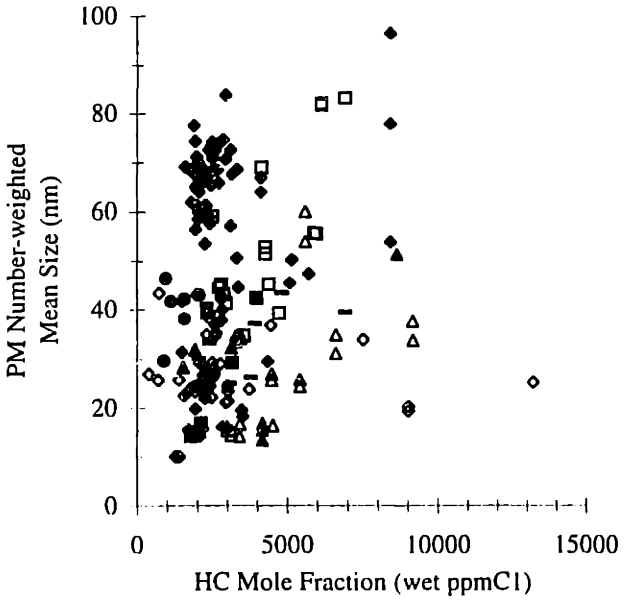

(a) Number-weighted

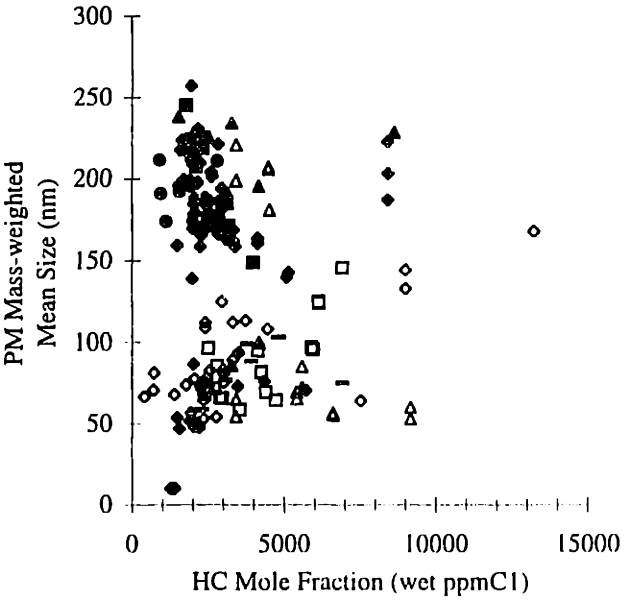

(b) Mass-weighted

Figure 6.3 Comparison between mean PM size and HC concentrations in various experiments: (a) number-weighted, (b) mass-weighted. Symbols represent same things as in previous figures.

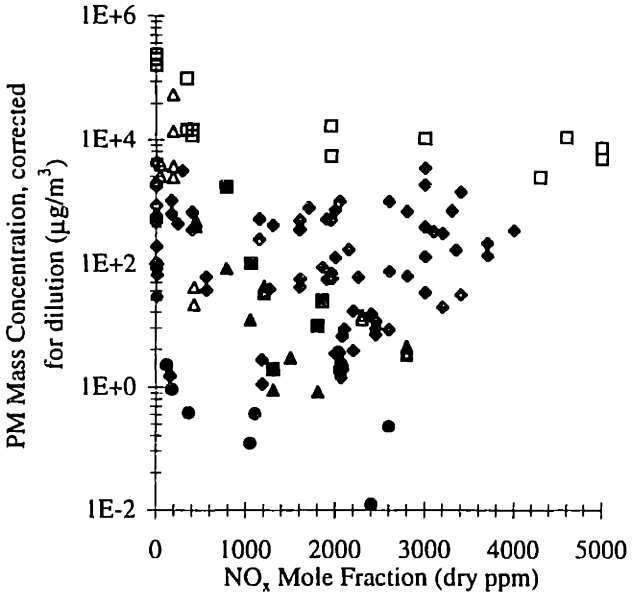

Figure 6.4 Comparison between PM and NO_x concentrations in various experiments. Symbols represent same things as in previous figures.

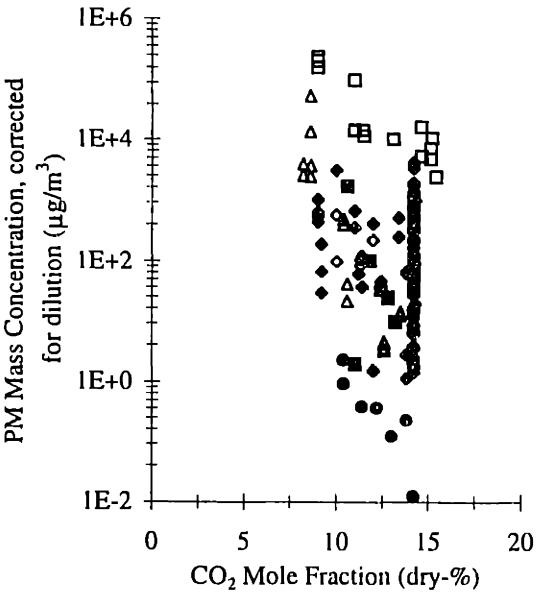

Figure 6.6 Comparison between PM and CO_2 concentrations in various experiments. Symbols represent same things as in previous figures.

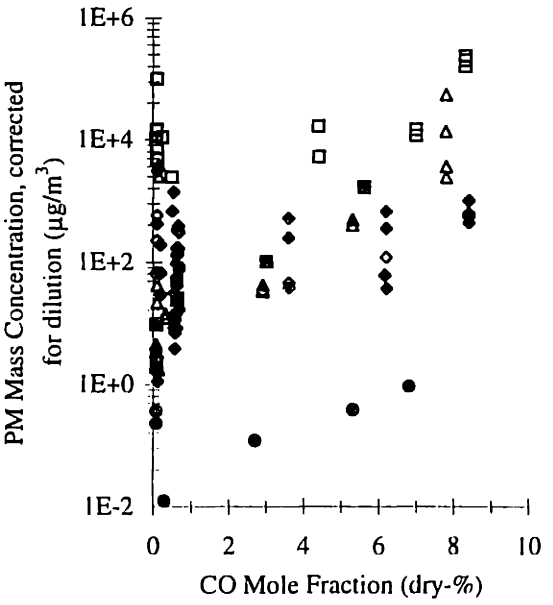

Figure 6.5 Comparison between PM and CO concentrations in various experiments. Symbols represent same things as in previous figures.

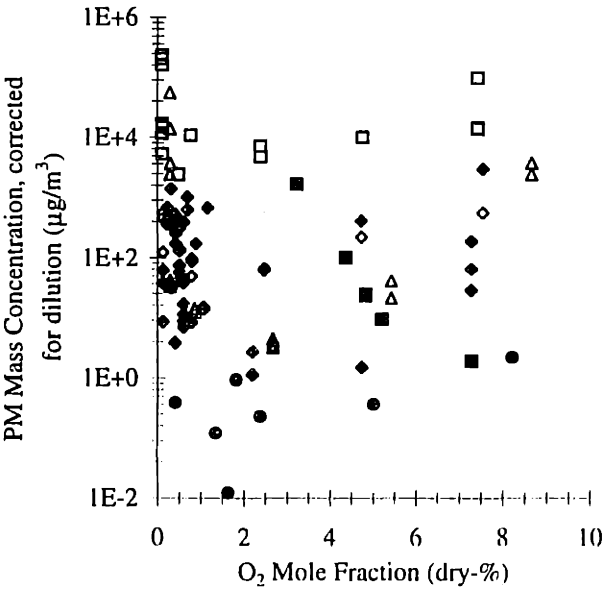

Figure 6.7 Comparison between PM and O_2 concentrations in various experiments. Symbols represent same things as in previous figures.

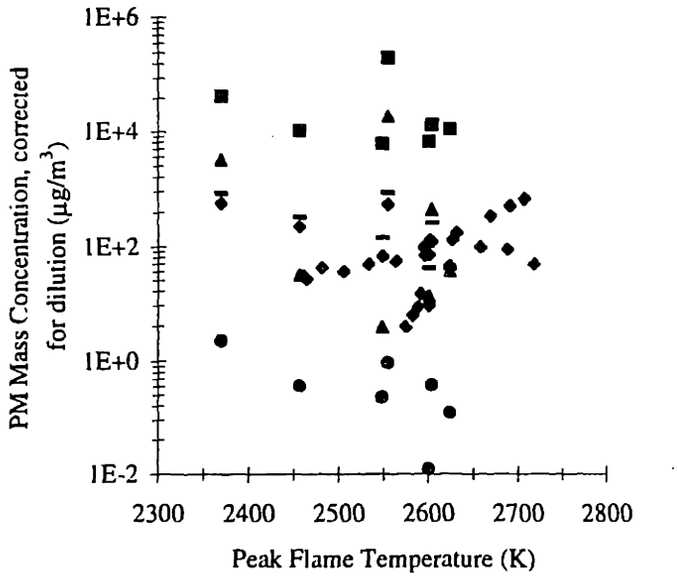

Figure 6.8 Comparison between PM concentration and peak temperature. Peak temperature calculated by GM Engine-Simulation Program [51]. Symbols represent same things as in previous figures.

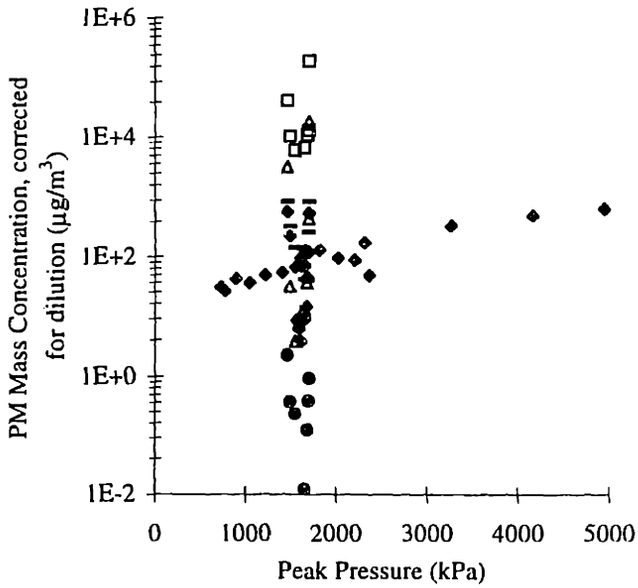

Figure 6.10 Comparison between PM concentration and peak cylinder pressure. Peak cylinder pressure calculated by GM Engine-Simulation Program [51]. Symbols represent same things as in previous figures.

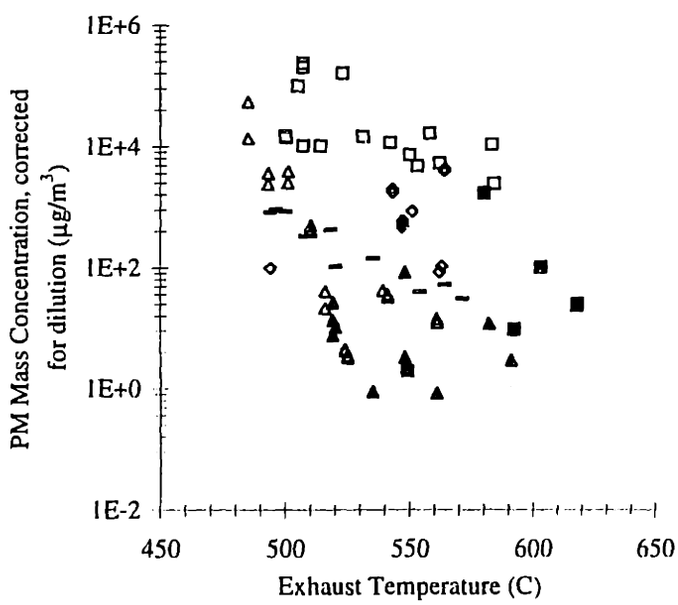

Figure 6.9 Comparison between PM concentration and exhaust temperature for tests in which exhaust temperature data is available. Exhaust temperature measured by thermocouples in exhaust ports. Symbols represent same things as in previous figures.

CHAPTER 7

MODEL OF PM EMISSIONS

7.1 Background

Results in previous chapters have shown the strong effect that air/fuel ratio, in-cylinder liquid fuel, and characteristic temperatures have on PM formation and emissions. However, the results show that PM is not directly correlated to any one parameter; rather, a variety of factors abet in the formation, growth, oxidation, and emissions of PM. The present chapter describes a model of these processes, starting with some background into previous modeling work done on PM in the context of different combustion processes. The next chapter compares model results to experimental data and discusses the modeled effect of engine operating parameters on individual particle dynamic processes.

The following is a brief recap of the experimental results insofar as they motivate the elements in the model of PM formation. Parameters that affect global and local air/fuel ratios strongly affect PM. For example, minimum PM number and mass concentrations are emitted at a global air/fuel ratio within 10% of stoichiometric (although the exact value depends on the particular fuel), and concentrations increase by as many as three orders of magnitude when the fuel/air equivalence ratio (ϕ) is either increased or decreased 30% from stoichiometric. Further, open valve fuel injection increases PM number and mass concentration by up to three orders of magnitude relative to closed valve injection, emphasizing the importance that liquid fuel in the combustion chamber has on PM nucleation. Coolant and oil temperatures, spark timing, and EGR affect PM, but to a lesser extent than ϕ and fuel injection timing. Lubricating oil consumption was observed to affect PM concentrations in only one case: when a synthetic oil was used; for other cases, emissions of oil-derived particles are negligible compared to those of combustion-derived particles. Consequently, the present paper addresses a model for only combustion derived particles. The catalytic converter was not found to eliminate a statistically significant amount of PM. A more thorough understanding of catalytic effects on PM is needed before the present model can treat the catalyst effectively; consequently, the present model quantifies only "engine-out" particle emissions (i.e., emissions without catalytic after-treatment).

PM was not found to correlate with any measured gaseous species (HCs, oxides of nitrogen, and oxides of carbon) or with either peak temperature or exhaust temperature. In particular, contrary to what was initially presumed, the lack of correlation between HC and PM emissions suggests that the mechanisms of PM formation are not the same as the mechanisms of unburned HC emissions, but rather that HCs transform into PM as a result of only certain engine conditions.

The experimental results above suggest the probable mechanisms of PM formation. Particles can nucleate in either homogeneously mixed or heterogeneously mixed regions. Homogeneous nucleation is the particle nucleation that occurs in the main premixed combustion event and, according to [59], is favored by richer equivalence ratios and presumably explains the increase in PM emissions as the global fuel/air equivalence ratio increases beyond stoichiometric. Heterogeneous nucleation is that that occurs in regions other than the homogeneously mixed region. Heterogeneously mixed regions include sites where fuel can be preferentially stored and released (such as oil layers and combustion chamber deposits [61]), sites of liquid fuel, and fuel rich regions near a site from which liquid fuel has recently evaporated. Although particles can presumably nucleate as a result of the fuel rich gas emerging from oil layers and combustion chamber deposits into post-flame gases, experiments (described above and in previous chapters) do not suggest this to be a significant source of particles, at least in comparison to particle nucleation as a result of in-cylinder liquid fuel. Consequently, the only heterogeneously mixed regions that will be considered in the present model are heterogeneous phase regions: sites of liquid fuel or sites where liquid fuel has recently evaporated, leaving a fuel rich mixture.

The following is a discussion of previous research regarding relevant particle nucleation mechanisms: nucleation in the homogeneous regions and in those regions where liquid fuel has caused heterogeneity (hereafter referred to as the homogeneous and heterogeneous phase nucleation mechanisms). Following discussion of nucleation mechanisms is a discussion of post-nucleation phenomena: growth and oxidation.

While the evidence above suggests that liquid fuel in the cylinder is associated with increased exhaust PM, recent research by Witze and Green corroborates the effect that liquid fuel in the cylinder can have on the formation of PM [28]. In-cylinder visualization during cold starts indicates that pools of liquid fuel may be ignited after the flame passes, resulting in sooty flames. Although Witze and Green's measurements were made at cold start conditions, the occurrence of sooty pool fires had a relatively slight dependence on coolant temperature; thus, the

mechanism of soot production via liquid fuel combustion, observed during the warm-up, may also occur in steady-state operation.

PM production from in-cylinder liquid fuel is presumably associated with the following processes: (a) ignition of liquid fuel, whether in the form of droplets or pools on cylinder walls, and (b) subsequent locally fuel-rich diffusion burning. Liquid fuel can ignite when oxygen concentrations and surrounding temperatures are high enough, either during flame passage or in the post-flame regions, provided enough oxygen remains in the burned gas (i.e., the mixture is sufficiently lean) [71]. For instance, Witze and Green observed sooty pool fires in SI engines after flame passage when oxygen concentration is low (relative to that in the unburned gas), but temperatures are high [28]. The model that follows assumes therefore that the formation of PM via liquid fuel combustion is directly related to the amount of liquid fuel in the cylinder and the likelihood that that fuel will ignite into a diffusion flame. The model is based on conditions for spray ignition developed by Law [72], but whereas Law's treatment applies specifically to suspended droplets alone or in a spray, it is here generalized to include both droplets and pools.

As discussed above, in addition to particles formed by heterogeneous-phase combustion, particles may also be formed by homogeneous or gas phase combustion, in particular under rich conditions. According to the Edelman expression, which models soot formation in well-stirred toluene combustion and is discussed in section 7.2, the rate of homogeneous phase soot production is approximately proportional to the square of HC concentration [59]. However, experimentally measured PM concentrations are higher at both rich *and* lean conditions than at stoichiometric (Chapter 5), suggesting that homogeneous phase combustion does not influence PM emissions alone; both homogeneous and heterogeneous phase combustion are examined in the Model section (7.2) to follow.

Once particles nucleate, they can undergo growth and/or diminution. HC vapors can bond either physically or chemically to the surface of the particles and thereby increase the particle size and mass. The Langmuir adsorption concept, which is treated more fully in the Model section of the present Chapter (7.2), has been used to treat physical and chemical bonding in the case of diesel exhaust but is only truly valid where the vapor present does not overwhelm the amount of adsorption sites available on particulate surfaces [16, 53], a condition that may not be true for either diesel or SI engine exhaust. For instance, chemical analysis of PM from SI engines indicates that 38 to 75% of the PM mass comes from organic carbon as opposed to the 4 to 37% from the soot or elemental carbon that makes up the nucleus [34], therefore indicating that the layer of adsorbed material on the particles may be significantly larger than a molecular layer. Rather, adsorption may account for the first layer of trapped vapors, after

which vapor absorption on previously adsorbed material dominates the particle growth. Nonetheless, insofar as the models of absorption and adsorption are similar in derivation and mathematical form, as will be discussed; consequently, the present model treats the two in a lumped fashion.

Oxidation causes particles to diminish in size, but to date, there has been no model specific to the oxidation of PM generated by SI engines. Although the widely used Nagle and Strickland-Constable model of soot oxidation [62] is applicable to soot over a broad range of temperatures [63], its applicability to SI engine-derived particles is questionable because they consist of as little as 4% soot by mass [34]. The present model uses a general expression based on the parameters used in the Nagle and Strickland-Constable model, but whose form is derived by comparison to experimental data, as will be discussed shortly.

The objectives of the present chapter (Chapter 7) are to formulate a model of PM emissions and to compare it to experimentally measured PM concentrations in order to understand which are the important mechanisms in the PM emission process (Chapter 8). The model incorporates the two types of nucleation (homogeneous and heterogeneous phase reactions), the three growth mechanisms (condensation, adsorption, and absorption), and oxidation. All submodels are based upon models of soot formation, growth, and oxidation found in literature and summarized above.

7.2 Model

A physically based model has been formulated for the formation, growth, oxidation, and subsequent emissions of PM. The model takes into account only particulate mass, due to the complexity of modeling the effects of coagulation on PM number concentration and size. The following section describes the model; afterwards, coefficients involved in the model are evaluated by comparison to experimental data.

NUCLEATION —

Homogeneous (Gas Phase) Nucleation Mechanism: Particles can nucleate in regions of either homogeneous or heterogeneous combustion. The homogeneous combustion is the main premixed combustion event in the bulk of the combustion chamber. The model for particle formation in the homogeneous combustion is taken directly from the literature. Experiments using a well-stirred spherical combustor suggest the so-called Edelman expression for soot formation during toluene combustion [59]:

$$\frac{d[S_{ee}]}{dt} = A_{ee} T^{a} [HC]^{b} [O_2]^{c} \exp\left(-\frac{T_{a,sp}}{T}\right) \tag{7.1}$$

where $d[S_{ee}]/dt$ = the rate of change of soot mass concentration due to formation in g/cm^3-s, with subscript ee referring to the Edelman expression

A_{ee} = 4.7 x 10^{14} (cgs units)
T = gas temperature in K
$[HC]$ = hydrocarbon concentration in mole/cm^3
$[O_2]$ = oxygen concentration in mole/cm^3
$T_{a,sp}$ = activation temperature = 16,110 K
a = -1.94
b = 1.81
c = -0.50

The use of an expression derived for a well-stirred reactor in the context of the premixed homogeneous-phase combustion within the SI engine cylinder does not necessitate that the model be modified in order to account for the difference between the engine and reactor geometries. However, differences in fuel types necessitate modifications to the expression. The Edelman expression was derived for prevaporized toluene combustion in air, while the present model concerns combustion of a variety of fuels. Hence, in order to apply Edelman expression, the present model assumes that only precursors of soot — aromatic species and acetylene — formed by partial oxidation of fuel can nucleate particles, even if the fuel is toluene (when the fuel is toluene, this alteration results in < 4% difference between the soot formation rate calculated with the present model compared to that calculated with expression (7.1), as will be discussed shortly). Therefore, rather than using the total HC concentration where the Edelman expression calls for $[HC]$, the model uses the portion of total HC concentration that are soot precursors. However, the portion of total HCs inside the flame that are soot precursors is not known. In order to overcome the lack of information regarding speciated HC concentrations in the flame-front as a function of fuel type, the following assumption is made: the fraction of HCs that break down into soot precursors in the flame equals the fraction of unburned exhaust HCs that are soot precursors. (In other words, soot precursors are no more or less likely than soot non-precursors to be consumed by post-flame oxidation. Admittedly, this may not be true, but it is the only assumption for which data is available.) The model scales the HC concentration by the fraction (A_{sp}) of combustion products that are precursors of soot (aromatic species or acetylene), as measured by Kaiser *et al.* using a gas chromatograph to speciate the exhaust of a SI engine operating on a number of single component fuels as well as a fully blended gasoline [68, 73]. Table 7.1 lists values of the scaling factor A_{sp} for the fuels in the test matrix. The

work of Kaiser *et al.* did not involve the indolene/MTBE mixture used in the present work, so for that case A_{sp} is assumed to be that for pure indolene times one minus the fraction of oxygenate in the fuel.

Table 7.1 Unitless scaling factor A_{sp} for each fuel used

Fuel	A_{sp}
indolene	0.25
indolene/MTBE	0.25 [a]
isooctane	0.026
propane	0.025
toluene	0.98 [b]

[a] A_{sp} for indolene times one minus fraction of oxygenate in the mixture. [b] A_{sp} is 0.98 for toluene in the present model, rather than the implicit 1.00 used in the original Edelman expression. Soot formation rates calculated with present model using A_{sp} equal to 0.98 differ from those calculated with expression (7.1) by less than 4%, which is indiscernible from noise in the present experiments.

Equation (7.1) — modified by the scaling factor A_{sp} — needs to be integrated over the time available for nucleation, and in order to facilitate the integration process some simplifications must be made. Due to the strong dependence of soot formation on HC concentration and the exponential dependence on temperature, particles are formed right behind the flame front at essentially the peak flame temperature. Consequently, it makes sense to evaluate equation (7.1) the peak flame temperature in the engine rather than integrating with a time resolved flame temperature, which itself is not trivial to calculate. Peak temperatures are calculated using an engine-simulation program [51]. Since particles are assumed to form within or right behind the flame front, the soot precursor concentration used in equation (7.1) is the HC concentration in the unburned gas multiplied by A_{sp} (as opposed to HC concentration in the burned gas multiplied by A_{sp}). Although the time (τ_{gp}) that any parcel of gas spends in the flame region producing soot is a small fraction of the total combustion duration, the exact value of τ_{gp} is unknown. Consequently, equation (7.1) is integrated over a time period proportional to the total combustion duration (τ_{cd} , approximated to be the time from spark ignition until the exhaust valve opens and reactions quench), with the proportionality factor being A_{gp}, the value of which is evaluated in an upcoming section by comparison to experimental data. The mass concentration of PM formed by the homogeneous or gas phase mechanism, $[PM]_{m,gp}$, then becomes:

$$[PM]_{m,gp} = \int_{\tau_{gp}} \frac{d[S_{ee}]}{dt} dt \equiv A_{gp} \cdot \tau_{cd} \cdot \left. \frac{d[S_{ee}]}{dt} \right|_{T_{pf}}$$
$$= A_{gp} \cdot \tau_{cd} \cdot \left\{ A_{ee} \cdot T_{pf}^{a} \cdot \left(A_{sp} \cdot [HC] \right)^{b} \cdot [O_2]^{c} \exp\left(-\frac{T_{a,gp}}{T_{pf}} \right) \right\} \tag{7.2}$$

where the subscript *pf* on temperature refers to the peak value in the flame, and all other symbols were defined above.

Heterogeneous (Liquid Fuel) Nucleation Mechanism: As discussed in section 7.1, another mechanism by which soot nuclei may form is thermal ignition heterogeneously mixed regions, particularly regions at or near liquid fuel; burning droplets or pools are locally fuel rich combustion sites and are therefore capable of producing particulates [28, 71]. The model of heterogeneous combustion is based on available models from the literature and has the same form as the homogeneous mechanism.

In order to have a general model of heterogeneous PM formation with as few assumptions as possible, the following model is used. The mass of PM formed by heterogeneous combustion is assumed proportional to the mass concentration of liquid fuel present in the combustion chamber to a power (use of a power reflects the fact that the heterogeneous phase PM nucleation rate may depend on liquid fuel concentration in a stronger-than-linear fashion — the power will be determined by comparison to experimental data), times the probability that the liquid fuel droplet/pool will ignite, times a coefficient reflecting the mass of particulate formed per unit mass of ignited liquid fuel (therefore reflecting the difference in PM forming potential between fuel types). The heterogeneous phase mechanism, therefore, is identical in form to the homogenous mechanism: a pre-exponential coefficient times the concentration of fuel or HCs available to a power times the concentration of oxygen available to another power times an Arrhenius-type temperature exponential (which is incorporated into the probability of ignition). But whereas in the homogeneous mechanism, it is assumed that ignition occurs, in the heterogeneous mechanism, the probability of ignition is not necessarily unity. The following discussion addresses each of the terms in the heterogeneous nucleation mechanism.

The mass concentration of liquid fuel in the cylinder during combustion is calculated using the following technique. First, the mass concentration of liquid fuel in the cylinder during combustion for the baseline conditions is calculated following the work of Meyer and Heywood [57]: in the present case, about 2% of the fuel injected at steady state survives in liquid form until combustion. (For example, this corresponds to a liquid fuel concentration

of 2.4 x 10^{-6} g/cm^3 in the cylinder in the baseline conditions at the time of peak pressure.) At any operating condition other than the baseline, the amount of liquid fuel in the cylinder is assumed equal to the amount of in-cylinder liquid fuel at the baseline conditions times the mass of fuel (m_f) injected relative to that in the baseline conditions, times the probability of fuel evaporation in the intake port, again relative to that in the baseline conditions. The probability of fuel evaporation in the intake port is assumed to be proportional to the temperature difference between the port air and the fuel droplet, times the time available for evaporation (τ_{ev}), divided by the heat of vaporization of the fuel (h_{fg}). The mass concentration of liquid fuel ($[F_l]$) at any given crank angle is proportional to the mass of liquid fuel ($m_{f,l}$); $[F_l]$ at any condition can be expressed relative to that at the baseline condition by:

$$\frac{[F_l]}{([F_l])_{bc}} = \frac{m_{f,l}}{(m_{f,l})_{bc}} = \frac{m_{f,in}}{(m_{f,in})_{bc}} \cdot \frac{(T_\infty - T_{dr})_{bc}}{(T_\infty - T_{dr})} \cdot \frac{(\tau_{ev})_{bc}}{\tau_{ev}} \cdot \frac{h_{fg}}{(h_{fg})_{bc}} \tag{7.3}$$

where the subscript *in* refers to the amount injected; T is the temperature, with the subscript ∞ referring to the bulk gas in the intake port and *dr* referring to the droplet conditions; and subscript *bc* refers to the baseline condition. All other symbols were defined above.

The intake port air temperature used in equation (7.3) was measured via a thermocouple and found to be about 50°C for the baseline conditions, and was found to vary most significantly as a function of EGR, increasing by as much as 38°C at the highest EGR level used. As engine speed increased 500 rpm from the baseline, intake port temperature decreased by 1°C, and as it decreased 500 rpm, that temperature increased 2°C. At intake manifold pressures of 7 x 10^5 and 1 x 10^6 dynes/cm^2 (0.7 and 1.0 bar absolute, respectively), the port temperature was 3 and 4°C below the baseline case, respectively. When the engine was operated with cold coolant and oil, the intake port temperature was approximately 29°C, or 21°C below the baseline conditions. Intake port air temperature was not found to depend on air/fuel ratio. The droplet temperature is estimated to be the temperature measured by a thermocouple in the fuel injection system, and is generally about 25°C.

Clearly, a more sophisticated model of droplet transport and evaporation, such as that formulated by Ladommatos and Rose [54], would better characterize the liquid fuel droplets in the cylinder. However, such a model is beyond the scope of the present research; rather, the simple model presented above and used in the present work, is described, even if only heuristically. One limitation of this simple model is its inability to calculate the amount of liquid fuel entering the cylinder as a function of fuel injection timing. Specifically, calculating the

complex time-resolved air and fuel flows in the intake port would involve a model of droplet travel and evaporation that is beyond the scope of the present paper.

In order to account for the variation of in-cylinder liquid fuel concentration as a function of fuel injection timing, the following simplification is made. Previous research has suggested a correlation between in-cylinder liquid fuel and HC emissions (measured experimentally and presented in Figure 5.5, and also measured by Arcoumanis *et al.* [55] and Alkidas [56]), prompting use of HC emissions a surrogate for in-cylinder liquid fuel mass, in the following manner. As fuel injection timing is adjusted with all other conditions held fixed, HC emissions are only affected by the amount of liquid fuel in the cylinder. Therefore, a sensitivity analysis of HC emissions as a function of fuel injection timing can be used to evaluate the amount of liquid fuel in the cylinder as a function of fuel injection timing. Cheng *et al.* estimate that 20% of HC emissions at steady state CVI operation result from liquid fuel in the combustion chamber [61]. Measured HC emissions in the experimental sweep of injection timing increase from 2050 ppmC1 to 3300 ppmC1 from CVI to OVI (data from Chapter 5). The difference in HC emissions between any OVI fuel injection timing and the CVI operation — assumed to be due solely to the presence of additional liquid fuel — gives the relative amount of liquid fuel in the cylinder by the equation:

$$\frac{[F_l]_{OVI}}{[F_l]_{bc}} = \frac{[HC]_{e,OVI} - (1 - f_{l,bc}) \cdot [HC]_{e,bc}}{f_{l,bc} \cdot [HC]_{e,bc}} \tag{7.4}$$

where f_l is the fraction of HC emissions derived from liquid fuel droplets (20%). Subscript e refers to concentrations measured in the exhaust, *bc* refers to measurements at the baseline conditions, and *OVI* refers to conditions of Open Valve Injection.

Not all liquid fuel present in the combustion chamber will ignite to form particles: for example, Law found that droplets ignite only if their Damköhler number (*Da*) exceeds a critical value [72]. The Damköhler number for the case of a droplet in a uniform environment is given by:

$$Da = \left(\frac{BQ^2 T_{a,dr}^2 Y_{ox,\infty}}{M \rho_\infty d_\infty R_g^2 c_p^2} \right) \left(\frac{p^2}{T_\infty^6} \right) \exp\left(-\frac{T_{a,dr}}{T_\infty} \right) \left(\frac{D_{dr}}{2} \right)^2 \Psi_{dr}^2 \tag{7.5}$$

where B is a constant (equal to 3.5 x 10^9 cm^3/mol-s for the case of n-hexadecane fuel relevant to diesel combustion, but has yet to be evaluated for gasoline); Q is the lower heating value of the fuel; $T_{a,dr}$ is the activation temperature for the droplet ignition (equal to 12,900 K for the n-hexadecane combustion), with the subscript *dr* referring to

Law's droplet ignition model; $Y_{ox,\infty}$ is the oxygen mass fraction in the gas surrounding the droplet; M is the average molecular weight of the gas; ρ_∞ is the density in the bulk gas; d_∞ is the diffusivity of fuel in the bulk gas; R_g is the universal gas constant; c_p is the specific heat of the fuel/air mixture; p is the pressure; T_∞ is the temperature in the bulk gas; D_{dr} is the diameter of the particular droplet; and Ψ_{dr} is the non-dimensional droplet vaporization rate:

$$\Psi_{dr} = \ln\left(1+\frac{T_\infty - T_{dr}}{h_{fg}/c_p}\right). \tag{7.6}$$

where T_∞ is the temperature of the bulk gas, and T_{dr} is the temperature of the droplet.

The probability that liquid fuel in the combustion chamber will ignite is related to the Damköhler number. But clearly, Da cannot be calculated for every individual droplet and fuel pool, nor can it be calculated for the variety of pressures, densities, and temperatures encountered during the cycle. Therefore, in order to apply Law's model (or, more generally, an expression similar in form to Law's) to find the likelihood of heterogeneous phase combustion for the variety of droplets and pools present at the variety of conditions encountered during the cycle, the following assumption is made: the probability any droplet or pool will ignite (P_i) is proportional to a modified Damköhler number (Da_∞), which is only a function of bulk gas and liquid properties, as opposed to properties of individual droplets or pools:

$$P_i \propto Da_\infty \Rightarrow P_i = A_i\left(\frac{Q^2 T_{a,dr}^2 Y_{ox,\infty}}{M\rho_\infty R_g^2 c_p^2}\right)\left(\frac{p^2}{T_\infty^6}\right)\exp\left(-\frac{T_{a,dr}}{T_\infty}\right)\Psi_{dr}^2 \tag{7.7}$$

where A_i is a dimensional constant of proportionality incorporating B, the square of the droplet radius, and d_∞ as well as any differences in the likelihood of liquid ignition between a suspended droplet and a liquid fuel pool or film; A_i is lumped into a more universal constant that is determined by comparison to experimental data. Because Witze and Green's observations [28] suggest that liquid fuel pools ignite only after flame passage when temperatures are significantly high, parameters in equation (7.7) must be evaluated at the conditions in the post-flame gas.

The discussion above detailed calculations of the amount of liquid fuel in the combustion chamber and the probability that it will ignite; however, ignited droplets or pools of different fuels will produce different amounts of particles (aromatics for example will produce more of the soot precursors necessary to nucleate PM than will paraffins). In order to reflect this, the relative amount of PM produced by any given ignited droplet or pool is assumed to be proportional to the fraction of fuel oxidation products that are soot precursors. That fraction is equal

to the constant A_{sp} defined in the context of the homogeneous phase mechanism (Table 7.1), although in the present context A_{sp} refers to the mass of PM precursor produced per unit of mass of ignited droplet. Further, in order that the model of heterogeneous phase PM nucleation can reflect the strong experimentally measured dependence of nucleation on liquid fuel and oxygen concentrations, the nucleation rate includes these two terms raised to powers (d and e respectively), which will be determined by comparison to experimental data and are expected to be positive numbers greater than unity. Consequently, the rate at which PM mass, $[PM]_{m,lf}$, is nucleated by the heterogeneous or liquid fuel mechanism is assumed to be:

$$\frac{d[PM]_{m,lf}}{dt} = A_{dr} A_{sp} P_i \left[F_l\right]^d Y_{ox,\infty}^e \tag{7.8}$$

where A_{dr} is a pre-exponential constant that will be discussed shortly and $[F_l]$ is the mass concentration of liquid fuel in the combustion chamber at some arbitrary time during combustion expressed in grams of fuel per cubic centimeter of cylinder volume. The time during the cycle at which $[F_l]$ is evaluated only impacts the value of A_{dr}; the present paper evaluates $[F_l]$ at 15°CA After Top Center (ATC), the time of peak cylinder pressure when using MBT timing. As discussed above, PM formation via the liquid fuel mechanism is most rapid after the flame passage when pressures and temperatures are high. Therefore, equation (7.8) is evaluated at the peak temperature and pressure, calculated using an engine-simulation program [51]. Any given droplet or pool will not burn for the entire combustion duration (τ_{cd}), but rather for a unknown, smaller time (τ_{lf}). As was done in the case of the homogeneous phase mechanism above, the total concentration of PM formed is assumed proportional to the rate of formation evaluated at peak temperature and pressure multiplied by the combustion duration. The coefficient A_{dr} accounts for this constant of proportionality and expresses the amount of particulate mass formed per unit mass of soot precursor derived by the liquid fuel combustion; A_{dr} is incorporated together with the constant A_i into the constant A_{lf}, which is evaluated in section 7.4. Finally, the mass concentration of PM nucleated by the liquid fuel mechanism is:

$$\begin{aligned}
[PM]_{m,lf} &= \int_{\tau_{lf}} \frac{d[PM]_{m,lf}}{dt} dt \equiv A_{dr} \tau_{cd} A_{sp} P_i \left[F_l\right]^d Y_{ox,\infty}^e \\
&= A_{lf} A_{sp} \tau_{cd} \left[F_l\right]^d \cdot \left(\frac{Q^2 T_{a,dr}^2 Y_{ox,\infty}^{e+1}}{M \rho_\infty R_g^2 c_p^2} \right) \left(\frac{p^2}{T_\infty^6} \right) \exp\left(-\frac{T_{a,dr}}{T_\infty} \right) \Psi_{dr}^2
\end{aligned} \tag{7.9}$$

where A_{lf} equals A_{dr} times A_i and all other symbols were defined above. All parameters are in cgs units. The form of the heterogeneous phase mechanism is identical to that of the homogeneous mechanism — a pre-exponential coefficient times fuel and oxygen concentrations, each to a power, times an Arrhenius-type exponential term, times a probability of ignition — although added terms are involved in equation (7.9) relative to (7.2) to model liquid fuel ignition and combustion characteristics.

Deposit break-up: Graskow *et al.* conjectured that the break-up of intake valve and combustion chamber deposits may be a significant source of nucleation mode particles (particles with size on the order of 10 nm) [49]. They observed that these nucleation mode particles often caused the total particle number concentration to increase by two orders of magnitude above the baseline level and were associated with a bimodal size distribution (a nucleation mode and a larger agglomeration mode). Nucleation mode particles were also observed in the present experiments during engine conditioning periods, but the size distributions and concentrations were observed to be unsteady and did not persist past the conditioning period, when the engine was operating at steady-state. Rather, as time passed, the distributions settled to a steady-state roughly log-normal distribution (for example, Figure 3.3) consisting only of agglomeration mode particles (i.e., no peak corresponding to a nucleation mode). Since steady-state particle size distributions are observed to be purely agglomeration mode it can be assumed that deposit buildup/breakdown is a only a significant source of particulate nuclei during transient operation such as conditioning periods or accelerations/decelerations. Therefore PM derived from deposit break-up is not relevant to the present model of steady-state PM emissions.

Intake air: Another potential source of particle nuclei is the intake air, which may be laden with atmospheric particles not filtered by the engine air filter. Experimental measurements of particulate emissions from the Ford engine operating on propane fuel (discussed in Chapter 5) showed that exhaust particle concentrations are orders of magnitude lower than particle emissions during operation with liquid fuels, so low in fact that the particle concentrations were approximately equal to that of diluent air passing through the HEPA filter into the dilution tunnel. For the case of propane fuel, which cannot form particles via liquid phase nucleation mechanism, the intake air may be a non-negligible source of particles compared to the extremely low concentration of combustion derived particles. By contrast, even the highest emissions with propane fuel are negligible compared to the PM emissions of all other fuels used in the present experiments, which suggests that *even if* all particles observed using propane fuel

did come from the intake air, intake air particles would still be a negligible source of particles for the liquid fuels. For example, intake air particles contribute at most 0.6% of the number concentration and 0.1% of the mass concentration emitted at the baseline conditions using indolene fuel (based on measurements using the indolene and propane on the same day of experiments, in order to eliminate any possible error from day-to-day variability).

Given the above evidence, the model neglects the contribution of intake air particles to the emitted liquid fuel-derived particle concentrations. In the case where propane emissions are modeled, in which intake air particles may have a non-negligible contribution, the intake concentration of is assumed to be the average of the experimentally measured concentrations using propane fuel: 1,900 particles/cm^3 with mean diameter 40 nm. These intake air particles are added to the particles nucleated via the gas-phase mechanism, and the total amount undergoes the oxidation and growth processes, to be described in the upcoming section.

OXIDATION —

In-Cylinder Oxidation: As discussed in section 7.1, the widely used Nagle and Strickland-Constable soot oxidation model may not be valid for gasoline engine derived PM, so the present paper models PM oxidation as a more general function of the parameters in the Nagle and Strickland-Constable expression: oxygen partial pressure and temperature. Like the Nagle and Strickland-Constable model [62], the present surface mass recession rate (ω in g/cm^2-s) is given as an Arrhenius expression:

$$\omega = A_{sr}\, p_{ox}^{f}\, T^{g}\, \exp\left(-\frac{T_{a,ox}}{T}\right) \tag{7.10}$$

where exponents f and g on the oxygen partial pressure (p_{ox} in dynes/cm^2) and temperature (T in K) are determined by comparison to experimental data in section 7.4. The value of the pre-exponential coefficient for the surface recession rate, A_{sr}, is lumped into a larger constant, which is evaluated in section 7.4. As was the case for the nucleation sub-models, equation (7.10) is evaluated at the peak temperature and pressure conditions in the cylinder, corresponding to the time at which oxidation is the most rapid. The calculated rate of particle recession due to oxidation (expressed as a decrease in PM mass concentration in g/cm^3-s) is:

$$\frac{d[PM]_{m,ox}}{dt} = -\omega \cdot [PM]_{su} \tag{7.11}$$

where $[PM]_{sa}$ is the surface area-weighted PM concentration. The area- and mass-weighted PM concentrations are related by the particle density, ρ_p, and the surface area- and volume-weighted mean particle sizes, $\overline{D}_{p,sa}$ and $\overline{D}_{p,v}$, respectively:

$$[PM]_m = \frac{\rho_p}{6} \cdot \frac{\overline{D}_{p,v}^3}{\overline{D}_{p,sa}^2} \cdot [PM]_{sa} \tag{7.12}$$

where $[PM]_m$ is the mass-weighted PM concentration, and $[PM]_{sa}$ is the surface area-weighted concentration. Values of $\overline{D}_{p,sa}$ and $\overline{D}_{p,v}$ in the combustion chamber are not known. Values measured in the dilution tunnel are approximately 100 and 150 nm, respectively; for lack of better information, the relative sizes — used in equation (7.12) — are assumed to remain constant throughout the emission process.

Equation (7.12) is used to substitute $[PM]_m$ for $[PM]_{sa}$ in equation (7.11), which is then integrated in order to yield an expression for the mass concentration of particles surviving oxidation ($[PM]_{m,fin}$) in terms of that before oxidation ($[PM]_{m,o}$) and the time available for oxidation (τ_{ox}):

$$\begin{aligned} [PM]_{m,fin} &= [PM]_{m,o} \cdot \exp\left(-\omega \cdot \frac{6\overline{D}_{p,sa}^2}{\rho_p \overline{D}_{p,v}^3} \cdot \tau_{ox} \right) \\ &\equiv [PM]_{m,o} \cdot \exp\left(-A_{ox} p_{ox}^f T^g \exp\left\{ \frac{-T_{a,ox}}{T} \right\} \cdot \frac{6\overline{D}_{p,sa}^2}{\rho_p \overline{D}_{p,v}^3} \cdot \tau_{cd} \right) \equiv \Pi_{ox} \cdot [PM]_{m,o} \end{aligned} \tag{7.13}$$

where Π_{ox} refers to the portion of mass retained after oxidation. Oxidation begins as soon as the first particle is formed and may continue indefinitely (albeit at a decreasing rate as temperatures drop). The value of τ_{ox} represents an average time associated with the temperature and pressure at which equation (7.10) is evaluated. In order to be consistent with the nucleation sub-models, τ_{ox} is designated as being proportional to the combustion duration, τ_{cd}, with the constant of proportionality being incorporated with A_{sr} into the constant A_{ox}, the value of which is calculated in section 7.4. The PM concentration before oxidation, $[PM]_{m,o}$, is by definition the concentration of particles from nucleation, $[PM]_{m,n}$.

The fraction of PM oxidized at the baseline engine operating conditions is calculated to be 33%, evaluating the above equations at the peak in-cylinder temperature and pressure calculated by an engine-simulation program [51]. Although a comparison between oxidation rates in diesel and SI engines is not necessarily valid, the estimated

33% oxidation rate is smaller in magnitude than the 67% rate of oxidation measured in diesel engines [74], presumably due to the relatively lower temperatures and oxygen concentrations.

Exhaust Oxidation: Oxidation occurs in the exhaust pipes, as well as in the cylinder. In order to evaluate exhaust oxidation, the same set of equations for in-cylinder oxidation is applied, except that the temperatures and pressures are average values in the exhaust. The exhaust temperature used in equations (7.10) through (7.13) is the value measured with a thermocouple inserted in the exhaust port, and the exhaust pressure is approximately atmospheric for all engine conditions (exhaust oxygen partial pressure is exhaust pressure times measured oxygen mole fraction). The amount of time during which particles in the exhaust undergo a significant rate of oxidation is estimated, following a study of exhaust port HC oxidation [21], to be on the order of 24 milliseconds at the baseline engine operating conditions. If the equations used for in-cylinder oxidation are used to evaluate the exhaust oxidation given this short time scale and the low temperatures and pressures in the exhaust port, then the result is that less than 1% of the PM mass oxidizes in the exhaust at conditions experienced in the present test matrix — the Π factor associated with exhaust oxidation is nearly unity. Consequently, exhaust oxidation is considered negligible in comparison to in-cylinder oxidation, even if the time scale for exhaust oxidation were grossly underestimated.

GROWTH —

Particles begin to grow as soon as they are formed: HC vapors may adhere to their surface either physically or chemically, causing the particle mass and size to increase. However, particle growth by condensation, adsorption, and absorption increases as temperature decreases, such that if a dilution tunnel is used, the growth can be dominated by growth in the tunnel. The following discussion treats the growth processes in regard to that occurring in the dilution tunnel insofar as the experiments (Chapters 4 and 5) were measurements of PM concentrations in a dilution tunnel, as are most if not all measurements of PM concentrations. However, the model statement is general enough that it can be used to evaluate particle concentrations in undiluted exhaust, as will be discussed in the section called Dilution Issues (7.3).

Condensation: HC vapor condenses on particles if the HC vapor pressure exceeds the saturation vapor pressure. Thus, particles measured at the monitoring port of the dilution tunnel only have condensed matter on them if the HC vapor pressure at that location exceeds the saturation vapor pressure corresponding to the temperature at that location. The HC vapor pressure, p_{HC}, is:

$$p_{HC} = \frac{X_{HC}}{\Lambda} p_d \tag{7.14}$$

where X_{HC} is the mole fraction of HCs, Λ is the dilution ratio (defined above), and p_d is the pressure in the dilution tunnel. In no case is p_{HC} observed to exceed the saturation vapor pressure, which ranges from 5×10^4 dynes/cm^2 for toluene to a pressure greater than atmospheric for propane, with indolene and isooctane falling in between. (Indolene vapor pressure is estimated following the work of Chen *et al.* [75].) In order for condensation to occur, with a dilution ratio of 15:1, X_{HC} would have to be at least 50,000 ppmC1, while the maximum observed value was 13,200 ppmC1 in the case of extreme EGR. Consequently, condensation is neglected as a mechanism of mass accretion (i.e., the Π factor associated with condensation, Π_{cond}, is unity).

Adsorption: Even if the HC concentration is insufficient for condensation, particles can retain HC vapors by physical or chemical bonds [16], both of which fall under the names of adsorption and absorption. Previous research has mainly dealt with adsorption, the process where vapor sticks to the solid surface of a particle. (Absorption, where vapor sticks to the previously adsorbed or absorbed vapor covering the solid surface of the particle, will be discussed shortly.) The Langmuir adsorption concept — originally derived for plane surfaces by Langmuir [53] but used for diesel exhaust particles/vapors by researchers such as Plee and MacDonald [16] — treats physical and chemical adsorption given the following assumptions:

1. The particle surface contains a fixed number of adsorption sites, each of which can adsorb one molecule.
2. The heat of adsorption is constant and independent of location. (Although this assumption is not necessarily true over a large temperature range, it is reasonable for addressing adsorption occurring in the dilution tunnel inside of which conditions do not vary significantly.)
3. Molecules at different sites do not interact.
4. The adsorption and desorption processes are in equilibrium. (The effect of tunnel residence time on measured PM concentrations was found less than measurement uncertainty as discussed in Chapter 4, which suggests that the adsorption/desorption processes have equilibrated by the time that measurements are made.)

Using a kinetic approach governed by these assumptions, Plee and MacDonald calculate the fraction of sites occupied by adsorbed molecules (Θ_{ad}) to be:

$$\Theta_{ad} = \frac{1}{1 + \frac{A_{ad} \cdot \Lambda}{X_{HC}} \exp\left(-T_{a,ad}/T\right)} \tag{7.15}$$

where A_{ad} is a constant, which Plee and MacDonald calculate to be 15,400 for particles from a diesel engine [16]; Λ is the dilution ratio; X_{HC} is the mole fraction of HC in the exhaust gas; and $T_{a,ad}$ is the activation temperature for the adsorption process, which Plee and MacDonald calculate to be 3,500 K for diesel exhaust particles/vapor [16]. They conclude that the physical adsorption process is highly reversible because no change of composition is involved and allude that this may be the reason for the low activation temperature. The value of Θ_{ad} ranges from zero to one, representing respectively the case of no adsorption and the case where the entire particulate surface is covered in an adsorbate film.

If only adsorption occurred, then the layer of HCs on the particles would be a film of molecular thickness, since adsorption only accounts for the process of particles sticking to the solid particulate surface. However, chemical analysis of particles from SI engines suggests that a significant fraction of the particle mass (38 to 75%) can come from adsorbed HCs, in which case the layer of HCs would have to be significantly larger than a film of molecule-sized thickness [34]. Rather, for the size of particles measured for SI engines (see Chapter 3 for particle size distributions), the layer of adsorbate would have to be on the order of 100 molecular diameters thick; i.e., vapor has to stick to previously adsorbed or absorbed vapor. Consequently, the present model expands the Langmuir adsorption concept to include absorption — when HC vapors stick to the vapor already adhering to particle surfaces. Although Plee and MacDonald do not rigorously model absorption, they and MacDonald *et al.* estimate that as much as about 35% of the particle mass is extractable (or adsorbed/absorbed) material [15, 16, 17], which would require a layer of adsorbed/absorbed material as large as 50 molecular diameters thick. The fact that such a large fraction of mass comes from so-called "adsorbed" material suggests that their model may really account for absorption as well as adsorption. For the sake of generality, the mass of absorbed material will be derived separately in the upcoming section.

Adsorption and Absorption: Derivation of the combined adsorption/absorption model follows that of the adsorption model, using the assumptions described above[3]. For the combined adsorption/absorption model, assumption number 1 above is relaxed, but assumptions 2 and 3 above are retained. Then, following the derivation for the adsorption model in [53], the rate of adsorption and absorption (r_{ab}) is:

$$r_{ab} = k_{ab} \cdot p_{HC} \cdot [PM]_{sa} \tag{7.16}$$

and the rate of desorption (r_{de}) is:

$$r_{de} = k_{de} \cdot [PM]_{sa} \cdot \Theta_{ab} \tag{7.17}$$

where Θ_{ab} is the fraction of $[PM]_{sa}$ that is absorbed or adsorbed material; k_{ab} and k_{de} are Arrhenius rates for the absorption and desorption mechanisms, respectively; and p_{HC} is the HC partial pressure. Following assumption 4 above, r_{ab} equals r_{de}, so:

$$k_{ab} \cdot p_{HC} = k_{de} \cdot \Theta_{ab} \Rightarrow \Theta_{ab} = \frac{1}{k_{de} / k_{ab} \cdot p_{HC}} \equiv \frac{1}{A_{ab} \frac{\Lambda}{X_{HC}} \exp\left(-T_{a,ab}/T\right)} \tag{7.18}$$

where A_{ab} is a pre-exponential coefficient, and $T_{a,ab}$ is an activation temperature, both of which incorporate the respective coefficients and activation temperatures of k_{de} and k_{ab}.

Thus, the form of the absorption model in equation (7.18) is similar to that of the adsorption model in equation (7.15), although the activation temperature and pre-exponential coefficients may differ from those of Plee and MacDonald's adsorption model [16] (not only because their model is strictly valid only for adsorption, but also because it treats diesel-derived PM, rather than gasoline-derived PM). Values of the pre-exponential coefficient and activation temperature for the combined absorption/adsorption model, A_{ab} and $T_{a,ab}$ respectively, will be calculated in section 7.4. The Arrhenius dependence on temperature in the denominator of equation (7.18) makes adsorption and absorption increasingly prevalent at lower temperatures; hence when applying the model, equation (7.18) is evaluated at the lowest temperature experienced by the particles — in applying the present model to the conditions used in experiments described in previous chapters, Θ_{ab} is evaluated at the dilution tunnel temperature.

[3] In what follows, parameters in the combined absorption/adsorption model will be labeled with the subscript *ab*, in order to distinguish from the adsorption model, labeled *ad*. Note that the derivation of the combined adsorption/absorption model could have been based upon application of Henry's Law, rather than assumptions paralleling those of the Langmuir adsorption concept (as is described presently), with the final result being the same.

The infinitesimal change in PM mass concentration at any instant in time is equal to the infinitesimal change in the amount of PM surface area concentration occupied by adsorbate/absorbate times the mass of adsorbate/absorbate per unit area (ψ). Equivalently, it is equal to the available PM surface area concentration times the fraction of adsorption/absorption sites occupied (not merely surface sites but also "sites" within the absorbate film) times the mass of adsorbate/absorbate per unit area (ψ), as given by the following equation:

$$d[PM]_{m,ab} = [PM]_{sa} \cdot \psi \cdot d\Theta_{ab} \tag{7.19}$$

where the subscript *ab* refers to combined adsorption/absorption process, Θ_{ab} represents the fraction of PM surface area that is adsorbed/absorbed material (evaluated at the conditions in the dilution tunnel), $[PM]_{m,ab}$ is the mass of HCs adsorbed/absorbed on particles per unit volume of diluted exhaust, and $[PM]_{sa}$ is the surface area-weighted PM concentration.

With adsorption/absorption (as opposed to merely adsorption), the particles may accumulate enough mass to significantly increase their size and hence the surface area on which HCs can absorb. In order to reflect this, equation (7.19) is rewritten in terms of only the particle mass concentration, using equation (7.12) to equate PM mass and surface area-weighted concentrations through the instantaneous particle sizes:

$$d[PM]_{m,ab} = [PM]_m \cdot \frac{6\overline{D}_{p,sa}^2}{\rho_p \overline{D}_{p,v}^3} \cdot \psi \cdot d\Theta_{ab} \equiv [PM]_m \cdot \beta \cdot d\Theta_{ab} \tag{7.20}$$

where $d[PM]_{m,ab}$ is the increase in PM mass via adsorption/absorption per unit volume of diluted exhaust, β is a constant of proportionality, $d\Theta_{ab}$ is the incremental change in the fraction of filled absorption sites, and all other symbols were defined above. To account for the fact that the values of $\overline{D}_{p,sa}$ and $\overline{D}_{p,v}$ change during the adsorption/absorption process, the two diameters are incorporated into the constant β, the value of which represents the average value of surface area per unit mass times ψ. The values of β and the Arrhenius-type constants used in Θ_{ab} are calculated by comparison to experimental data, as is discussed in section 7.4.

Rewriting equation (7.20), maintaining the time-independent form, and integrating from the start of the adsorption/absorption process to its completion yields the following equation:

$$d\ln[PM]_{m,ab} = \beta \cdot d\Theta_{ab} \Rightarrow \ln\left(\frac{[PM]_{m,fin}}{[PM]_{m,o}}\right) = \beta \cdot \left(\Theta_{ab,fin} - \Theta_{ab,o}\right) \Rightarrow$$
$$[PM]_{m,fin} = [PM]_{m,o} \cdot \exp\left(\beta \cdot \Theta_{ab,fin}\right) \equiv \Pi_{ab} \cdot [PM]_{m,o} \tag{7.21}$$

where the subscript *o* refers to the original PM concentration, which is by definition the PM concentration derived from nucleation less the amount oxidized, and the subscript *fin* refers to the final concentration. The initial value of Θ_{ab} is zero, by definition; the final value is evaluated using equation (7.18). As in the case of the oxidation mechanism, the Π factor for the adsorption/absorption process (Π_{ab}) refers to the amount of mass after adsorption/adsorption per unit mass before, but unlike Π_{ox}, is greater than unity.

COMPLETE MECHANISM —

The nucleation, oxidation, and growth submodels are incorporated in the following manner. The total PM mass concentration measured at the monitoring port of the dilution tunnel is the mass of PM nucleated via the homogeneous and heterogeneous mechanisms, minus the mass oxidized both in the cylinder and in the port (although that in the port is negligible), plus the mass added by the condensation, adsorption, and absorption mechanisms:

$$[PM]_{m,fin} = [PM]_{m,n} \cdot \Pi_{ox} \cdot \Pi_{con} \cdot \Pi_{ab} \tag{7.22}$$

where $[PM]_{m,n} = \left([PM]_{m,gp} + [PM]_{m,lf}\right)$; Π_{ox} was defined in equation (7.13), and refers only to in-cylinder oxidation since exhaust oxidation is negligible; Π_{con} is unity as discussed in the section on condensation growth; and Π_{ab} was defined in equation (7.21) referring to the combined adsorption/absorption process. Subscripts *m*, *fin*, *n*, *ox*, *con*, *ab*, *gp*, and *lf* refer to mass, final, nucleation, oxidation, condensation, absorption/adsorption, gas phase (or homogeneous), and liquid fuel (or heterogeneous) mechanisms, respectively.

PM concentrations at any condition are calculated relative to the baseline concentrations for several reasons. Firstly, day-to-day variations in engine operation produced a daily variation in PM emissions at the baseline conditions. While concentrations at the baseline engine operating conditions were usually within 50% of each other, on a few days the concentrations varied from the average by one to two orders of magnitude. Nevertheless, baseline concentrations are repeatable on any given day: repeated tests on a given day vary by no more than 20% on a number- or mass-weighted basis, as discussed in Chapter 3. Because modeling day-to-day variability is beyond the

scope of this project, the effect on PM of a change in engine operating conditions is calculated as the PM emissions relative to PM emissions at the baseline conditions on the same day of experiments.

Unknown coefficients were evaluated by fitting modeled data to experimental data. The next section discusses the fact that the model can be applied to general dilution systems, not only the one in the present experiments. Section 7.4 discusses the values of the coefficients and presents a comparison of modeled PM emissions to experimentally measured ones.

7.3 Dilution Issues

As alluded to above, although the model is framed in such a way as to capture the effect of the experimental dilution process, dilution conditions such as temperature and dilution ratio (Λ) are inputs to the model, so the model should work for other dilution conditions including no dilution at all, corresponding to original engine-out exhaust. Due to sampling constraints, PM concentrations in the exhaust (prior to dilution) could not be reliably measured (as discussed in section 2.3); therefore, the PM formation model can only be compared to post-dilution PM measurements (such as the data presented in previous chapters). Nonetheless, PM concentration as a function of dilution ratio was experimentally measured in Chapter 4 and is compared to modeled data in the present chapter in order to show that the model captures the effect of dilution — the implication being that the model need not only be applied to the conditions (Λ = 15) used in the present experiments, but can be applied to a variety of dilution conditions, and presumably to the condition of no dilution at all (Λ = 1), representing the case where samples are drawn from the exhaust.

The model used to calculate PM concentrations in the exhaust or at the exit plane of the cylinder is no different than the complete model, except for the values of parameters used: for concentrations prior to dilution, the dilution ratio used in the model is Λ = 1. Temperature at which condensation, absorption, and adsorption occur is simply the lowest temperature reached by the exhaust, be it the temperature near the exhaust valve, in the exhaust system, or in the dilution tunnel, depending on what stage of the emission process at which one wants to estimate the PM concentration. The length of time available for PM oxidation in the exhaust system is an input to the system, for which the present paper suggests the value 24 milliseconds at baseline conditions; if one wants to estimate PM

concentrations at the exit to the cylinder, then the time available for exhaust system oxidation is zero, but all other parameters are unaffected.

Experimental particulate measurements, taken in the dilution tunnel and presented in figures that follow for comparison to the present model, are corrected for dilution ratio so that they reflect the particle number or volume per unit volume of exhaust cooled to standard temperature and pressure. Calculated PM concentrations $[PM]_{m,fin}$ are the mass of particulate matter per unit volume of undiluted exhaust, as well.

7.4 Calculation Of Model Coefficients

The 84 experimental data points (Table 5.1) were used to calculate the values of the 16 unknown coefficients in the present model (Table 7.2, next page) by evaluating the model at the 84 test conditions and maximizing the R^2 correlation coefficient between the modeled and experimentally measured PM concentrations. (Kowalik *et al.* determined the value of $T_{a,gl}$ for toluene [59]; their value is assumed to hold for the present experimental conditions, and is listed in Table 7.2 for comparison to $T_{a,gl}$ for the other fuels.) The resulting R^2 correlation coefficient is 0.81, showing good correlation between the model and experimental data. The best fit expression used to find this R^2 correlation coefficient (the power law expression shown in Figure 7.1 along with a comparison between modeled and experimental data) deviates in value from the diagonal line of slope unity that corresponds to exact coincidence between modeled and experimental data by no more than 37% over the seven-decade range of measured/modeled PM concentrations (compared to the approximately 25% experimental uncertainty). The coefficient and exponent in the power-law fit used to find the R^2 correlation coefficient differ from unity by 5% and 4%, respectively, suggesting the model has only small systematic error.

The value calculated from the best fit for the activation temperature of the liquid fuel mechanism is 13,000 K, while that calculated for the droplet combustion experiments using n-hexadecane fuel (relevant to diesel combustion) is 12,900 K [72]. This similarity does not necessarily imply similarity between the chemical processes involved in the liquid fuel combustion.

Table 7.2 Coefficients for model of PM emission and the equations in which they are used

Coefficient (units)	Value	Equation
A_{gp}, constant in homogeneous mechanism (-)	4.0×10^{-5}	(7.2)
$T_{a,gp}$, activation temperature in homogeneous mechanism (K)	32,000 for indolene and indolene/MTBE mixture 14,000 for isooctane 40,000 for propane 16,110 for toluene, as specified by [59]	(7.1), (7.2)
$A_{lf} = A_l * A_{dr}$, coefficient in heterogeneous mechanism (cgs units)	7.6×10^{18}	(7.9)
d, exponent in heterogeneous mechanism (-)	3.5	(7.8), (7.9)
e, exponent in heterogeneous mechanism (-)	1.9	(7.8), (7.9)
$T_{a,dr}$, activation temperature in heterogeneous mechanism (K)	13,000	(7.5), (7.9)
A_{ox} coefficient in oxidation mechanism (cgs units)	0.14	(7.13)
f, exponent in oxidation mechanism (-)	0.5	(7.10), (7.13)
g, exponent in oxidation mechanism (-)	-0.5	(7.10), (7.13)
$T_{a,ox}$, activation temperature in oxidation mechanism (K)	20,000	(7.10), (7.13)
A_{ab}, constant in adsorption/absorption mechanism (-)	15,400, equal to value calculated by [16]	(7.15), (7.18)
$T_{a,ab}$, activation temperature in adsorption/absorption mechanism (K)	3,500, equal to value calculated by [16]	(7.15), (7.18)
β, constant in adsorption/absorption mechanism (-)	850	(7.20), (7.21)

The values calculated from the best fit for constants in the lumped absorption/adsorption mechanism (A_{ab} and $T_{a,ab}$) come out within 3% of those Plee and MacDonald calculated for the simple Langmuir adsorption concept. This equality may be due to the lack of strict distinction between the completion of adsorption and the onset of absorption: it is possible that previous measurements and experiments by Plee and MacDonald and MacDonald *et al.* [16, 17] did not solely involve adsorption, but may have incorporated the effect of absorption, especially given their calculation that up to 35% of the particle mass is soluble matter [17]. In fact, the numerical values of Θ_{ad} and Θ_{ab} differ by far less than 1% over the range of temperatures encountered in the present experiments and by no more than 1.4% over the range of diluted exhaust HC concentrations encountered. Even if the most extreme HC concentration possible (maximum EGR, no dilution) were encountered, the two values would differ by less than 9%. Considering that 9% error is indistinguishable from measurement/modeling uncertainty, even if Plee and MacDonald mislabeled the combined adsorption/absorption processes as simply adsorption, their numerical results would not be noticeably affected by this syntactical mistake. On the other hand, it is possible (although unlikely) that that absorption does not occur at all: while adsorption is a surface bond, absorption is a bond in which the vapor can permeate into the bonding surface material. So, it may be the case that the supposed mass accreted by absorption is really just layer

upon layer of adsorbed material. Were this the case, the derivation of the mass accreted through repeated adsorption would be the same as the one above for mass accreted through absorption, and the results above would still hold.

The model calculates that at the baseline conditions, the fraction of PM derived from adsorbed/absorbed vapors is 76%. By comparison, Hildemann *et al.*, who chemically analyzed PM emitted by SI engines during the Federal Test Procedure, found that between 38 and 75% (or about 70 to 90% of the elemental/organic carbon mass) is derived from adsorbed/absorbed vapors [34], suggesting that the model captures the effect of adsorption/absorption reasonably well.

While the present analysis starts with the assumption that the Nagle and Strickland-Constable expression for soot oxidation [62] may not be valid because of the small soot content in SI engine particles, the reaction rates calculated using the present model and the Nagle and Strickland-Constable model during (for example) the baseline engine cycle differ by only about 20%. Moreover, if a simple Arrhenius expression is fit to the Nagle and Strickland-Constable rate over the range of pressures and temperatures encountered in the baseline engine cycle, the activation temperature equals that for the present model (20,000 K). Although, the two rates may be approximately identical, the analysis in the upcoming sections uses the rate previously described insofar as it is applicable to PM from SI engines rather than the Nagle and Strickland-Constable rate, since the latter is only strictly valid for soot.

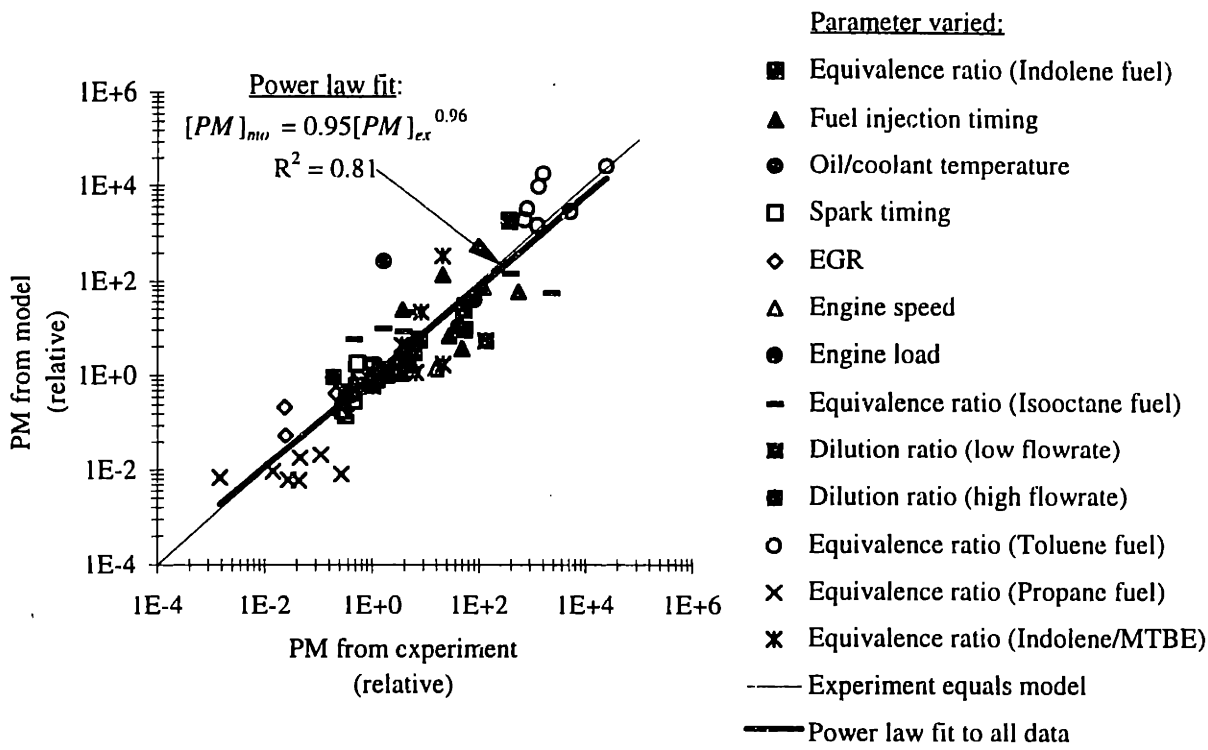

Figure 7.1 Comparison between modeled and experimentally measured PM concentrations. All data scaled relative to PM concentration at baseline conditions.

CHAPTER 8

MODEL RESULTS AND DISCUSSION

8.1 Matrix of Operating Conditions

The matrix of experimental operating conditions (developed to test the effect of engine operating parameters, fuel delivery parameters, and fuel type on particulate emissions) was discussed in a previous chapter; the model will be used to calculate PM emissions at the conditions in this matrix. The matrix centers about the "baseline operating conditions" defined in the context of the experimental conditions (Table 2.2). Comparison is made between model results and all experimental conditions presented in Chapter 5 except for the experiments to measure the effect of lubricating oil and the catalytic converter: the present model is not capable of explaining particle dynamics within the catalyst nor does it attempt to explain the effect of oil composition on PM formation, as indicated in the Background section, above.

The effect of fuel injection control strategy was discussed in Chapter 5. The reason that Proportional/Integral (PI) controller with the Universal Exhaust Gas O_2 Sensor (UEGO) emitted less PM than the standard Ford EEC IV controller with a Heated O_2 Sensor (HO2S) was deemed to be that the former maintained fluctuations in the ϕ within a narrower bound around stoichiometric — the point of minimum PM emissions — than the latter. However, the present model is a steady-state model and does not consider *fluctuations* in ϕ, so if the model is to be applied in order to estimate the effect of control strategy on PM emissions, it must be done in a quasi-steady-state mode. This point is addressed in Appendix 1.

The model relies upon some inputs regarding the geometry of the engine used (in particular, for use in an engine-simulation program to calculate peak cylinder temperature and pressure [51]); parameters used in the present research are those of the Ford Zetec engine described in Chapter 2. The geometry of the Saturn engine, also used for experimental measurements is quite similar: both are 1.9 to 2.0 liter engines with 4-valves per cylinder, pent-roof chambers, and compression ratios 9.5 to 9.6.

8.2 Experimental Comparison

The present model captures the effect of all measured operating conditions on PM concentrations qualitatively if not flawlessly quantitatively; however, its high correlation coefficient (see previous chapter) demonstrates that quantitative comparison is quite good considering the number of fitted constants used. The following figures show comparison of the model to experimental data when various engine operating parameters are varied one at a time. (Absolute concentrations and detailed discussion of experimental apparatus/procedure can be found in preceding chapters.)

Whereas it was expected that PM concentrations would increase as the ϕ becomes rich, it was originally difficult to interpret the increase at lean ϕ. However, analysis of the contributions of individual mechanisms to the total PM concentration clarifies the experimentally observed behavior as a function of fuel/air equivalence ratio (Figure 8.1). The model shows that PM concentrations increase as equivalence ratio becomes leaner than stoichiometric because of the liquid fuel mechanism: although the concentration of liquid-phase fuel in the cylinder increases proportionally to ϕ, the oxygen concentration necessary to ignite the liquid fuel is far more prevalent as ϕ decreases, as shown in Figure 5.2. Gas phase nucleation becomes more prevalent as ϕ is enriched up to $\phi = 1.2$, after which the decrease in temperature overwhelms the increase in HC availability. The oxidation mechanism shows more of an oxygen dependence than a dependence on temperature: the fraction of PM oxidized decreases monotonically with increased ϕ from 50% at $\phi = 0.7$ to 13% at $\phi = 1.3$. Fractional contributions of each mechanism to the total PM mass are illustrated in Figure 8.2, as is the fractional change in mass due to oxidation.

When fuel injection timing is varied, virtually all parameters (e.g., oxygen availability, in-cylinder temperatures and pressures) are unaffected. Rather, fuel injection timing only affects the in-cylinder concentration of liquid-phase fuel and the HC concentration available for post-flame adsorption/absorption. The strong sensitivity of PM nucleation to liquid-phase fuel is reflected in the fact that the model calculates two orders of magnitude higher PM during OVI than during CVI (Figure 8.3). The amount of adsorption/absorption does not vary as significantly as the amount of PM nucleated: Θ_{ab} varies by no more than 70% of the value during CVI.

The model calculates an exponential decrease in PM as the level of EGR is increased (Figure 8.4), in accordance with experimental measurements. This decrease is due to three factors: increased intake temperature resulting from the increased amount of recirculated, hot exhaust gas (at zero EGR, the intake port temperature was measured to be 50°C versus 88°C at the highest EGR rate), in turn resulting in an increased fuel evaporation rate; decreased amount of fuel injected, since EGR displaces air/fuel in order to maintain constant intake pressure, resulting in further decreased availability of liquid fuel in the cylinder; and decreased temperatures and pressures in the cylinder, resulting in decreased Arrhenius terms in the gas phase nucleation rate. According to the model, the above factors overwhelm the countering effects that, as EGR increases, decreased temperatures restrict oxidation and, as EGR increases so do HC emissions, thereby increasing the availability of vapor for adsorption/adsorption. The competing mechanisms cause the kink in calculated PM concentration at the EGR level of 75%: more HC mass is adsorbed/absorbed at the 75% EGR condition than at either the 50 or 100% EGR conditions, the reason being relatively high concentrations of both HCs (9,000 ppmC1) and PM as compared to (a) the 50% EGR condition, at which the HC concentration is lower (3,100 ppmC1), but the PM surface area on which HCs can adsorb/absorb is higher, and (b) the 100% EGR condition, at which the HC concentration is higher (13,200 ppmC1), but the PM surface area on which HCs can adsorb/absorb is overwhelmingly less. The measured PM concentration, by contrast, does not have the "kink" at 75% EGR, but rather shows an exponential decrease in PM with increased EGR across the range of EGR values used. The discrepancy suggests that the model may overestimate the amount of HC adsorbed/absorbed at the 75% EGR condition. Fractional contributions of each mechanism to the total PM mass are illustrated in Figure 8.5, as is the fractional change in mass due to oxidation.

Use of the model to calculate the effect of coolant and oil temperature on PM emissions is complicated by the indirect link between those temperatures and the intake port temperature. The model calculates as much as two orders of magnitude increase in PM as coolant and oil temperatures decrease from 87°C to 34°C. However, the exact magnitude of the increase depends strongly upon the intake port temperature inducing fuel evaporation, measurement of which is complicated by the fact that fuel at different locations in the port may evaporate at different rates. Specifically, a thermocouple inserted close to the port, but not

touching the intake valve, reads approximately 30°C at the colder engine conditions, which is about 20°C cooler than at baseline operating conditions. When this port temperature is used in the model, the model calculates approximately 270 times as much PM at the cold condition as at the warm one, primarily due to the effect of poor fuel vaporization. On the other hand, the intake valve is significantly warmer than 30°C even in the cold operating conditions, and may be as warm as the intake valve at the warm operating conditions, in which case, the effects of the liquid fuel PM nucleation mechanism would be equal for the two cases. Were the amount of PM generated by the liquid fuel mechanism equal for the two cases, the model would calculate a 20% increase in PM emissions relative to the baseline conditions — compared to the measured 60% increase — due solely to the fact that colder engine temperatures result in higher HC emissions (Figure 5.6). These two bounds encompass the measured 60% increase in PM emissions. The fact that the actual measured emissions fall closer to the latter bound suggest that the fuel evaporation rate is primarily determined by conditions on or near the intake valve.

According to the model, the effect of advanced spark timing on PM emissions is a competition between increased nucleation — via both the homogeneous and heterogeneous mechanisms due to higher cylinder temperatures — and increased oxidation, again because of increased temperature and pressure. (Temperatures measured in the intake port are not affected by spark timing, hence fuel evaporation is not affected.) While advancing the spark timing does decrease exhaust temperatures (Figure 5.8), the decrease does not strongly affect the calculated exhaust PM oxidation rate, since far less than 1% of the PM is oxidized in the exhaust at these conditions. However, as the spark is advanced, exhaust temperatures decrease, causing an increased exhaust HC concentration and thus increased availability of vapor for adsorption/absorption. The model results show the correct trend (Figure 8.6); nevertheless, at the most advanced spark timings, the model either overestimates the amount of PM nucleation and/or growth, or it underestimates the amount of oxidation, while at the most retarded spark timings, it does the opposite.

The model calculates increased PM emissions with increased load at fixed engine speed; however, it underestimates the magnitude of the measured increase (Figure 8.7). While the measured PM concentration at wide open throttle and 2000 rpm is 80 times that of the baseline condition, the modeled concentration is only 40 times higher. Model calculations suggest that, when load is increased from the baseline con-

dition to wide open throttle, the amount of PM nucleated via the liquid fuel mechanism increases by a factor of 150, for the following reasons. First, higher load results in higher intake flowrate, which results in lower intake port temperature (the difference was measured to be 4°C), which in turn decreases the fuel evaporation rate. Second, more fuel is injected into the port and less residual gas is retained in the cylinder (residual gas fraction drops from 12% to 5% [51]), resulting in a greater amount of liquid fuel in the cylinder. Third, higher load results in an increased amount of fuel/air charge in the cylinder, which causes higher peak temperatures, thus accelerating the PM nucleation rates. The reason that the model underestimates the effect of load on PM may be that the model underestimates the full magnitude to which load effects intake port fuel evaporation, particularly because a sophisticated submodel for backflow (and the resulting, turbulence) is beyond the scope of the present project. The model calculates that as load increases, particle formation via the gas phase nucleation mechanism increases by a factor of six, because of higher temperatures and higher fuel concentrations. However, as load increases, exhaust HC concentration decreases, limiting the extent of adsorption/absorption. Moreover, as load increases, cylinder temperature and pressure both increase which, according to the model, causes the fraction of PM oxidized to increase from 32% to 54%.

As with load, the model calculates that PM emissions should increase with engine speed, but the model underestimates the magnitude of that increase (Figure 8.8). Increased engine speed decreases the time for heat transfer, so temperatures of gases and engine surfaces increase. For example, as engine speed increases, intake port temperature was measured to increase by 3°C. However, the time for fuel evaporation decreases inversely with increased speed, which — according to model calculations — overwhelms the measured increase in temperature; consequently as speed increases, the model calculates a higher concentration of liquid-phase fuel in the combustion chamber. Plus, as engine speed increases, gas exchange improves so the residual fraction drops from 13% to 11% (according to the engine-simulation program [51]); hence as speed increases, the amount of air/fuel mixture ingested into the cylinder (thus the amount of liquid fuel) further increases. The result is that, as engine speed increases over the range of 1500 to 2500 rpm, the calculated rate of PM nucleation via the liquid fuel mechanism increases by a factor of ten, and the total amount of PM nucleated via this mechanism increases by a factor of six. Moreover, as speed increases, cylinder temperatures increase (again due to the decreased time available for heat transfer), causing the cal-

culated gas phase PM nucleation rate to increase by 20%; however, the decrease in time available for nucleation overwhelms the slight increase. Similarly, model calculations show that, although increased temperatures at increased speeds cause an increased oxidation rate, the total fraction of PM mass oxidized decreases (from 38% at 1500 rpm to 27% at 2500 rpm) because the increase in oxidation rate is overwhelmed by the decrease in time available for oxidation.

In order to test that the model correctly captures the effect of the dilution process on PM concentration, model calculations are compared to experimental results presented in Chapter 4, in which PM was measured while the dilution ratio was varied while all other engine operating parameters remained fixed. With all engine parameters fixed, dilution ratio affects PM mass concentration solely through its affect on the particle dynamics of adsorption/absorption in the dilution tunnel. Calculated PM concentrations as a function of dilution ratio were compared to measured PM concentrations for two cases. In one case, the diluted exhaust flowrate was sufficiently fast to limit heat transfer from the diluted exhaust through the dilution tunnel walls to the atmosphere, such that decreased dilution ratio resulted in increased diluted exhaust temperature (the reasons for which are described in Chapter 4), while at the same time increasing the concentration of the particles and vapors undergoing adsorption/absorption. In the other case, the flowrate of diluted exhaust through the dilution tunnel was so slow as to render the diluted exhaust temperature independent of dilution ratio by allowing sufficient time for heat transfer from the diluted exhaust to the atmosphere. Hence the only effect of increased dilution was to decrease the concentration of the diluted exhaust particles and vapors undergoing adsorption/absorption.

Comparisons of the modeled and measured effect of dilution ratio on PM concentrations in these two sets of conditions are shown in Figures 10 and 11 (scaled by dilution ratio to represent PM concentration per unit of cooled exhaust, as discussed previously). Note that PM concentrations could not be reliably measured via the SMPS without dilution ($\Lambda = 1$) because the conditions in the exhaust can give the SMPS bias that results in ever-decreasing PM concentrations (Chapter 2). Given this disclaimer, the most reliable datum measured at $\Lambda = 1$ (the one with least bias, i.e., the highest measured concentration) is presented in Figure 8.9 for the sake of illustrating the trend. In the case of the low flowrate (Figure 8.10), no measurement could be made at all (moreover, day-to-day variability in PM emissions prohibit use of data presented

in Figure 8.9, since that was collected on a different day). Therefore, the datum at $\Lambda = 1$ is estimated by extrapolating the curve of measured PM as a function of dilution ratio: the value at $\Lambda = 1$ of the best-fit polynomial through the data at Λ from 6 through 16 is chosen as the "estimated experimental datum" (Figure 8.10).

Dilution ratio affects calculated PM concentrations (via its effect on adsorption/absorption) in the following manner. In the low flowrate case, the model calculates a decrease in measured PM concentration as dilution ratio is increased up to about 9:1, above which the PM concentration becomes unaffected by further increases in dilution ratio. While this is the same trend as the measured PM concentrations, the point above which the PM becomes insensitive to further dilution was measured to be about 15:1 rather than 9:1. On the other hand, in the case of high flowrate, the model correctly calculates the dilution ratio at which the PM concentration becomes insensitive to changes in dilution ratio (the model calculates 14:1 and experiments show 13 or 14:1), but it does not calculate as large a variation in PM concentration with dilution ratio as was measured.

The model accurately estimates the relative PM emissions from the different fuels (Figure 8.11), but the model's accuracy may be due *in part* to the fact that the activation energies in the homogeneous mechanism for each fuel were chosen by comparison to experimental data. Nonetheless, the calculated amount of PM nucleated by the homogeneous mechanism does not overwhelm that nucleated by the heterogeneous mechanism across the range of fuel types and equivalence ratios, which suggests that the accuracy of the model is not solely due to the fact that activation energies in the homogeneous mechanism are chosen by comparison to experimental data. The model is designed to reflect how PM is affected by fuel parameters such as (a) the propensity of the fuel molecule to break down into a soot precursor, (b) physical characteristics related to evaporation and heat release as involved in the heterogeneous nucleation mechanism, and (c) the activation energy required to form PM from the soot precursors present in the gas phase. The fact that the model can accurately estimate the effect of fuel type on PM suggests these fuel parameters may be the truly important ones.

8.3 Discussion

In order to decide whether any mechanism in the model is extraneous, each mechanism was individually shut off, the remaining coefficients were optimized, and the correlation coefficient was re-evaluated. In all cases, the correlation coefficient became significantly worse, except for the case when oxidation was shut off, suggesting that all mechanisms with the possible exception of oxidation are important. Explanations of trends in PM emissions as a function of each engine operating condition (above and in Chapter 5) support the assertion that no mechanism is extraneous; that is, reasons for the trends in PM emissions involve all of the mechanisms.

The present model can only be accepted with an important caveat about the uniqueness of the model and its chosen parameters. While every attempt was made to restrict the model to reasonable physical and chemical processes, neither the model nor the present paper gives a unique description of the particle formation and emission processes. Specifically, although the model involves plausible physical and chemical descriptions of particle dynamics and reasonable (if simplified) descriptions of the physical phenomena involved, a model with more detailed physics and chemistry would supersede the present one.

The results of the model suggest that the major contributions to PM are liquid fuel nucleation in fuel-lean conditions or conditions where in-cylinder liquid plentiful (such as open valve fuel injection), gas phase nucleation in fuel-rich conditions, and adsorption/absorption in conditions where the availability of HC vapors and PM surface are both high.

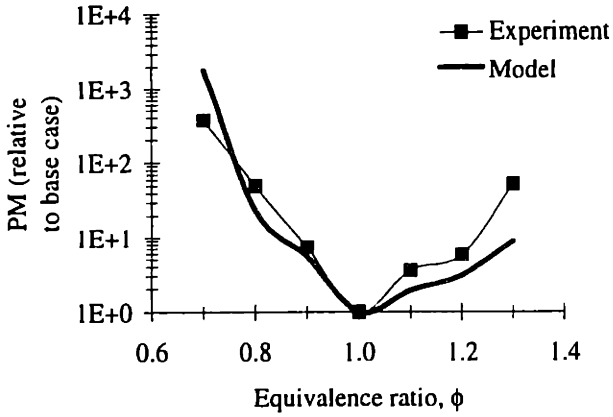

Figure 8.1 Modeled and experimentally measured PM concentrations as a function of fuel/air equivalence ratio. All data scaled relative to PM concentration at baseline conditions.

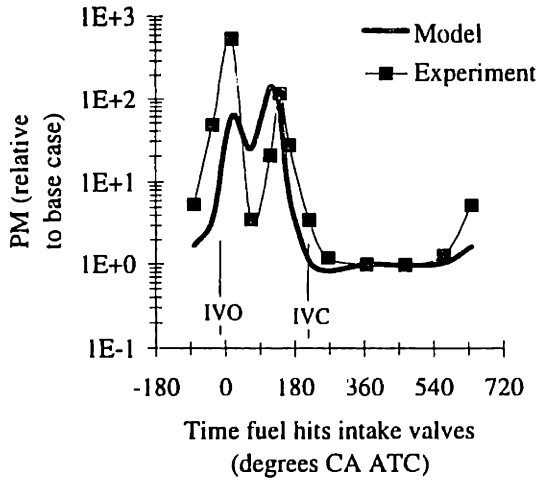

Figure 8.3 Modeled and experimentally measured PM concentrations as a function of fuel injection timing. All data scaled relative to PM concentration at baseline conditions.

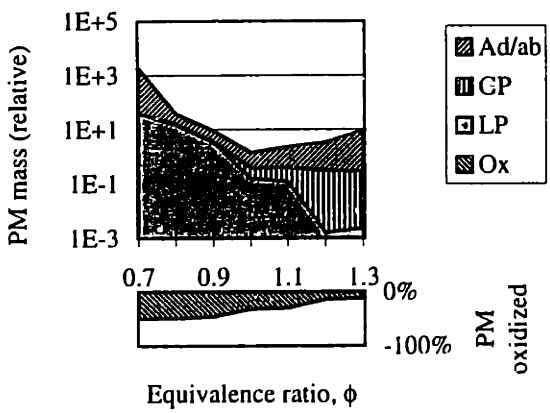

Figure 8.2 Fractional contributions of each mechanism to the total PM mass as a function of fuel/air equivalence ratio, and fractional change in mass due to oxidation. Note that the left hand scale is logarithmic. "Ad/ab" is mass from the adsorption/absorption mechanism; "GP" is from gas phase nucleation mechanism; "LP" is from liquid phase nucleation mechanism; "Ox" is fractional change in mass due to oxidation.

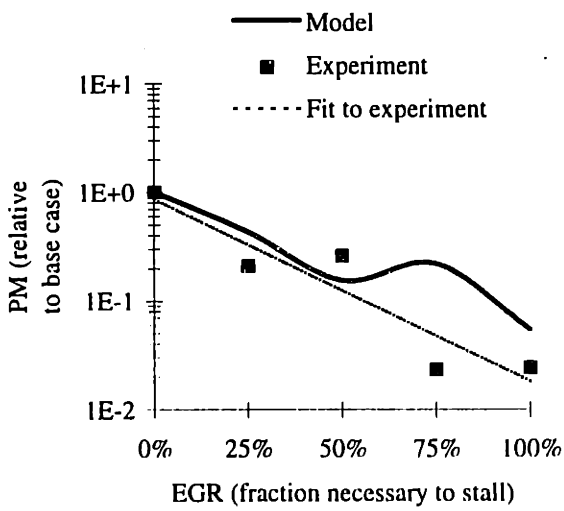

Figure 8.4 Modeled and experimentally measured PM concentrations as a function of EGR rate (measured as the fraction of the amount necessary to stall the engine). All data scaled relative to PM concentration at baseline conditions. Curve labeled "fit to experiment" is an exponential fit to the experimental data.

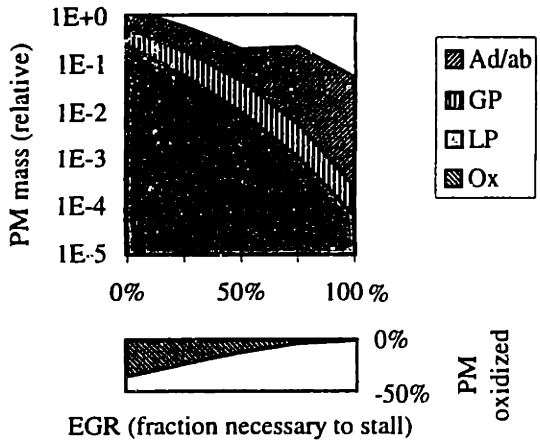

Figure 8.5 Fractional contributions of each mechanism to the total PM mass as a function of EGR rate, and fractional change in mass due to oxidation. Note that the left hand scale is logarithmic. Definitions of symbols same as in Figure 8.2.

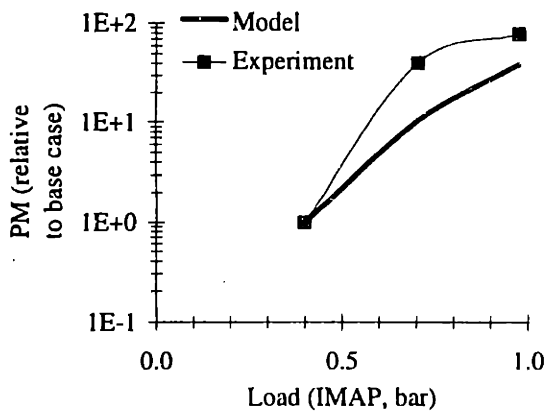

Figure 8.7 Modeled and experimentally measured PM concentrations as a function of load (intake manifold absolute pressure). All data scaled relative to PM concentration at baseline conditions.

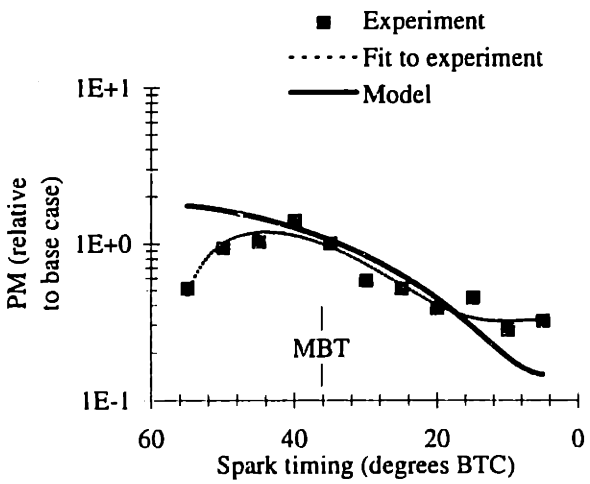

Figure 8.6 Modeled and experimentally measured PM concentrations as a function of spark timing. All data scaled relative to PM concentration at baseline conditions. Curve labeled "fit to experiment" is a fourth order polynomial fit to the experimental data.

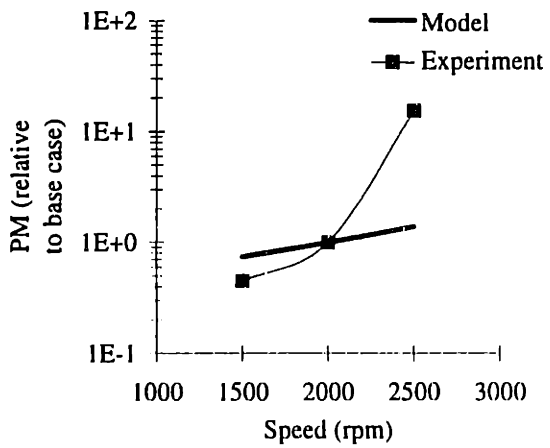

Figure 8.8 Modeled and experimentally measured PM concentrations as a function of engine speed. All data scaled relative to PM concentration at baseline conditions.

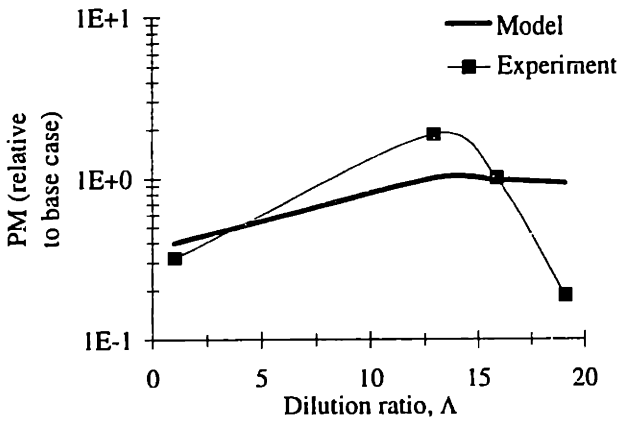

Figure 8.9 Modeled and experimentally measured PM concentrations as a function of dilution ratio in the high flowrate case (Re = 57,000). All data scaled relative to PM concentration at baseline conditions. PM concentration at dilution ratio of unity could not be measured accurately: subsequent measurements will be progressively lower; therefore the datum presented in this figure is the maximum measured concentration at Λ = 1.

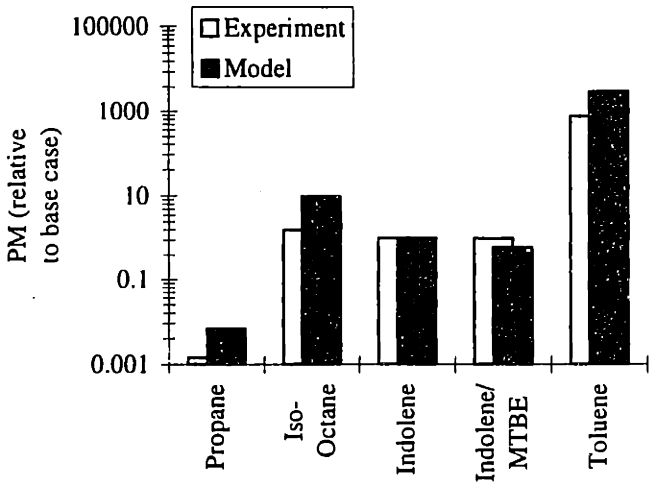

Figure 8.11 Modeled and experimentally measured PM concentrations using the different fuels at the baseline operating conditions. All data scaled relative to PM concentration using indolene fuel.

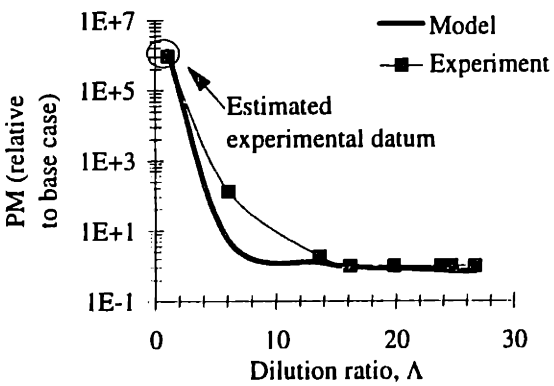

Figure 8.10 Modeled and experimentally measured PM concentrations as a function of dilution ratio in the low flowrate case (Re = 9,000). All data scaled relative to PM concentration at baseline conditions. PM concentration at dilution ratio of unity could not be measured at all, so datum in figure is the extrapolation of the curve through the other data, as explained in the text.

CHAPTER 9

TRANSIENT PM EMISSIONS

9.1 Experimental Methodology and Conditions

METHODOLOGY

The description of the experimental apparatus and the data analysis procedure were given in Chapters 2 and 3. A similar technique is used for apparatus conditioning as in the steady state experiments; because of slight differences, the apparatus technique will be briefly summarized and recapped here. At the beginning of a test day, the SMPS is warmed up and used to measure the atmospheric particulate concentration. Then the SMPS is used to measure the particle concentration in the diluent air, i.e., the air without any engine exhaust that is drawn into the dilution tunnel through the HEPA and charcoal filters. Experiments begin only after the particulate mass concentration in the diluent air drops below 0.4% of the atmospheric concentration, which corresponds to less 0.1% of the measured particle concentration at the baseline engine operating conditions and approximately 0.4% of the minimum measured PM concentration (corrected for dilution ratio) using indolene fuel (data presented in Chapter 5).

Conditioning of the engine is handled as follows. Before any day of experiments, the engine is warmed up at the baseline engine speed and load until the temperatures of the coolant and oil are within 2° of the 87°C set point. Once the engine is fully warmed, the dilution ratio is adjusted in order to achieve good sensitivity in PM measurements at the various engine operating conditions used on the given day of testing — generally the dilution ratio at the baseline engine operating conditions is approximately 15:1. The method for setting the dilution ratio is discussed in Chapter 3.

OPERATING CONDITIONS

As discussed previously, the transient experiments involve cycling between a two sets of engine operating conditions at regular intervals and measuring the time resolved particulate emissions. The baseline engine operating conditions for the present tests are the same as those used in steady state PM emissions studies: 2000 rpm, 40 kPa (absolute) intake manifold air pressure (IMAP), no exhaust gas

recirculation, stoichiometric fuel/air equivalence ratio, coolant and oil temperatures 87 ± 2°C, spark timing set for Maximum Brake Torque ± 3° crank angle, closed valve fuel injection. In experiments where the IMAP is varied, 70 kPa (absolute) is used as the pressure to which IMAP is alternated. In experiments where ϕ is varied, ϕ = 1.3 (30% rich) is used as the value to which equivalence ratio is alternated. In experiments where the engine is started, operated for two minutes, shut down for two minutes, and then restarted, the conditions during firing operation are the baseline conditions, and when the engine is not firing, the engine is still motored at 2000 rpm by the dynamometer with the throttle in the same position as during firing, but with fuel injection and spark ignition turned off.

As discussed in Chapter 2, repeated tests of transient operating conditions are performed by supplying a "square wave" input to the engine controller (Figure 3.1a), be it a square wave in IMAP, ϕ, or fuel supply and ignition. Simultaneous to a change in IMAP, the engine controller changes the spark timing to maintain MBT timing to within ± 3° crank angle. As introduced in Chapter 3, the PM emissions have a response function that is a series of first order responses, as in equation (3.4). The purpose of the data analysis (as described in Chapter 3) is to find the time constant for the first order response of PM emissions to transient engine operation in order to determine whether that time constant differs from that of the diagnostics by a statistically significant margin, and — if so — to infer the cause of the engine's time response. The next section of this chapter will describe the results of experiments in which the time response of the diagnostics are quantified, and the following section will describe the results of experiments in which the Saturn engine is operated in transient mode. Following is a discussion of the reasons for the observed engine responses, the information obtained from these experiments, and their implications on the modeling of PM formation during transient engine operation.

9.2 Time Response of Individual Components

In order to distinguish the time response of the engine from that of the measurement diagnostics, a series of tests were performed, each of which isolate the various subsystems of the measurement apparatus — firstly, the SMPS and, secondly, the SMPS together with the pipes between the exhaust system and the SMPS (that including the dilution tunnel and everything downstream of the exhaust tee in Figure 2.1).

SMPS

The SMPS was isolated by connecting a three-way valve to the SMPS inlet, on one side of which was an opening to the atmosphere, and on the other side of which was a HEPA filter. When the three-way valve was set to the atmosphere, ambient air containing approximately 20,000 particles/cm^3 in the size range from 9 to 378 nm, with approximately 60 particles/cm^3 at the nominal size of 50 nm, was drawn into the SMPS. (For the sake of comparison, the measured mass concentration corresponding to the concentration of 20,000 particles/cm^3 is 17 μg/m^3, which is 13% above the newly enacted annual National Ambient Air Quality Standard, but not beyond the range of concentrations encountered in the laboratory environment.) In the other valve position, filtered air containing only 500 particles/cm^3 between 9 and 378 nm, with approximately 1 particle/cm^3 at the nominal size of 50 nm, was drawn into the SMPS. With the three-way valve in either position, the SMPS inlet temperature and pressure conditions were approximately equal to those encountered when sampling from the monitoring port of the dilution tunnel, which means that the flow conditions were the same.

At periodic intervals, the three-way valve was switched between the two settings, with the resulting SMPS data recorded by the data acquisition computer. Particles of several sizes were measured: Figure 9.1a shows the time response of 50 nm particles and first order fits for both the rising and falling edges of the PM concentration, both of which have time constants of 7 ± 2 seconds. It appears that data in Figure 9.1a has a sudden change in the time constant about 15 to 20 seconds after responding to the step change in SMPS input conditions (shown for the falling edge of the particle response function in the right-hand portion of Figure 9.1a, on a log scale in order that the first order function appears linear, thereby clearly showing the change in slope, corresponding to the change in time constant). The cause of this behavior is unclear: it may be that there is a 15 to 20 second delay between the initial SMPS response and the beginning of a secondary response within the same diagnostic, with the net result looking like a change in time constant 15 to 20 seconds after the response begins. However, this abrupt change in the slope of the SMPS response does not occur at all particle sizes (e.g., Figure 9.1b), and therefore may be attributable to a measurement artifact rather than a real physical particle dynamic phenomenon. Moreover, no abrupt changes in the slope of particle time responses have been observed for any experiments using the dilution

tunnel together with the SMPS, nor when using the engine and the entire PM measurement apparatus; therefore, the matter is not investigated further.

Time constants measured for the various particle sizes were 4 to 7 seconds with error bounds of ± 2 seconds. Figure 9.1 shows first order fits for both the rising and falling edges of the PM concentration, for which the time constants are equal or do not differ by a statistically significant margin (in some cases, to be discussed in upcoming sections, the rising and falling time constants differ significantly). Maricq [11] has also observed that the SMPS has a fairly long time response compared to the one second scanning time of the Electrostatic Classifier (as described in Chapter 2). Limitations on the study of transient PM emissions imposed by the finite time resolution of the SMPS will be discussed in an upcoming section.

SMPS AND DILUTION TUNNEL

The time response of the subsystem encompassing the exhaust, dilution tunnel, and SMPS was measured by supplying particle-laden engine exhaust to the subsystem and periodically shutting off the exhaust flow by closing the more upstream of the valves between the exhaust tee and the dilution tunnel, shown in Figure 2.1. (The second valve, further downstream, was maintained in such a position that, when the upstream valve was open, the dilution ratio in the tunnel was 11.) The particle concentration in the diluted exhaust was 2.5×10^6 particles/cm^3 (with a concentration of approximately 1700 particles/cm^3 at the nominal size of 25 nm), as compared to the order of 100 particles/cm^3 (with a concentration on the order of 20 particles/cm^3 at the nominal size of 25 nm) in the filtered air that constituted the sole contents drawn through the dilution tunnel when the engine exhaust flow was shut off.

Particle concentration data, measured by the SMPS, was recorded while periodically closing the valve that isolates the engine from the tunnel, as described above. Figure 9.2 shows the time response of 25 nm particles and first order fits for only the falling edge of the PM concentration, corresponding to the event when the exhaust flow through the dilution tunnel is abruptly shut off. The rising edge, when exhaust begins to fill the section of pipe downstream of the valves and the exhaust tee, is not shown because it was found to be an unrepeatable time-response function uncharacteristic of anything measured in the present engine experiments. That is, the event in which the exhaust pipe initially contains no exhaust and *gradually*

fills — as opposed to engine transients in the present project, which are step changes in engine operating conditions while exhaust constantly flows through the exhaust pipe — results in an unrepeatable particulate response function, the like of which never occurs in the engine experiments that are of primary interest in the present project. For this reason, the rising edge PM responses are not plotted or discussed further.

Measured time constants were 4 ± 1 seconds. The fact that the time response for the entire system of plumbing as well as the SMPS equals that for the SMPS alone — to within a statistically significant margin — demonstrates that the SMPS is the limiting factor regarding measurement time resolution. Along another line, the fact that particle concentration drops by orders of magnitude in the minimum time-scale observable with the SMPS verifies that particle storage in the transfer tubes and dilution tunnel is negligible. (Note that this conclusion does not necessarily apply to the engine itself; rather, storage in exhaust ports or runners may be significant, as will be discussed.) The result of these two observations is that any observed time response that is slower than that of the SMPS should presumably be due to particle formation and/or storage effects in the engine itself, as opposed to limitations in the SMPS response time or storage in the transfer tubes and/or dilution tunnel. The following experiments isolate the responses of PM emissions to various engine transients and discuss how those time responses compare to the limitations imposed by the diagnostics.

9.3 Results

RESPONSE TO TRANSIENT LOAD

In experiments where the intake manifold absolute pressure is varied between 40 and 70 kPa, the measured time response of PM generally follows a first order response (Figure 9.3). (One exceptional case will be presented and discussed in an upcoming portion of this section.) The time constants for both the rising and falling edges of the PM response function are between 4 and 21 seconds for different PM sizes (Table 9.1); however, the value for the rising edge is not always equal to that for the falling edge. Possible reasons for this inequality are measurement uncertainty or the fact that different intake manifold pressures between the rising and falling edges of the PM wave result in different exhaust flowrates, which in turn affects the degree to which PM mixes and diffuses within the exhaust pipes and dilution tunnel. Another

possibility is that each different load condition has a correspondingly different rate at which the liquid fuel pools in the intake port are filled and depleted, and therefore enhances or retards to a different degree the formation of PM at in-cylinder sites of burning liquid fuel.

Table 9.1 Time constants measured for rising and falling edges of particulate response for experiments with varying intake manifold pressure [a]

Size (nm)	12.5	25	50	75	100	200
τ_{re}, rising edge time constant (seconds)	20 ± 4	14 ± 6	21 ± 5	14 ± 5	(b)	(c)
τ_{fe}, falling edge time constant (seconds)	19 ± 4	11 ± 8	11 ± 5	11 ± 7	(b)	(c)

[a] Bounds on the time constants are listed as a range of values above and below the median value, as discussed in Chapter 3.
[b] Time constants for the emissions of 100 nm particles were discussed in the Uncertainty Analysis in Chapter 3: data measured on different days for the rising time differed significantly, although the falling time was found to be 4 ± 1 second on one day and 7 ± 3 seconds on the second, which is not a statistically significant difference.
[c] Particles in the nominal 200 nm size range had too low a concentration to yield acceptable signal to noise, as discussed in Chapter 3.

Clearly the time constants measured in the present experiment (4 to 21 seconds) are not always longer by a statistically significant margin than the time constants associated with the pipes, dilution tunnel, and diagnostics (4 to 7 seconds). In cases where the engine response time does not exceed that of the diagnostic, the time response of the diagnostic may be the limiting characteristic in measuring the engine's time response. However, in cases where the engine response time does exceed that of the diagnostic (specified in Table 9.1, above), it can be concluded that the engine creates some kind of time delay. One possible source of the delay is the liquid fuel pool in each intake port: when the engine makes a transition from one load to another, a larger or smaller supply of fuel must be injected per cycle, and a similarly larger or smaller supply of fuel must leave liquid fuel pools in the intake ports either in liquid or vapor phase. The fact that the air/fuel ratio is generally within 5% of the nominal stoichiometric value (example, Figure 3.1b, as well as Figures 9.7a and b) does not necessarily mean that the vapor-to-liquid fractionation does not vary during the transient operation. Rather, parameters relating to fuel evaporation such as the temperature of the intake valve and the amount of fuel pooled in the intake port vary during load transients (see section 7.2 and [76]), and as a result, the relative fractionation between liquid and vapor phase fuel transported from the intake port into the cylinder may change. Since the amount of liquid fuel present in the combustion chamber strongly influences the amount of PM formed (as discussed in Chapters 5, 7, and 8), transient

settling of the vapor-to-liquid ratio (or, equivalently, the amount of liquid phase fuel in the combustion chamber) from its initial value to its final one may affect the rate at which transient PM emissions settle to a steady state. Aquino *et al.* measured the intake valve bulk temperature during a transition in intake pressures approximately equivalent to the present one (from 40 kPa to just less than 80 kPa); these data show a time constant for valve temperature response on the order of 20 seconds [76]. Intake valve temperature significantly affects the amount of liquid fuel in the cylinder that may form PM (as was inferred and discussed in Chapter 7), and therefore, the similarity between the time scales of intake valve temperature change and PM response lends evidence to the assertion that the observed time response for PM emissions is due (at least, in part) to changes in liquid fuel vaporization characteristics in the intake port, and the subsequent availability of liquid fuel in the cylinder for formation of PM.

Another possible factor determining the time constant for PM emission response is that particles are stored on and released from the walls of the exhaust port or runner: at a change in IMAP, the exhaust flowrate changes as does the PM concentration in the exhaust, thereby forcing a change in the amount of PM stored on and released from engine surfaces per unit time. In contrast to storage and release in the pipes leading from the exhaust tee to the dilution tunnel (Figure 2.1) as well as in the tunnel itself, storage and release in the exhaust port and/or runner may be significant. However, time-scales over which these processes occur have not been investigated, owing among other reasons to the difficulty of exhaust sampling for PM measurement (see Chapter 2).

The fact that rise time is always greater than or equal to falling time has not been attributed to any engine characteristic, but may simply be coincidental. Rather, in experiments with variable air/fuel ratio (upcoming section), rise times are sometimes larger, sometimes equal, and sometimes smaller than falling times.

RESPONSE TO TRANSIENT FUEL/AIR RATIO

In experiments where the fuel/air equivalence ratio is varied between 1.0 and 1.3, the measured time response of PM again follows a first order response, at least for small — 12.5 and 25 nm — particles (Figure 9.4a). For the larger particles, the response starts out as first order, but after a "peak" concentration is reached, the quasi-steady state emission level is observed to drift up or down. However, the drift is not

repeatable: measured PM concentrations sometimes drift up, sometimes down (Figure 9.4b). The drift has been found to exceed the 30% uncertainty bound on only one occasion, and then for a duration of only two seconds (circled in Figure 9.4b); whether this drift is merely noise or a systematic variation is unclear.

The time constants for both the rising and falling edges of the PM response function are between 6 and 25 seconds (Table 9.2). Again, the value for the rising edge is not always equal to that for the falling edge, possibly because of different rates at which liquid fuel pools in the intake port are filled and depleted.

Table 9.2 Time constants measured for rising and falling edges of particulate response for experiments with varying fuel/air equivalence ratio [a]

Size (nm)	12.5	25	50	100	200
τ_{re}, rising edge time constant (seconds)	6 ± 4	18 ± 6	13 ± 4	(b)	(b)
τ_{fe}, falling edge time constant (seconds)	15 ± 4	17 ± 4	25 ± 4	(b)	(b)

[a] Bounds on the time constants are listed as a range of values above and below the median value, as in Table 9.1, above.
[b] Particles in the nominal 100 and 200 nm size ranges had poor signal to noise.

In the case of 12.5 nm particles, the rising time does not differ from that of the diagnostics (4 to 7 seconds) by a statistically significant margin. For 50 nm particles, the range of values on the rising time just overlap with that of the diagnostics, given its 2 second uncertainty bound. But for all of the other conditions summarized in Table 9.2, time constants associated with the engine emissions are longer than the time constants associated with the dilution tunnel and diagnostics by a statistically significant margin. Moreover, for these latter cases in which the engine time constants differ from diagnostic ones by a statistically significant margin, the time constants for the experiment with varying ϕ are similar to those in the experiment with varying load, which suggests that the factors causing PM versus time response function might be similar for the two experiments. Specifically, the reason for the relatively slow transition from one steady state PM concentration to the other (in comparison to the time required for the fuel/air ratio to reach its new value and the time for the diagnostic to respond to step input changes) may be the gradual rate at which the liquid fuel pools in the intake ports equilibrate to the new conditions, and the subsequent gradual equilibration in in-cylinder liquid fuel concentrations. Further, the time response may reflect the rate at which exhaust pipe storage/release effects occur.

RESPONSE OF PM DURING START-UP EXPERIMENTS

Experiments were performed in which the engine was motored at 2000 rpm while the ignition and fuel injection were simultaneously turned on or off every two minutes. The engine was fully warmed up, in order that start-up and shut down tests would be readily repeatable without possible interference from day-to-day engine variability, which might be problematic if, for example, cold start tests were performed on several consecutive days. Moreover, the fully warmed conditions guarantee that the effect of the start-up itself on PM emissions will be separated from effects of the warm-up process on PM emissions. (The effects of warm-up on PM emissions will be discussed separately.) The engine and control configuration were those described previously; although the control computer was set for stoichiometric operation, during the open loop control that occurs for the first few cycles of warmed-up operation, the engine may override the controller by enriching the fuel flow. However, if such enrichment occurred, then it was over such a short time scale as to be immeasurable with the Universal Exhaust Gas Oxygen (UEGO) sensor.

The results of these experiments are similar for all of particle sizes tested (for example, Figures 9.5a and b) except 200 nm which had too few particles to yield a reasonable signal to noise ratio. Unlike the experiments with variable load and air/fuel ratio, these data are not normalized since they will not yield information about a time constant; rather they are plotted as the measured number concentration. In two experiments, the SMPS saturated during the shut down when measuring 25 nm particles: the SMPS measurement range was set for optimal sensitivity during most iterations of the current experiment. No evidence suggests that the curves cut off by the SMPS detection limit would have been qualitatively different from the others. Concentration levels from one curve to the next in both Figures 9.5a and b show neither a consistent increasing nor decreasing trend, suggesting that variations between PM concentrations on the different curves at any given time are merely the result of the combined engine and measurement uncertainty. (Variations between curves in Figures 9.5a and b serve to quantify the level of uncertainty attributed to the present start-up and shut-down experiments.)

Measured trends in PM emissions during the start-up and shut-down experiments are the following (reasons for these phenomena will be discussed in upcoming paragraphs). At start-up, PM emissions are dramatically higher than the emission level immediately following the start-up event but before the shut-down event; i.e., start-up causes a burst of particles. Similarly, at shut-down, PM emissions are higher

(though not necessarily dramatically higher) than the baseline level. The measured PM response is what is observed when two short bursts of particles and baseline emission level in between are subject to a first order time lag, such as that caused by the mixing and transit through the exhaust pipes, dilution tunnel, and SMPS (as schematically demonstrated in Figure 9.6a). The following is a discussion of the reasons for the two bursts of particles and an explanation of the PM emissions trends between those peaks.

High emissions during the start-up are most likely due to the high liquid-to-vapor ratio of the fuel entering the cylinder, if not directly due to a higher than stoichiometric fuel/air ratio. As alluded to above, although many engine controllers will intentionally enrich the first cycle of operation, the oxygen sensor used for the present experiment registered a stoichiometric fuel/air ratio for the entire two minute period when the engine was running. This may mean that (a) the particular control strategy did not involve enrichment, or if it did involve enrichment, then (b) any enrichment occurs over an immeasurably short time-scale, or (c) the sole effect was to rapidly build up enough of a liquid fuel pool in the intake port that a stoichiometric amount of fuel is transported from the pool to the cylinder, either in liquid or in vapor phase. However, even if enrichment does not occur, when the engine first starts, the intake valve is cooler than during steady state operation, leading to poorer fuel evaporation. Hence, whether or not enrichment occurs, the start-up would be accompanied by a brief period when in-cylinder liquid fuel concentration exceeds that during steady state operation, and would therefore lead to a short burst of high PM emissions due to the strong dependence of PM nucleation on in-cylinder liquid fuel, as discussed in Chapters 5 through 7. In summary, a combination of a high liquid-to-vapor fuel ratio and/or enrichment is consistent with the observed peak in PM emissions at start-up.

Since the engine operating conditions between the start-up and shut down are ostensibly steady-state, it might be expected that the PM emission rate would be steady to within the 20-30% uncertainty (described in Chapter 3). However, as can be seen for the 25 nm particles particularly (and slightly for the 50 nm particles), the so-called "baseline level" in between the start-up and shut-down events is anything but level. The reason why 25 nm particles increase in concentration during the steady operation for the first two minutes after the start-up may be that storage- and release-related growth processes in the engine (presumably the exhaust port and runner) cause particles to grow over time. That is, when the engine is being motored, essentially no particles accompany the air blown through the exhaust pipes, so particles are

stripped from pipe walls and not replaced. Then, when the engine starts to fire, the amount of particles on the exhaust walls is below the equilibrium level, so there is a net settling of particles on the walls where they may undergo coagulation and growth by adherence of HCs. But as time progresses, more particles are present on pipe walls, so more are available to be stripped off; therefore, in time the particles emitted from the engine are more numerous and larger. The result is that the size distribution shifts upward and to larger particles (as schematically demonstrated in Figure 9.6b), and either of these changes may account for the increase in "baseline" PM emission levels over the first few minutes of steady operation. Another possibility is that the liquid fuel conditions in the intake and cylinder — particularly the equilibration of the in-cylinder liquid-to-vapor fractionation — may lead to a gradual increase from small nuclei of particles (around 10 nm in diameter) to larger agglomerates (closer to 30 to 50 nm).

It is not clear that PM emissions are peak during shut-down or whether they are simply rising at the same time as the engine is shut off. If emissions do peak, the reason for that peak is unclear: perhaps dramatically unstable combustion in a few cycles, thus producing markedly higher PM concentrations than the baseline level. The oxygen sensor becomes overwhelmed by noise during shut down, so it is impossible to discern whether the last few cycles are excessively rich or lean. On the other hand, it may be the case that the trend toward higher emissions during the baseline operation period merely overlaps with the shut-down event, masking whatever really happens during shut-down. Future work for the present project involves further investing the shut-down event, using the experimental apparatus at Ford Motor Company.

After engine shut-down and before the engine is started up again, the particulate emissions levels decay to relatively low levels, so low in fact that they are roughly equivalent to the PM levels drawn through the dilution tunnel when the engine is shut off altogether, which is to suggest that the engine produces no measurable PM concentration when being motored. (Example PM levels drawn through the dilution tunnel with the engine off were cited in the section 9.2.) Previous experiments have shown that only a negligible fraction of the present engine's PM emissions come from a source other than combustion such as oil consumption (Chapter 5), so that PM emissions during motored engine operation (as opposed to fired) are not expected to be measurably different from the background tunnel levels.

NON-FIRST ORDER RESPONSE

On one day of testing, experiments showed a response to transient intake manifold pressure that was not first order; rather, the response had an overshoot, which is to say that it showed a higher-than-first order response in transition between steady state emission levels (Figure 9.7a)[4]. Although these results were duplicated several times on the same day (repeated results shown in Figure 9.7a), they could not be duplicated on any other day of testing. Rather, on all other days, the data showed a first order response like data in Figure 9.3 (Figure 9.3b shows the response function for the same conditions and particle size as does Figure 9.7a).

For the experiment in Figure 9.7a, when load is increased from 40 to 70 kPa (time = 0 after correction for the transit time), the concentration of 12.5 nm particles gradually drifts up, as if the primary change in the size distribution is a shift from smaller particles to larger ones — i.e., the whole size distribution is shifting along the particle diameter axis toward larger particles. However, it should be noted that the response in Figure 9.7a is not first order, which is characterized by a sudden change in slope at time = 0 — i.e., an abrupt change in the derivative of the time response like that in Figures 9.3a and b at time = 0, as opposed to the gradual drift at time = 0 in Figure 9.7a. After three to six minutes, the concentration in Figure 9.7a begins to decrease, as if the size distribution continues to move toward larger particle sizes, but now the mode particle size has passed 12.5 nm. When the intake pressure is reduced, however, the concentration of 12.5 nm particles increases dramatically (on some occasions, saturating the highest measurement range of the SMPS), only to settle to its original level after several minutes. Data taken at 25 nm corroborates the drift in the particle size distribution along the size axis: the concentration of 25 nm particles does not even start to increase until approximately four minutes after the step change in load, which is consistent with the size distribution moving gradually to higher particle sizes. However, once the concentration of 25 nm particles does increase, it quickly saturates the SMPS at even its highest setting, so that when the downward step in load occurs, an overshoot in PM concentration (if it occurs) cannot be measured. Data taken at 50 nm further corroborates the aforementioned drift: the concentration of 50 nm particles does not start to increase until nearly seven minutes after the step change in load. When the

[4] Note that Figure 9.7 is not normalized between 0 and 100% of a steady state emission level because no steady state level is reached.

downward step in load occurs, the response is first order, and no overshoot is observed. (The measured concentration at 50 nm is shown in Figure 9.7b for comparison to the first order response function with respect to changes in load, shown in Figure 9.3a.)

The occurrence of these overshoots and drifts in particle sizes is troubling from a research perspective because they were unrepeatable events: it was only on this one day that they were observed to occur. The fact that the lengths of time between steps were different between the present experiments and those experiments resulting in a simple first order response function might be suggested as the crucial difference. However, a variety of step durations were used in the present experiments (although the results are not shown for all experiments), and only on this occasion was a non-first order response observed. Moreover, results presented in Chapter 3 show that the particulate time response does not depend on the duration of the time steps between load changes. In fact, no matter what length the step duration is, a first order response can be recognized simply by its sudden change in slope at the time when the step occurs followed by a smooth, monotonic rise to the final steady state value. Data in Figures 3.1 and 9.1 through 9.5 show that sudden change in slope and smooth, monotonic increase, while data in Figure 9.7a do not.

9.4 Discussion

A few factors may account for long time (tens of seconds) that it takes the PM emissions to reach a steady state after a change in engine conditions. (The present discussion considers only those cases where the PM emissions had a time constant that differed from that of the diagnostic by a statistically significant margin so that the response time of PM emissions could be distinguished from that of the diagnostic.) Firstly, although the engine controller is programmed to maintain the desired air/fuel ratio without over- or under-shooting (and, according to data presented in Figures 3.1 and 9.7, it does so to within 1-2% excluding what are thought to be outliers, as marked in Figure 9.7b), the controller is not programmed to maintain the steady state in-cylinder fractionation between liquid- and vapor-phase fuel. For example, at a step increase in the input value of equivalence ratio versus time, when the desired equivalence ratio is suddenly enriched by 30%, the control system measures the exhaust equivalence ratio and adjusts input conditions until the desired value is reached (likely using a built in fuel injection control strategy or a so-called "tip-in" strategy to reach the desired value as quickly as possible); but the fact that exhaust equivalence ratio quickly reaches

the correct steady state value does not mean that the in-cylinder liquid-to-vapor fractionation has reached the steady state value. On the contrary, for the first few seconds after the engine input conditions demand 30% higher equivalence ratio, the engine controller has to inject more than an additional 30% of fuel per cycle into the pools of fuel already in the intake port, the reason being that the rate of fuel evaporation does not increase by 30%. Consequently, the 30% increase in exhaust equivalence ratio is partly an increase in ingested fuel vapor and partly an increase in ingested liquid fuel; in fact, the amount of ingested fuel vapor may not ever increase by the full 30%. Nonetheless, it is only after the intake conditions (i.e., temperature, amount of fuel injected per cycle, and other parameters affecting the amount of fuel evaporating per cycle within the intake port) equilibrate that the amount of in-cylinder vapor fuel will increase to its full equilibrium value. Thus, it is only after intake conditions equilibrate that the amount of PM formed from this in-cylinder vapor fuel will themselves reach an equilibrium value. Similarly, it is only after intake conditions equilibrate that PM emissions from in-cylinder liquid fuel reach their equilibrium value, although the opposite effect is occurring as occurs for vapor phase fuel: a given amount of liquid fuel becomes less likely to nucleate particles in the increasingly more fuel-rich global environment (according to the model presented in Chapters 7 and 8), but increasingly less liquid fuel is present as time progresses. The net result is that, when the input equivalence ratio increases, the particle nucleation rate increases to an equilibrium value only as fast as intake port conditions equilibrate, because of the effect on in-cylinder liquid-to-vapor fuel fractionation.

The second factor that may account for long time it takes the PM emissions to reach a steady state after a change in engine conditions is the gradual equilibration of storage and release processes on walls of engine parts (for instance, the exhaust port). Specifically, emitted particles may consist of particle nuclei (defined above) and adhered vapor, either of which may be stored and released from walls of engine parts. Although tests isolating the SMPS, the dilution tunnel, and the exhaust pipes downstream of the exhaust tee show that storage in those parts is negligible, the tests do not prove that particles and/or vapor cannot be stored in the exhaust port or the exhaust pipe leading up to the exhaust tee (Figure 2.1). Rather, a portion of particle growth via adherence of vapor may occur in the exhaust port as a result of particles/vapors being stored and released from engine walls. Were this the case then, at times when particle and/or vapor emissions from the cylinder suddenly increase (i.e., at a change in engine operating conditions), the rate at

which particles and/or vapors become stored on exhaust port walls will exceed the rate at which they are released, and those rates may not equilibrate for several seconds or several tens of seconds. Specifically, when engine operating conditions change, the exhaust gas particulate concentration changes, hence the size of the particulate concentration gradient between the exhaust gas and exhaust port walls changes, so the rate at which particles are stored on and released from port walls changes. But, equilibration of the storage and release process inherently takes some time. The time constant with which engine-out PM emissions respond to transient engine operating conditions may reflect the combined rates of equilibration of liquid fuel pools in the intake port and particle dynamics in the exhaust system.

Time constants for engine response functions are longer than those for the measurement diagnostic alone by a statistically significant margin in many but not all cases. This suggests that the time response of the tunnel and SMPS set-up *may* limit the ability to accurately resolve transient PM emissions. Although data in preceding figures generally show a first order response to transient operating conditions, as described by equation (3.4), measurement of a first order response is consistent with either of the two following scenarios: (a) exhaust particulate emissions truly respond to transient engine operation with a first order transition between the initial and final emissions levels, and (b) the engine responds in to transient engine operation with a higher-than-first order response function, but either mixing in the exhaust, tunnel, and SMPS or limitations on the time response of the SMPS result in measured data that only resembles a first order response. The temporal limitation of the SMPS leads to the recommendation that the response of PM emissions to transient conditions be verified with a diagnostic capable of better time resolution, such as Laser-Induced Incandescence, which has been used by other researchers [77, 78, 79] in applications other than SI engine studies.

Moreover, as alluded to in Footnote 1, the fact that a first order response function is measured in almost every case does not necessarily mean that no higher order response actually occurred. Rather, PM emissions may have (for example) a second order response, which overshoots the steady state PM emission value, but which is measured to be first order because of the effect of mixing in the exhaust, dilution tunnel, and SMPS. Notwithstanding, it is more reasonable to accept the data in Figures 3.1 and 9.1 through 9.5 at face value than to believe that a variety of factors conspire to yield a deceptively simple looking response. Insofar as intake, in-cylinder, and exhaust conditions change in first order fashion to transient engine

conditions (example: [76]), and insofar as these conditions control PM emissions in steady state, the accepted first order PM response function is consistent with instantaneous PM emissions being equivalent to the quasi-steady state emissions governed by instantaneous engine conditions.

Were this the case and were all governing conditions as a function of time well known, then steady state models of PM formation and emission could be used to predict the quasi-steady state emissions at several points during any period of transient PM emission. For example, PM emissions during the FTP could be predicted using the model in Chapter 7 based upon a knowledge of the temperature history of relevant engine parts, engine speed, load, spark timing, fuel injection timing, and exhaust gas recirculation conditions at any given instant, as well as exhaust conditions and dilution ratio. (Appendix 3 addresses this point and predicts PM emissions during the FTP, albeit with a limited data set.) When used to calculate transient PM emissions in this manner, the model predicts that the high PM emissions measured during the acceleration transients in FTP tests ([12, 36], as discussed in the Introduction) may not be due to an overshoot in PM emissions during transients and may not necessarily be due to non-stoichiometric air/fuel ratios. Rather, the model predicts that high PM emissions are simply due to the fact that periods of acceleration require high engine load, which leads to orders of magnitude increases in PM emissions for the reasons discussed in Chapter 8.

Higher PM emissions during Bag 1 of the FTP than Bag 3 can also be explained by either quasi-steady application of the model in Chapter 7 or simply the assumption that quasi-steady state sensitivity to engine temperature is the same as that measured in steady state (Chapter 5). Specifically, the response of PM emissions to cold starting conditions, as opposed to the warm ones used in the present experiments, should be the superposition of the PM response to a warm start-up with the PM response to cold steady state conditions. The colder the steady state engine operation, the higher the PM emissions. Consequently, if the intake port temperature conditions for a cold start — coldest right at the start but with a gradual warm up [57] — were encountered during operation that was steady state in all other respects, then the emissions would start high and gradually decrease. Going one step further, if the gradual intake port warm-up were encountered at the same time as the engine was started (which is to say: if the conditions were a cold start), then PM emissions should show a higher peak (or the burst of particles, described above) than in the warmed-up starting case, but as the engine warms, PM emissions would gradually approach those for the

warmed-up starting case. In summary, higher PM emissions in the cold Bag 1 than in Bag 3 [12, 36] is consistent with a quasi-steady state response to differences in the temperatures of engine parts.

While the present experiments did not address the effect of the catalytic converter on transient PM emissions, it is possible to speculate that the time response of catalyst-out PM emissions follow a quasi-steady state response to governing engine/catalyst conditions. If they do follow quasi-steady governing conditions, then the observed decrease in tailpipe PM emissions from Bag 1 to Bag 3 of the FTP [12, 36] is consistent with the fact that the catalyst warms up after the engine is started and the fact that the catalyst *may* oxidize PM when warm. (Chapter 5 presented data showing that, at high catalyst temperature, PM concentrations may decrease, though not by a statistically significant amount.)

The response of engine-out PM emissions to step changes in engine speed at constant load — an experimental condition that cannot be performed with the author's dynamometer — might have a non-first order response, *even though* it follows the quasi-steady state PM emissions. The reason is that variations in speed affect two factors influencing measured PM emissions: (a) the time available for processes like fuel evaporation and post-formation particle dynamics, and (b) temperatures in the intake, cylinder, and exhaust. When engine speed is suddenly increased, the time available for the above processes immediately decreases, while temperatures increase only gradually. Consequently, immediately after a step increase in engine speed, quasi-steady state conditions might make PM emissions increase at first, overshooting the eventual steady state level, but soon decrease slightly.

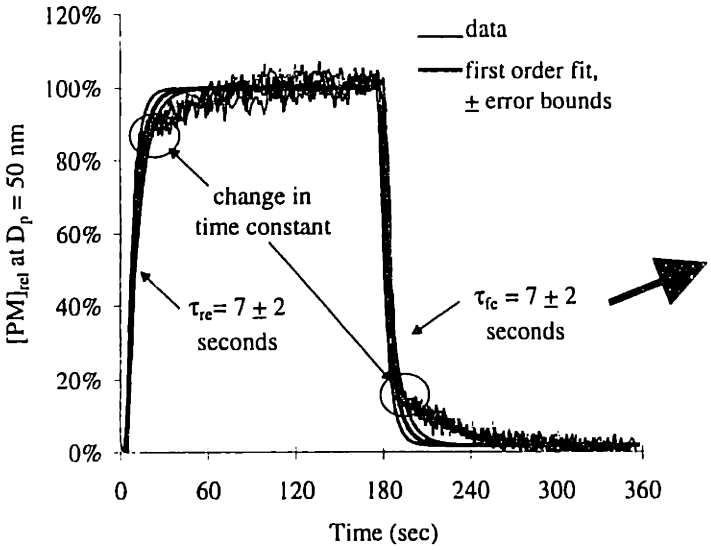

(a) 50 nm particles

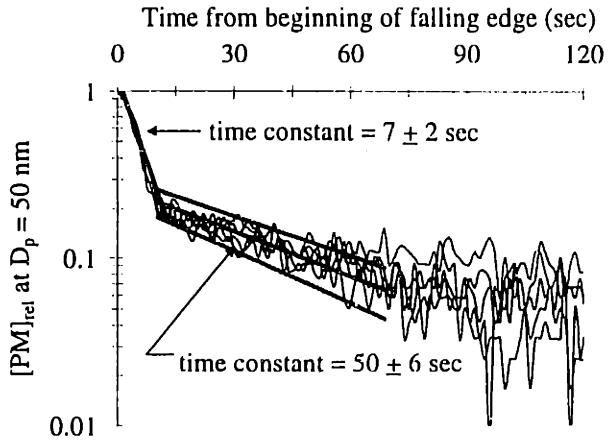

(a, continued) blow-up of falling edge for 50 nm particles on a log scale

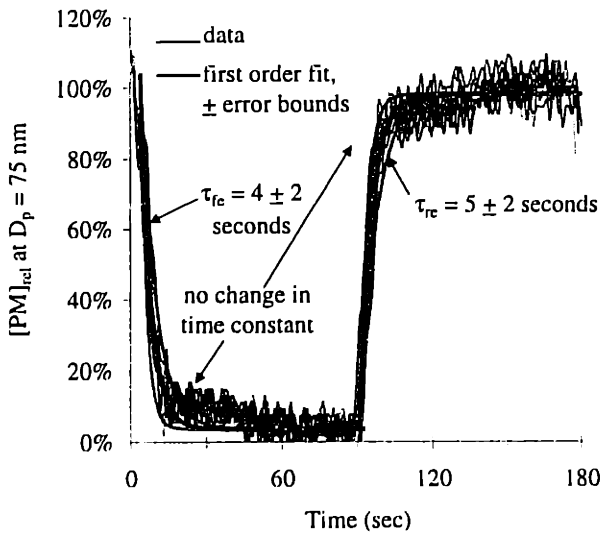

(b) 75 nm particles

Figure 9.1 Time response of SMPS to step changes in PM concentration. Particle size measured: (a) 50 nm, (b) 75 nm. The 50 nm PM emissions have a sudden change in the time response, while at 75 nm, if such change occurs, it is indistinguishable from measurement noise.

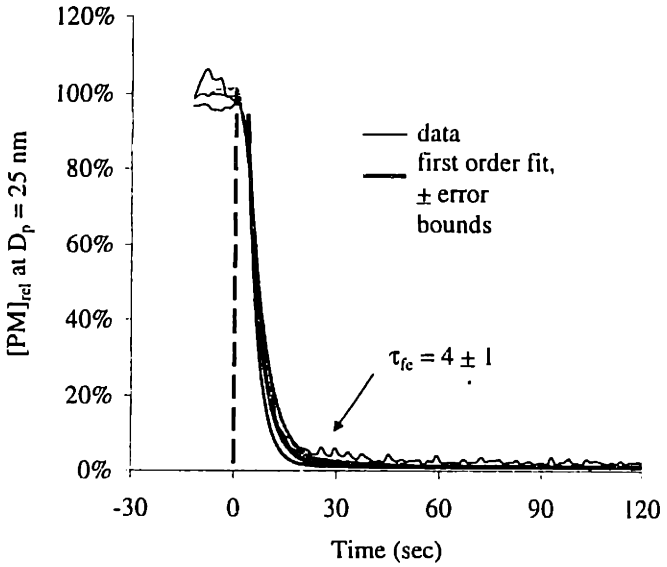

Figure 9.2 Time response of exhaust piping, dilution tunnel, and SMPS to step changes in PM concentration. Particle size measured: 25 nm. Time between step changes: several minutes (in order for conditions to reach steady state before any step change in input conditions). Vertical dashed line at time = 0 denotes beginning of transient response after the steady state period during time < 0.

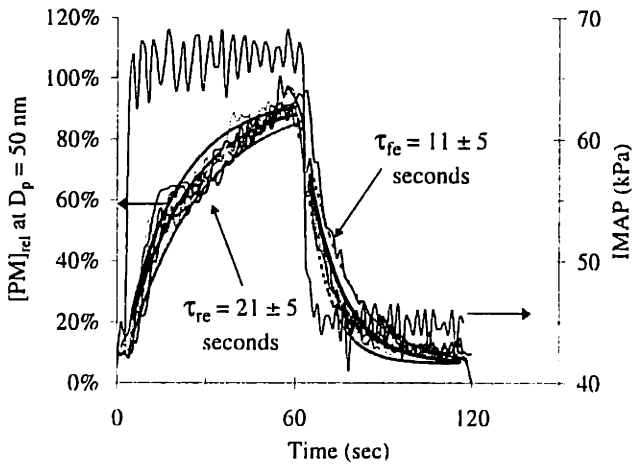

(a) 50 nm particles

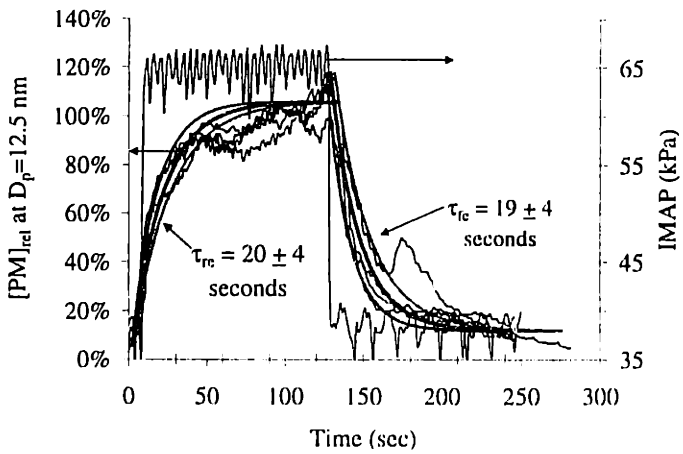

(b) 12.5 nm particles

Figure 9.3 Response of PM emissions to transient intake pressure. Particle size: (a) 50 nm, (b) 12.5 nm. Baseline conditions at the 40 kPa IMAP case, with a dilution ratio of 7:1. Baseline conditions except for intake pressure at the 70 kPa IMAP case, with a dilution ratio of 5:1. Air/fuel ratio remains within same bounds about stoichiometric as in Figure 3.1b, and thus is not plotted. Although the durations of the time steps differ between figures a and b (1 and 2 minutes, respectively), Chapter 3 has shown that the duration does not affect the particulate time response.

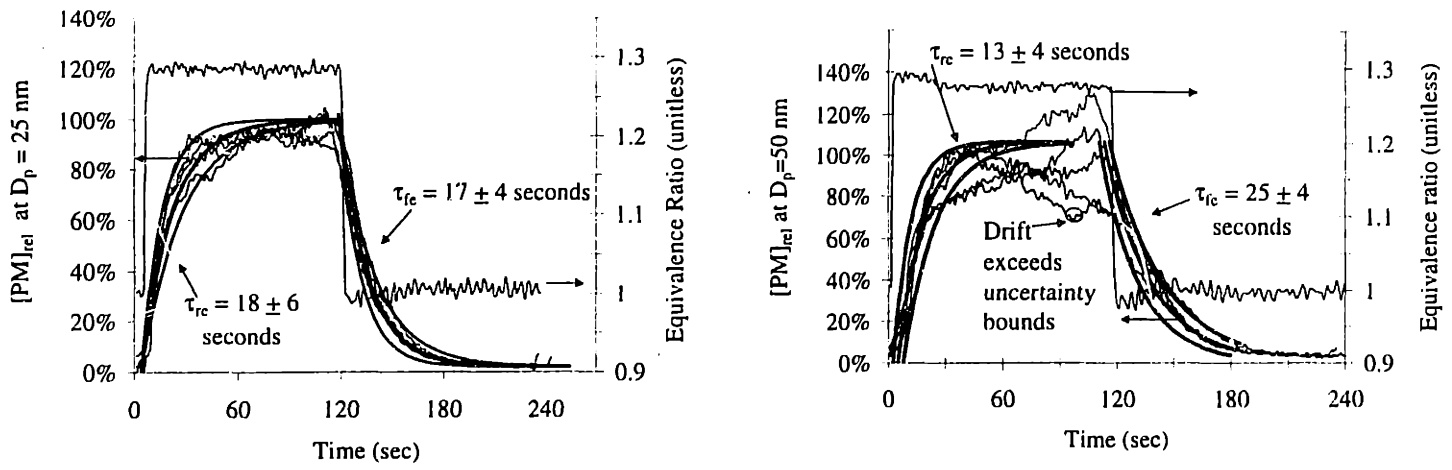

(a) 25 nm particles

(b) 50 nm particles

Figure 9.4 Response of PM emissions to transient equivalence ratio. Particle sizes: (a) 25 nm, (b) 50 nm. Baseline conditions except equivalence ratio. Dilution ratio = 7:1. Time between step changes: 2 minutes. Figure 9.4a shows no drift, and Figure 9.4b shows unrepeatable drift following first order response. Drift is within the 30% uncertainty bounds for all but the two second period circled in Figure 9.4b.

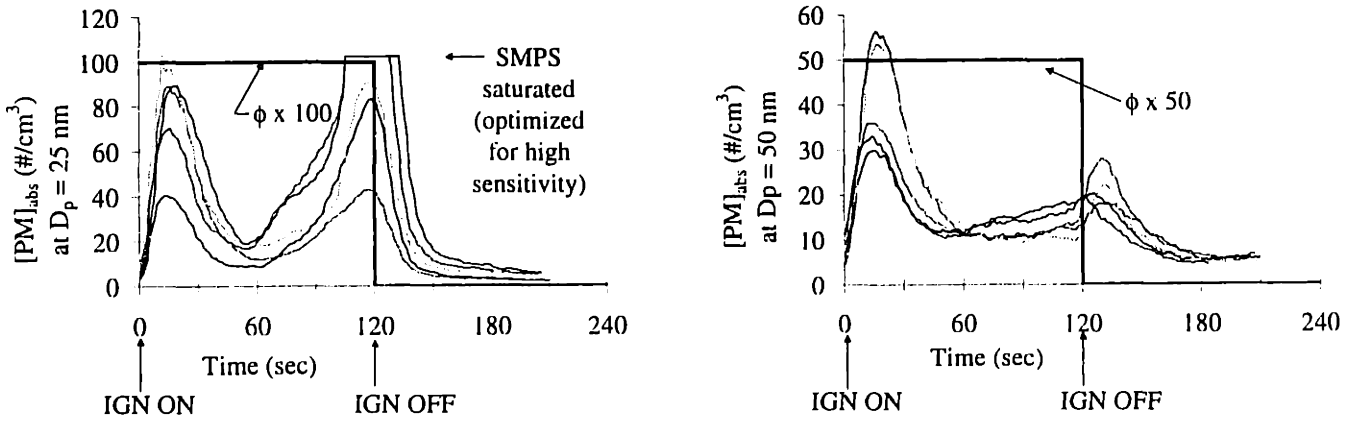

(a) 25 nm particles

(b) 50 nm particles

Figure 9.5 PM emissions during repeated start-up and shut-down experiments and schematic representation of fuel/air equivalence ratio. Conditions: baseline engine operating conditions when the engine is firing; when it is being motored, speed and throttle position remain same as in firing conditions, but no fuel is injected and the spark is not ignited. Dilution ratio = 7:1. Time between ignition on and ignition off events: 2 minutes.

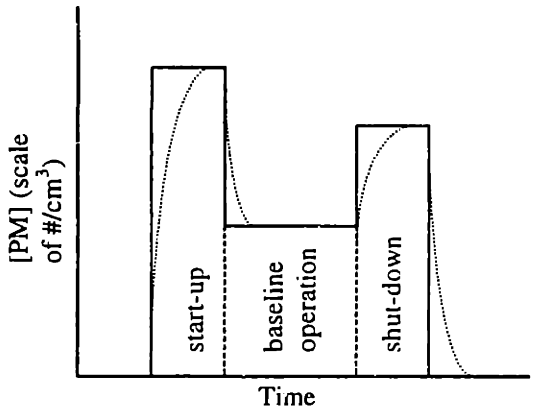

(a) Schematic of PM emissions during start-up and shut-down experiment, with phases of experiment denoted in corresponding regions.

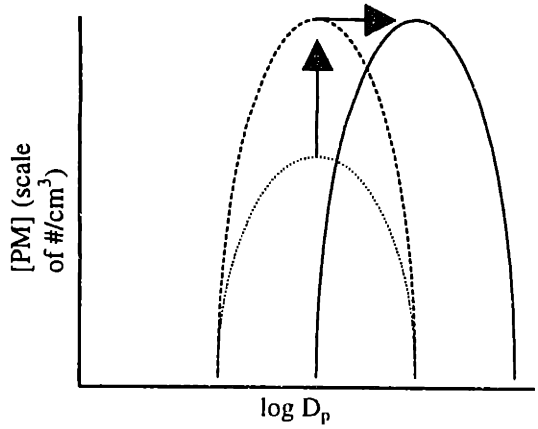

(b) Schematic of changes in size distribution

Figure 9.6. Schematics of (a) PM emissions as might be measured in the exhaust during start-up and shut-down experiments (bursts of particles and baseline level shown as solid lines) and the measured PM emissions that result from the first-order time lag between exhaust and SMPS (dotted lines); (b) PM size distribution — plotted versus the log of particle size, D_p — shifting upward and to larger particle sizes: dotted curve is original size distribution, longer dashes is that size distribution scaled up in particle concentration, solid curve is the scaled size distribution moving along the size axis toward larger particles.

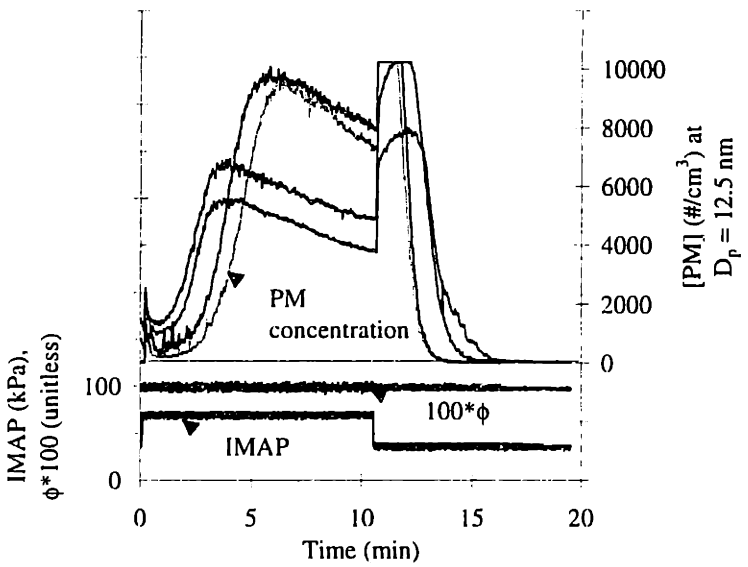

(a) 12.5 nm particles and associated engine parameters for four separate tests, all performed on the same day. Data is not normalized, as discussed in text.

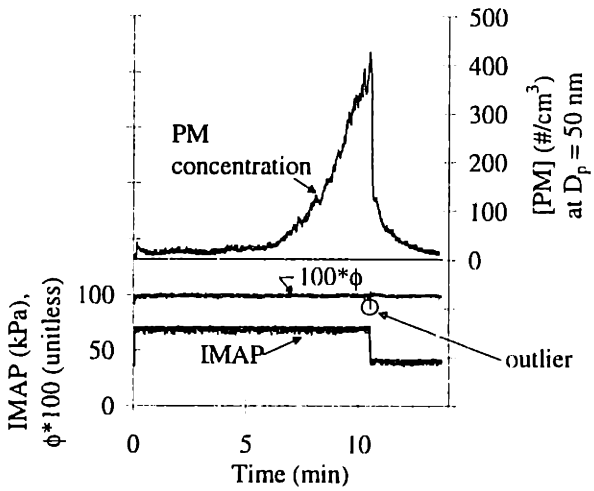

(b) 50 nm particles and associated engine parameters for one representative test. One outlying datum for equivalence ratio circled: this data point is likely an outlier rather than an actual undershoot in ϕ because the time scale over which it occurs (about one second) is far faster than time scales associated with liquid fuel phenomena, as discussed in the present paper and in [76].

Figure 9.7 Response of PM emissions to transient intake manifold pressure. Particle size: (a) 12.5 nm, (b) 50 nm. Baseline conditions at the 40 kPa IMAP case, with a dilution ratio of 22:1. Baseline conditions except for intake pressure at the 70 kPa IMAP case, with a dilution ratio of 11:1. IMAP and equivalence ratio (ϕ) plotted. Time between step changes: 10 minutes.

CHAPTER 10

CONCLUSIONS

10.1 Dilution Experiments

The dilution process for the purpose of measuring particulates from SI engines has been systematically investigated to determine the effects of dilution ratio and flowrate on measurement quality and uncertainty. The main conclusions are:

Instrumentation Issues

1. SMPS measurements are likely to drift if water is allowed to condense within sampling tubes. This problem can be avoided if samples have sufficiently low relative humidity, e.g. samples are taken from diluted SI engine exhaust or exhaust from a diesel engine operating at low load.
2. Strong turbulence in the tunnel, especially that caused by turbulent Re or a turbulence-enhancing orifice, allows thorough mixing so that particle and gas species concentrations are uniform — within 4 to 6% for the present experiments — across the radius of the tunnel.

Measurement Uncertainties

3. Uncertainties in concentration measurements depend on the size of the particles, and can be as much as 50% at sizes around 10 nm. However, for measurements of integrated concentrations, the upper bound on the uncertainty of the SMPS alone is 20%. The uncertainty added by the dilution process is undetectably small. Uncertainty in measurements of number concentrations made via the SI-engine/tunnel/SMPS system are approximately 20%; for volume or mass concentration measurements, it is 25%.
4. Uncertainty in measurements of mean particle sizes made via the SMPS alone is approximately 3%. For mode particle sizes, it is 7%. Uncertainty in measurements of mean particle sizes made via the entire SI-engine/tunnel/SMPS system is approximately 3%. For mode particle sizes, it is 10%.

Recommendations for Dilution Tunnel Design

5. Choices of dilution tunnel diameter and flowrate requires a compromise between acceptable levels of mixing and particle losses. Larger tunnel diameters result in lower a loss rate for a fixed mass flux, but require more powerful vacuum pumps or blowers to generate a given Re. Recommended parameters based on the present study are: dilution ratios of 15:1 and dilution tunnel diameters of the order of 15 cm or larger. The effect of tunnel residence time on particle characteristics is less than measurement uncertainty.

Dilution ratio effects

6. Dilution ratio may strongly affect the temperature of the diluted exhaust as well as the dynamics of particle growth and equilibration. The current USEPA guidelines requirement that samples be taken below 52°C constrains the minimum dilution ratio to be on the order of 10:1 depending on the temperature of the exhaust gas.
7. At a high flowrate of diluted exhaust (flowrate = 6400 lpm, Re ≈ 57000), when the dilution ratio is increased from 1:1 until about 13 - 18:1, measured particle number and volume concentrations (corrected for dilution ratio) increase due to particle growth dynamics. Above dilution ratios of 13 - 18:1, resistance to condensation, adsorption, absorption, and coagulation prohibits growth and decreases particle concentrations.
8. At low enough flowrate (flowrate = 950 lpm, Re ≈ 9000) that temperature and dilution ratio become decoupled, increased dilution ratio from unity to 13 or 15:1 results in decreased measured particle concentrations (corrected for the dilution ratio). Beyond 13 or 15:1, the dilution is sufficient to disallow particle dynamics, so PM concentrations stay fixed with respect to dilution ratio.

Particle losses and mass accretion

9. The dilution process affects diesel exhaust particles by reducing the number concentration and increasing the volume concentration by less than the measurement uncertainty. Although it was not possible to measure the corresponding processes in the SI engine exhaust, it might be inferred that the

behavior is similar in a qualitative sense, but that the higher vapor concentration will tend to make the increase in volume (or mass) due to vapor accretion more significant.

Comparison between SMPS and gravimetric filter analysis

10. The SMPS proved more accurate than gravimetric filter analysis due to the problem of HCs adsorbing on the filter quickly enough to overwhelm the amount of PM mass trapped.

10.2 Steady State Experiments

In order to understand the process of PM formation in SI engines, a modeling effort was performed in conjunction with a series of experimental measurements using a SMPS; the results of the experimental work are the following:

Effect of engine parameters

1. Open valve fuel injection increases PM number and mass concentration by up to three orders of magnitude relative to closed valve injection, emphasizing the importance that liquid fuel in the combustion chamber has on PM nucleation.
2. When the oil and coolant temperatures are decreased by about 50°C, PM mass emissions increase by 60%, again due to liquid fuel in the combustion chamber.
3. Retarding spark timing thirty crank angle degrees from MBT timing causes PM number and mass emissions to decrease by a factor of three, while advancing spark beyond MBT timing causes PM emissions to plateau. The behavior of PM as a function of spark timing is due to the conflicting effects of temperature on Arrhenius-type PM nucleation and oxidation mechanisms, as well as the effect of post-flame temperatures on unburned HCs.
4. As EGR increases, PM number and mass emissions decrease exponentially, because of the Arrhenius dependency in the nucleation mechanism and the strong dependence of the amount of fuel present in liquid phase in the combustion chamber on intake conditions.

5. As engine load increases from 40% throttle to wide open throttle, PM number and mass concentrations increase as many as three orders of magnitude, due to increased availability of liquid fuel and increased in-cylinder temperatures and pressures.
6. PM shows no universal trend with respect to engine speed.

Effect of fuel, oil, and catalyst parameters

7. In tests where the air/fuel ratio is varied with all other conditions fixed, PM number and mass concentrations attain a minimum within 10% of stoichiometric (the exact air/fuel ratio depends on the particular fuel) and increase by as many as three orders of magnitude when the air/fuel ratio either increases or decreases 30% from stoichiometric.
8. Negligible amounts of PM form as a result of lubricating oil consumption with conventional mineral oils of either 30 or 40 weight; however, use of synthetic 30 weight oil results in a 70% increase in PM relative to the 30 weight mineral oil.
9. The catalytic converter does not eliminate a statistically significant amount of PM.

Correlations between PM emissions and other parameters

10. PM emissions do not have a strong correlation with any gaseous species, with either peak cylinder temperature or pressure, or with exhaust temperature.

10.3 Model of PM Formation During Steady State Operation

The results of the modeling work, done in conjunction with the experimental investigation of the effect of steady state engine operating parameters on PM emissions, are the following:

Model formulation

1. The model of PM formation and emission — consisting of submodels in which PM nucleates at sites of burning liquid fuel and in gas phase chemical reactions, and in which PM can grow by condensation, chemical and/or physical adsorption, and absorption, and in which PM can shrink by oxidation — accurately captures trends in PM emission as a function of engine operating conditions.

Model results

2. The R^2 correlation coefficient between the modeled and measured PM emissions is 0.81.
3. The model shows the strong influences of in-cylinder liquid fuel, air/fuel ratio, and port/cylinder temperatures on PM emissions. Moreover, it suggests that fuel type affects PM emissions through (a) the propensity of the fuel molecule to break down into soot precursors, (b) physical characteristics related to evaporation and heat release as involved in the heterogeneous nucleation mechanism, and (c) the activation energy required to form PM from the soot precursors present in the gas phase.
4. The model has been tested against a variety of dilution conditions, and is not unique to the present experimental setup.

10.4 PM Formation During Transient Operation

Transient particulate emissions from a spark-ignition engine were studied. In most cases, the results show a first order (i.e., $1-\exp(-t/\tau_{re})$) response to the transient conditions.

Time resolution of diagnostics

1. Time constants measured for the instrumentation are 4 to 7 seconds, while time constants for engine responses to transients are from 4 to 25 seconds, which are larger by a statistically significant margin than those of the diagnostics in many but not all cases. The fact that time constants for the engine are not always larger than those measured for the diagnostics by a statistically significant margin suggests that the diagnostics may limit observation of actual engine behavior in certain cases.

Transient response during engine operation

2. PM emissions follow a first order response, presumably because of gradual equilibration of intake port fuel evaporation and exhaust port storage effects. If this is the case, then PM emissions during transient operation should be predictable by evaluating the model of PM formation with sufficient time-resolved data.
3. One case occurred in which a higher than first order response function was observed, but this could not be duplicated.

Transient response during engine start-up and shut-down

4. During controlled, motored start-up tests, PM emissions are consistent with a peak just at start-up, followed by a period of level emissions during which time the particle size distribution may shift upward and/or along the particle size axis in response to equilibration of intake, in-cylinder, or exhaust processes. When the ignition and fuel injection are simultaneously shut off, PM emissions may peak again — although this peak may be masked by a generally increasing PM concentration — but quickly decrease.

REFERENCES

[1] Natural Resources Defense Council, *Breath-Taking: Premature Mortality Due to Particulate Air Pollution in 239 American Cities* (1996).

[2] Pope III, C. A., Dockery, D. W., "Acute Health Effects Of PM10 Pollution on Symptomatic and Asymptomatic Children," *Am. Rev., Respir. Dis.*, vol. 145, pp. 1123-1128 (1992).

[3] USEPA, "EPA's Proposal For the Particulate Matter Standard: Fact Sheet," (1996).

[4] Seinfeld, J. H., Atmospheric Chemistry and Physics of Air Pollution, John Wiley and Sons Publishing, New York, p. 51 (1986).

[5] "National Ambient Air Quality Standards for Particulate Matter; Final Rule," *Federal Register*, vol. 62, p. 38652 (1997).

[6] Rogge, W. F., Hildemann, L. M., Mazurek, M. A., Cass, G. R., "Sources of Fine Organic Aerosol. 2. Noncatalyst and Catalyst-Equipped Automobiles and Heavy-Duty Diesel Trucks," *Environ. Sci. Technol.* vol. 27, pp. 636-651 (1993).

[7] Rickeard, D. J., Bateman, J. R., Kwon, Y. K., McAughey, J. J., Dickens, C. J., "Exhaust Particulate Size Distribution: Vehicle and Fuel Influences in Light Duty Vehicles," *SAE Paper 961980* (1996).

[8] Greenwood, S. J., Coxon, J. E., Biddulph, T., Bennett, J., "An Investigation to Determine the Exhaust Particulate Size Distributions for Diesel, Petrol, and Compressed Natural Gas Fueled Vehicles," *SAE Paper 961085* (1996).

[9] Hildemann, L. M., Markowski, G. R., Jones, M. C., Cass, G. R., "Submicrometer Aerosol Mass Distributions of Emissions from Boiler, Fireplaces, Automobiles, Diesel Trucks, and Meat-Cooking Operations," *Aerosol Sci. and Tech.*, vol 14, pp. 138-152 (1991).

[10] Motor Vehicles Manufacturers Association, *MVMA Motor Vehicle Facts & Figures '93* (1993).

[11] Maricq, M., "Vehicle Particulate Emissions: A Comparison of ELPI, SMPS, and mass measurement," International Seminar on Particle Size Distribution Measurement from Combustion Engines, Espoo, Finland, 18 May 1998.

[12] Williams, D. J., Milne, J. W., Roberts, D. B., Kimberlee, M. C., "Particulate Emissions From 'In-Use' Motor Vehicles - I. Spark Ignition Vehicles," *Atmospheric Environment*, vol. 23, pp. 2639-2645 (1989).

[13] Williams, D. J., Milne, J. W., Quigley, S. M., Roberts, D. B., Kimberlee, M. C., "Particulate Emissions From 'In-Use' Motor Vehicles - II. Diesel Vehicles," *Atmospheric Environment*, vol. 23, pp. 2647-2661 (1989).

[14] Siegl, W. O., Zinbo, M., Korniski, T. J., Richert, J. F. O., Chladek, E., Paputa Peck, M. C., Weir, J. E., Schuetzle, D., Jensen, T. E., "Air Toxics: A Comparison of the Gas- and Particle-Phase Emissions from a High-Emitter Vehicle with Those from a Normal-Emitter Vehicle," *SAE Paper 940581* (1994).

[15] Amann, C. A., Stivender, D. L., Plee, S. L., MacDonald, J. S., "Some Rudiments of Diesel Particulate Emissions," *SAE Paper 800251* (1980).

[16] Plee, S. L., MacDonald, J. S., "Some Mechanisms Affecting the Mass of Diesel Exhaust Particulate Collected Following a Dilution Process," *SAE Paper 800186* (1980).

[17] MacDonald, J. S., Plee, S. L., D'Arcy, J. B., Schreck, R. M., "Experimental Measurements of the Independent Effects of Dilution Ratio and Filter Temperature on Diesel Exhaust Particulate Samples," *SAE Paper 800185* (1980).

[18] Abbass, M. K., Andrews, G. E., Williams, P. T., Bartle, K. D., "Diesel Particulate Composition Changes Along an Air Cooled Exhaust Pipe and Dilution Tunnel," *SAE Paper 890789* (1989).

[19] Kosowski, M. G., "Soot Formation in a Multipoint-Fuel-Injected Spark-Ignited Engine," *SAE Paper 850294* (1985).

[20] Quader, A. A., "How Injector, Engine, and Fuel Variables Impact Smoke and Hydrocarbon Emissions with Port Fuel Injection," *SAE Paper 890623* (1989).

[21] Kayes, D., Hochgreb, S., "Time, Space, and Species Resolved Measurements of Engine-Out Hydrocarbon Emissions from Spark-Ignited Engines," *Combust. Sci. and Tech.*, vol. 127, pp. 333-362 (1997).

[22] Thompson, N. D., Wallace, J. S., "Effect of Engine Operating Variables and Piston and Ring Parameters on Crevice Hydrocarbon Emissions," *SAE Paper 940480* (1994).

[23] Min, K., Cheng, W. K., Heywood, J. B., "The Effects of Crevices on the Engine-Out Hydrocarbon Emissions in SI Engines," *SAE Paper 940306* (1994).

[24] Pedersen, P. S., Ingwersen, J., Nielsen, T., Larsen, E., "Effects of Fuel, Lubricant, and Engine Operating Parameters on the Emission of Polycyclic Aromatic Hydrocarbons," *Environ. Sci. Technol.*, vol. 14, pp. 71-79 (1980).

[25] Fanick, E. R., Whitney, K. A., Bailey, B. K., "Particulate Characterization Using Five Fuels," *SAE Paper 961089* (1996).

[26] Kittelson, D. B., Dolan, D. F., Beaver, M. C., "Exhaust Particle Size Distributions Produced By Diesel And Spark Ignition Engines: Comparison Of Theory And Experiment," *Central States Section of the Combustion Institute, Paper CSS/CI-79-09* (1979).

[27] Maricq, M. M., Dearth, M. A., Chase, R. E., Ball, J. C., "Particulate Size Measurements," Health Effects Institute Workshop on Particle Characterization, 3 December 1996.

[28] Witze, P. O., Green, R. M., "LIF and Flame-Emission Imaging of Liquid Fuel Films and Pool Fires in an SI Engine During a Simulated Cold Start," *SAE Paper 970866* (1997).

[29] Alkidas, A. C., Drews, R. J., "Effects of Mixture Preparation on HC Emissions of a S.I. Engine Operating Under Steady-State Cold Conditions," *SAE 961958* (1996).

[30] Fulcher, S. K., Gajdeczko, B. F., Felton, P. G., Bracco, F. V., "The Effects of Fuel Atomization, Vaporization, and Mixing on the Cold-Start UHC Emissions of a Contemporary S.I. Engine with Intake-Manifold Injection," *SAE Paper 952482* (1995).

[31] Koehl, W. J., Benson, J. D., Burns, V., Gorse, R. A., Hochhauser, A. M., Reuter, R. M., "Effects of Gasoline Composition and Properties on Vehicle Emissions: A Review of Prior Studies — Auto/Oil Air Quality Improvement Research Program," *SAE Paper 912321* (1991).

[32] Westerholm, R. N., Alsberg, T. E., Frommelin, A. B., Strandell, M. E., Rannug, U., Winquist, L., Grigoriadis, V., Egeback, K. E., "Effect of Fuel Polycyclic Aromatic Hydrocarbon Content on the Emissions of Polycyclic Aromatic Hydrocarbons and Other Mutagenic Substances from a Gasoline-Fueled Automobile," *Environ. Sci. Technol.* vol. 22, pp. 925-930 (1988).

[33] Handbook of Chemistry and Physics, ed. Hodgman, C. D., Chemical Rubber Publishing, Cleveland, pp. 1142, 1143, 1246, 1247 (1958).

[34] Hildemann, L. M., Markowski, G. R., Cass, G. R., "Chemical Composition of Emissions from Urban Sources of Fine Organic Aerosol," *Environ. Sci. Technol.*, vol. 25, pp. 744-759 (1991).

[35] Laurence, R. B., Wong, V. W., Brown, A. J., "Effects of Lubrication System Parameters on Diesel Particulate Emission Characteristics," *SAE Paper No. 960318* (1996).

[36] Maricq, M. M., Podsiadlik, D. H., Chase, R. E., "Beyond mass emissions: An examination of the size resolved and transient nature of particle emissions from motor vehicles," *Ford Motor Company internal communication.*

[37] Takeda, K., Yaegashi, T., Sekiguchi, K., Saito, K., Imatake, N., "Mixture Preparation and HC Emissions of a 4-Valve Engine with Port Fuel Injection During Cold Starting and Warm-up," *SAE Paper 950074* (1995).

[38] Crane, M. E., Thring, R. H., Podnar, D. J., Dodge, L. G., "Reduced Cold-Start Emissions Using Rapid Exhaust Port Oxidation (REPO) in a Spark-Ignition Engine," *SAE Paper 970264*, (1997).

[39] Hildemann, L. M., Cass, G. R., Markowski, G. R., "A Dilution Stack Sampler for Collection of Organic Aerosol Emissions: Design, Characterization and Field Tests," *Aerosol Sci. and Technol.*, vol. 10, pp. 193-204 (1989).

[40] TSI Incorporated, *Model 3934 SMPS (Scanning Mobility Particle Sizer) Instruction Manual*, 1996, pp. A-1, B-2-5, B-12-13, B-17-19.

[41] Kittelson, D. B., "Engines and Nanoparticles: A Review," *J. Aerosol Sci.*, vol. 29, no. 5/6, pp. 575-588 (1998).

[42] Hofeldt, D. L., "Real-Time Soot Concentration Measurement Technique for Engine Exhaust Streams," *SAE Paper 930079* (1993).

[43] Roessler, D. M., Faxvog, F. R., Stevenson, R., Smith, G. W., "Optical Properties and Morphology of Particulate Carbon: Variation with Air/Fuel Ratio," Particulate Carbon: Formation During Combustion, ed. Siegla and Smith, Plenum Press, New York, 1981.

[44] Dyer, T. M., Flower, W. L., "A Phenomenological Description of Particulate Formation During Constant Volume Combustion," Particulate Carbon: Formation During Combustion, ed. Siegla and Smith, Plenum Press, New York, 1981.

[45] Kadota, T., Henein, N. A., "Time-Resolved Soot Particulates in Diesel Spray Combustion," Particulate Carbon: Formation During Combustion, ed. Siegla and Smith, Plenum Press, New York, 1981.

[46] Lindstedt, P. R., "Simplified Soot Nucleation and Surface Growth Steps for Non-Premixed Flames," Soot Formation in Combustion, ed. Bockhorn, Springer-Verlag Publishing, New York, pp. 417-441 (1994).

[47] Melton, L. A., "Soot diagnostics based on laser heating," *Applied Optics*, vol. 23, no. 13, pp. 2201-2207.

[48] Trayser, D. A., Creswick, F. A., Gieseke, J. A., Hazard, H. R., Weller, A. E., Locklin, D. W., "A Study of the Influence of fuel Atomization, Vaporization, and Mixing Processes on Pollutant Emissions from Motor-Vehicle Powerplants," Phase Report to Division of Motor Vehicle Research and Development, National Air Pollution Control Administration (1969).

[49] Graskow, B. R., Kittelson, D. B., Ahmadi, M. R., and Morris, J. E., "Characterization of Exhaust Particulate Emissions from a Spark Ignition Engine," *SAE Paper 980528* (1998).

[50] Heywood, J. B., Internal Combustion Engine Fundamentals, McGraw-Hill, Inc., New York, pp. 567, 915 (1988).

[51] Meintjes, K., *General Motors Engine-Simulation Program (CSC)*, version 1.0, General Motors, Warren, Michigan, 1987.

[52] Reynolds, W. C., "The Element Potential Method for Chemical Equilibrium Analysis: Implementation in the Interactive Program STANJAN," Department of Mechanical Engineering, Stanford, University (1986).

[53] Langmuir, I., "The Adsorption of Gases on Plane Surfaces of Glass, Mica and Platinum," *Journal of American Chemical Society*, vol. 40, pp. 1361-1402 (1918).

[54] Ladommatos, N., Rose, D. W., "A Model of Droplet Thermodynamic and Dynamic Behavior in the Port of a Port-Injected Engine," *SAE Paper 960467* (1996).

[55] Arcoumanis, C., Gold, M. R., Whitelaw, J. H., Xu, H. M., Gaade, J. E., Wallace, S., "Droplet Velocity/Size and Mixture Distribution in a Single-Cylinder Four-Valve Spark-Ignition Engine," *SAE Paper 981186* (1998).

[56] Alkidas, A. C., "The Effects of Fuel Preparation on Hydrocarbon Emissions of a S.I. Engine Operating Under Steady-State Conditions," *SAE 941959* (1994).

[57] Meyer, R., Heywood, J. B., "Evaporation of In-Cylinder Liquid Fuel Droplets in an SI Engine: A Diagnostic-Based Modeling Study," *paper submitted to SAE, 1998.*

[58] Ladommatos, N., Rose, D. W., "Results of a Computer Model of Droplet Thermodynamic and Dynamic Behavior in the Port of a Port-Injected Engine," *SAE Paper 960468* (1996).

[59] Kowalik, R. M., Ruth, L. A., Edelman, R. B., Farmer, R. C., Wong, E., Wang, T. S., "Fundamental Characterization of Alternative Fuel Effects in Continuous Combustion Systems," U. S. Dept. of Energy Report DOE/ET/11313-11 (1982).

[60] Gelfand, B. E., "Droplet Breakup Phenomena In Flows With Velocity Lag," *Prog. Energy Combust. Sci.*, vol. 22, pp. 201-265 (1996).

[61] Cheng, W. K., Hamrin, D., Heywood, J. B., Hochgreb, S., Min, K., Norris, M., "An Overview of Hydrocarbon Emissions Mechanisms in Spark-Ignition Engines," *SAE Paper 932708* (1993).

[62] Nagle, J., Strickland-Constable, R. F., "Oxidation of Carbon Between 1000-2000°C," *Proc. Fifth Carbon Conf.*, 1, 154 (1962).

[63] Appleton, J. P., Park, C., "Shock-Tube Measurements of Soot Oxidation Rates," *Combustion and Flame*, vol. 20, pp. 369-379 (1973).

[64] Quader, A. A., "Why Intake Charge Dilution Decreases Nitric Oxide Emissions from Spark Ignition Engines," *SAE Paper 710009* (1971).

[65] Fox, J. W., Cheng, W. K., Heywood, J. B., "A Model for Predicting Residual Gas Fraction in Spark-Ignition Engines," *SAE Paper 931025* (1993).

[66] Posylkin, M., Taylor, A. M. K. P., Vannobel, F., Whitelaw, J. H., "Fuel Droplets Inside a Firing Spark-Ignition Engine," *SAE Paper 941989* (1994).

[67] Chevron Company, "California Phase 2 Reformulated Gasoline," Technical Bulletin, 1995.

[68] Kaiser, E. W., Siegl, W. O., Henig, Y. I., Anderson, R. W., Trinker, F. H., "Effect of Fuel Structure on Emissions from a Spark-Ignited Engine," *Environ. Sci. Technol.*, vol. 25, no. 12, pp. 2005- 2012 (1991).

[69] Kummer, J. T., "Catalysts for Automobile Emission Control," *Prog. Energy Combust. Sci.*, vol. 6, pp. 177-199 (1980).

[70] Montgomery and Reitz, "Six-Mode Cycle Evaluation of the Effect of EGR and Multiple Injections on Particulate and NO_x Emissions from a D.I. Diesel Engine," *SAE Paper 960316* (1996).

[71] Williams, A., Combustion of Liquid Fuel Sprays, Butterworths Publishing, Boston, pp. 93, 99, 102 (1990).

[72] Law, C. K., "Theory of Thermal Ignition in Fuel Droplet Burning," *Combust. and Flame*, vol. 31, pp. 285-296 (1978).

[73] Kaiser, E. W., Siegl, W. O., Cotton, D. F., Anderson, R. W., "Effect of Fuel Structure on Emissions from a Spark-Ignited Engine. 2. Napthene and Aromatic Fuels," *Environ. Sci. Technol.*, vol. 26, no. 8, pp. 1581-1586 (1992).

[74] Du, C. J., Kittelson, D. B., "Total Cylinder Sampling from a Diesel Engine: Part III - Particle Measurements," *SAE Paper 830243* (1983).

[75] Chen, K. C., DeWitte, K., Cheng, W. K., "A Species-Based Multi-Component Volatility Model for Gasoline," *SAE Paper 941877* (1994).

[76] Aquino, C. F., Plensdorf, W. D., Lavoie, G. A., Curtis, E. W., "The Occurrence of Flash Boiling In a Port Injected Gasoline Engine," *SAE Paper 982522* (1998).

[77] Dec, J. E., "Soot Distribution in a D.I. Diesel Engine Using 2-D Imaging of Laser-Induced Incandescence, Elastic Scattering, and Flame Luminosity," *SAE Paper 920115* (1992).

[78] Vander Wal, R. L., Dietrich, D. L., Zhou, Z., Choi, M. Y., "Development and Applications of Laser-Induced Incandescence," *Proceedings of the Third International Microgravity Combustion Workshop*, Cleveland, OH, 11-13 April, 1995.

[79] Pinson, J. A., Mitchell, D. L., Santoro, R. J., Litzinger, T. A., "Quantitative, Planar Soot Measurements in a D.I. Diesel Engine Using Laser-Induced Incandescence and Light Scattering," *SAE Paper 932650* (1993).

[80] Lafleur, A., Plummer, E., *personal communication* (1998).

APPENDIX 1

Model Prediction Of PM Versus Fuel Control Strategy

The present model of PM formation and emission (Chapter 7) is a steady state model, while the effect of control strategy and oxygen sensor on PM emissions is largely due to the magnitude of *unsteady* air/fuel ratio fluctuations permitted by each control strategy/sensor (Chapter 5). Therefore, the model cannot not be used to estimate the aforementioned effect. However, the model should theoretically be capable of finding the bounds on the effect of control strategy, as follows. If a particular control strategy and oxygen sensor combination allows fluctuations in air/fuel ratio within a certain range, then the PM emissions should be bounded by the maximum and minimum PM emissions in that range. Consequently, when one control strategy/sensor combination allows greater fluctuations about stoichiometric than another, the model correctly predicts the experimental observation that the former should have higher emissions than the latter.

Although the model can capture the qualitative difference in PM emissions with control strategy/sensor, the model does not capture the quantitative difference. Following the above logic, the model predicts that the standard Ford engine control strategy (EEC IV) using the HO2S, which allows a 2-3% fluctuation in air/fuel ratio (as measured with a UEGO sensor in the exhaust), will have 20% higher emissions than the PI controller with a UEGO sensor, which allows only 1% fluctuation. However, the experimentally measured difference in emission rates was a factor of 10 higher emissions with the former than with the latter. The discrepancy may be that the oxygen sensors measure only fluctuations in ϕ of the total exhaust, as opposed to fluctuations in ϕ during individual cycles, which may be significantly larger than 2-3%. Were this the case, then the fact that larger fluctuations result in higher PM emissions would make the PM emissions calculated with the assumption of 2-3% fluctuations an underestimate of the true PM emissions.

APPENDIX 2

Chemical Analyses of PM

The original intent of chemical analysis of engine-out PM was to quantify the proportion of PM mass derived from fuel versus that from oil. However, this proved unnecessary, since that proportion could be deduced through experiments using the SMPS as described in Chapter 5. Nonetheless, a limited number of filter samples were chemically analyzed and tested for mutagenicity. Filters were collected using the Ford Zetec engine at 2000 rpm and ½ throttle (0.5 bar IMAP) with a dilution ratio of 15:1. Resulting chromatograms are shown on the following pages. Fourteen PAH species were identified, all of which resemble products of fuel combustion, as compared to those of oil combustion. The chromatogram of the diluted engine exhaust is similar to the "signature" of atmospheric PM [80], lending further evidence to the assertion that a significant portion of airborne PM comes from automobiles. The samples proved mutagenic, using a bioassay test [80].

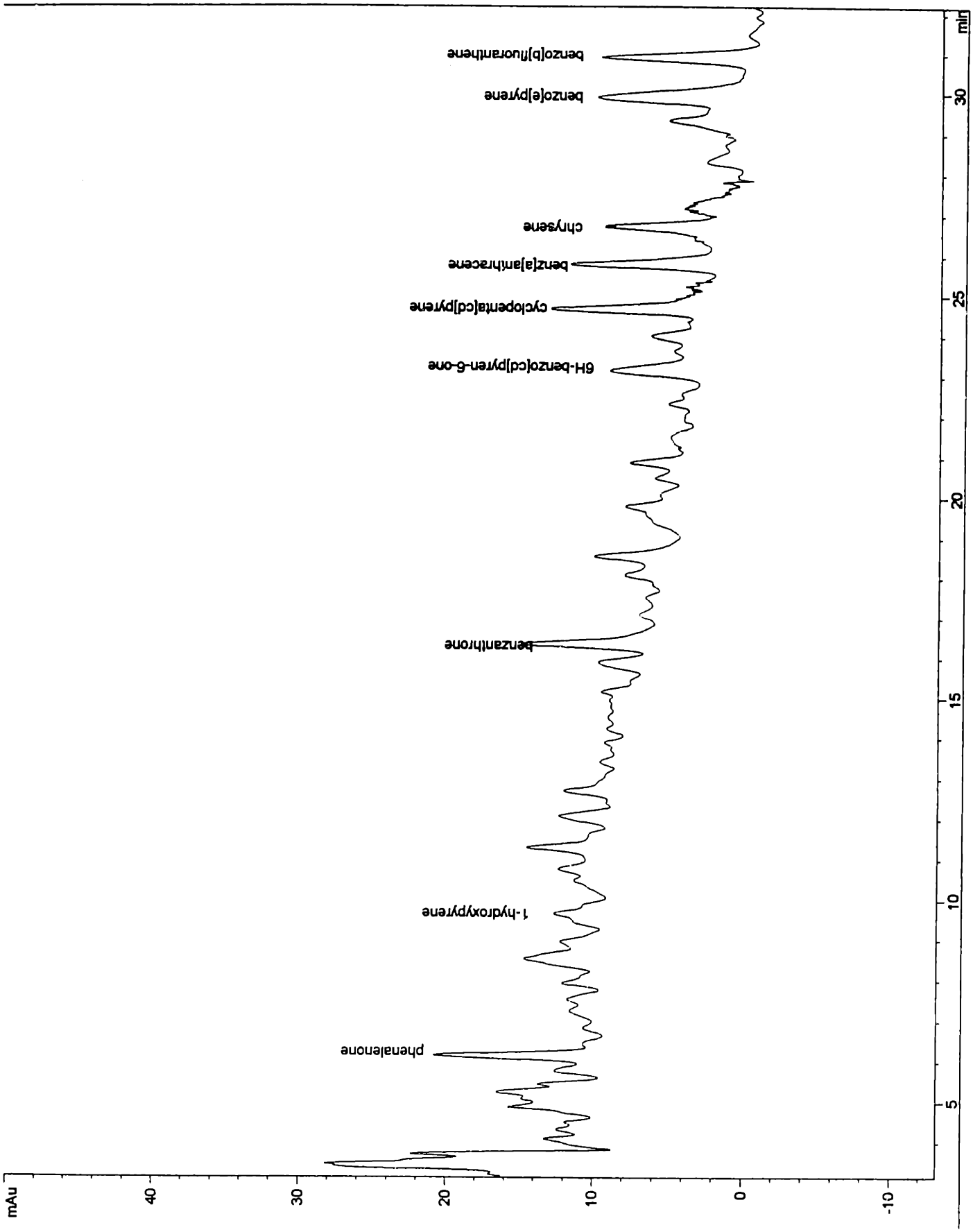

Figure A2.1 (a) Chromatogram (page 1) of diluted exhaust PM. Dilution ratio = 15:1. Conditions: fully warmed operation, 2000 rpm, ½ throttle.

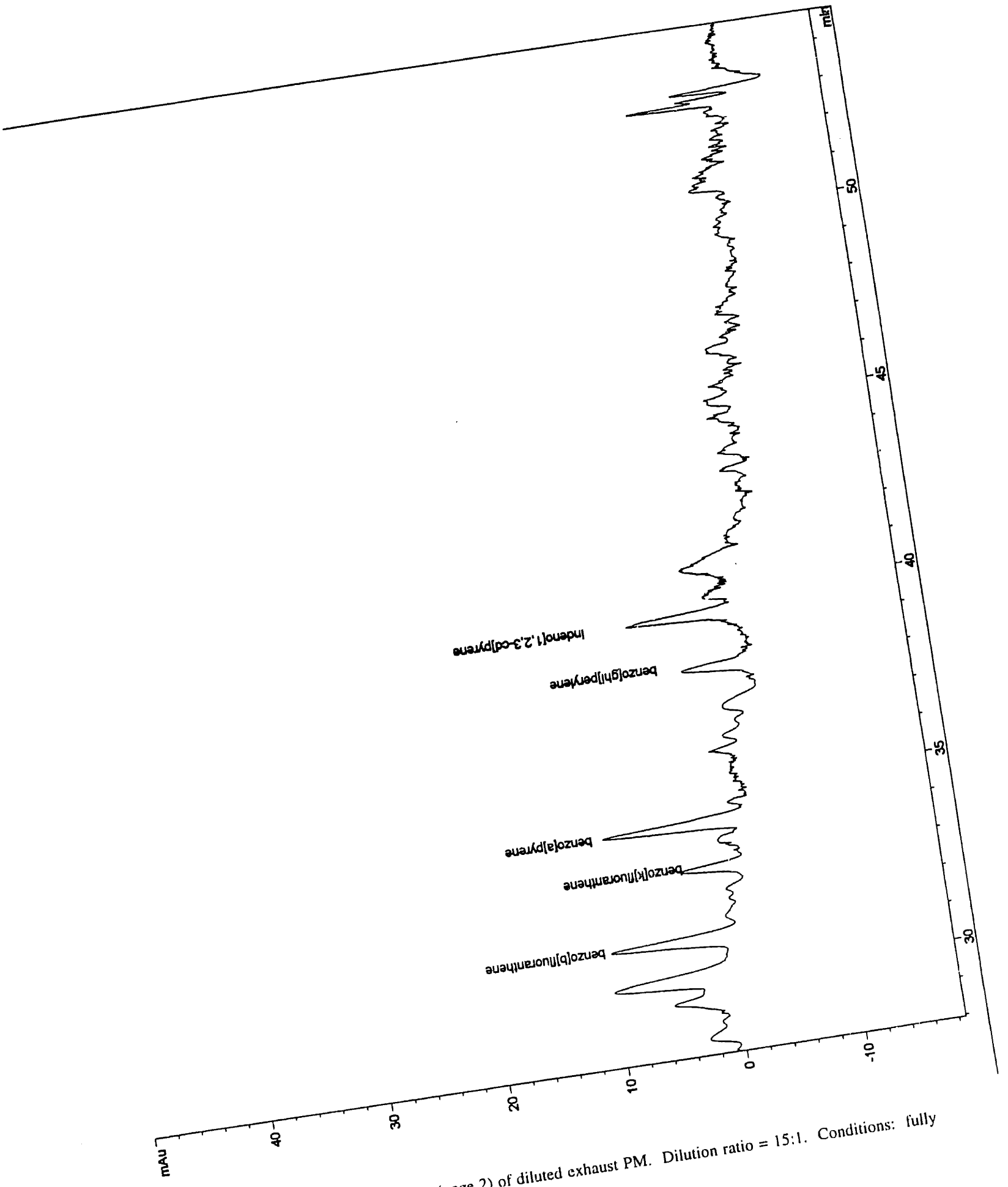

Figure A2.1 (b) Chromatogram (page 2) of diluted exhaust PM. Dilution ratio = 15:1. Conditions: fully warmed operation, 2000 rpm, ½ throttle.

APPENDIX 3

PM Emissions During FTP Test

In Chapter 9, the model of PM formation and emissions was applied qualitatively to the FTP in order to explain why emissions peak during periods of high acceleration. The present appendix details quantitative application of the model during the FTP, and a comparison between the model results and experimental data for a Ford vehicle with a blank-brick catalyst (i.e., experimental data correspond to engine-out emissions, as do the model results). This quantitative application of the model and comparison to experimental data is left to an appendix because there are a number of important caveats regarding the data that separate these data from the more broadly applicable data presented in the text of the thesis. First, application of the model requires sufficient time resolved data, including equivalence ratio, engine speed and load, spark timing, and intake port temperature; however, the only data set presently available includes all information *except* intake port temperatures, therefore a temperature history had to be assumed. Since model results are extremely sensitive to the intake port temperature (as discussed in Chapter 8), the assumption of a temperature history is a strong source of uncertainty. In the present case, temperature was assumed to rise exponentially from the cold engine temperature to the steady state warmed-up temperature with a time constant on the order of that measured for transient engine operation by [76] and was assumed to be equally affected by load and speed as is the Saturn engine, for which intake temperatures are discussed in Chapter 8. Second, the experimental data was obtained from a vehicle with a V8 engine of significantly different design than the engine that was used to calculate the values of model coefficients; consequently, the model may not accurately predict the relative weightings between the different nucleation mechanisms (as is expressed by the values of the different pre-exponential coefficients) and, therefore, may not accurately predict PM emissions.

Given these caveats, a data set collected once every second during Bag 1 the FTP at Ford has been used in the model. The results are plotted relative to the peak PM emissions, as are measured PM emissions, for reasons discussed in section 7.3 of the text. As can be seen in Figure A3.1, the model correctly predicts when PM emissions will peak, though it does not calculate quantitatively correct PM concentrations, presumably because of the two reasons above.

PM emissions — both measured and predicted — are highest during the acceleration periods; the reason for the peaks PM emission rates are as follows. Although the fuel/air equivalence ratio is within 5% of stoichiometric throughout the accelerations, the model suggests that PM emissions are so high because the load on the engine is so high: a lot of fuel is injected into the intake and (as discussed in Chapter 8) intake temperatures drop during periods of high load, leading to poor fuel evaporation and thus exacerbating the problem of liquid fuel in the cylinder. Moreover, for the present experimental conditions, the total flowrate of diluted exhaust is fixed, so high load conditions lead to low dilution ratios, which in turn leads to high absorbtivity for the following reasons. In the experimental set-up used at Ford to obtain this data, the temperature of the diluted exhaust is (according to measurements) approximately fixed at 300 K. Therefore, as discussed in Chapter 8 in the case where the model was applied to the experiment of variable dilution ratios using the low (isothermal) flowrate of diluted exhaust, low dilution ratios lead to high absorbtivity and thus high PM mass concentrations. The net result is peak PM emissions during periods of high load, despite the approximately constant, stoichiometric air/fuel ratio.

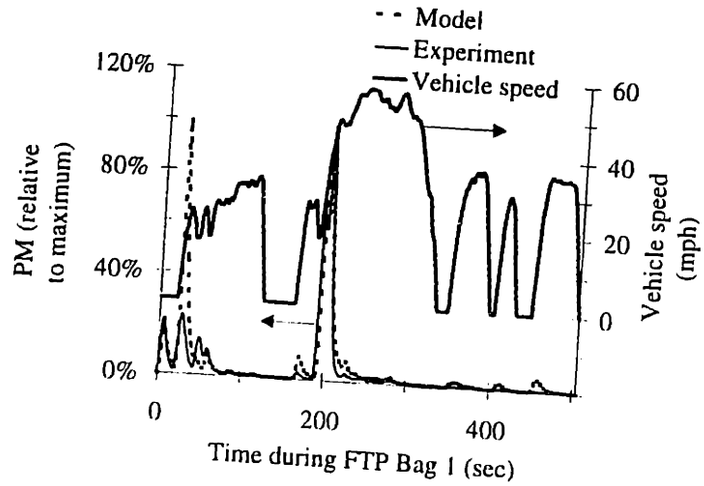

Figure A3.1 Modeled PM emissions during Bag 1 of the FTP and experimental data for a V8 blank-brick catalyst vehicle. PM emissions are plotted relative to the peak PM concentration. Plotted on the second ordinate axis is the trace of speed versus time for Bag 1 of the FTP, in order to show that peaks of PM emissions occur during acceleration periods.

APPENDIX 4

Data Used In Chapter 6

Several parameters were measured during experiments in which air/fuel ratio, fuel type, and several engine operating conditions were varied, and several other parameters were calculated for the same conditions. Although these were data were used in the chapter regarding correlations between PM emissions and other parameters (Chapter 6), the data were not presented on their own. In order to make this data available, Appendix 4 presents measured concentrations of nitrogen oxides, carbon oxides, and oxygen, as well as calculated temperatures and pressures in the cylinder, plus measured exhaust temperatures as a function of air/fuel ratio. In addition, this appendix presents calculated in-cylinder and exhaust parameters as a function of engine load, speed, spark timing, and EGR mass fraction. As mentioned in the section regarding results from steady state experiments, the GM Engine-Simulation Program was used to calculate peak temperatures and pressures in the cylinder [51], but calculations performed by this program are based on the physical and chemical properties of isooctane fuel. The peak flame temperatures were calculated for the Otto Cycle using STANJAN [52] and showed that peak flame temperature varies by no more than 3% or 100 K at any given ϕ for indolene, isooctane, propane, and toluene. Thus GM Engine-Simulation results using isooctane fuel should be generalizable to the other fuels. The figure showing peak in-cylinder temperatures given by the Otto Cycle analysis also shows the curve of peak temperature as a function of air/fuel ratio calculated by the GM Engine-Simulation Program; the difference between the results of the program and those of the Otto Cycle analysis is due to the idealizations inherent in the Otto Cycle analysis.

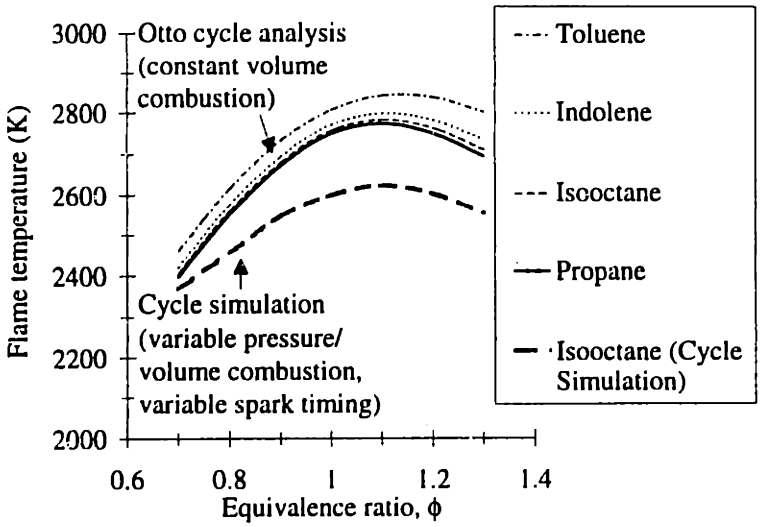

Figure A4.1 Peak flame temperature as a function of fuel/air equivalence ratio as calculated for Otto Cycle and for real cycle, the latter using the GM Engine-Simulation Program [51]. Inputs: baseline engine operating conditions except equivalence ratio, with engine geometry equal to that for Ford Zetec.

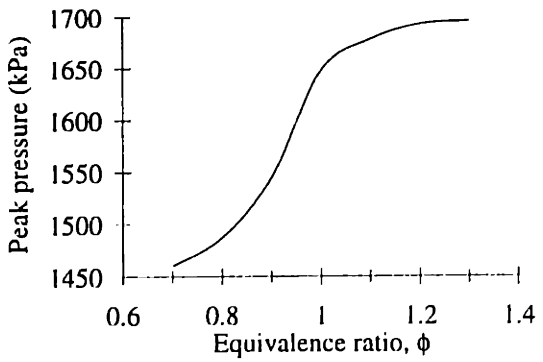

Figure A4.2 Peak cylinder pressure as a function of fuel/air equivalence ratio as calculated using the GM Engine-Simulation Program [51]. Inputs: baseline engine operating conditions except equivalence ratio, with engine geometry equal to that for Ford Zetec. Isooctane fuel.

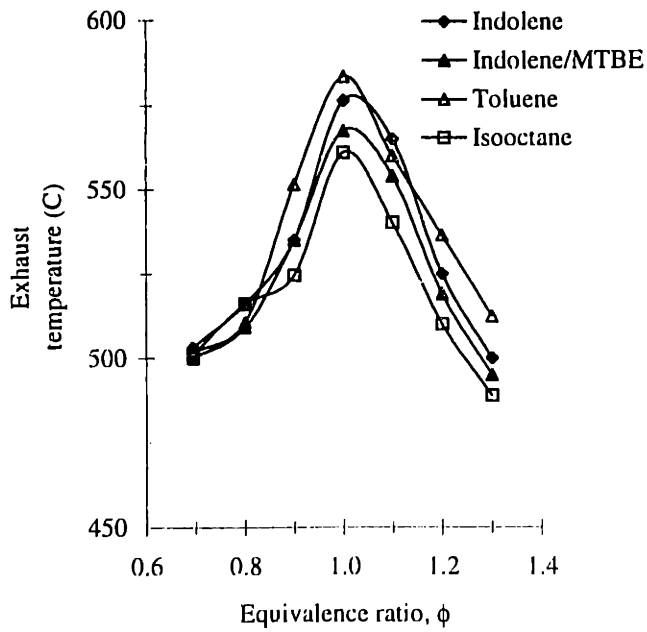

Figure A4.3 Measured exhaust temperature as a function of fuel/air equivalence ratio. Baseline engine operating conditions except equivalence ratio, using Saturn engine. Data for propane (using Ford Zetec engine) not available.

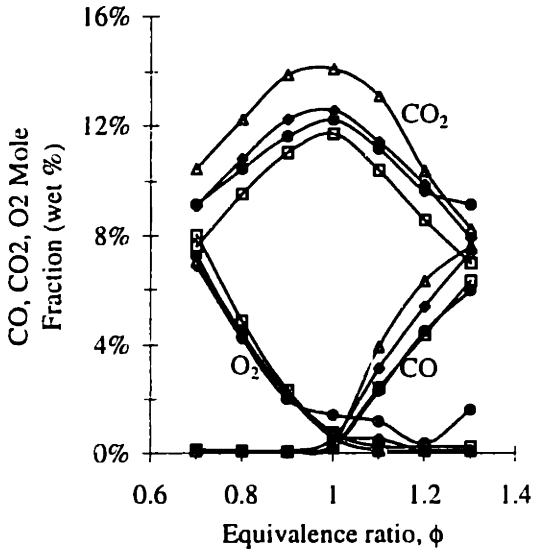

Figure A4.4 Measured exhaust concentrations of CO, CO_2, and O_2 as a function of fuel/air equivalence ratio. Baseline engine operating conditions except equivalence ratio. Symbols represent same things as in previous figure.

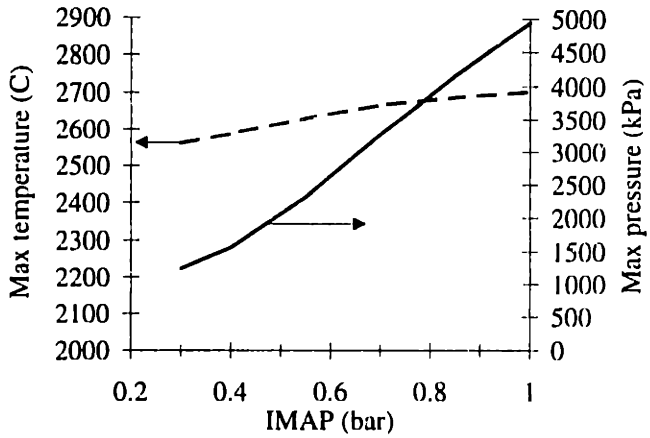

Figure A4.6 Peak cylinder temperature and pressure as a function of IMAP as calculated using the GM Engine-Simulation Program [51]. Inputs: baseline engine operating conditions except IMAP, with engine geometry equal to that for Ford Zetec. Isooctane fuel.

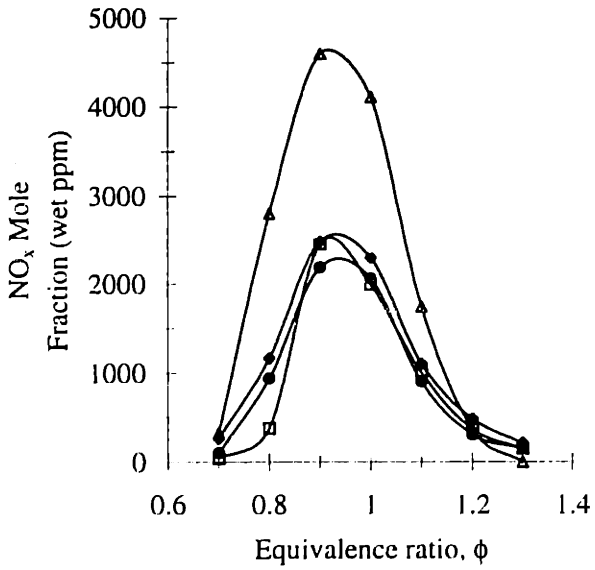

Figure A4.5 Measured exhaust concentrations of NO_x as a function of fuel/air equivalence ratio. Baseline engine operating conditions except equivalence ratio. Symbols represent same things as in previous figures.

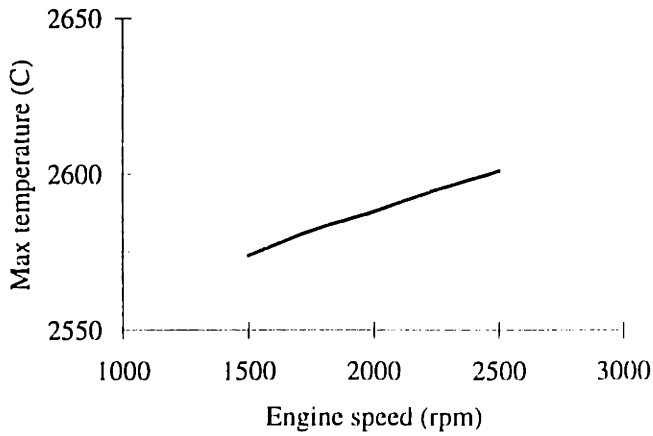

Figure A4.7 Peak cylinder temperature as a function of engine speed as calculated using the GM Engine-Simulation Program [51]. Inputs: baseline engine operating conditions except speed, with engine geometry equal to that for Ford Zetec. Isooctane fuel.

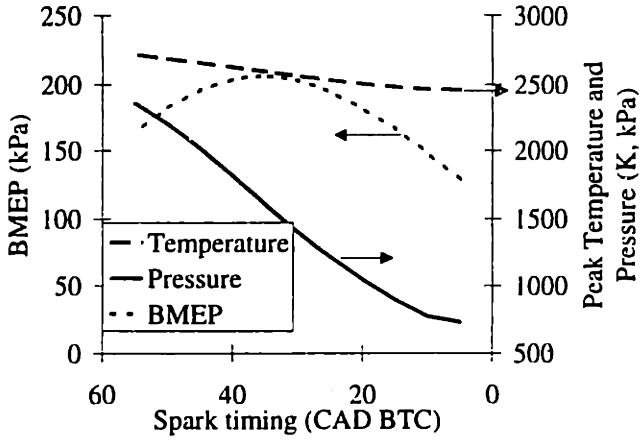

Figure A4.8 Peak cylinder temperature and pressure, as well as Brake Mean Effective Pressure (BMEP), as a function of engine spark timing as calculated using the GM Engine-Simulation Program [51]. Inputs: baseline engine operating conditions except speed, with engine geometry equal to that for Ford Zetec. Isooctane fuel.

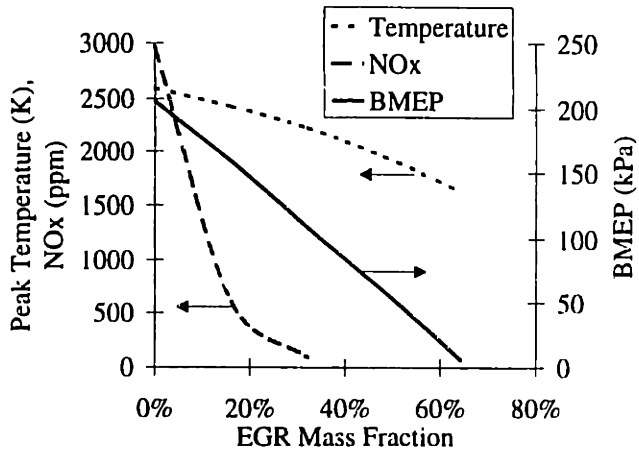

Figure A4.9 Peak cylinder temperature, NO_x emissions, and Brake Mean Effective Pressure (BMEP) as a function of EGR mass fraction as calculated using the GM Engine-Simulation Program [51]. Calculated EGR mass fraction corresponding to 100% of that needed to stall the engine (the metric used in the text) is 64%. Inputs to engine-simulation program: baseline engine operating conditions except residual gas fraction, with engine geometry equal to that for Ford Zetec. Isooctane fuel.